

SQUAMISH-LILLOOET REGIONAL DISTRICT

MOUNT CURRIE LANDSLIDE RISK ASSESSMENT

FINAL

PROJECT NO.: 1358004

DATE: January 16, 2018

January 16, 2018
Project No.: 1358004

Ryan Wainwright, Emergency Program Manager
Squamish-Lillooet Regional District
Box 219
Pemberton, BC, V0N 2L0

Dear Mr. Wainwright,

Re: Mount Currie Landslide Risk Assessment – FINAL

Please find enclosed a final copy of the above referenced report. This version of the document incorporates comments and suggestions from the Squamish-Lillooet Regional District on a draft of the report issued on December 22, 2017. This final version of the report also supersedes the December 22, 2017 draft. Should you have any questions or comments please do not hesitate to contact the undersigned.

We appreciate the opportunity to work on this most interesting project.

Yours sincerely,

BGC ENGINEERING INC.
per:



Matthias Jakob, Ph.D., P.Geo.
Principal Geoscientist

EXECUTIVE SUMMARY

Squamish-Lillooet Regional District (SLRD) retained BGC Engineering Inc. (BGC) to assess landslide and associated flood risk of the north face of Mount Currie. The project was initiated by SLRD following a series of rock fall events towards the top of the mountain occurring in 2015 and 2016. The rock fall events raised concerns about the risk to the public in the area around Pemberton and near the hamlet of Mount Currie.

The types of geohazards within the study area that were considered by BGC are: rock avalanches, rock falls, debris flows, rock slides / debris slides, landslide damming and associated flooding.

Study Area Description

Mount Currie is located immediately south of the village of Pemberton and the hamlet of Mount Currie, which lie in the floodplain of the Lillooet River upstream of Lillooet Lake. The mountain range is delimited to the north by the Lillooet River Valley, to the west and northwest by Green River Valley, and to the southeast by Gravell Creek. Mount Currie's rugged topography and geology contribute to the occurrence of landsliding. The area receives substantial precipitation in the form of rain and snow.

The main rock type in the study area is a fine- to medium-grained diorite, a rock type similar to granite. The diorite has a well-developed steeply dipping foliation (alignment of the minerals that form the rock). Volcanic rocks prevail at the eastern end of Mount Currie ridge. Two northwest-southeast trending faults have been previously mapped along Mount Currie ridge.

Geohazard Analysis

BGC undertook the following work to characterize landslide geohazards:

- Desktop analysis
- Geomorphic mapping
- Fieldwork including seismic survey
- Rock avalanche probability of occurrence estimate and runout modelling
- Landslide damming and flood modelling
- Debris flow magnitude-frequency analysis.

The desktop analysis reviewed and interpreted the literature, geotechnical reports, Google Earth and Bing imagery, available historical aerial photographs, and LiDAR data.

The Mount Currie ridge was traversed by foot to check the geomorphic mapping, and to characterize the rock mass. Temperature was measured in tension cracks to investigate the possible presence of frozen ground. While no sub-zero temperatures were encountered, the strong temperature gradient, and the elevation and aspect of the Mount Currie ridge, indicates that permafrost may prevail at depth.

Select locations on the Green and Lillooet rivers floodplain were inspected for evidence of pre-historic rock avalanche debris deposits. A geophysical investigation program was conducted in

the valley bottom to search for buried rock avalanche deposits. Neither the ground inspection nor geophysical survey found evidence of buried rock avalanche deposits.

The results of the geohazard assessment found that based on the desktop analysis and fieldwork observations, the area impacted by past rock falls, rock slides, debris avalanches and debris flows is confined to the south side of Green River and, as such, are not considered to represent significant hazards to infrastructure and residents below Mount Currie.

Through geomorphic mapping, BGC documented the distribution and orientation of “lineaments”, which are distinct linear features in the rock mass and may represent significant geological structures. The distribution of these lineaments and other geomorphic features allowed the identification of 19 potential rock avalanche source zones.

The review of the potential rock avalanche sources identified four main sources based on a qualitative ranking of the hazard. The qualitative ranking was based on activity level (evidence of recent deformation), kinematics (orientation of joints in consideration of slope stability), and volume estimate.

Computer models were used to estimate the potential rock avalanche travel distance and the associated flooding due to potential landslide blocking of the Green and Lillooet rivers. The numerical models of the rock avalanches runout and flooding associated with the damming of Green and Lillooet River showed that two of the four potential rock avalanche sources have the potential to affect areas on the north side of Green River.

The estimated annual probability of the modeled rock avalanche scenario 1 (from potential source identified near Currie NE3 Peak) is approximately 1 in 5,000, or a 0.02% chance of occurrence in any given year. The estimated annual probability of the modelled rock avalanche scenario 2 (from potential source identified along ridge east of Currie NE3 Peak) is approximately 1 in 11,000 or 0.009% chance of occurrence in any given year, under current conditions (including weathering/erosion rates). These probability estimates are subject to uncertainty, and could be adjusted up or down based on the results of further assessment and/or monitoring data.

Projected climate change is expected to further deteriorate rock slope stability, but how this might increase rock avalanche probability in the future cannot be reliably quantified due to the unknown distribution of permafrost and strength reduction associated with loss of ice cohesion in the rock mass. A subjective two-fold and ten-fold increase in the annual rock avalanche probability as a consequence of climate change was used to test the sensitivity of rock avalanche hazard to climate change. These two rock avalanche scenarios were carried forward in the geohazard risk assessment.

Geohazard Risk Assessment

The first step of the risk assessment identified and characterized the elements which could potentially be exposed to the geohazard scenarios considered in the risk analysis. These included persons, buildings, critical facilities, business activities, power and communication lines.

Risk was assessed for direct impact of a rock avalanche and vulnerability was assessed for flooding associated with the potential damming of the Green and Lillooet rivers.

On Mount Currie, rock avalanches are expected to travel at over 100 km/hr and involve volumes up to approximately 8 Million m³ of material. This would likely lead to total destruction of everything in their path. The two rock avalanche scenarios with the longest runout (greatest damage potential) were included in the risk assessment. The risk was calculated for an individual person and for groups of people and compared to risk tolerance criteria developed elsewhere. Occupants in up to 15 parcels could be exposed to risks that exceed individual risk tolerance criteria. For the group risk, depending on the rock avalanche scenario and the climate sensitivity analysis, the results indicated the risk could range from tolerable to unacceptable.

For the flooding hazard, the water depth as a result of a landslide dam is expected to increase over minutes to hours allowing for people to respond to the hazard. This response is difficult to quantify as it varies in different sections of the valley (due to different road networks providing exit routes) and it varies in time (whether the flooding occurs during the day or night, summer or winter). Furthermore, the timing and location of a breach of a landslide dam would impact the flood hazard and risk, but are extremely difficult to quantify. Approximately 160 buildings were identified as being potentially impacted by flooding associated with one of the rock avalanche scenarios, however the probability of flood-related losses has not been quantified.

Preliminary economic loss estimates were provided in association with direct impact and flooding for building damage (between \$1.6 million and \$16 million depending on the rock avalanche scenario) and business activity (between \$2 million and \$31.5 million depending on the rock avalanche scenario). Critical infrastructure and lifelines potentially affected by rock avalanche direct impact or flooding include the waste water treatment plant and various water and sewer infrastructure (i.e. mains and lift stations), Pemberton search & rescue base, and Ministry of Forest fire base.

Although there is considerable uncertainty in the risk estimates, the results of the study indicate that rock avalanche hazards from Mount Currie pose risks that likely exceed individual and group risk tolerance criteria. Given the uncertainties and potential risks, additional investigation, analysis, and implementation of a monitoring system likely represent the most practical and cost-effective approach to risk management. This would also allow future refinements or revisions of the current hazard and risk estimates.

SLRD might consider restricting land use in parts or all of the areas within modeled rock avalanche runout zones as any increase in development density in these areas would further increase the risk estimates.

TABLE OF CONTENTS

| | |
|--|-------------|
| EXECUTIVE SUMMARY | i |
| TABLE OF CONTENTS | iv |
| LIST OF TABLES | vi |
| LIST OF FIGURES | vii |
| LIST OF APPENDICES | ix |
| LIST OF DRAWINGS | viii |
| LIMITATIONS | x |
| 1.0 INTRODUCTION | 1 |
| 1.1. General | 1 |
| 1.2. Risk Assessment Framework | 2 |
| 1.3. Previous Geohazard Work | 3 |
| 1.3.1. Mount Currie | 3 |
| 1.3.2. Mount Currie Ridge Scarp | 4 |
| 2.0 STUDY AREA DESCRIPTION | 6 |
| 2.1. Physiography and Surficial Geology | 6 |
| 2.2. Geology | 7 |
| 2.3. Climate | 7 |
| 2.3.1. Climate Change | 9 |
| 2.4. Seismicity | 12 |
| 3.0 GEOHAZARD ANALYSIS | 14 |
| 3.1. Definitions | 14 |
| 3.2. Desktop Analysis | 16 |
| 3.3. Fieldwork | 16 |
| 3.4. Geomorphic Mapping | 17 |
| 3.4.1. Lineaments | 17 |
| 3.4.2. Deep-Seated Gravitational Slope Deformation | 18 |
| 3.4.3. Rock Fall and Rock / Debris Slides | 19 |
| 3.4.4. Debris Flows | 20 |
| 3.4.5. Limitations and Uncertainties | 20 |
| 3.5. Rock Avalanche Geohazard Analysis | 23 |
| 3.5.1. Frequency Estimation Method | 23 |
| 3.5.2. Regional Rock Avalanche Inventory | 23 |
| 3.5.3. Seismic Survey | 24 |
| 3.5.4. Rock Mass Characterization and Kinematic Analysis | 25 |
| 3.5.5. Temperature Profiles | 29 |
| 3.5.6. Frequency Estimation | 31 |
| 3.5.7. Climate Change and Hazard Frequency | 33 |
| 3.5.8. Uncertainties and Limitations | 34 |
| 3.6. Rock Fall and Rock / Debris Slide Geohazard Analysis | 35 |
| 3.6.1. Climate Change and Hazard Frequency | 35 |

| | |
|---|-----------|
| 3.6.2. Uncertainty and Limitations | 35 |
| 3.7. Debris Flow Geohazard Analysis | 36 |
| 3.7.1. Introduction | 36 |
| 3.7.2. Debris Flow Inventory..... | 36 |
| 3.7.3. Regional Frequency-Magnitude Relationship | 37 |
| 3.7.3.1. Methodology | 38 |
| 3.7.3.2. Results | 39 |
| 3.7.3.3. Climate Change Effects | 40 |
| 3.7.4. Uncertainties | 40 |
| 3.8. Preliminary Geohazard Assessment Results | 41 |
| 3.9. Rock Avalanche Runout Modelling | 41 |
| 3.9.1. Runout Methodology | 41 |
| 3.9.2. Inputs for Runout Modelling..... | 42 |
| 3.9.2.1. Sliding Surface | 42 |
| 3.9.2.2. Failure Volume and Source Location | 42 |
| 3.9.2.3. Resistance Parameters | 42 |
| 3.9.3. Excess Runout (“Splash Zone”)..... | 43 |
| 3.9.4. Runout Modelling Results..... | 44 |
| 3.9.5. Rock Avalanche Flow Intensity Index | 45 |
| 3.9.6. Uncertainties and Limitations..... | 45 |
| 3.10. Landslide Damming and Flood Modelling | 45 |
| 3.10.1. Flood Modelling Methodology..... | 46 |
| 3.10.2. Flood Modelling Input Parameters..... | 46 |
| 3.10.3. Flood Modelling Results | 46 |
| 3.10.4. Uncertainties and Limitations..... | 47 |
| 3.11. Results of Geohazard Numerical Modelling | 47 |
| 4.0 ELEMENTS AT RISK ANALYSIS | 48 |
| 4.1. Background | 48 |
| 4.2. Buildings..... | 49 |
| 4.3. Critical Facilities | 50 |
| 4.4. Persons | 51 |
| 4.5. Business Activity..... | 52 |
| 4.6. Lifelines..... | 53 |
| 5.0 VULNERABILITY AND RISK ESTIMATION | 54 |
| 5.1. Introduction | 54 |
| 5.2. Safety Risk Tolerance Criteria | 54 |
| 5.3. Results | 56 |
| 5.4. Individual Safety Risk..... | 56 |
| 5.5. Group Safety Risk | 57 |
| 5.6. Human Vulnerability | 59 |
| 5.7. Building Damage | 59 |
| 5.8. Business Activity..... | 60 |
| 5.9. Loss of Function..... | 61 |

6.0 CONCEPTUAL MITIGATION STRATEGIES 64
7.0 CONCLUSIONS AND RECOMMENDATIONS..... 66
 7.1. Conclusions..... 66
 7.2. Recommendations 67
8.0 CLOSURE..... 68
REFERENCES 69

LIST OF TABLES

Table 1-1. Overview of the general risk management framework to be used in this project (adapted from CSA 1997; AGS 2007; VanDine 2012; ISO 31000:2009).....3

Table 1-2. Discontinuity sets identified by Evans (1987) and Bovis and Evans (1995) along the northeast ridge of Mount Currie.5

Table 3-1. Historical aerial photographs used in this assessment. 16

Table 3-2. Potential rock avalanche sources on the north face of Mount Currie.21

Table 3-3. Discontinuity characteristics for the southwest structural domain.29

Table 3-4. Discontinuity characteristics for the northeast structural domain.29

Table 3-5. Summary of the spatial rock avalanche density estimate and rock avalanche annual probability of occurrence for the potential rock avalanche source zones. 33

Table 3-6. Summary of the assumed annual probability of rock avalanche occurrence climate change adjustment for the potential rock avalanche source zones..... 33

Table 3-7. Inventory of debris flow events reaching the lower part of the fan at the base of Flow Paths A, B, C and D; based on historical aerial photographs listed in Table 3-1 and Google Earth Imagery.....37

Table 3-8. Debris Flow frequency-volume summary for Fans A, B, C and D on the north face of Mount Currie based on a regional analysis approach. 39

Table 3-9. Source and entrainment volumes considered in the DAN3D simulations. 42

Table 3-10. Input parameters used in the DAN3D simulations of rock avalanches initiating from Mount Currie. 43

Table 3-11. Elements at risk simulated by DAN3D and splash zone. 45

Table 4-1. Elements at risk within the rock avalanche direct impact and splash zones, and flood inundation zone..... 49

| | | |
|------------|---|----|
| Table 4-2. | Building data uncertainties. | 50 |
| Table 4-3. | Summary of calculated population estimates used in risk analysis..... | 52 |
| Table 4-4. | Uncertainties associated with estimating the number of occupants of a building. | 52 |
| Table 4-5. | Business data uncertainties. | 53 |
| Table 5-1. | Number of parcels exceeding individual risk tolerance thresholds for current conditions and with consideration of climate change..... | 57 |
| Table 5-2. | Summary of building consequence estimates. | 60 |
| Table 5-3. | Summary of business consequence estimates..... | 61 |
| Table 5-4. | Summary of critical facilities impacted by Scenario 1 and 2 rock avalanche and flooding. | 61 |
| Table 5-5. | Summary of roads impacted by Scenario 1 and 2 rock avalanche and flooding. | 62 |
| Table 6-1. | Hierarchical approach to potential rock slope monitoring techniques applicable to Mount Currie. | 64 |

LIST OF FIGURES

| | | |
|-------------|--|----|
| Figure 1-1. | Location map (August 2014 imagery from arcgis.com)..... | 2 |
| Figure 1-2. | Stereonet of contoured poles to discontinuities measured at Mount Currie (Bovis and Evans 1995). | 5 |
| Figure 2-1. | Monthly climate normal for (A) Pemberton Airport between April 1984 and December 2011, and (B) Pemberton between June 1969 and December 2000 (data from PCIC, 2017). | 8 |
| Figure 2-2. | A) Projected change in mean annual temperature for western Canada B) Projected change in mean annual temperature at the Pemberton airport..... | 9 |
| Figure 2-3. | Daily ground temperatures measured in selected boreholes at ca. 10 m and 20 m depth in Switzerland. | 10 |
| Figure 2-4. | Maximum active layer thickness measured at selected reference sites in the past 15 years at Stockhorn Mountain in Switzerland..... | 11 |
| Figure 2-5. | Projected changes in hourly extreme precipitation by the late 21 st century assuming a high end (RCP 8.5) emission scenario..... | 11 |
| Figure 2-6. | A) Earthquakes in Natural Resource Canada database (Halchuk et al., 2015) for southwestern British Columbia. B) Empirical relationship of earthquake magnitude and distance at which landslides were | |

| | | |
|-------------|---|----|
| | seismically triggered and the magnitude of the earthquake (Keefer, 1984). | 13 |
| Figure 3-1. | Summary diagram outlining which geohazard scenarios were identified and which were analyzed in each step of the geohazard analysis. | 14 |
| Figure 3-2. | Geological Strength Index (GSI) and main discontinuity sets of the Southwest Domain. | 26 |
| Figure 3-3. | Geological Strength Index (GSI) and main discontinuity sets of the Northeast Domain. | 27 |
| Figure 3-4. | Stereonet of the two structural domains for both compass and photogrammetry measurements. | 28 |
| Figure 3-5. | Temperature profiles obtained from thermistor string lowered in trenches. See Drawing 03 for location. | 30 |
| Figure 3-6. | Schematic of permafrost distribution on Mount Currie. | 31 |
| Figure 3-7. | Debris-flow frequency-volume estimates for major creeks draining the North Face of Mount Currie based on regional analysis. | 38 |
| Figure 3-8. | Cumulative frequency of the splash zone ratio from published literature on rock avalanches | 44 |
| Figure 5-1. | DNV individual risk tolerance criteria for landslides compared with Canadian mortality rates (all causes) in 2008. | 55 |
| Figure 5-2. | Group risk tolerance criteria as defined by GEO (1998). | 56 |
| Figure 5-3. | F-N curve showing the range of group risk analysis results for Scenarios 1a (purple) and 2b (red) in the current climate and projected future climate conditions. | 58 |
| Figure 5-4. | F-N plot for group risk for debris flows from Mount Meager (Friele et. al. 2008) with Rock Avalanche Scenario 1a and 2b group risk results from the current study shown for comparison (purple and red ovals). | 59 |

LIST OF DRAWINGS

| | |
|------------|--|
| DRAWING 01 | Bedrock and Surficial Geology |
| DRAWING 02 | Regional Earthquake Inventory and Inventory of Post-glacial Rock Avalanches |
| DRAWING 03 | Site Investigation |
| DRAWING 04 | Geohazard and Landslide Features Inventory on Mount Currie |
| DRAWING 05 | Overview of Potential Rock Avalanche Sources on Mount Currie |
| DRAWING 06 | Regional Rock Avalanche Inventory Area and Concentric Areas Used in the Estimation of Rock Avalanche Frequency |

- DRAWING 07 Rock Avalanche Deposit
- DRAWING 08 Flood and Rock Avalanche Hazard Scenario Map: Zone 1a
- DRAWING 09 Flood and Rock Avalanche Hazard Scenario Map: Zone 2b
- DRAWING 10 Risk Assessment Basemap
- DRAWING 11 Results, Vulnerability Map: Flood and Rock Avalanche Scenario Zone 2b

LIST OF APPENDICES

- APPENDIX A ROCK AVALANCHE AND DEEP-SEATED GRAVITATIONAL SLOPE DEFORMATION (DSGSD) REGIONAL INVENTORY
- APPENDIX B DETAILS OF PHOTOGRAMMETRY METHODOLOGY TO GENERATE 3D SURFACES AND EXTRACT DISCONTINUITY SURFACE ORIENTATIONS
- APPENDIX C GEOPHYSICAL SURVEY REPORT FROM FRONTIER GEOSCIENCE INC.
- APPENDIX D DETAILS OF KINEMATIC ANALYSES CONDUCTED FOR THE VARIOUS SECTIONS OF THE NORTH SLOPE OF MOUNT CURRIE
- APPENDIX E ROCK AVALANCHE PROBABILITY OF OCCURRENCE ESTIMATE USING THE NORWEGIAN ROCK SLOPE ASSESSMENT APPROACH
- APPENDIX F JAKOB ET AL., 2016. REGIONAL DEBRIS-FLOW AND DEBRIS-FLOOD FREQUENCY-MAGNITUDE CURVES. PROCEEDINGS OF GEOVANCOUVER 2016
- APPENDIX G DETAILS ON THE DAN3D ROCK AVALANCHE MODELLING
- APPENDIX H RISK ASSESSMENT METHODOLOGY

LIMITATIONS

BGC Engineering Inc. (BGC) prepared this document for the account of Squamish-Lillooet Regional District. The material in it reflects the judgment of BGC staff in light of the information available to BGC at the time of document preparation. Any use which a third party makes of this document or any reliance on decisions to be based on it is the responsibility of such third parties. BGC accepts no responsibility for damages, if any, suffered by any third party as a result of decisions made or actions based on this document.

As a mutual protection to our client, the public, and ourselves, all documents and drawings are submitted for the confidential information of our client for a specific project. Authorization for any use and/or publication of this document or any data, statements, conclusions or abstracts from or regarding our documents and drawings, through any form of print or electronic media, including without limitation, posting or reproduction of same on any website, is reserved pending BGC's written approval. A record copy of this document is on file at BGC. That copy takes precedence over any other copy or reproduction of this document.

1.0 INTRODUCTION

1.1. General

Squamish-Lillooet Regional District (SLRD) retained BGC Engineering Inc. (BGC) to assess landslide risk of the north face of Mount Currie (Figure 1-1). The project was initiated by SLRD following a series of rock fall events from the top of the mountain occurring in 2015 and 2016. The rock falls raised concerns about the risk to the public in the area around Pemberton and near the hamlet of Mount Currie from landslide hazards. Funding for this project is provided by Emergency Preparedness BC (EMBC). A steering committee assembled by SLRD oversees the project and is composed of representatives from SLRD, Village of Pemberton, Lil'wat Nation, EMBC, and BC Ministry of Forests Land and Natural Resource Operations (MFLNRO).

A preliminary report (BGC 2017) summarizing the findings of the desktop study component of this project was presented to the SLRD and steering committee on July 7, 2017. The interim report identified and characterized, at a preliminary level of detail, the following types of geohazards within the study area: rock avalanches, large rock falls, debris flows, rock slides / debris slides, along with landslide damming and associated floods. The present report updates the preliminary geohazard assessment results of the interim report based on field work, review of LiDAR, numerical modelling. This report also provides a landslide risk assessment based on the updated geohazard assessment.

BGC provided SLRD with a March 9, 2017 proposal describing the scope of work, which was accepted by the SLRD on March 28, 2017. BGC's scope of work excludes assessment of the following hazards and elements at risk:

- An assessment of geohazards west of Nairn Fall Provincial Park, as agreed with the steering committee during a July 11, 2017 meeting
- An assessment of hydrotechnical hazard other than floods associated with the potential damming of the Green River and Lillooet River by landslides initiating from the north face of Mount Currie, in the project area of interest defined in BGC's proposal issued on March 9, 2017
- An assessment of snow avalanche hazard
- An assessment of liquefaction potential due to earthquake
- Potential impact of all hazards to forestry operations for the area between the base of the north face of Mount Currie and Green River (as per guidance from the steering committee during an April 24, 2017 meeting)
- Potential impact of hazard on future developments in the study area (as per guidance from the steering committee during the April 24, 2017 meeting).

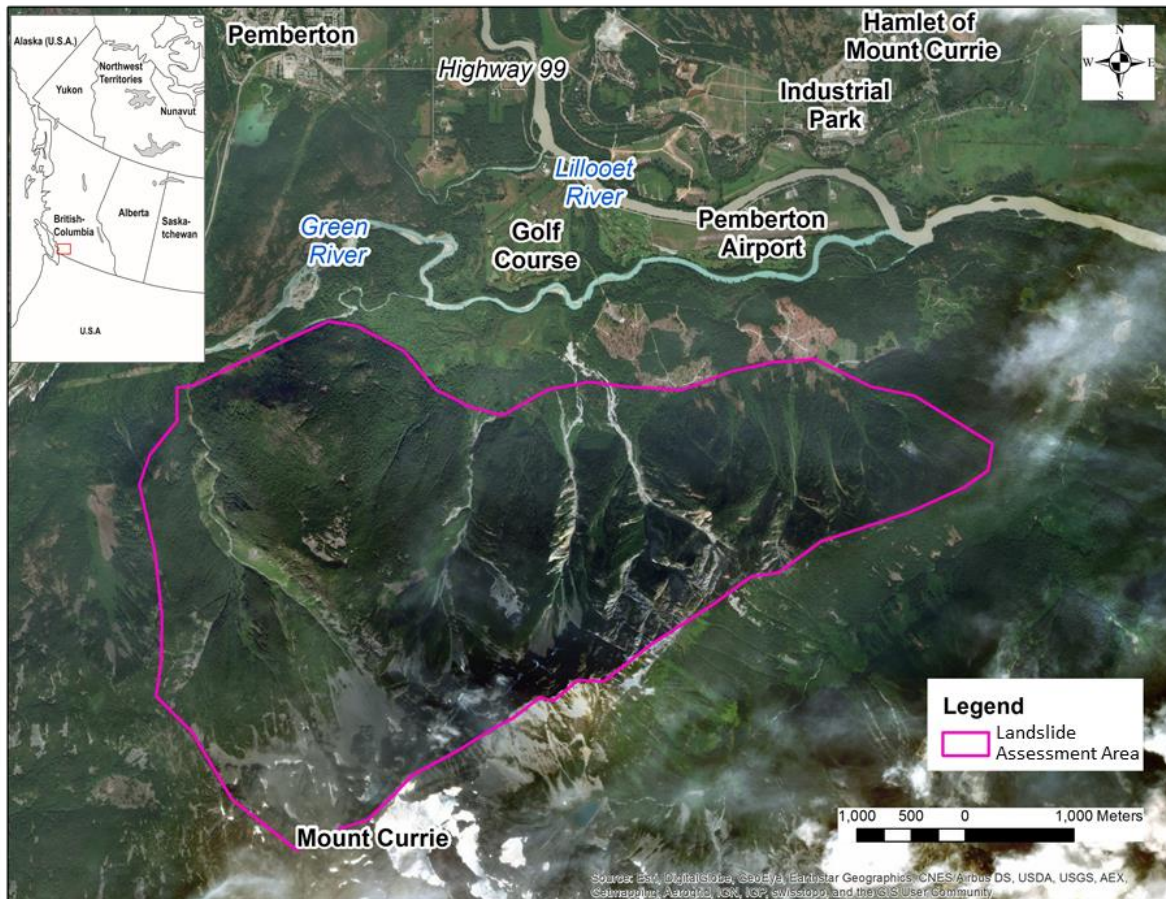


Figure 1-1. Location map (August 2014 imagery from arcgis.com).

1.2. Risk Assessment Framework

Risk is a measure of the probability and severity of an adverse effect to health, property or the environment, and is estimated by the product of hazard probability (or likelihood) and consequences (AGS 2007). As applied to geohazards, it involves estimation of the likelihood that a geohazard will occur, impact elements at risk, and cause particular types and severities of consequences. Each of these components are estimated separately and then combined. The objective is to provide a systematic, repeatable assessment with an appropriate level of detail for the information available.

Table 1-1 provides an overview of a risk management framework, after Canadian Standards Association (CSA 1997), AGS (2007), and ISO 31000:2009. This assessment comprises the first five phases and part of the sixth phase of the risk management framework for Mount Currie.

Table 1-1. Overview of the general risk management framework to be used in this project (adapted from CSA 1997; AGS 2007; VanDine 2012; ISO 31000:2009).

| | | | | | | | |
|----------------------|-------------------------------|-------------------------|---------------------------|--|--|---|--|
| Geohazard Assessment | Geohazard Risk Identification | Geohazard Risk Analysis | Geohazard Risk Assessment | Geohazard Risk Management | Risk Communication and Consultation Informing stakeholders about the risk management process | 1. Scope Definition a. Recognize the potential hazard b. Define the study area and level of effort c. Define roles of the client, regulator, stakeholders, and Qualified Registered Professional (QRP) d. Identify 'key' consequences to be considered for risk estimation | Monitoring and Review Ongoing review of risk scenarios and risk management process |
| | | | | 2. Geohazard Analysis a. Identify the geohazard process, characterize the geohazard in terms of factors such as mechanism, causal factors, and trigger factors; estimate frequency and magnitude; develop geohazard scenarios; and estimate extent and intensity of geohazard scenarios. | | | |
| | | | | 3. Elements at Risk Analysis a. Identify elements at risk b. Characterize elements at risk with parameters that can be used to estimate vulnerability to geohazard impact. | | | |
| | | | | 4. Geohazard Risk Estimation a. Develop geohazard risk scenarios b. Estimate consequences c. Estimate geohazard risk | | | |
| | | | | 5. Geohazard Risk Evaluation a. Compare the estimated risk against local or other tolerance criteria b. Prioritize risks for risk control and monitoring | | | |
| | | | | 6. Geohazard Risk Control a. Identify options to reduce risks to levels considered tolerable by the client or governing jurisdiction b. Select option(s) with the greatest risk reduction at least cost c. Estimate residual risk for preferred option(s) | | | |
| | | | | 7. Action a. Implement chosen risk control options b. Define and document ongoing monitoring and maintenance requirements | | | |

1.3. Previous Geohazard Work

A review of the previous geohazard work was completed in the Mount Currie area to provide context for the current work.

1.3.1. Mount Currie

Previous geohazard assessment of the Mount Currie area included the work by Jakob (1996) which provided a detailed estimate of debris flow frequency in one of the main gullies of the north face of the mountain. Blais-Stevens et al. (2012) highlighted the high debris flow and rock fall / rock slide susceptibility of the north face of Mount Currie. Fournier (2016) reported a series of small to moderate scale rock fall events, which occurred between 2015 and 2016 along the southwest end of Mount Currie Ridge.

1.3.2. Mount Currie Ridge Scarp

Eisbacher (1983) identified a major linear feature (antisllope scarp and tension-crack trench) along the northeast ridge of Mount Currie. Although the origin of this feature was initially interpreted to be tectonic (or seismic), Thompson et al. (1997) provided evidence that it is likely the result of gravitational deformation of the ridge. The linear feature has an orientation of 043° and an approximate length of 1,750 m (Evans 1987). The scarp increases in height from less than 2 m to more than 20 m when traced to the northeast (Bovis and Evans 1995).

Bovis and Evans (1995) described the rock mass, mapped the discontinuity set orientations (Table 1-2 and Figure 1-2), and studied the displacement mechanisms along the prominent antisllope scarp and tension-crack trench on the northeast end of Mount Currie scarp (i.e., closest to the cliff face). They identified two main movement trends on four rock mass blocks located along the trench:

- Northeast displacement interpreted to be associated with toppling along sub-vertical, northwest trending foliation planes (D1 in Table 1-2 and Figure 1-2)
- Northwest displacement interpreted to be associated with sliding on flat-lying joints (D3 and D4): the greater scarp height to the northeast was hypothesized to be the surface expression of sliding along D3/D4. Ground displacement ranging between 15 and 60 mm were measured by Bovis and Evans (1995) for the period from 1987 to 1991.

Bovis and Evans (1995) identified toppling along D1 as a predominant mechanism, which could lead to progressive development of through-going shear surfaces. However, due to the northerly to northeasterly direction of toppling, they concluded that this mechanism is unlikely to pose a significant hazard to the Green River area. This finding was reevaluated as part of the analyses completed for this project (Section 3.5.4). Bovis and Evans (1995) did not comment on the hazard related to the displacement recorded towards the northwest.

A later study by Thompson et al. (1997) based on the characterization and analysis of a trench across the Mount Currie scarp's southwest end (i.e. furthers to the cliff face) provided evidence that displacement has occurred episodically from late Pleistocene to mid-Holocene time along the scarp. Thompson et al (1997) found no evidence of current or very recent movement along the Mount Currie scarp's southwestern end. The direction of slope movement was consistent with the northeast displacement interpreted by Bovis and Evans (1995). Thompson et al. (1997) found no definitive evidence for present or recent deformation at the location of the trench, i.e., just southeast of Currie NE3.

In summary, previous work documented the occurrence of rock fall, rock slide, debris flows and slow rock slope deformation (also called deep-seated gravitational slope deformation in Section 3.1. With the exception of debris flows, no systematic mapping of geohazard over the whole north face of Mount Currie or magnitude-frequency relationship has previously been conducted. No risk assessment was previously conducted for any of the geohazards associated with Mount Currie.

Table 1-2. Discontinuity sets identified by Evans (1987) and Bovis and Evans (1995) along the northeast ridge of Mount Currie.

| Discontinuity Set | Type | Orientation | Spacing (m) | Surface Characteristics | Possible Failure Mechanism |
|-------------------|-----------|--|---------------|-------------------------|----------------------------|
| D1 | Foliation | Sub-vertical, dipping towards 040° to 050° | 0.5 to 2 | Smooth | Toppling |
| D2 | Joint | Dipping steeply towards 130° to 140° | Not available | Smooth | Toppling |
| D3 | Joint | Flat-lying (< 30°), dipping to the southwest | Not available | Not available | Sliding |
| D4 | Joint | Flat-lying, dipping to the west | Not available | Not available | Sliding |

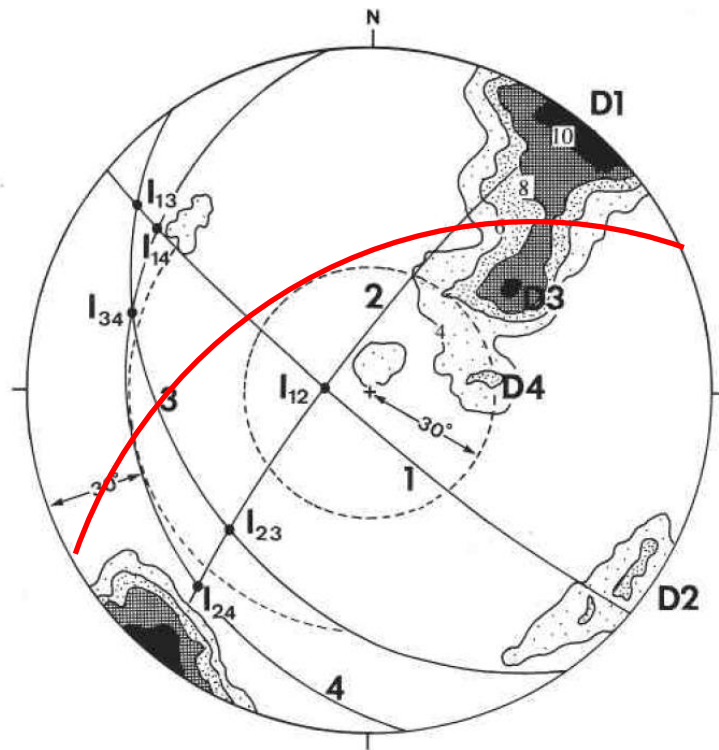


Figure 1-2. Stereonet of contoured poles to discontinuities measured at Mount Currie (Bovis and Evans 1995). This stereonet is a lower hemisphere equal area projection. Contours are percentage of total pole measurements per 1% area. D1, D2, D3, D4 refers to the discontinuity set nomenclature presented in Table 1-2. I₁₂, I₁₃, I₁₄, I₂₃, I₂₄, I₃₄ refers to the discontinuity set intersection orientation. Red great circle representing the approximate orientation of the upper Mount Currie Ridge was annotated by BGC.

2.0 STUDY AREA DESCRIPTION

This section describes the overall project setting, including physiography, geology, climate, and seismicity. Descriptions of project area geomorphology and engineering geology are included in Section 3.0 as they relate to hazard identification and characterization.

2.1. Physiography and Surficial Geology

Mount Currie is a mountain range located immediately south of the village of Pemberton and the hamlet of Mount Currie, which lie in the floodplain of Lillooet River upstream of Lillooet Lake. The mountain range consists of six main summits: Mount Currie Peak, Currie W1, Currie NW1, Currie N1, Currie NE2, and Currie NE3 (Drawing 01). The summits are located along a seven-kilometer long crest oriented SW-NE, except for Mount Currie Peak, which lies approximately 800 m south of the main crest line. The range is delimited to the north by the Lillooet River Valley, to the west and northwest by Green River Valley, and to the southeast by Gravell Creek. Mount Currie Peak has an elevation of 2,591 m above sea level (asl), almost 2,400 vertical meters above the Lillooet River Valley. The rugged topography of Mount Currie affects the stress distribution in the rock mass and overlying surficial material making them both susceptible to landsliding.

Mount Currie and the surrounding landscape has been shaped by repeated glaciations over the past 2,600,000 years combined with erosion and landslide activity. The last, or Fraser glaciation, reached its maximum extent about 14,500 years when the Cordilleran ice sheet reached an elevation of 2,000 m asl in the Southern Coast Mountains, and the main valley was ice-free by about 10,500 years ago (Eisbacher 1983; Clague and Ward 2011). Since then, alpine glaciers reached their maximum during the mid-19th century at the peak of the Little Ice Age and have since retreated to the upper, northeast facing side of Mount Currie Peak. A rock glacier has also been identified north of Currie W1 (Drawing 01), indicating the presence of alpine permafrost (consistent with permafrost zonation models by Gruber; 2012 and MFLNRO; 2013 for the study area). As a result of glacial erosion, upper slopes are steep and rocky and contain numerous escarpments (scars) and counter-slope scarps.

Part of the west and northwest sides of Mount Currie is overlain by landslide debris (Blais-Stevens 2008). Rubble talus and block accumulations are present along lineaments and at the bottom of steep rock slopes. The north face contains four watersheds with multiple, colluvium-filled gullies with debris flow deposits at their outlets inferred to be up to 10 m thick. The west side of the north face is covered by a veneer (inferred to be 1 m thickness on average) of till material with abundant bedrock outcrops.

The Green River valley bottom on the west and northwest sides of Mount Currie is filled with a combination of fluvial sediment and glaciofluvial deposits (Blais-Stevens 2008). A review by BGC of water well logs (MoE 2017) in Nairn Falls Provincial Park found a mix of sediment textures including silt, sand, gravel with the presence of boulders in gravel.

Green River and Lillooet River floodplain consists of fluvial deposits (Blais-Stevens 2008). A review by BGC of water well logs (MoE 2017) located in Pemberton Golf Course, along Highway

99 and near the Pemberton airport shows sediment consistent with a fluvial dominated depositional environment potentially overlying glacio-fluvial or glacio-lacustrine sediments. The depth of the available water wells ranges between 3 and 81 m, and well logs report sediment textures include clay, silt, sand, minor gravel, and minor peat.

2.2. Geology

The previously mapped regional geology was reviewed as part of the desktop study to provide context to the rock types and major tectonic structures observed during the fieldwork at Mount Currie. The study area is in the western Coast Belt of the Western Canadian Cordillera characterized by Middle Jurassic to mid-Cretaceous plutonic rocks which intrude low-grade metamorphosed sedimentary and volcanic rocks (Journeay and Monger 1994). Drawing 01 shows that bedrock on Mount Currie consists of diorite and quartz diorite plutonic rocks, and stratified rocks of the Brockenback Hill Formation (Gambier Group).

The Early Cretaceous Pemberton Diorite Complex forms the western side of Mount Currie. The diorite is fine- to medium-grained with local gradations into quartz diorite and coarse-grained hornblendite (Roddick and Hutchison 1973). It is in contact along the northwest trending Miller Creek Thrust Fault with Jurassic quartz diorite, which outcrops in the center of the mountain (Journeay and Monger 1994). The Miller Creek Thrust Fault is a west dipping tectonic feature considered to represent the boundary between the southeast and southwest Coast Mountain (Bustin et al. 2013). The quartz diorite contains abundant inclusions, gneissic zones and irregular areas of dark dioritic rock (Roddick and Hutchison 1973). Well-developed foliation in both diorite and quartz diorite is northwest-trending and dips steeply to the northeast or southwest (Roddick and Hutchison 1973; Woodsworth 1977). Dykes can be observed in both diorite and quartz diorite (Photograph 1).

The Gambier Group forms the east side of Mount Currie and consists mostly of the Brokenback Hill Formation (Journeay and Monger 1994). The rock types include andesite breccia, tuff and greenstone derived from a combination of flows and pyroclastic rocks (Roddick and Hutchison 1973). An unnamed fault trends to the northwest within the Gambier Group (Drawing 01).

2.3. Climate

The Pemberton valley floodplain is part of the Coastal Western Hemlock Dry Submarine biogeoclimatic zone (MFLNRO 2016). While the Coastal Western Hemlock zone is generally characterized by wet climate and mild temperature, the valley bottom around Pemberton is drier than the lower section of Mount Currie, which consists of the Coastal Western Hemlock Moist Submarine zone. At mid-elevation on the mountain, there is a transition to the Mountain Hemlock Moist Maritime zone, characterized by short, cool summers and long, cool, and wet winters. The upper part of the mountain, above tree line, is in the Coastal Mountain-Heather Alpine zone, where snowpack is deep and persistent, and summers are moderated by maritime influences (MFLRO 2016).

Climate normal were derived from Pemberton Airport weather station for the period between April 1984 and December 2011, and from Pemberton weather station for the period between June 1969 and December 2000 (PCIC 2017). Mean daily temperature reaches its maximum in July and August, and falls below 0°C between November and February (Figure 2-1). Monthly precipitation ranges between approximately 40 mm during the summer and up to 200 mm in January. The amount of fall and winter precipitation (September to March) is greater at Pemberton weather station between 1969 and 2000 than at Pemberton weather station between 1984 and 2011.

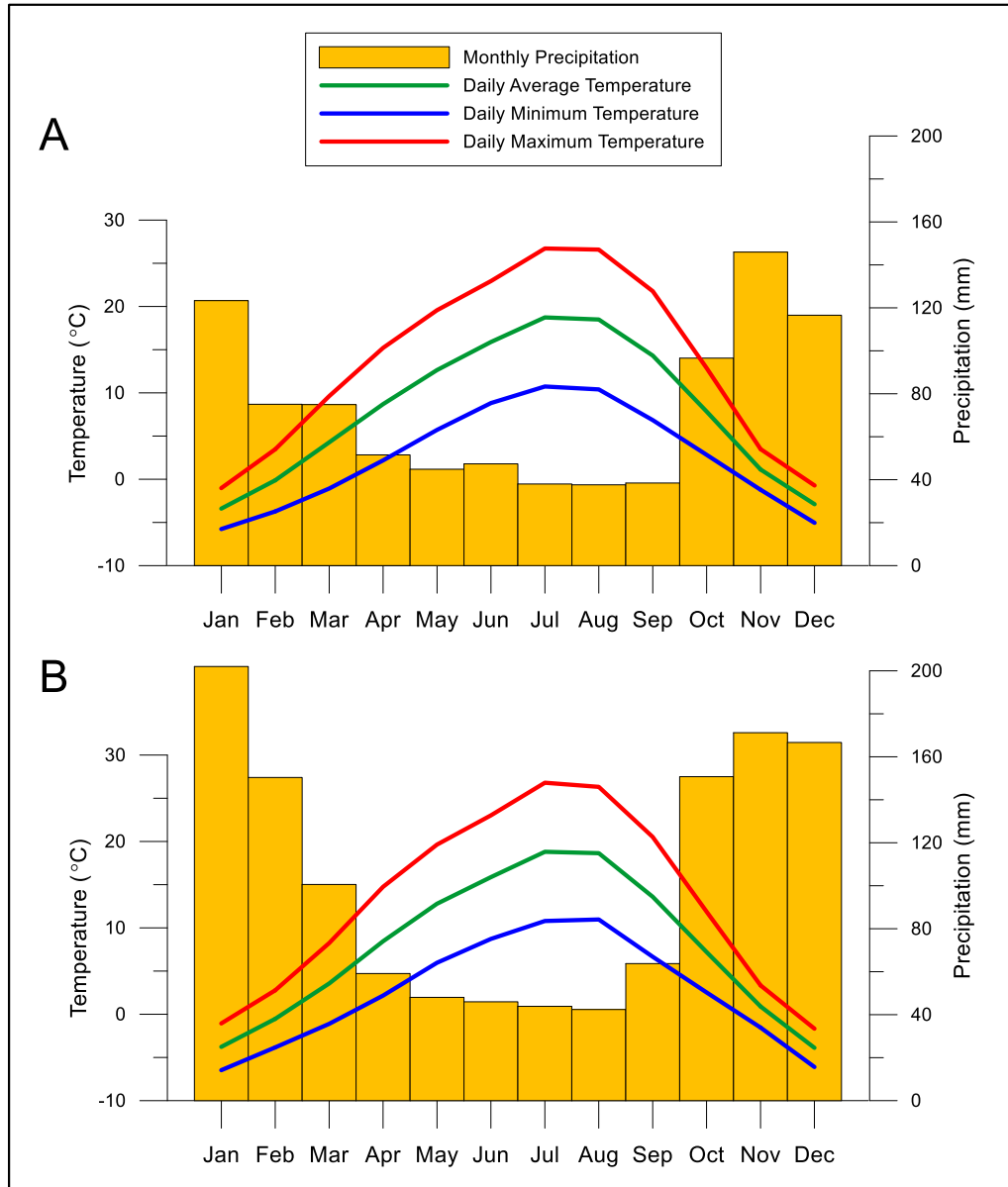


Figure 2-1. Monthly climate normal for (A) Pemberton Airport between April 1984 and December 2011, and (B) Pemberton between June 1969 and December 2000 (data from PCIC, 2017).

2.3.1. Climate Change

Climate change since the 1950s is unprecedented, compared to prior decades and millennia (IPCC, 2014). Changes in climate need to be considered as part of land use planning which includes geohazards. The two climate metrics most relevant to the present study area are temperature and precipitation changes. Climate projections from numerical models based on assumed greenhouse gas concentrations along with technological and socio-economic conditions are relied on for studies similar to the current project. One such set of assumptions is called “representative concentration pathways” (RCP) 8.5 (Riahi et al., 2011) and was used by others to estimate the temperature and precipitation in western North America until the year 2100. The mean annual temperature projections for western Canada between 2017 and 2100 are shown in (Figure 2-2A). Based on this model the mean annual temperature increase anticipated at the Pemberton Airport is approximately 4°C by 2100 (Figure 2-2B).

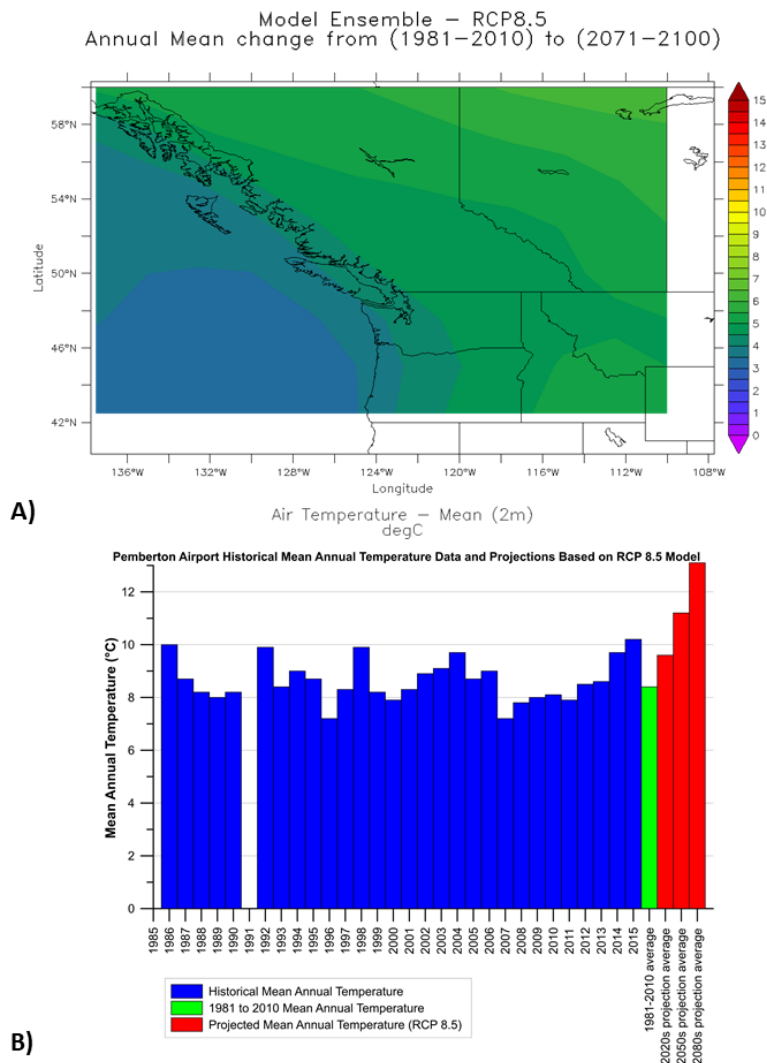


Figure 2-2. A) Projected change in mean annual temperature for western Canada B) Projected change in mean annual temperature at the Pemberton airport. Both figures are based on data assuming the RCP 8.5 climate model obtained from CCHIP 2017.

The projected increases of the air temperature will also affect the permafrost distribution. The progressive degradation of permafrost would reduce ice cohesion in the rock mass. Figure 2-3 shows borehole temperature measurements in mountain permafrost in Switzerland, most of which show a warming trend accentuated over the past 10 years. This is accompanied by a thickening active layer, particularly in “warm” permafrost, i.e. permafrost between zero and -1° Celsius. Figure 2-4 provides an example of active layer thickening at Stockhorn Mountain where random fluctuations in active layer thickness prior to 2009 were replaced with a sudden increase in active layer depth from 3.4 to 4.8 m. This implies that during that time ice that had persisted between 3.4 and 4.8 m depth melted and the associated cohesion bond between rock slabs was lost.

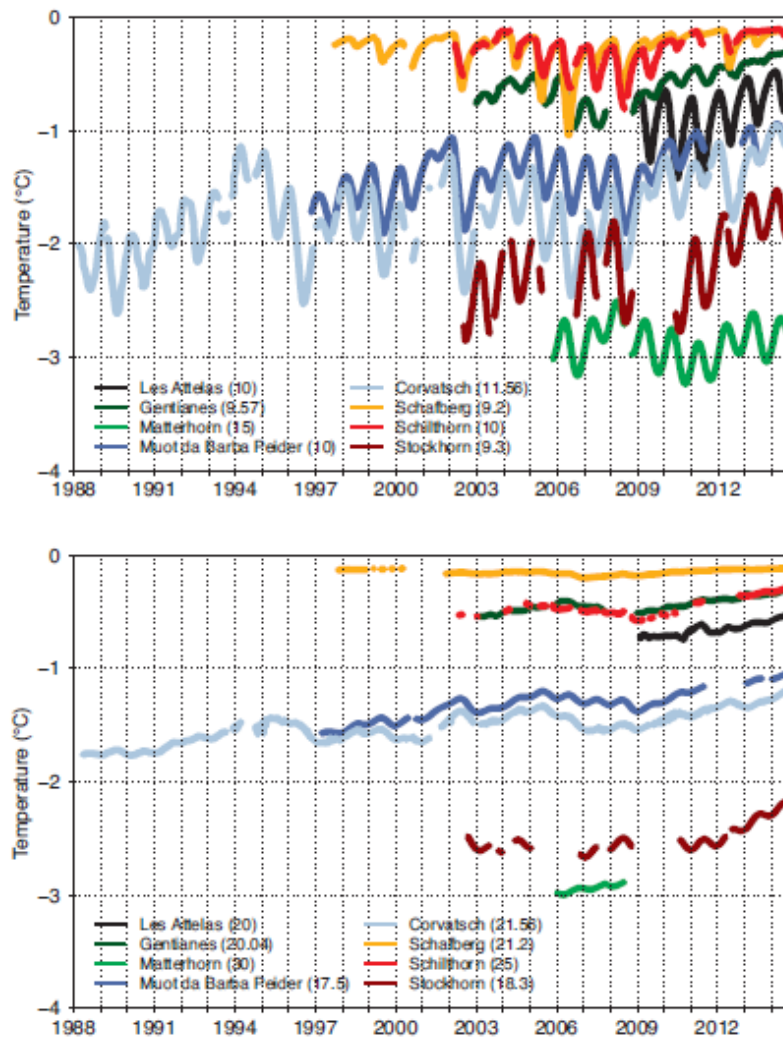


Figure 2-3. Daily ground temperatures measured in selected boreholes at ca. 10 m and 20 m depth in Switzerland. The exact depth is metres in indicated in brackets in the legend (Source: Noetzli et al. 2016).

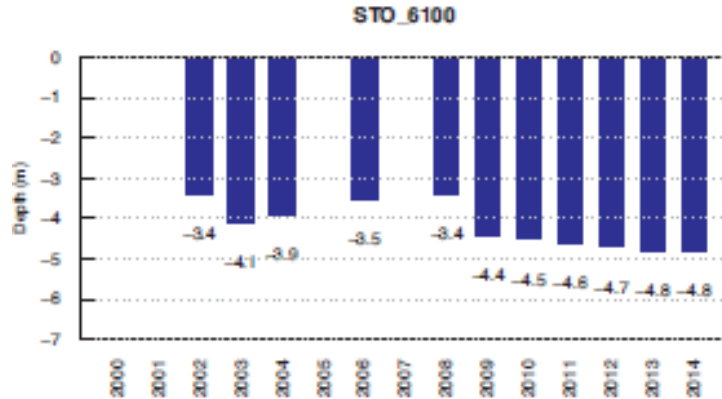


Figure 2-4. Maximum active layer thickness measured at selected reference sites in the past 15 years at Stockhorn Mountain in Switzerland. (Source: Noetzli et al. 2016).

In addition to the projected changes in temperature, recent work (i.e. Prein et al. 2016) has identified a projected substantial increase in the frequency of high intensity rainfall in southwestern British Columbia, with up to a 4-fold increase in the frequency of peak hourly rainfall (Figure 2-5). This implies a higher frequency of debris-flow threshold exceedances.

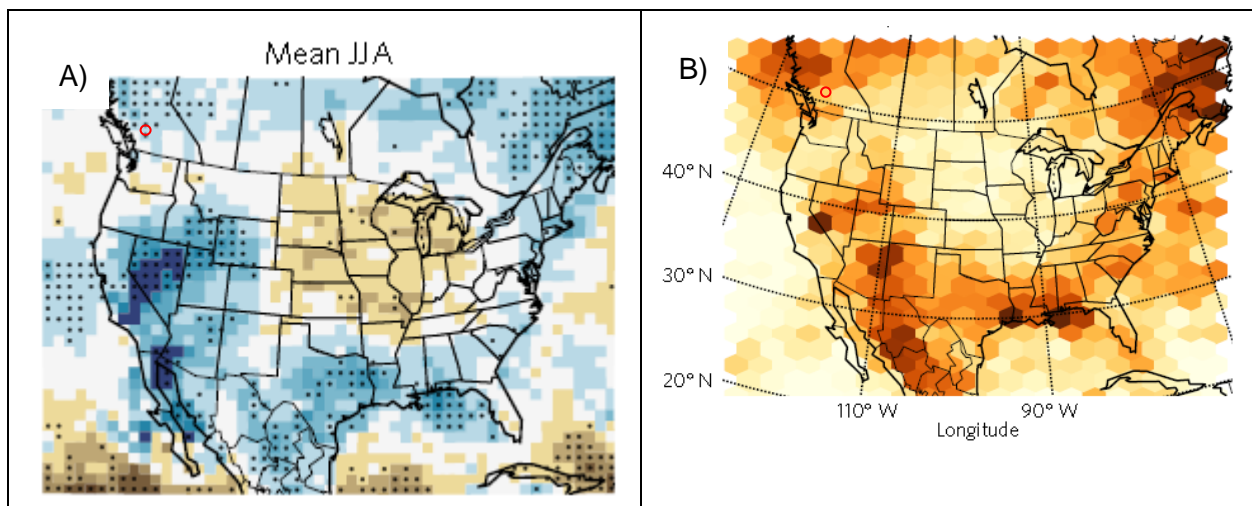


Figure 2-5. Projected changes in hourly extreme precipitation by the late 21st century assuming a high end (RCP 8.5) emission scenario. A) shows the projected changes in the magnitude of hourly extreme precipitation for June, July, August. The light blue colour applicable to the research site (see red circle) indicates an increase of up to 35%, B) shows the projected increase in the frequency of high intensity rainfall. The light brown colour indicates an approximate 3-fold increase in the frequency of extreme hourly rainfall.

Pemberton Valley receives significant precipitation between October and March. The temperature at the valley floor is below zero between November and February with frequent daily freeze-thaw conditions both of which can influence slope stability. Modeled temperature and precipitation increases would be accompanied by increases in the frequency and magnitude of meteorological events that could trigger landslides.

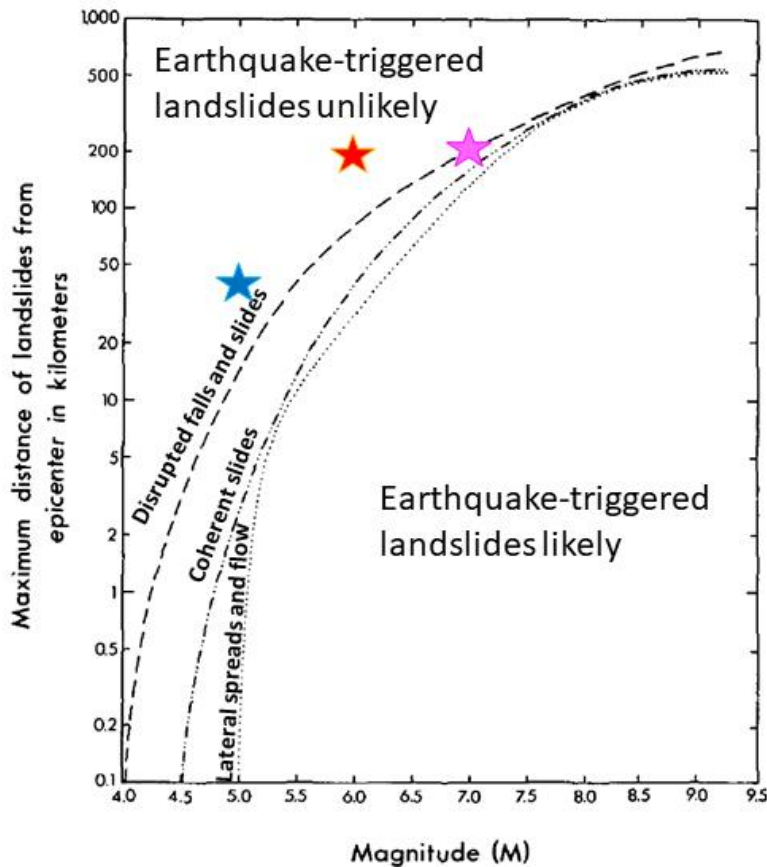
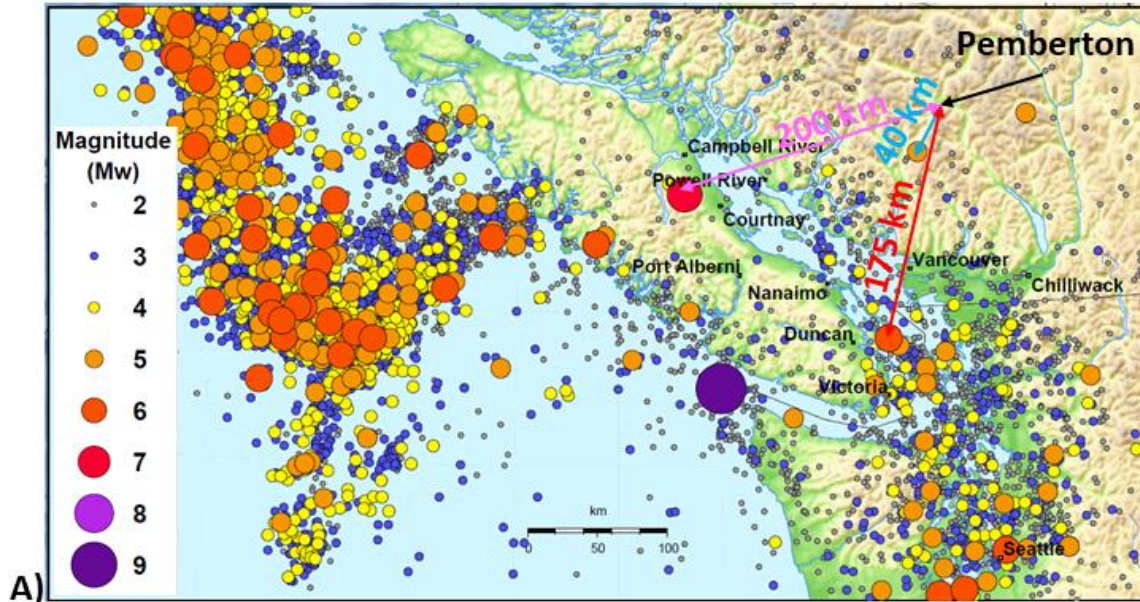
2.4. Seismicity

The regional seismicity is reviewed to estimate the potential for earthquakes to trigger landslides on the north face of Mount Currie. Using a worldwide database of earthquake-triggered landslides, Keefer (1984; 2002) suggest that earthquakes larger than moment magnitude (M) 6 can trigger rock avalanches, and those greater than M4 can trigger rock fall and rock slides. Drawing 02 shows the distribution of M4 and larger earthquakes recorded between 1700 and 2017 in southwestern British Columbia and northwestern Washington (Halchuk et al. 2015; NEDB, 2017). Nearby M6 and larger earthquakes have, to date, occurred almost exclusively on shallow-crustal faults on Vancouver Island and in western Washington; along the subducted Juan de Fuca plate deep beneath Salish Sea and Puget Sound; and along offshore plate-boundary faults west and north of Vancouver Island (Figure 2-6).

Keefer (1984) proposes relationships between earthquake magnitude and the likely maximum distance from epicenters at which landslides can be triggered (Figure 2-6B). Based on the seismic record and using Keefer's relationships, Figure 2-6 suggests that an earthquake could possibly trigger landslides on Mount Currie, but the likelihood is relatively low due to (1) the low frequency of recorded earthquakes with magnitude greater than M4 within the region of interest, and (2) the large distance to regions that more frequently generate M6 or larger earthquakes: Vancouver Island, northwestern Washington State, and along offshore plate-boundary faults west and north of Vancouver Island.

The empirical relationships by Keefer (1984) are useful for a preliminary estimate of the likelihood of landslide triggered by earthquakes at a specific location. However, other parameters, such as the degree of rock mass fracturing and damage (Keefer 1984), or progressive rock mass weakening through cyclic loading from numerous small earthquakes (e.g., numerical investigation by Gishig et al. 2016) can influence the sensitivity of rock slopes to seismicity.

In summary, earthquake-triggered landslides can occur in the study area but it is anticipated that they do so with a lower frequency than landslides from other triggers (e.g., climatic events for rock fall and debris flows). As such earthquakes are not considered to be the main driver of instability along Mount Currie.



B)
 Figure 2-6. A) Earthquakes in Natural Resource Canada database (Halchuk et al., 2015) for southwestern British Columbia. Estimated distance to the nearest M5 (blue), M6 (red), and M7 (magenta) earthquakes are shown. B) Empirical relationship of earthquake magnitude and distance at which landslides were seismically triggered and the magnitude of the earthquake (Keefer, 1984). The three nearest major earthquakes from A are shown using the same colours.

3.0 GEOHAZARD ANALYSIS

This section presents the methodology and results of the geohazard analysis for the north face of Mount Currie. The geohazards investigated were identified during the desktop analysis component of this project. Based on that work, the following geohazards were identified to be studied in more detail within the study area: rock avalanches; large rock falls / rock slides; landslide dams and associated floods; debris flows, debris slides and debris avalanches. Figure 3-1 provides a flow chart summarizing the geohazard identified for the north face of Mount Currie, the sequence of analyses conducted and the outcome of the geohazard assessment.

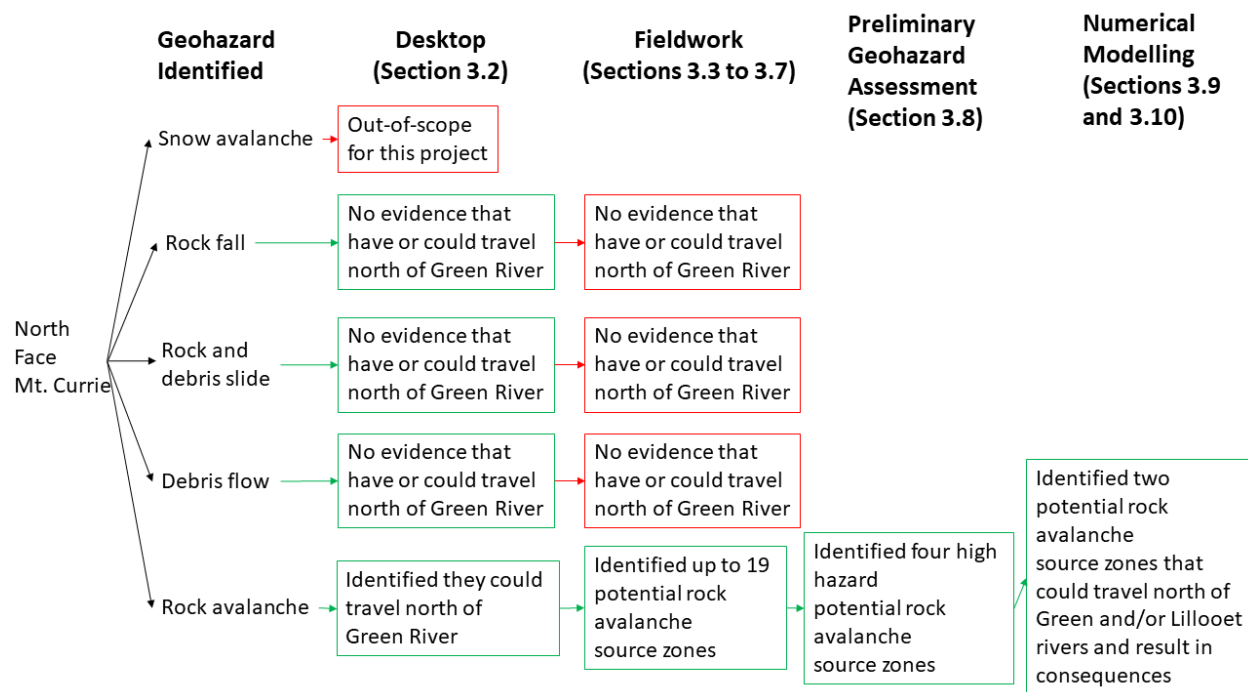


Figure 3-1. Summary diagram outlining which geohazard scenarios were identified and which were analyzed in each step of the geohazard analysis.

3.1. Definitions

A few definitions are introduced at this stage to clarify to the reader what the different processes and geomorphic features mean that are being discussed herein.

Deep-seated gravitational slope deformation (DSGSD), also called mountain slope deformation, sackung, or rock mass creep, are defined by Hungr et al. (2014) as: *Large-scale gravitational deformation of steep, high mountain slopes, manifested by scarps, benches, cracks, trenches and bulges, but lacking a fully defined rupture surface. Extremely slow or unmeasurable movement rates.* Over time, slow mountain slope deformations can either evolve into extremely rapid rock avalanches (Pedrazzini et al. 2013), or they can deform at a slow to very slow rate for millennia (Hippolyte et al. 2012).

Rock avalanche is defined by Hungr et al. (2014) as: *Extremely rapid (> 5 m/s), massive, flow-like motion of fragmented rock from a large rock slide or rock fall.* Only rock slope failures with a volume greater than 1,000,000 m³ were considered as rock avalanche in this project. This corresponds to a volume threshold commonly used in references for rock avalanches with high mobility (Hsu 1975; Glastonbury and Fell 2010). Where no volume information was available from the published literature for the rock slopes considered in this study, a scar area of 100,000 m² was used as a proxy (i.e., assuming a 10 m thick failure depth); or a debris area of 120,000 - 130,000 m² (i.e., assuming a 10 m depth and a bulking factor of 1.2 – 1.3; Brückl 2001).

Rock fall consists of the detachment, fall, rolling, and bouncing of rock fragments (Hungr et al., 2014). The process may occur singly or in clusters, but there is little dynamic interaction between the most mobile moving fragments, which interact mainly with the substrate.

Rock (and debris) slides involve sliding of a mass of rock (and debris) on a rupture surface. In strong rock, this failure surface is generally planar or stepped, defined at least partially by pre-existing rock mass discontinuities. In this study, rock falls and rock / debris¹ slides are differentiated from rock avalanches primarily based on their volume. Our inventory focused on large rock fall and rock / debris slide events with volumes ranging between approximately 50,000 m³ and 1,000,000 m³.

Debris flow consists of rapid to extremely rapid surging flow of saturated debris in a steep channel (Hungr et al., 2014). It can involve significant volumetric entrainment of material and water from the flow path. Debris material is expected to consist of a mixture of sand, gravel, cobbles, and boulders with varying proportion of silt and trace of clay (Hungr, 2005).

Lineaments refer to linear depressions in alpine environments. They are common features in high alpine environments of British Columbia that can be interpreted as symptoms of and precursors to large-scale slope failures. Linear depressions can be the expression of one of four processes:

- Preferential erosion along a geological or tectonic boundary.
- Erosion along a lateral glacial meltwater channel.
- Slope deformation associated with glacial debuitressing.
- Deep-seated gravitational slope deformation.

Frequency, hazard probability, and return period are used interchangeably in this report, depending on the context. Frequency is defined as the annual probability of occurrence of a hazard scenario. Return period is the inverse of frequency, and is defined as the average recurrence interval (in years) of a hazard scenario. For example, an annual frequency of 0.01 corresponds to a 100-year return period.

¹ The term 'debris' is here included with 'rock' to indicate that some shallow rock slides may involve surficial material such as weathered rock, granular material, and vegetation.

3.2. Desktop Analysis

Through the desktop analysis BGC reviewed the published literature (Section 1.3), geotechnical reports (Section 1.3.1), Google Earth and Bing imagery, available historical aerial photographs (Table 3-1), and LiDAR data relevant to the study area. The LiDAR data and orthophotos were collected on August 26, 2017 by McElhanney Consulting Services Ltd. (McElhanney) for this project. A regional rock avalanche regional inventory was also prepared as part of the desktop analysis (Appendix A) and discussed in more detail in Section 3.5.2.

Table 3-1. Historical aerial photographs used in this assessment.

| Photo ID | Date | Approx. Scale |
|----------------------------------|--------------------|------------------------|
| BC400:2-3 | August 1-2, 1947 | 1:30,000 |
| BC497:15-18 | June 29, 1948 | 1:30,000 |
| BC911:98-100 | 1948 | 1:50,000 |
| BCB5341:029-031/049-051 | 1969 | 1:50,000 |
| BCB81114:125-129/174-175 | 1981 | 1:25,000 |
| 30BCC94135:091-095 | August 13, 1994 | 1:25,000 |
| 30BCC94120:034-035 | August 1, 1994 | 1:15,000 |
| 16733-0 R352 | August 23, 1999 | 1:25,000 |
| BCC04052:003-004/023-028/110-114 | September 24, 2004 | 1:25,000 |
| Orthophotos | August 26, 2017 | 20 cm pixel resolution |

3.3. Fieldwork

Fieldwork was undertaken by BGC staff Drs. Matthias Jakob, P.Geo., Marc-André Brideau, P.Geo., and Matthieu Sturzenegger, P.Geo. on August 8 and 9, 2017 with a follow up field visit by Marc-André Brideau and Matthieu Sturzenegger on September 23, 2017. Ground traverses along the Mount Currie (Drawing 03) allowed for ground-truthing of the geomorphic mapping (Section 3.4), along with collecting rock mass description and discontinuity orientation measurements which provided input for the rock avalanche (Section 3.5), and rock fall and rock / debris avalanche characterization (Section 1). Air temperature profiles were collected in three tension cracks on a southeast facing slope to determine indicators for the presence of permafrost in the rock mass. The fans at the base of the north slope of Mount Currie were inspected during a ground traverse to provide input for the geohazard characterization of debris flow (Section 3.7). Select locations on the Green and Lillooet rivers floodplain were visually inspected for pre-historic rock avalanche debris deposit.

Digital photographs were collected during helicopter flights along Mount Currie to generate three-dimensional surface models using the photogrammetry structure-from-motion (SfM) methodology. These digital surface models were then used to measure the orientation of major discontinuities. Additional information on photogrammetry can be found in Appendix B. General

observations about the geomorphology, rock mass characteristics, and debris flow activity on the fans were recorded during three helicopter flights.

A geophysical investigation program comprised of one seismic refraction and one seismic reflection survey lines was conducted by Frontier Geoscience Inc. on a debris flow fan and along the section of the Green River Forest Service Road that runs between the two parts of the Big Sky Golf Club Resort (Drawing 03). The geophysical investigation aimed to search for the presence of a buried rock avalanche deposit beneath the fluvial sediments of the Green and Lillooet rivers. Details of the geophysical methodology and results can be found in Appendix C.

A series of photographs providing highlights of key features observed during the fieldwork is provided after the main text of the report. The photographs are numbered in the order in which they are first referred to in the report and their location is provided on Drawing 03.

3.4. Geomorphic Mapping

The objectives of geomorphic mapping were to identify and characterize terrain and geohazards including geohazard locations, extents, and factors contributing to slope instability. These interpretations support the geohazard frequency and magnitude analyses described in Sections 3.5.1 to 3.5.6.

Geomorphic features were mapped based on a combination of airborne LiDAR, historical aerial photographs (Table 3-1), Google Earth imagery, and complemented with helicopter- and field-based observations made in August and September 2017.

The geomorphic mapping involved the following tasks:

- Mapping of geomorphic and past landslide features on the north face of Mount Currie to identify the predominant geohazard types (Drawing 04)
- Mapping typical failure or deformation features, such as landslide scars, tension cracks, lineaments, and counter-slope scarps, in order to identify possible rock avalanche source zones on the north face of Mount Currie (Drawings 04 and 05)
- Inventory and frequency estimates of large rock fall, rock slide, and debris slide events on the north face of Mount Currie
- Inventory and frequency estimates of debris flows on the north face of the Mount Currie.

Definitions for each of these processes is provided in Section 3.1. Snow avalanche potential along rock fall and debris flow paths was noted, but not quantified as it is outside the current scope.

3.4.1. Lineaments

One set of lineaments trends approximately SW-NE and dips steeply to the northwest (consistent with the orientation of discontinuity set D2 in Table 1-2 and Section 3.5.4). This first lineament trend includes the main tension cracks along Mount Currie Ridge. A second set of lineaments trends SE-NW to SSE-NNW (consistent with the orientation of foliation S1/D1 in Table 1-2 and Section 3.5.4). This second lineament trend corresponds to numerous scars and may be associated with tension cracks on the west side of Mount Currie. A third set of lineaments

(consistent with orientation of D5 in Section 3.5.4) was observed during fieldwork which corresponds to orientation of gullies and persistent traces on the steep rock slope of the north face of Mount Currie. D5 was also mapped on the southeastern slopes of the mountain, just downslope of the ridgeline (Photograph 2).

3.4.2. Deep-Seated Gravitational Slope Deformation

Features associated with DSGSD, such as uphill facing scarps, ridge top trenches and grabens, or scarps with talus were identified at numerous locations within the assessment area. DSGSDs represent potential rock avalanche source zones, such as Source ID 1, 2, 3, 4, 13 and 15 within the assessment area (Table 3-2 and Drawing 05).

DSGSD ID 1 is delimited by wide tension cracks and lineaments along the ridgeline and appears to be controlled by sub-vertical foliation planes on the northeast side of Currie NE2 (Drawings 04 and 05; Photographs 3, 4 and 5). The observed failure mechanism is toppling along foliation planes tilted by approximately 30° (Photograph 6; see Section 3.5.4 and Appendix D for additional discussion of failure mechanisms). The depth of rock mass disturbed by this mechanism may be up to approximately 100 m, as shown in Photographs 7 to 10 by the hinge where foliation planes change from undisturbed to tilted. A wide scar in the middle of DSGSD ID 1 (Photograph 8) may correspond to the detachment zone of a previous landslide. This feature separates the DSGSD into two parts (ID 1a and ID 1b). Photograph 11 shows that significant displacement, in the order of 20 m (as described in Bovis and Evans 1995), has occurred on the upper section of ID 1b.

DSGSD ID 2 has an elongated outline along the eastern section of Mount Currie. It is delimited by a series of tension cracks on the southeast side of the ridge (Drawing 04, and Photographs 12 and 13) and is subject to frequent rock falls on the northwest side (Photographs 14 and 15). This DSGSD has been subdivided into three parts (ID 2a, ID 2b and ID 2c) based on morphological features (Drawing 05). Photographs 16 and 17 shows lineaments and talus slopes oblique to the ridge orientation, suggesting that a displacement component is to the northeast.

DSGSD ID 3 is characterized by a main upper cliff, and a series of smaller escarpment separated by talus zones (Drawing 05 and Photograph 18). The blocks in the talus appear weathered on surface and/or covered with lichen, suggesting that deformation is currently not active (or is deforming at a slow rate).

DSGSD ID 4 is defined at the top by tension cracks in a forested area (Drawing 05 and Photograph 19). The southeast section of this DSGSD corresponds the detachment zone of a past landslide event (Photographs 20 and 21). Unstable and disturbed rock masses suggest that that further rock slope instabilities are possible (Source ID 16 on Drawing 05).

DSGSD ID 13 is characterized by a dilated rock mass (Photograph 22), tension cracks (Photograph 23), and a frontal cliff (Drawing 05 and Photograph 24). Rock debris in both the talus at the base of the cliff, and within tension cracks appear weathered on surface and/or covered with lichen (Photographs 23 and 24), suggesting that deformation is currently not active (or is deforming at a slow rate).

DSGSD ID 15 is located between Watersheds B and C and is bounded by tension cracks (Drawing 05). DSGSD ID 19 is characterized by an upper and lateral depression potentially defining upper and lateral scars (Drawing 05).

3.4.3. Rock Fall and Rock / Debris Slides

Rock falls are widespread on Mount Currie and often form talus slope with limited runout distance at the base of rock slopes (measured shadow angle² ranging between 27° and 37°, consistent with literature, e.g., Evans and Hungr 1993; Jaboyedoff and Labiouse 2011). A broad colluvium cone on the east side of Mount Currie's north face is characterized by a slope angle of 30° to 35° and appears to be an active fragmental rock fall and small rock / debris slide zone (Drawing 01; Drawing 04; Photographs 25 to 27).

A rock fall event was mapped on Currie NE3, where a fresh scar and runout paths are visible (Photographs 28). This failure may have triggered failure of a disturbed mass of rock already subject by flexural toppling (Photograph 29). Tension cracks near the ridge (Photograph 30) suggest that this location may be the source of further instability (Source ID 7). Similarly, tension cracks on the ridge to the west, appear to be defining another instability (Source ID 12 in Table 3-2, on Drawing 05 and on Photograph 31).

Two recorded clusters of rock fall events occurred in 2015 (Currie NW1, Photograph 32, Source ID 10) and 2016 (below Currie N1, Photograph 33 to 35, Source ID 11). Both clusters were described by Fournier (2016). The failure mechanism of the 2016 events appears to involve wedge sliding along discontinuity sets S1 (foliation) and D5 (see Section 3.5.4 and Appendix D). A scar can be observed at the top of the instability (Photographs 33 to 35). Kinematic analyses and almost constant rock fall activity in the gullies below this location suggest that this area is a potential source of further instability (ID 11 in Table 3-2 and on Drawing 05).

Rock slides have been observed at several locations on Mount Currie. Large landslide scars delineated on Drawing 04 are evidence of past rock slide events. A common failure mechanism observed over the assessment area is toppling along foliation planes. This mechanism seems to tilt columnar blocks of bedrock generating a disturbed and dilated mass along a well-defined surface (e.g., Photographs 6, 8, 36, 37). The disturbed mass may remain in place or slide along this surface.

The debris of another sizable rock slide event was observed below Currie NE2 (Photographs 38 and 39). The debris sits on a bench at the top of steep rock slopes and gullies. This position is considered potentially unstable and part of the debris may be re-mobilized and fail (Source ID 6).

Well-defined, persistent structures defining potentially unstable zones were observed at other locations (e.g., Photographs 40 and 41). These locations include Source ID 14, 17 and 18 (Table 3-2 and on Drawing 05).

² The shadow angle is here defined as the angle between the horizontal and a line linking the base of a rock slope and farthest extent of the generated rock fall debris.

Three active rock / debris slides (Source ID 5, 8 and 9 in Table 3-2 and on Drawing 05) were observed in the assessment area. They appear to generate frequent but relatively small volumes of material, however historical aerial photographs show that ID 5 generated a significant event, which ran out for approximately 1 km in Mount Currie easternmost gully. Part of the scar of this event seems to be progressively re-vegetating (Photograph 42).

3.4.4. Debris Flows

Four main debris flow paths (along watersheds A, B, C and D on Drawing 04) were identified on the north face of Mount Currie. Deeply incised flow paths (Photographs 43 and 44) and fans (Drawing 01 and Photographs 45 to 48) are the main landforms associated with these processes. Active rock falls and rock / debris slides on the upper sections of the north face of Mount Currie provide the debris supply to the channels which can be subsequently remobilized as debris flows.

Debris flow activity in the watershed that experienced the recent rock falls has increase as a response of the much higher sediment recruitment in the upper watershed. Now the debris flow deposits are extending well beyond its former limit into the Green River floodplain (Photographs 45 to 48).

3.4.5. Limitations and Uncertainties

The main limitations associated with the geomorphic mapping relate to the spatial resolution and temporal coverage of the imagery used. The spatial resolution of the aerial photographs is on the order of a few metres while the pixel size of the 2017 orthophotograph and LiDAR is 0.1 m and 0.5 m respectively. This means that the 2017 data can resolve smaller features than the historical one which could introduce a bias in subsequent analyses. The temporal coverage available in the photographs ranges from 1947 to 2017. This means that only big geomorphic events that leave a persistent trace in the landscape (Guthrie and Evans, 2007) can be recognized and documented. Only one LiDAR dataset was available for this project which means that a change detection analysis (where one digital elevation model generated from LiDAR is subtracted from another to characterize zones of movement) was not possible. This means that slow slope movements that initiated recently and do not yet have a well-expressed surface expression could have been missed.

Table 3-2. Potential rock avalanche sources on the north face of Mount Currie.

| Source ID | Activity | Kinematic* | Estimated Potential Unstable Volume (m ³) | Qualitative Rating* |
|-----------|---|---|---|---------------------|
| 1 | Deep-seated gravitational slope deformation delimited by well-defined tension cracks; displacement was measured along the cracks by Bovis and Evans (1995); numerous fresh scar on the sides of disturbed mass indicate frequent rock fall activity | Ongoing toppling along S1 with long tension crack developing along D2 | 5,000,000 | High |
| 2 | Deep-seated gravitational slope deformation delimited by well-defined tension cracks and lineaments; numerous fresh scars on the sides of the disturbed mass indicate frequent rock fall activity | Ongoing toppling along S1 with long tension crack developing along D2 | 12,000,000 | High |
| 3 | Deep-seated gravitational slope deformation delimited by a well-defined upper scar; escarpments and talus are present in the disturbed mass; no evidence of recent activity; rock debris are partially vegetated in the talus | Likely mechanism is toppling along S1 | 8,000,000 | Moderate |
| 4 | Deep-seated gravitational slope deformation delimited by a back scar; location of a past rock avalanche (see ID 16); tension cracks developing in the disturbed mass | Possible mechanism is wedge sliding along S1-D7 | 1,800,000 | High |
| 5 | Potential retrogression behind a recent rock and debris slide; location of a recent event, which occurred between 1948 and 1969; no sign of recent activity except for surficial raveling; scar seems to be progressively re-vegetating | Possible mechanisms include wedge sliding (S1-D7) and toppling (S1) | 1,300,000 | Moderate |
| 6 | Debris sitting on a bench above steep gullies and rock slopes; rock fall activity inferred | n/a | 90,000 | Low |
| 7 | Rock mass dilation and open fractures; location of a recent rock fall event | Possible mechanism is wedge sliding (S1-D7) | 10,000 | Low |
| 8 | Potential retrogression behind an active source of raveling material; no sign of developing cracks; ongoing raveling | Possible mechanisms include wedge sliding (S1-D7) and toppling (S1) | 700,000 | Moderate |
| 9 | Potential retrogression behind an active source of raveling material; no sign of developing cracks; ongoing raveling | Likely mechanism is toppling along S1 | 60,000 | Low |

| Source ID | Activity | Kinematic* | Estimated Potential Unstable Volume (m ³) | Qualitative Rating ⁺ |
|-----------|--|---|---|---------------------------------|
| 10 | Location of June 2015 rock fall event (Fournier 2016) | Possible mechanisms include planar sliding (D4) and wedge sliding (D2-D4) | 50,000 | Low |
| 11 | Location of two recent rock fall / slide events in September 2016 (Fournier 2016); constant fragmental rock fall activity in the gully below the rock fall failure observed during August 8, 2017 field work | Possible mechanism is wedge sliding (S1-D4) | 680,000 | High |
| 12 | Potential instability defined by a tension crack at the back | Possible mechanism is planar sliding along D4 | 10,000 | Low |
| 13 | Deep-seated gravitational slope deformation delimited by well-defined tension cracks; significant dilation occurred; blocks on talus and within the cracks are covered with vegetation and lichen | Likely mechanism is toppling along S1 | 13,300,000 | Moderate |
| 14 | Potential instability defined by two persistent lineaments | Possible mechanism is wedge sliding (D2-D5) | 500,000 | Low |
| 15 | Deep-seated gravitational slope deformation characterized by a network of tension cracks in the middle | Likely mechanism is toppling along S1 | 800,000 | Low |
| 16 | Location of a previous rock slide event; highly disturbed mass with relatively fresh-looking blocks | Ongoing flexural toppling | 600,000 | Moderate |
| 17 | Potential instability partially defined by persistent structures | Possible mechanism is wedge sliding (S1-D4) | 100,000 | Low |
| 18 | Potential instability partially defined by persistent structures | Possible mechanism is wedge sliding (S1-D4) | 200,000 | Low |
| 19 | Potentially developing deep-seated gravitational slope deformation | Likely mechanism is toppling along S1 | 2,900,000 | Moderate |

Notes:

* See Section 3.5.4 and Appendix D

+ Takes into consideration the size of the potential source, its activity, and the results of kinematic analyses

3.5. Rock Avalanche Geohazard Analysis

Of the 19 potential rock avalanche sources identified in the desktop study (Table 3-2), only potential sources 1, 2, 4, 6, 11, 14, 16, 17, 18 were carried forward in the rock avalanche geohazard analysis. The other potential sources were either likely to runout in a direction that they would not represent a hazard to the infrastructure considered in this project (potential source 3 and 10), they were located at a lower elevation on Mount Currie that they were unlikely to reach the infrastructure considered in this project (potential source 5, 8, 9, 15, 19), or their estimated potentially unstable volume were too small to develop in rock avalanches (potential source 7 and 12).

3.5.1. Frequency Estimation Method

Rock avalanches usually occur only once at a given location (or in the rare cases where they occur more than once, the time between events can range from hours to thousands of years). It is therefore not possible to calculate a probability of occurrence for a specific slope based on repeated events, such as commonly done for debris flows or rock falls. Instead, a combination of a regional rock avalanche inventory, a comparative assessment of specific slope attributes, an understanding of the historical performance of the Mount Currie slopes, and professional judgment have been used to assign a likely range of probabilities of rock avalanche occurrence.

Based on a regional scale rock avalanches inventory (see Section 3.5.2), a regional spatial average can be calculated by dividing the number of rock avalanches by the area of investigation. Given the assumption that all the catalogued rock avalanches occurred during the past 10,000 years (i.e., following deglaciation), one can then determine the annual regional average (the frequency) by dividing the spatial density average by 10,000 years. This regional frequency density can then be adjusted for the area of the slope of interest using site specific desktop and field observations to estimate a range of rock avalanche frequency specific to the area of interest. Site specific observations may include evidence for recent activity (see Section 3.4), and structural and kinematic considerations (see Section 3.5.4).

3.5.2. Regional Rock Avalanche Inventory

A regional inventory of rock avalanches and DSGSD was compiled using previously published work (Clague and Souther 1982; Evans and Brooks 1991 and 1992; Cruden and Lu 1992; Bauman and Yonin 1994; Holm et al., 2004; Blais-Stevens, 2008; Blais-Stevens et al. 2011; Hensold 2011) and by reviewing the available Google Earth imagery, aerial photographs and LiDAR data. The inventory area was centered on the Mount Currie and extended 70 km to the east and west and 70 km to the north and south (Drawing 02). The inventory for this project only included landslides that occurred since the last glaciation (~10,000 years ago), as pre-glacial or glacial rock avalanches are obscured or no longer identifiable due to glacial erosion.

Thirty-one rock avalanches were identified within a 4,900 km² area (Drawing 02) using the criteria defined in Section 3.1. A list of the rock avalanches identified, including their location and size

estimates, is provided in Appendix A. BGC believes that this inventory captures the majority of past rock avalanches since the last glaciation, because rock avalanches with volumes greater than 1,000,000 m³ leave a detectable legacy on the landscape (Guthrie and Evans, 2007). This is also consistent with previous inventories undertaken by BGC in southwestern British Columbia.

The DSGSDs were not included in the frequency estimation, because they have not failed catastrophically. However, they are included in Drawing 02 and in Appendix A for completeness, and because this type of gravitational processes could, as explained in Section 3.1, result in catastrophic failure in some cases.

3.5.3. Seismic Survey

Based on the review of the LiDAR-based terrain model and initial ground inspection at selected sites in the valley, there is no surface evidence suggesting that past landslide events ran out further than Green River. However, it is possible that longer runout events were subsequently buried by floodplain aggradation and are thus no longer visible. Water well logs (see Section 2.1) located in Pemberton Golf Course, along Highway 99 and near the airport do not describe or identify obvious landslide-related sediments. However, these logs are not detailed nor are they typically created by qualified geoscientists trained to identify landslide deposits. Therefore, the well logs could not be relied on to confirm the absence of buried landslide deposits. For this reason, a seismic survey was completed along one of the debris flow fan at the base of the north face of Mount Currie. The goal was to provide additional subsurface information about possible rock avalanche debris overlain by floodplain deposits. Seismic survey results and details about the methodology used are provided in Appendix C.

Results along Seismic Line 1 (SL-1 in Drawing 03) indicate the presence of a layer up to 25-metre thick of poorly compacted earth material, underlain by a layer up to 116-metre thick of material with a higher degree of compaction. Within the more compacted layer, two zones with higher P-wave velocity (2,250 – 2,260 m/s) may correspond to coarser material such as cobbles and boulders within the sediments. These high wave velocity zones could be indicative of rock avalanche debris. The more compacted layer overlies bedrock and terminates within the current colluvial fan (Drawing 03). As such it is considered likely that these high P-wave velocity zones correspond to the coarse fraction of large old debris flow or a rock slide deposit but due to the limited runout distance are unlikely to be associated with a large rock avalanche.

Results along Seismic Line 2 (SL-2 in Drawing 03) highlight four major reflectors. The lowest one, at depth ranging between approximately 0 and 50 m asl is interpreted to correspond to the top of bedrock. The second reflector is subhorizontal at approximately 80 m asl and is interpreted to correspond to lacustrine silts and clay. The two upper reflectors are at depth of approx. 140 m asl and 190 m asl to the south and are both dipping to the north of the profile. The nature of the sediments below these reflectors could not be interpreted with confidence. The material above the upper reflector is shown to correspond to low compaction, fine-grained material, based on material logged on water wells W-73896 and W-78542 (Drawing 03).

These results are consistent with water well logs and field observations in the floodplain of both Green River and Lillooet River (Drawing 03). Water well logs report fluvial dominated depositional environment potentially overlying glacio-fluvial or glacio-lacustrine sediments (see Section 2.1). Field observations indicate surface material consisting of fine-grained fluvial sediments (Photographs 49 and 50) and no evidence of past rock avalanche events, such as unsorted coarse debris and large boulders.

In summary, the geophysical investigations do not allow the conclusion that a large rock avalanche is buried beneath flood plain deposits. This implies that the rock avalanche runout models (Section 3.9) will have to be calibrated from events nearby, but not on a known rock avalanche at the base of Mount Currie. The results also indicate that rock avalanching on the north face of Mount Currie is infrequent.

3.5.4. Rock Mass Characterization and Kinematic Analysis

BGC characterized rock mass at 11 stations on Mount Currie (Drawing 03). At each station, rock mass characteristics were described as per ISRM (1978 and 1981) and using the Geological Strength Index (GSI) (Marinos et al. 2005, 2007). Discontinuity orientation measurements were undertaken at each station using a compass and was complemented by helicopter-based photogrammetry. Photogrammetry allowed the quantitation of discontinuities geometrical parameters (orientation, persistence) on 3D models generated from digital photographs which augmented the discontinuity orientation dataset collected using a compass. This technique has the advantage of allowing safe measurements on the steep and inaccessible rock slopes of the north face of Mount Currie (Appendix B).

Discontinuity measurements suggest that two main structural domains³ can be defined on Mount Currie. The principal difference between the domains is the inclination of foliation planes (S1), which are subvertical to steeply dipping to the southwest in the Northeast Domain, whereas they are steeply dipping to the northeast in the Southwest Domain (Figure 3-2 and Figure 3-3). This structural difference may have important implication for the potential failure mechanisms of the mountain, flexural toppling being predominant in the Northeast Domain.

Bedrock consists of diorite or quartz diorite intrusive rock, as described in Section 2.2. Intact rock strength was estimated to be between R4 (requires more than one blow from rock hammer to be fractured) and R5 (requires many blows from rock hammer to be fractured), and weathering was observed along the major discontinuities (W 1.5 – 2). The rock mass has a foliated or gneissic fabric and its GSI ranges between 40 and 60 in the Southwest Domain, and between 35 and 55 in the Northeast Domain (Figure 3-2 and Figure 3-3). The GSI range, strong strength and minor weathering suggest that discontinuity set orientation probably provide the major control on stability.

Six discontinuity sets were defined in the Southwest Domain, and five in the Northeast Domain (Figure 3-4, Table 3-3 and Table 3-4). The main set consists of pervasive foliation planes (S1).

³ Structural domains refer to zones with similar number and orientation of discontinuity sets.

Other important ones include steeply dipping discontinuities (D2), approximately perpendicular to the foliation, a set of subhorizontal discontinuities (D6) and a set of discontinuities dipping moderately to the east (D5). Discontinuity sets D3, D4, and D7 are less abundant, but may have important kinematic implications, as they have the potential to be adversely oriented (i.e., lead to failure see kinematic analysis below).

The discontinuity sets allowed a kinematic analysis. Kinematic analyses study the geometric relationship between rock mass discontinuities and rock slope orientation to assess feasible failure mechanisms. Details of the analyses are summarized in Appendix D and show that, due to the complexity of the morphology on the north face of Mount Currie, several failure mechanisms are feasible, explaining past failure events and defining potential further instabilities (see Table 3-2).

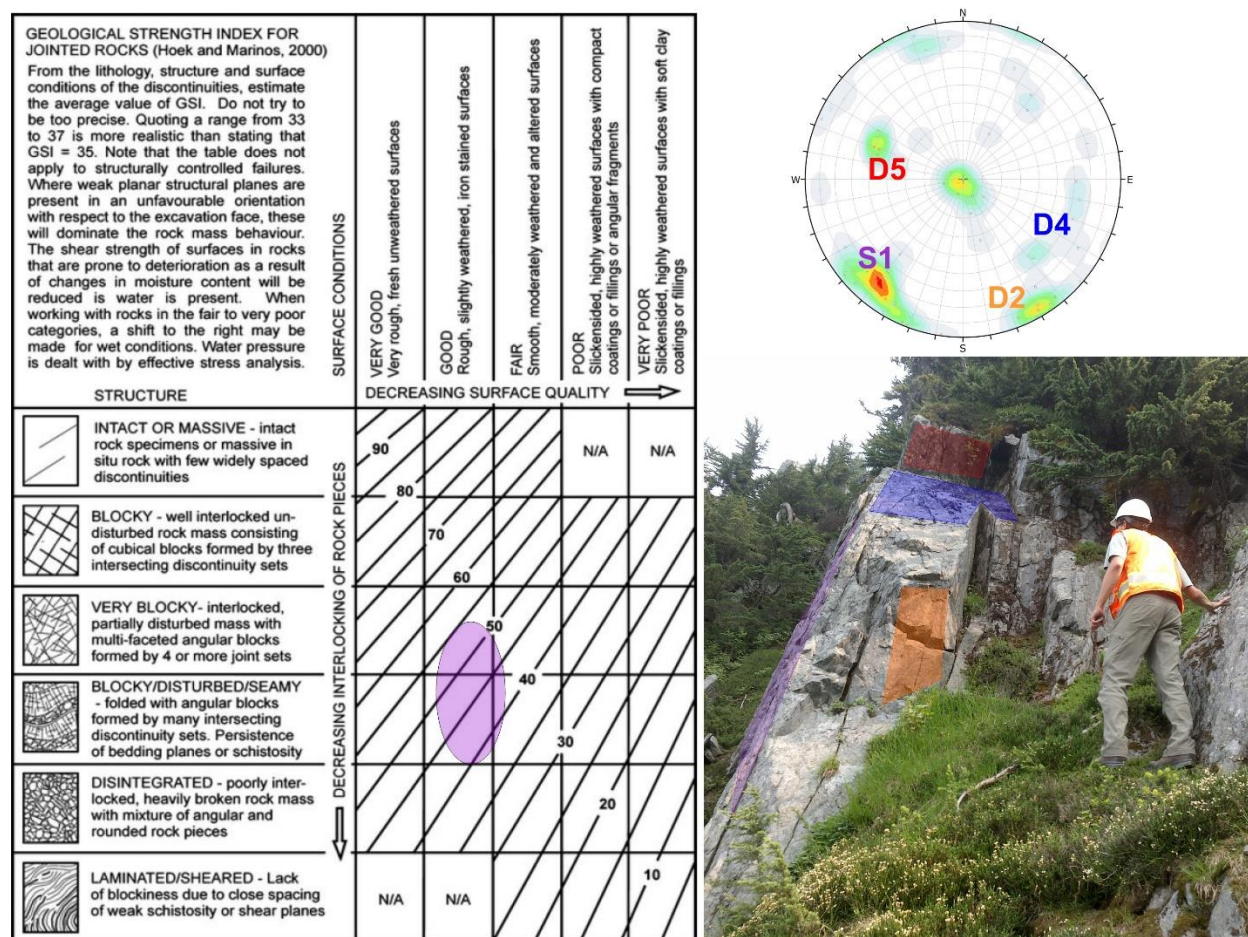


Figure 3-2. Geological Strength Index (GSI) and main discontinuity sets of the Southwest Domain.

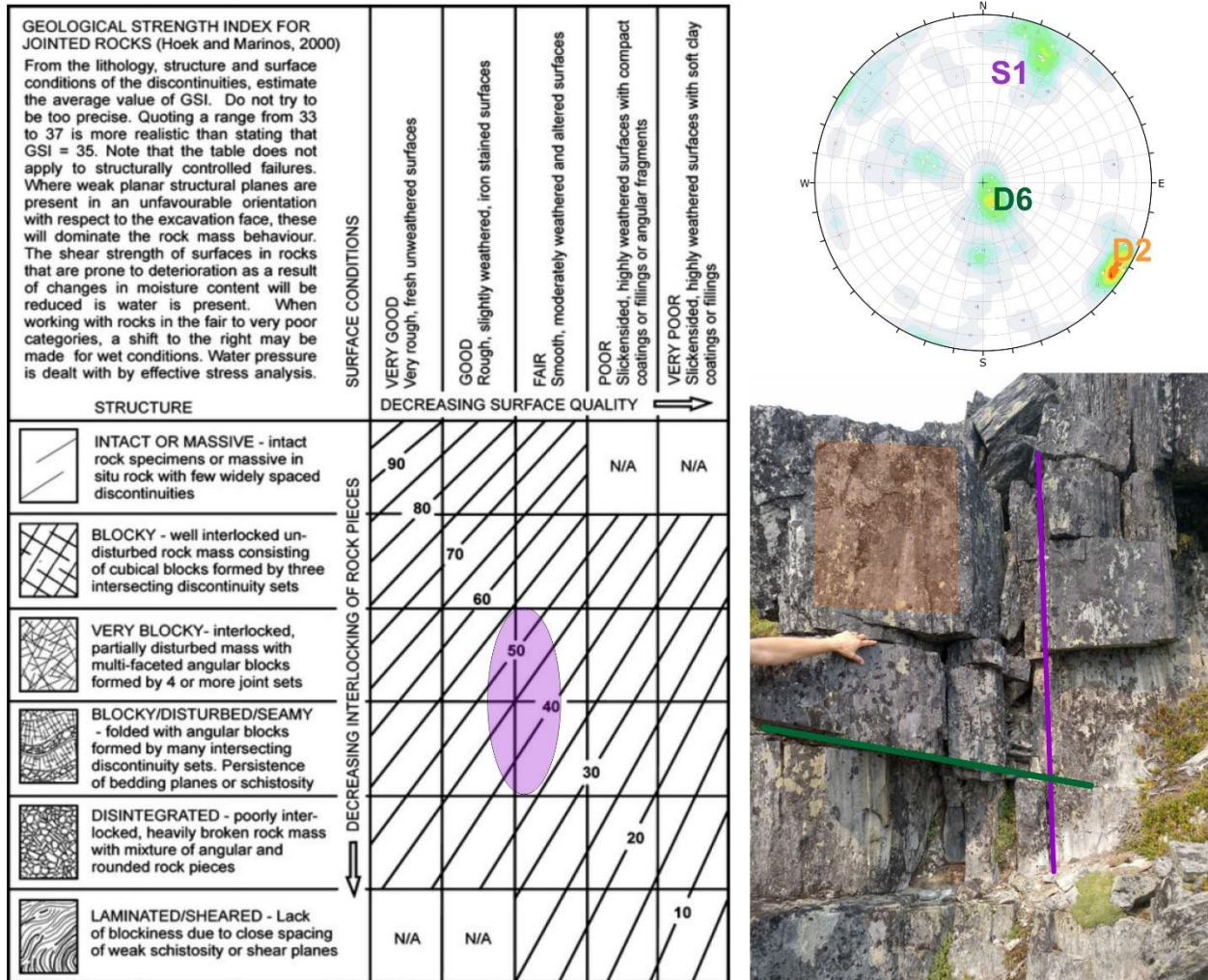


Figure 3-3. Geological Strength Index (GSI) and main discontinuity sets of the Northeast Domain.

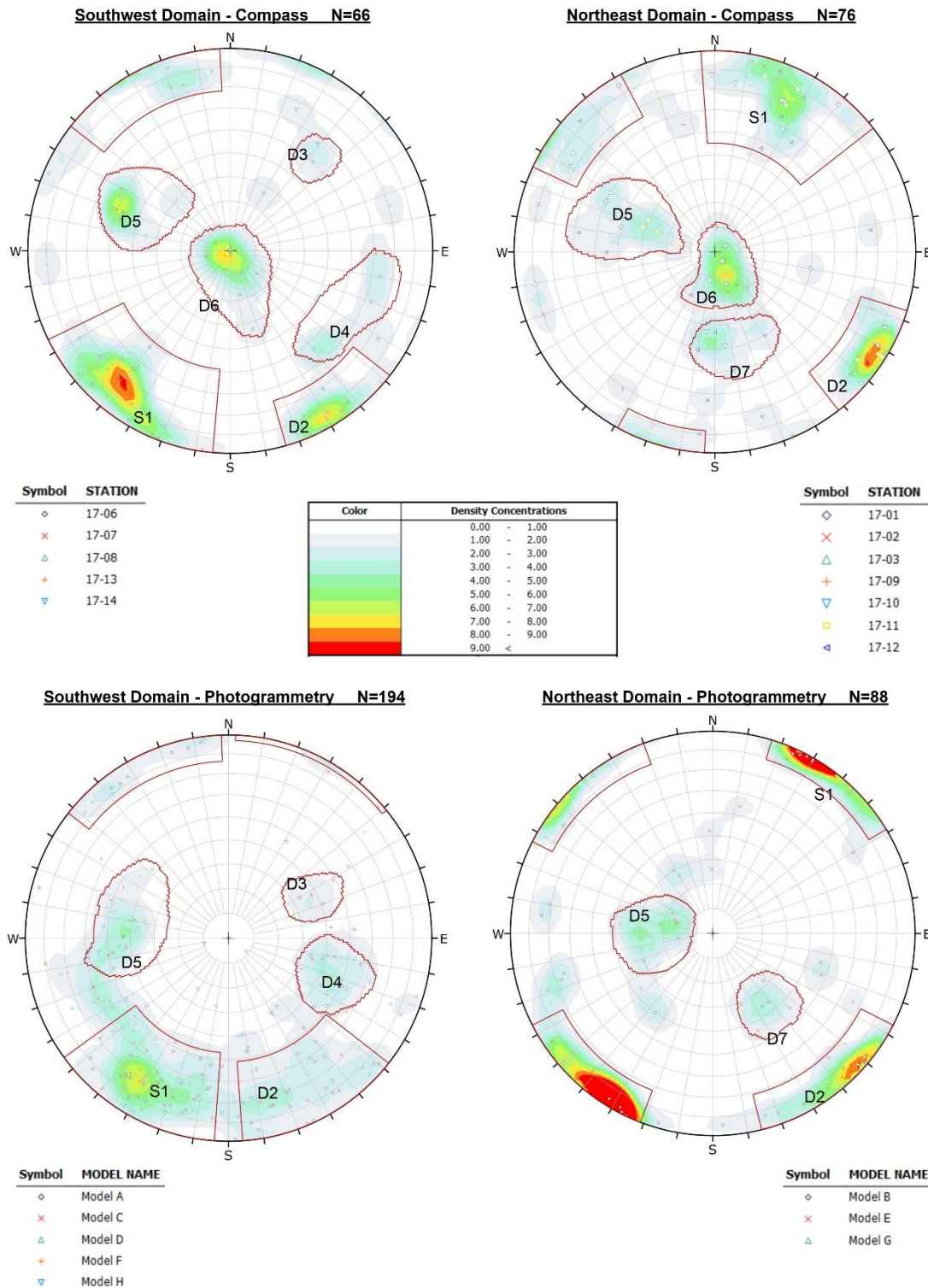


Figure 3-4. Stereonets of the two structural domains for both compass and photogrammetry measurements. The stereonet shows lower hemisphere equal area projections, and the contours symbolize the percentage of total pole measurements per 1% area. The symbols refer to the field station and model name for compass and photogrammetry measurements, respectively.

Table 3-3. Discontinuity characteristics for the southwest structural domain.

| Set | Dip ¹ (°) | Dip Direction ¹ (°) | Fisher's K ¹ | Persistence ² (m) | Spacing ² (m) | Roughness ² |
|-----|-------------------------|-----------------------------------|-------------------------|---------------------------------|-----------------------------|------------------------|
| S1 | 71 | 31 | 24 | 0.3 – 10.0+ | 0.1 – 2.0 | Planar - Rough |
| D2 | 78 | 331 | 17 | 0.3 – 5.0 | 0.2 – 1.2 | Undulating - Rough |
| D3 | 41 | 237 | 41 | 1 – 1.2 | 1.0 - 1.3 | Planar - Smooth |
| D4 | 48 | 288 | 45 | 0.2 – 5.0 | 0.1 – 1.0 | Undulating - Rough |
| D5 | 45 | 100 | 39 | 0.2 – 3.0 | 0.1 – 4.0 | Planar - Smooth |
| D6 | 8 | 353 | 44 | 0.2 – 2.0 | 0.2 – 2.0 | Undulating - Rough |

Notes:

1. Average of compass and photogrammetry measurements
2. Based on field characterization

Table 3-4. Discontinuity characteristics for the northeast structural domain.

| Set | Dip ¹ (°) | Dip Direction ¹ (°) | Fisher's K ¹ | Persistence ² (m) | Spacing ² (m) | Roughness ² |
|-----|-------------------------|-----------------------------------|-------------------------|---------------------------------|-----------------------------|------------------------|
| S1 | 87 | 212 | 22 | 0.5 – 10.0+ | 0.2 – 1.0 | Undulating - Rough |
| D2 | 87 | 312 | 27 | 0.5 – 3.0 | 0.2 – 1.5 | Planar - Smooth |
| D5 | 30 | 101 | 30 | 0.5 – 10.0 | 0.2 – 1.5 | Undulating - Smooth |
| D6 | 12 | 327 | 31 | 0.5 – 10.0 | 0.2 – 1.0 | Planar - Smooth |
| D7 | 37 | 344 | 47 | 0.3 – 2.0 | 0.3 – 0.5 | Planar - Rough |

Notes:

1. Average of compass and photogrammetry measurements
2. Based on field characterization

3.5.5. Temperature Profiles

Temperature profiles were collected in three tension cracks on the south side of the Mount Currie ridge. The fractures were all located on the upper southeast face of the mountain (Drawing 03 and Photograph 51). Figure 3-5 shows the temperatures measured in the tension cracks on August 8, 2017. Considering the uncertainties and limitation of using thermistor strings in existing tension cracks (see Section 3.5.8), the results suggest that the presence of warm permafrost (~0°C) is possible between 6 and 8 m depth. The observation that temperatures recorded at 6 m, 7 m and 8 m depth are identical between tension cracks supports the hypothesis that the bedrock is at 0°C (zero curtain effect). In addition, subsurface temperatures are most likely colder on the north face due to topography effects (Noetzli and Gruber 2009). Consequently, there is a high probability that warm permafrost is present on the north face of Mount Currie. Permafrost is ground defined as being below zero degree Celsius for at least 2 consecutive years. Figure 3-6 shows the postulated permafrost distribution in section and oblique view. This is consistent with

the presence of a rock glacier north of Currie W1 Summit (Drawing 01). With increasing and projected warming discussed in Section 2.3.1, the active layer (the seasonally unfrozen layer) will thicken and ice in joints melt. This could progressively lower the strength along surfaces of individual clasts but also larger rock masses. Once sufficient ice has disappeared from critical joint sets, a larger rock avalanche could detach. Thus, we postulate that rock avalanche hazard may increase over time.

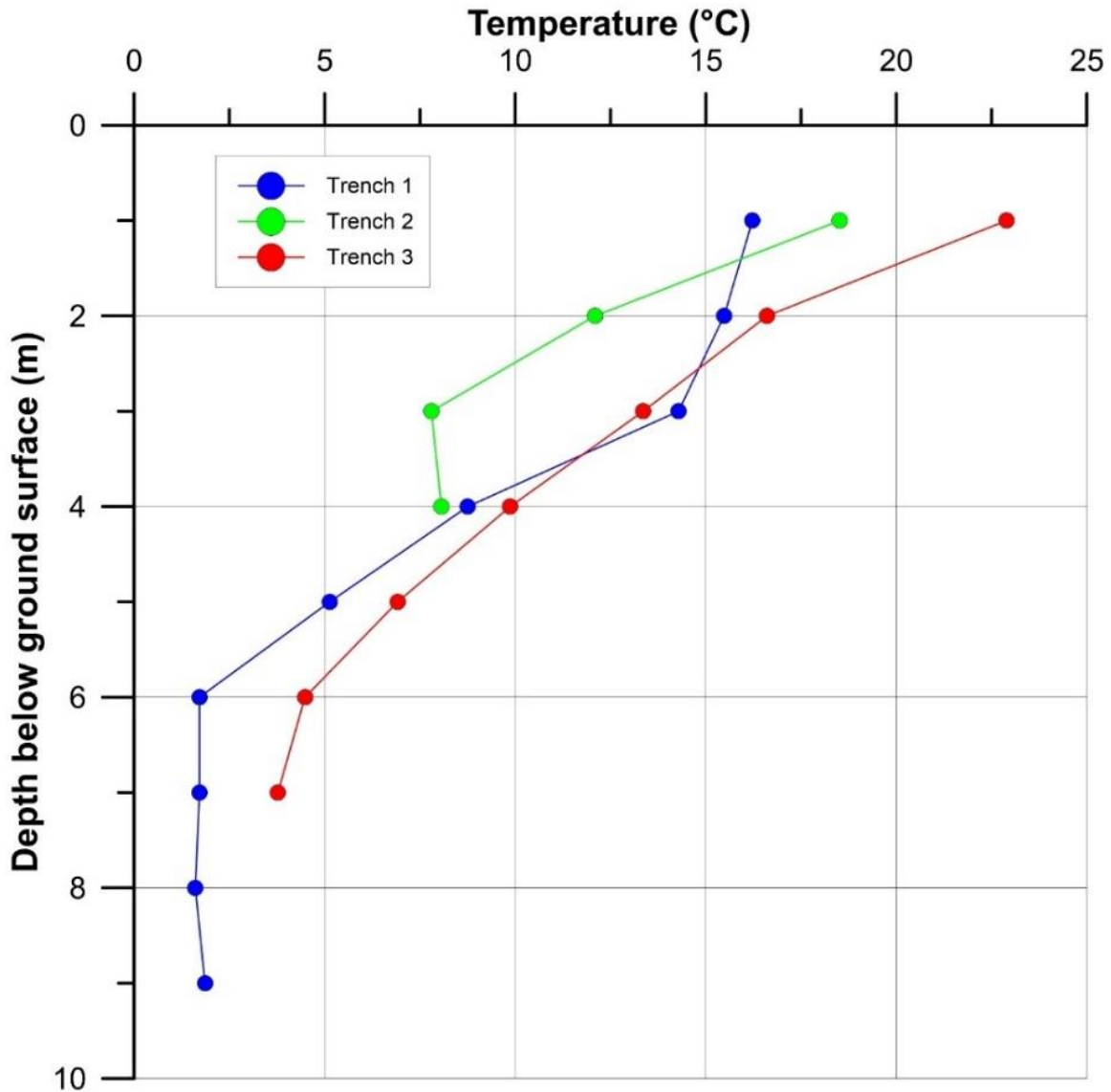


Figure 3-5. Temperature profiles obtained from thermistor string lowered in trenches. See Drawing 03 for location.

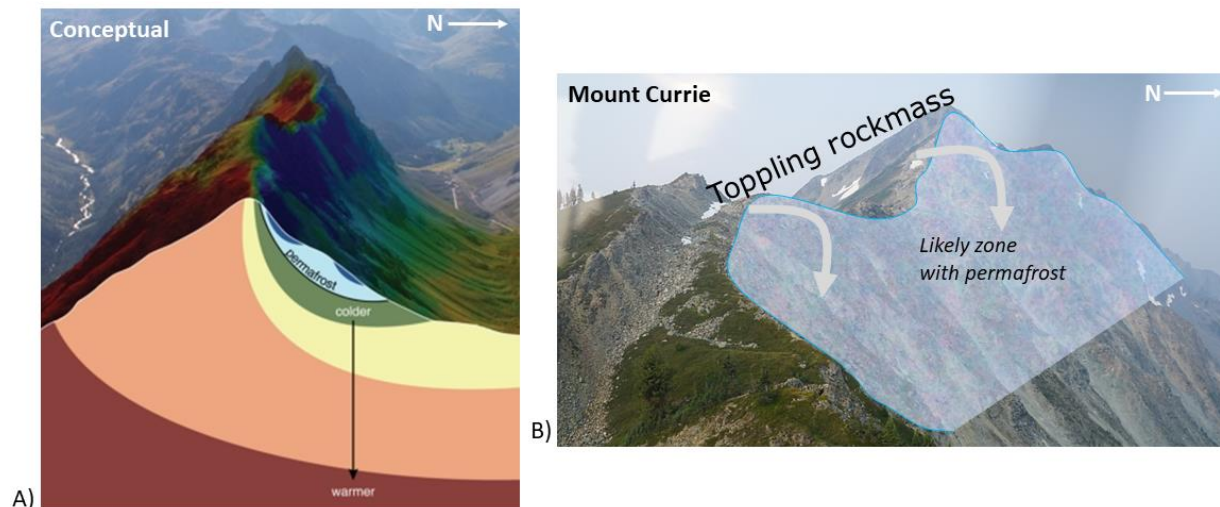


Figure 3-6. Schematic of permafrost distribution on Mount Currie. A) shows the conceptual distribution of permafrost on the north face and progressive warming with depth (image from Global Greenhouse, 2017). B) shows the summit ridge and North Face of Mount Currie with an approximation of permafrost limits (note these are schematic and not currently based on real data).

3.5.6. Frequency Estimation

The 31 rock avalanches identified in Section 3.5.2 within the regional inventory area correspond approximately to one rock avalanche per 158 km². This value is called the “spatial density” as it informs on how many rock avalanche occur in a given area. When normalized by time (the last 10,000 years), this value becomes a frequency: $(6.3 \times 10^{-7}$ rock avalanches per year per km²). This value is comparable to the number of rock avalanche per 140 km² reported by Savigny and Clague (1992) for the Fraser Valley and Fraser Canyon areas. This rock avalanche frequency estimate can be refined by subtracting areas with slope gradient less than 20° (e.g., valley bottoms, lakes and plateaus) from the inventory area, as these represent terrain with very low potential to generate rock avalanches. Based on this revised area, the estimate of the rock avalanche frequency during the last 10,000 years for the inventory area is one rock avalanche per 105 km² (i.e., 9.5×10^{-7} rock avalanches per year per km²).

The above result is an estimate of the regional rock avalanche frequency. It assumes that the potential for a rock avalanche to be triggered is constant over the entire inventory area (i.e., assuming average site-specific geological and structural conditions) and that there is no trend in rock avalanche activity due to climate change or rock mass relaxation. To assess the sensitivity of the rock avalanche frequency to geologic or structural conditions, the inventory was queried in terms of increasing distance from Mount Currie.

Drawing 06 summarizes the rock avalanche frequency estimates as a function of a circular area of increasing radius centered on Mount Currie. It shows that the annual frequency of rock avalanches decreases with increasing inventory area. For example, when only the slopes steeper than 20° are considered within a 5-km radius (area of 52 km²), one rock avalanche has occurred

within the past 10,000 years, giving an annual probability of $1.9 * 10^{-6}$ rock avalanches per year per $\text{km}^2 = (1 \text{ rock avalanches} / [52 \text{ km}^2 * 10,000 \text{ years}])$.

To provide an estimate of the annual probability of future rock avalanches for specific sections of Mount Currie, BGC subjectively adjusted the frequency based on site-specific conditions. In this project, the site-specific conditions considered include:

- Increasing the frequency by one order of magnitude when a feasible failure mechanism has been identified during the kinematic analysis, and
- Increasing the frequency by one order of magnitude when widespread deformation features without signs of recent activity or when localized deformation features with signs of recent activity has been identified, or
- Increasing the frequency by two orders of magnitude when widespread deformation features with signs of recent activity has been identified or ongoing minor rock fall events are reported.

For example, potential source zone 1, which includes zone 1a and 1b have kinematically feasible failure mechanism and widespread deformation with signs of recent activity. As such their frequency was increased by three orders of magnitude resulting in an estimated site specific annual probability of occurrence of $1.9 * 10^{-3}$ rock avalanches per year per km^2 or $1.9 * 10^{-4}$ rock avalanches per year (when multiplied by the combined area of Source ID 1a and zone 1b, respectively).

As a second example, the sum of all potentially unstable zones (Source ID 1 to 19) within the assessment area on the north side of Mount Currie has an area of approximately 1.3 km^2 (Drawing 06), so the annual frequency of rock avalanches on the north face of Mount Currie would be $1.9 * 10^{-4}$ rock avalanches per year per $\text{km}^2 * 1.3 \text{ km}^2 = 3.9 * 10^{-4}$ rock avalanches per year⁴. The rock avalanche frequency estimate for the sum of all potentially unstable zones was not considered in the risk assessment as it is a measure of the potential for instabilities over the entire assessment area, and not for specific instabilities representing a risk to the elements at risk listed in Section 4.0. Table 3-5 summarizes the spatial density of rock avalanches and estimated annual probability of occurrence for the potential rock avalanche source zones identified in Section 3.4.

To provide a comparison and validation of the rock avalanche probability of occurrence estimates summarized in Table 3-5, a Norwegian hazard and risk assessment methodology (Hermanns et al. 2012; Blikra et al., 2016) was applied to the potential rock avalanche zones 1 and 2 on Mount Currie (Appendix E). The mean rock avalanche probability of occurrence obtained using the Norwegian methodology compare favourably with the values estimated by BGC. The Norwegian methodology provided a way of estimating uncertainty around the probability of occurrence estimates.

⁴ When considered at the scale of all potentially unstable zones (Source ID 1 to 19), the order of magnitude kinematic correction is applied (as Appendix D documents that feasible mechanisms are identified over most of the landslide assessment area) and one order of magnitude correction associated with the deformation and activity (as only localized sections of the study area show signs of recent activity) is applied.

Table 3-5. Summary of the spatial rock avalanche density estimate and rock avalanche annual probability of occurrence for the potential rock avalanche source zones.

| Potential Rock Avalanche Source Zone ¹ | Area (km ²) | Rock Avalanche Spatial Density Estimate (event / (km ² * year)) | Mean Rock Avalanche Annual Probability of Occurrence Estimate |
|---|-------------------------|--|---|
| Sum of zone 1 | 0.10 | 1.9 * 10 ⁻³ | 1.9 * 10 ⁻⁴ |
| Sum of zone 2 | 0.49 | 1.9 * 10 ⁻⁴ | 9.3 * 10 ⁻⁵ |
| Sum of zones 4, 6, 11, 14, 16, 17,18 | 0.21 | 1.9 * 10 ⁻³ | 3.9 * 10 ⁻⁴ |
| Sum of zones 1 to 19 | 1.26 | 1.9 * 10 ⁻⁴ | 3.9 * 10 ⁻⁴ |

Notes:

1. Potential rock avalanche source zones outlined on Drawing 05.

3.5.7. Climate Change and Hazard Frequency

The increase in air temperature along with precipitation amounts and intensity discussed in Section 2.3.1 could influence the frequency and possibly magnitude of rock avalanches. Potential linkage between climate change and large-scale rock slope landslides have previously discussed for Canadian (e.g. Cloutier et al., 2016 and Brideau et al., 2016) and international (Huggel et al., 2010 and Coe et al., 2017) case studies.

It is notable that the recent (2016) rock slope failure on the eastern portion of the north face occurred in the area that is presumably underlain by “warm” permafrost and which is thus most sensitive to warming.

While detrimental effects of climate change on rock slope stability conditions is anticipated, it is impossible to quantify this potential effect without knowing the distribution of ground ice in the rock mass, nor having data to support the degradation of permafrost. In this study, adjustments to the annual probability of rock avalanche occurrence is suggested in Table 3-6 to reflect the anticipated changes.

Table 3-6. Summary of the assumed annual probability of rock avalanche occurrence climate change adjustment for the potential rock avalanche source zones.

| Potential Rock Avalanche Source Zone ¹ | Annual Probability of Occurrence Adjustment | Climate Change Factors |
|---|---|---|
| Sum of zone 1 | x 10 | Loss of ice cohesion Increase in frequency and magnitude of high intensity precipitation event |
| Sum of zone 2 | x 2 | Increase in frequency and magnitude of high intensity precipitation event |
| Sum of zones 4, 6, 11, 14, 16, 17,18 | x 10 | Loss of ice cohesion Increase in frequency and magnitude of high intensity precipitation event |

Note:

1. Potential rock avalanche source zones outlined on Drawing 05

The adjustment values presented in Table 3-6 are based on judgement and may be higher or lower. They are meant to indicate the potential sensitivity of the Mount Currie north face to projected climate change. To quantify these values, a substantial subsurface investigation program would have to be launched that includes drilling, temperature and ice content measurements as well as long-term monitoring to understand the rate of active layer thickening, ice loss and its manifestation in rock creep and rock fall frequency changes.

The values reported in Table 3-6 will be applied in the risk assessment (Section 5.0) to estimate the potential climate change sensitivity of rock avalanches and associated flooding risk in a changing climate.

3.5.8. Uncertainties and Limitations

A source of uncertainty associated with the rock avalanche geohazard characterization is that some remotely obtained or proxy data had to be used. For example, the rock mass description, discontinuity characterization, and temperature profiles are based on outcrops located along the south side of Mount Currie as the north side of the mountain is too steep to be accessed without rope access support. Photogrammetric three-dimensional surface model of outcrops on the north face were analysed as a remote tool for characterizing rock on that side of the mountain. Similarly, the interpretation of the seismic survey did not have a deep geotechnical borehole along the alignment to calibrate the interpretation and nearby water well logs had to be used.

The temperature profile measured in the tension cracks should only be used as a proxy for the actual ground temperatures because the thermistors were placed within an existing, air filled crack and due to logistical reasons, no time was allowed for the thermistors to properly stabilize. Together with the thermistor accuracy it is likely that the string are showing temperatures 1 to 2°C too warm.

The rock avalanche frequency estimation is based on a series of assumptions which are sources of uncertainty. One assumption relates to the distribution of rock avalanche through time. Cruden and Hu (1993) discussed that the steady state assumption for rock slide and rock avalanche frequency (i.e., the probability of a rock slide or rock avalanche remains constant through time) may be conservative as landslides may have been more frequent immediately after deglaciation. Cruden and Hu (1993) and Jackson (2002) did not have dates for multiple large rock slope failures in the Canadian Rocky Mountains to test their conceptual model. Sturzenegger et al. (2015) dated two rock avalanche events at the Palliser Rockslide in the Canadian Rocky Mountains; the results suggest that the steady state assumption is possible.

The correction factors applied to the regional rock avalanche frequency are also significant sources of uncertainty. While kinematic feasibility and level of activity (displacement rate and rock fall) are generally accepted as factors that are indicative of a greater susceptibility to rock avalanche, the quantification of this correction is based on BGC's judgement and by comparing estimates against those generated by methods developed by other others for application in Norway (Appendix E).

The uncertainties in the rock avalanche probability estimates have not been quantified. However, based on the information available, the probability estimates are considered to be within an order of magnitude of those reported in Table 3-5. Even with this degree of uncertainty, the overall conclusions of the assessment are expected to be valid.

3.6. Rock Fall and Rock / Debris Slide Geohazard Analysis

Our rock fall and rock / debris slide inventory focused on large events with volumes ranging between 50,000 m³ and 1,000,000 m³, and was undertaken by comparison of the historical aerial photographs captured from 1947 to 2004, with a period of 10 to 20 years between photographs (Table 3-1). The inventory was complemented with field observations. Recent large rock fall and rock slide events were recorded based on the “freshness” of rock slope scars and/or rock debris. We estimate that large rock fall and rock / debris slide events as old as 1937 (80-year time period) can be recorded based on the historical aerial photographs (i.e., approximately 10 years older than the oldest aerial photographs). Scar areas ranging from approximately 10,000 m² and 100,000 m² were used as a proxy, assuming 5 m and 10 m deep failures, respectively.

Geomorphic mapping suggests that two large rock fall and rock / debris slide events occurred between 1948 and 2017. These two events correspond to the location of potential sources ID 5 and 11 in Drawings 04 and 06. The resulting annual frequency is 0.001 events per year per km² (as the assessment area is 21 km²).

Since rock fall and rock / debris slides typically initiate on rock slopes steeper than approximately 40°⁵, it is appropriate to refine the annual frequency estimate considering only the slopes steeper than 40° within the assessment area (approx. 9 km²). Using this area, the annual frequency per km² is 0.003 events per year per km².

3.6.1. Climate Change and Hazard Frequency

The above rock fall and rock slide estimate assumes that past rock mass conditions will continue in the future. As discussed in Section 2.3.1 permafrost degradation on the north face of Mount Currie is expected to result in active layer thickening. The active layer thickening and associated loss of effective ice cohesion will result in more frequent rock fall activity and potentially larger rock fall volume. A similar effect has already been documented in the European Alps (e.g. Gruber et al., 2004).

3.6.2. Uncertainty and Limitations

The rock fall and rock slide assessment conducted is limited to events 50,000 m³ and 1,000,000 m³ as smaller events could typically not be observed in aerial photographs. Smaller but more frequent events can over the period of years, decades, or centuries be important contributors to the transfer of sediment/debris on Mount Currie. During the fieldwork in August

⁵ Various slope angles have been used in previous international studies (see Loyer et al., 2009 for summary) to identify slope sections susceptible to rock fall.

2017, BGC noted that raveling and small rock falls (1 to 10 m³) were occurring several times an hour. The delivery of debris from these small events can influence the frequency and magnitude of debris flows (Section 3.7).

3.7. Debris Flow Geohazard Analysis

3.7.1. Introduction

Frequency-magnitude relationships (FMRs) are defined as volumes or peak discharges of landslides related to specific return periods (or annual frequencies) of their occurrence. This relation forms the core of any hazard assessment because it combines the findings from frequency and magnitude analyses in a format suitable for numerical analysis. The frequency and magnitude of a hazardous event form a relationship where larger events occur more rarely than smaller events. The notion of debris flow return period and even frequency requires revision where there is evidence that the frequency-magnitude relationship may change over time as is postulated to be the case at Mount Currie.

Most debris-flow hazard assessments require that the magnitude of events is established for several return periods and this also forms the basis for risk assessments in which life loss and/or economic consequences are systematically included. The principal challenge lies in establishing reliable FMR. For longer return periods, this requires a combination of several absolute dating methods, test trenching, hydrology, sedimentology and creative geomatics applications. These techniques were outside the budget and scope for the present assignment.

Once debris flow events have been documented and their age and volume estimated, return periods need to be assigned to individual events that allow extrapolation and interpolation into annual probabilities beyond those extracted from the physical record. Such record extension is necessary to develop scenarios for different return periods. These scenarios then form the basis for debris-flow modelling and risk analysis.

In this context, judgement is required to assign magnitudes for very long return periods (thousands of years) and the degree of error is proportional to the length of the return period. This high degree of uncertainty can be addressed through secondary considerations or contingency plans should the channel aggrade significantly over time.

3.7.2. Debris Flow Inventory

Jakob (1996) generated a detailed inventory of debris flows reaching the lower part of the fan at the base of Flow Path D based on dendrochronology. He identified 9 debris flow events in 40 years (1954 to 1994) resulting in a frequency of 0.225, or a return period of 4 years. Most debris flow events were inferred to have occurred during the dormant tree growing season (i.e., October to May). BGC attempted to extend this inventory based on more recent aerial photographs and Google Earth imagery. No event after 1994 could be identified based on aerial imagery available until 2009. However, it is likely that the low spatial resolution of aerial imagery prevents from

recognizing smaller event, which may not have resulted in channel avulsion or significant channel erosion.

Similarly, an inventory of debris flows along Flow Paths A, B and C was built using aerial photographs and Google Earth imagery. Table 3-7 summarized the results of these observations. As for Flow Path D, the low spatial resolution of aerial imagery may prevent recognizing smaller events. In addition, the limited spatial resolution (i.e., period of time between two sets of photographs) may result in missing some events. Note that this data truncation of smaller but more frequent events is of lesser importance as smaller events travel less far and are less destructive. It would only be of importance if development were considered in the runout area of such small events.

Table 3-7. Inventory of debris flow events reaching the lower part of the fan at the base of Flow Paths A, B, C and D; based on historical aerial photographs listed in Table 3-1 and Google Earth Imagery. Their respective volumes are unknown.

| Debris Flow Path | Number of Events | Inventory Period | Frequency (Return Period) |
|------------------|------------------|-------------------------|---------------------------|
| A | 1 | 1969 to 2015 (48 years) | 0.021 (48) |
| B | 2 | 1948 to 2009 (61 years) | 0.033 (31) |
| C | 4 | 1948 to 2009 (61 years) | 0.066 (15) |
| D | 2 | 1948 to 1994 (46 years) | 0.043 (23) |

3.7.3. Regional Frequency-Magnitude Relationship

Any frequency-magnitude calculation that spans time scales of millennia necessarily includes some judgment and assumptions, both of which are subject to uncertainty. For this desktop study analysis, BGC supplemented the debris flow inventory with a novel approach (Jakob et al., 2016; Appendix F) to characterize debris-flow hazards and estimate their magnitude and frequency of occurrence. This work is particularly important in estimating rare, large debris flows with particularly long runout distances. In areas where comprehensive studies on debris-flow or debris flood frequencies and magnitude have been conducted, a simple normalization procedure based on fan area or fan volume can be applied to approximate FMR without the need for in-depth field investigation. These, however, should only be applied in similar environment and morphometrically similar watersheds. As few detailed FMR studies have been conducted in the drier environments of southwestern BC, the results of this analysis should be viewed as preliminary and not suitable for the detailed design of mitigation structures.

Previous work by Jakob (1996) provided an estimate of debris flow frequency and magnitude for Flow Path D at the base of the north face of Mount Currie. The frequency estimate was augmented with an inventory of recent events (Section 3.7.2) based on a combination of historical aerial photographs, Google Earth Imagery, and other available records. This work informed high frequency events that are of interest but would not govern any future mitigation efforts as they are of substantially lesser magnitude and impact force.

3.7.3.1. Methodology

Nine detailed debris-flow hazard and risk assessments have also been completed in southwestern BC for different clients by BGC and Cordilleran Geoscience over a period of approximately 15 years.

These hazard assessments in southwestern BC entailed the reconstruction of detailed FMRs for debris floods and debris flows. Various methods were applied to decipher magnitudes and frequencies of past events. For each project, a frequency-magnitude (F-M) curve was established. Details of the methods are provided in Appendix F. The individual F-M curves were normalized by fan area and plotted on the same graph (Figure 3-7). A best-fit line was plotted and a predictive equation extracted.

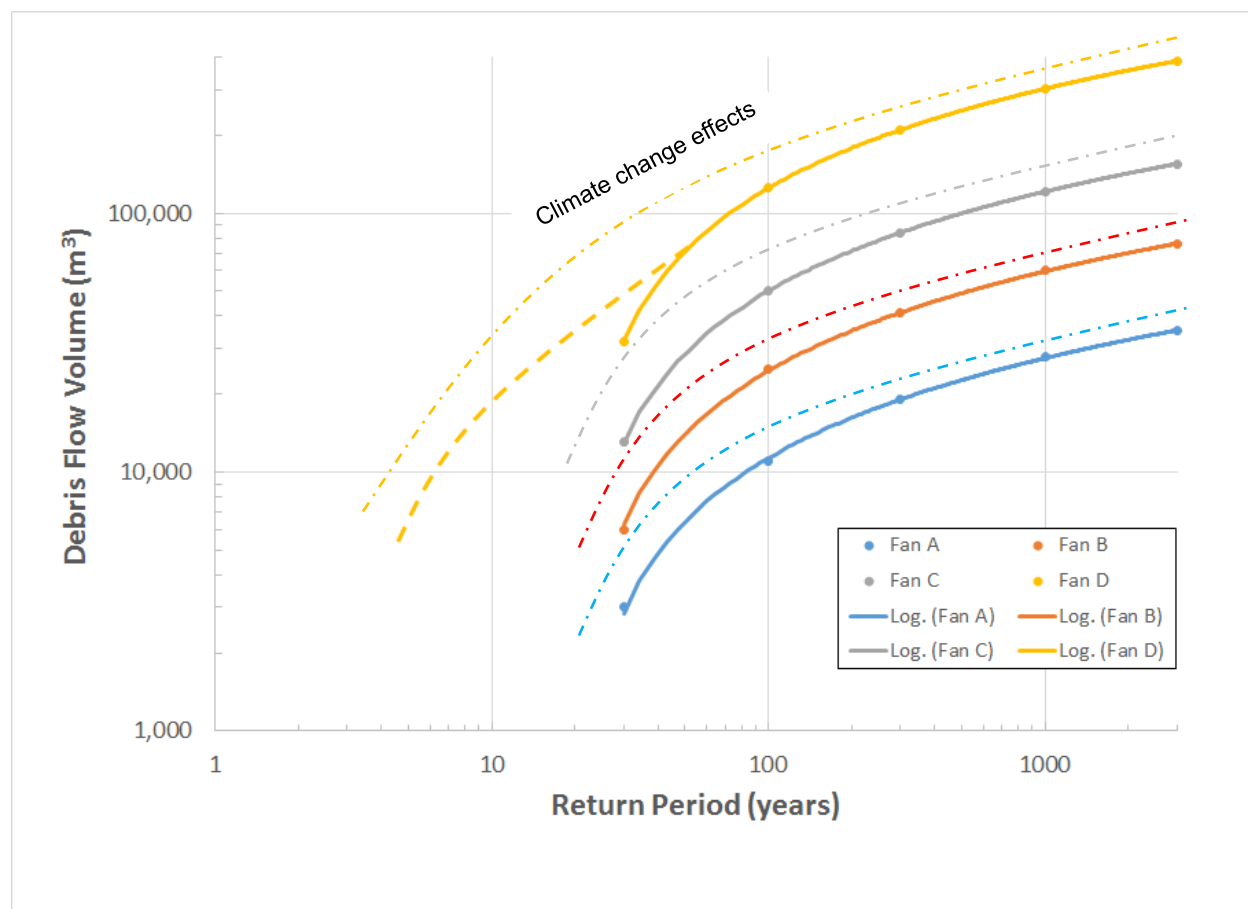


Figure 3-7. Debris-flow frequency-volume estimates for major creeks draining the North Face of Mount Currie based on regional analysis. The frequency-magnitude curve for Fan D was manually adjusted based on detailed investigations by Jakob (1996). A similar adjustment may be appropriate for Fan B and C, but without detailed field investigations is not warranted. Dashed lines show conceptually the effect of climate change.

The regional relations predict the sediment volume (V_S) in m^3 generated in various return period (T) events and normalized by fan area (A_f) in km^2 . Each relation is applicable for return period events ranging from approximately 30 to 3,000 years, noting that in some cases the minimum

return periods exceed 30 years. Higher return periods are too speculative with respect to their sediment volumes to be included in this analysis.

The regional debris-flow MFR (Equation 3-1) was developed by BGC from the detailed study of nine creeks in southwestern BC and has a coefficient of determination (R^2) of 0.65, which indicates goodness of curve fit.

$$V_s = A_f [54,230 \ln(T) - 161,714] \quad [\text{Equ. 3-1}]$$

3.7.3.2. Results

The relation expressed in Equation 3-1 is applied to Creeks A, B, C, and D (Drawing 04). According to Table 3-8, the typical debris flows as determined by Jakob (1996) for Creek D is less than a 30-year event and close to a 10-year event if Equation 3-1 were forced through the zero point. Table 3-8 also demonstrates that much larger debris flows are conceivable on Creeks A to D. Those would likely be associated with extreme rainstorms combined, at higher return periods, with debris-flow triggering rock slope failures in the upper watershed. The exact match between the maximum credible debris flow as per Jakob (1996) and the analysis presented herein is coincidental rather than constituting a verification of the validity of the work. The principal limiting factor for debris flow volumes in Creek D and the adjacent watershed may thus not be sediment availability, but the amount of rain, snowmelt and ground water available to entrain material.

Table 3-8. Debris Flow frequency-volume summary for Fans A, B, C and D on the north face of Mount Currie based on a regional analysis approach. Sediment volumes are rounded to the nearest 1,000 m³ to represent the uncertainty associated with these values. The volume estimate for Fan D is based on work by Jakob (1996).

| Return Period (years) | Fan A | Fan B | Fan C | Fan D |
|---|---|---|---|---|
| | Debris Flow Volume (m ³) | Debris Flow Volume (m ³) | Debris Flow Volume (m ³) | Debris Flow Volume (m ³) |
| 10 | n/a | ? | ? | 12,000 |
| 30 | 3000 | 6000 | 13,000 | 32,000 |
| 100 | 11,000 | 25,000 | 50,000 | 125,000 |
| 300 | 19,000 | 41,000 | 84,000 | 210,000 |
| 1000 | 28,000 | 60,000 | 121,000 | 300,000 |
| 3000 | 35,000 | 76,000 | 155,000 | 390,000 |
| Jakob (1996) Typical ⁶ Debris Flow | n/a | n/a | n/a | 12,000 |
| Jakob (1996) Maximum Debris Flow | n/a | n/a | n/a | 390,000 |

⁶ In weathering-limited basins, the debris source areas and channels contain limited amounts of transportable sediment that are recharged by weathering processes and mass movements after each debris flow (Jakob, 1996). "Typical" magnitude is demonstrated to be adequate for engineering and planning purposes in weathering-limited basins.

3.7.3.3. Climate Change Effects

The results presented in the previous section imply, to some degree that past conditions will remain valid in the future. As discussed in Section 2.3.1, climate models suggest that both the temperature and precipitation intensity will likely increase and as such past condition might not be valid in the future.

The result is an assumed increase in rock fall frequency and possibly magnitude should larger unstable rock masses become unfrozen. An increase in rock fall frequency implies a higher rate of recharge of erodible material to the debris flow channels. This, in turn, results in more material being available for debris flow transport when critical hydroclimatic thresholds are exceeded, or debris flows be initiated by rock slides or perhaps even wet snow avalanches. This may ultimately lead to more frequent (shorter recharge times) and possibly larger (more available material) debris flows.

In combination with the projected permafrost degradation, it can thus be expected that debris flows will increase in both frequency and magnitude in the future, which infers that the current fans will become more active and further encroach onto the Green River floodplain. The combined effect is indicated conceptually in Figure 3-7 as dashed lines. Given that there is no current or future proposed development planned for the northern fans of Mount Currie, this trend will have little bearing of risk to loss of life, but may eventually affect the sediment load and thus stream flow behaviour of Green River. Should debris flows eventually discharge directly into Green River, a channel change from meandering to anastomosing may be observed. This would lead to further channel bank instability.

3.7.4. Uncertainties

While based on typical assumptions and observations, estimates of landslide frequency and magnitude span time scales of millennia and require judgment and assumptions that are subject to some uncertainty listed below:

- BGC did not complete new dendrochronological investigations or test trenching. It relies on a regional approach supported by air photograph interpretation and an examination of the work done by Jakob (1996). Specifically, for event return periods of debris flows that are not captured by the air photograph record, this introduces some error.
- Older events are covered by new ones, thus obliterating evidence. Therefore, only the surface expression as viewed in the field aid in interpreting events of the past.
- The premise of stationarity over time (no long-term trend in the frequency of debris flows), and a stochastic process that is independence from initial conditions. This assumption can be questioned: For example, extrapolation of high return periods from the initial record length is done with only limited information on how climatic or geomorphic watershed conditions may have changed during this time. Changes in vegetation cover, changes in the frequency and/or magnitude of hydroclimatic events and the occurrence of cataclysmic events such as large landslides as observed in 2016 and to this day will influence levels of hazard and associated risk.

- The regional approach by Jakob (2016) bears uncertainties that are mostly associated with defining fan areas correctly in areas with aggrading adjacent floodplains.

BGC believes that the results are a reasonable estimate of the frequency-magnitude relationships of debris flows on creeks A to D.

3.8. Preliminary Geohazard Assessment Results

This section summarizes the results of the preliminary geohazard assessment and discusses the selection of geohazard scenarios carried forward in the numerical modelling phase of the geohazard assessment (Sections 3.9 and 3.10).

Based on the desktop analysis and fieldwork observations, the area impacted by past rock falls, rock slides, debris avalanches and debris flows is confined to south side of Green River (Sections 1 and 3.7). The potential impact of all hazards to forestry operations for the area between the base of the north face of Mount Currie and Green River is excluded from the scope of this work, and as such they will not be considered as geohazard scenarios in the risk assessment.

The review of the potential rock avalanche sources identified four main sources based on a qualitative ranking of the hazard. The qualitative ranking was based on activity level (from desktop and field observations), kinematics (based on field measurements), and volume estimate (based on desktop and field measurements). These four potential rock avalanche sources were considered in the runout modelling (Section 3.9).

3.9. Rock Avalanche Runout Modelling

Numerical modelling of potential rock avalanches provided the basis for the estimation of spatial impact probabilities and corresponding intensities, which serve as inputs to the risk analysis. This section describes the runout numerical modelling approaches, inputs and results. Further details are provided in Appendix G. Section 3.9.5 will build on the runout modelling results by focusing on the numerical modelling associated with a flood resulting from the disrupted river flow (Green and/or Lillooet) due to a rock avalanche.

3.9.1. Runout Methodology

Rock avalanches were modelled with the numerical modelling software *DAN3D* (McDougall and Hungr 2004). *DAN3D* was developed specifically for the analysis of rapid landslide motion across complex three-dimensional terrain. BGC has successfully applied *DAN3D* for the same purposes on other projects.

The model simulates landslide motion from initiation to deposition and requires the following inputs:

- A digital elevation model (DEM) of the topography in the study area, which defines the sliding surface across which the simulated landslide travels
- A corresponding DEM that delineates the extent and thickness of the initial landslide (i.e., source zone of failed rock mass)

- User-specified flow resistance parameters that control how fast and how far the simulated landslide travels.

3.9.2. Inputs for Runout Modelling

3.9.2.1. Sliding Surface

The sliding surface that was used for rock avalanche modelling was based on LiDAR data acquired in August 2017 specifically for this project. A topographic grid with a 10 x 10 m spacing was generated from the higher resolution LiDAR data.

3.9.2.2. Failure Volume and Source Location

Four failure scenarios representing different sections of the mountain that are potential rock avalanche sources, labelled source zone ID 1, 2b, 4, and 11 (Table 3-2) were considered for the analysis. These four scenarios were chosen based on their volume, level of activity and as representative of the potential rock avalanche in the different sections of Mount Currie (Table 3-2). The locations of these source zones are shown on Drawing 05. The geometry of the rupture surfaces bounding the potential rock avalanche source zone for the *DAN3D* analysis are based on discontinuity orientations measured in the corresponding section of Mount Currie (Section 3.5.4) and on lineaments mapped in the LiDAR (Section 3.4.1).

No entrainment was included in the analysis of source zone ID 1, as it is expected that the volume of entrainable material available along the runout path would be small in comparison to the source volume of the rock avalanche. The distribution and thickness of entrainable material for the other source zones was based on geomorphic mapping (Drawing 04) of talus along the runout path. The final simulated volumes are shown in Table 3-9.

Table 3-9. Source and entrainment volumes considered in the DAN3D simulations.

| Source Zone ID | Unbulked Volume (Mm ³) | Bulked Volume ¹ (Mm ³) | Entrained Volume (Mm ³) | Final Volume (Mm ³) |
|----------------|------------------------------------|---|-------------------------------------|---------------------------------|
| 1 | 3.3 | 4.1 | 0 | 4.1 |
| 2b | 8.3 | 10.4 | 1.5 | 11.9 |
| 4 | 1.8 | 2.3 | 0.60 | 2.9 |
| 11 | 0.68 | 0.85 | 0.45 | 1.3 |

Note:

1. Bulking of 25% was assumed for all cases.

3.9.2.3. Resistance Parameters

The user-specified basal resistance parameters are calibrated during back-analysis. To simulate the potential future rock avalanches, the Voellmy flow resistance model was used. The Voellmy model has been used by a number of researchers to successfully simulate rock avalanche motion (e.g., Hungr & Evans 1996; McDougall 2006; Aaron & Hungr 2016). Compared to alternative flow

resistance models, the Voellmy model tends to produce more realistic estimates of deposit distribution and velocity (McDougall 2017). The Voellmy model is governed by two parameters: 1) a friction coefficient, f ; and 2) a turbulence parameter, ξ , which produces a velocity-dependent resistance that tends to limit flow velocities (similar to air drag acting on a falling object) (McDougall and Hungr 2004). The values of f and ξ were determined with reference to typical values for rock avalanches.

The values used for the DAN3D models of potential rock avalanches at Mount Currie are summarized in Table 3-10. These values correspond to values back-analyzed for mobile rock avalanches (Hungr and Evans, 1996; McDougall 2006; Aaron and Hungr, 2016). They include back-analysis rock avalanches which travelled on flood plains (e.g. Frank Slide) as anticipated in the case of a rock avalanche initiating from Mount Currie.

Table 3-10. Input parameters used in the DAN3D simulations of rock avalanches initiating from Mount Currie.

| Mobility Case | Friction Coefficient - f | Turbulence Coefficient - ξ (m/s ²) |
|---------------|----------------------------|--|
| Case 1 | 0.1 | 500 |

3.9.3. Excess Runout (“Splash Zone”)

The “splash zone” is a feature sometimes observed on the outer margin of rock avalanche debris (e.g., Cruden and Hungr 1986; Mathews and McTaggart 1978; Iverson et al. 2015). It consists typically of an area of the landslide deposit at the margin of the main mass with relatively smooth surface morphology composed of a thin layer of fine-grained sediments, which contrasts with the otherwise hummocky, thick and coarse-grained rock avalanche deposit. The splash zone forms as the result of undrained loading and liquefaction when a rock avalanche impacts saturated alluvial sediments in a valley or floodplain.

Based on a review of 12 rock avalanche case studies (Figure 3-8), BGC estimates that the runout distance of a rock avalanche that generates undrained loading of valley/floodplain sediments, liquefaction, and formation of a splash zone could be increased by 60%, on average. This represents a splash zone ratio of 0.6 where the ratio is defined as the travel distance of the distal liquefied fine-grained material (as measured from the edge of coarse debris) divided by the travel distance of the main coarse rock avalanche debris. Based on the review of splash zone thickness from the same rock avalanche case studies, a value of 2 m was assumed for a potential splash zone associated with a rock avalanche from Mount Currie.

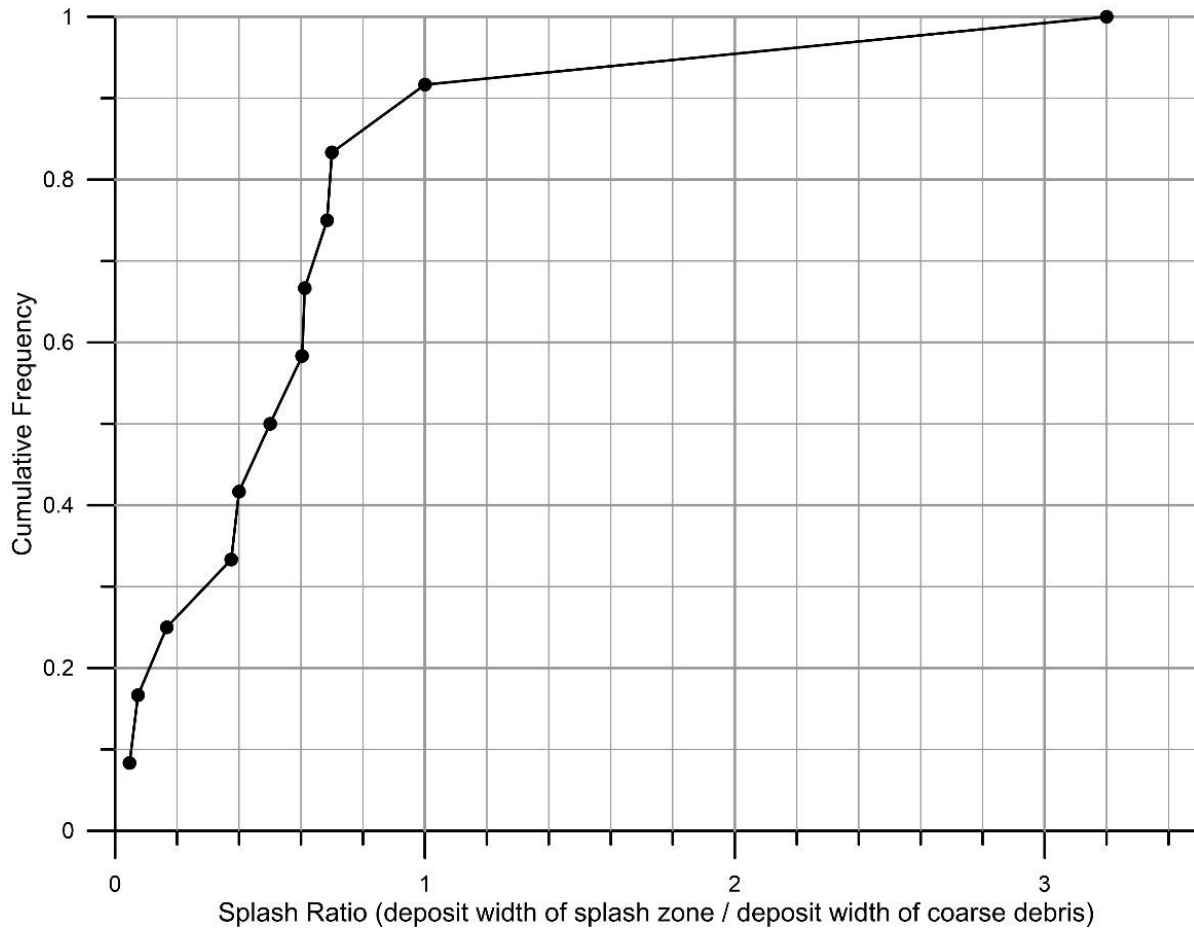


Figure 3-8. Cumulative frequency of the splash zone ratio from published literature on rock avalanches

3.9.4. Runout Modelling Results

The forward analysis results for the four scenarios modelled are shown on Drawing 07. The simulated impact area appears to be insensitive to the basal resistance parameters. This is likely because both sets of basal resistance parameters that were tested have the same turbulence coefficient, which limits the velocity (and therefore momentum) obtained by the moving mass as it descends Mount Currie. The potential elements at risk impacted by the four simulated rock avalanches are summarized in Table 3-11. Except for source zone ID 11, all cases are simulated to dam Green River. Only rock avalanches originating in source zone ID 2b are simulated to dam the Lillooet River.

Table 3-11. Elements at risk simulated by DAN3D and splash zone.

| Source Zone ID | Dam Green River | Dam Lillooet River | Impact Golf Course | Impact Airport |
|----------------|-----------------|--------------------|--------------------|----------------|
| 1 | Yes | No | Yes | No |
| 2b | Yes | Yes | Yes | Yes |
| 4 | Yes | No | Yes | No |
| 11 | Yes | No | No | No |

3.9.5. Rock Avalanche Flow Intensity Index

To characterize the potential destructiveness of the modelled rock avalanches, the flow intensity index (I_{DF}) was used for the models results of Source ID 1a (the potential source identified near Currie NE3 Peak) and 2b (the potential source identified along the ridge east of Currie NE3 Peak; Drawings 08 and 09). The flow intensity was defined as an index according to Jakob et al. (2011) as follows:

$$I_{DF} = d \times v^2$$

where

d is flow depth in metres; and

v is flow velocity in meters per second.

The potential runout path and main deposit (referred to as the rock avalanche direct impact zone) were assumed to have an equivalent I_{DF} greater than 1000. This reflects that this area would be impacted by over a metre of bouldery material travelling at speeds greater than 10 m/s. Total destruction of the infrastructure is expected in the rock avalanche direct impact zone. The splash zone was divided in two flow intensity index zones. The majority of the splash zone is assumed to have a I_{DF} between 100 and 1000. The distal part of the splash zone has an assumed I_{DF} between 10 and 100 to represent the transition between the hazard associated with the rock avalanche and the flooding.

3.9.6. Uncertainties and Limitations

Rock avalanche runout is sensitive to site specific conditions such as topography, nature of the source material, and nature of the material along the runout path. While topography is well constrained by LiDAR for this project, the behaviour of the material in the source and along the runout path has to be estimated based on back-analysis of similar past events in Canada and the world. Entrainment and the splash zone were incorporated in the numerical runout models but these aspects of the potential rock avalanche are also based on review of similar past events.

3.10. Landslide Damming and Flood Modelling

Based on the rock avalanche runout modelling results, a numerical hydrodynamic model was used to model the flooding resulting from landslide damming scenarios from source zone ID 1

and 2b. The location, extent, and size of the rock avalanche deposits for these scenarios matched the results of the runout modelling, described in Section 3.9 (Drawing 07).

3.10.1. Flood Modelling Methodology

The hydrodynamic modelling software package *TELEMAC* (Hervouet and Bates 2000) was used to model the extent, water velocity, water depth, and rate of flooding resulting from a rock avalanche damming the Lillooet and/or Green Rivers. *TELEMAC-2D* is a depth-averaged shallow flow numerical model that BGC has used to model similar events on other recent projects.

3.10.2. Flood Modelling Input Parameters

For each scenario, a DEM of the deposit was overlain on the LiDAR DEM of the project area, and used to generate a mesh for the model. The extent of the model domain was defined by the available LiDAR data. The LiDAR DEM includes the surface of the water in the Lillooet and Green Rivers; however, the bathymetry or the average depth of the rivers were not available for modelling. To correctly model the flow of water in these rivers, the elevations of the mesh points falling inside the rivers were reduced to approximate the bathymetry. The elevation was reduced until the water was contained within the river banks, with no flooding related to the ordinary flow of the river. This approach of estimating the river depth resulted in the elevations of the nodes being reduced by 4 m and 3 m in the Lillooet and Green Rivers, respectively. A variable edge-length triangular mesh was used, with an average edge length of 5 m along the river banks and toe of the deposits, increasing to 17 m elsewhere.

The median annual flood based on the daily average flow rates were used as input boundary conditions for the two rivers: 510 m³/s and 195 m³/s for the Lillooet and Green Rivers, respectively, as they provide a good estimator of the 2-year flood (Reed 2002). A discharge rating curve based on the assumption of normal flow was developed for the eastern outlet boundary condition, accounting for the flow of the Lillooet River and allowing flood waters to exit the model. In both scenarios, the model was run until steady-state between input and output flow volumes, indicating that the maximum extent of flooding in the model domain had been reached.

The flow velocity and water depth at each node at steady-state were extracted from the model. These values were used to calculate the hazard intensity index, I_{DF} , as explained in Section 3.9.5.

3.10.3. Flood Modelling Results

Drawings 08 and 09 show the peak modelled extent and destructive potential of landslide and flood Scenarios 1a and 2b, respectively. Destructive potential is shown in two different ways on the drawings: flow intensity index and flow depth.

The flow intensity index (IDF) defined in Section 3.9.5 provides a common measure of destructive potential in the landslide and flood impact areas. Drawings 08 and 09 display flood intensity at an order-of-magnitude level of detail where $I_{DF} > 1$. These flows have potential to result in structural building damage due to dynamic and static impact pressure. All areas of the landslide direct impact and splash zones display flow intensity index values.

Where I_{DF} does not exceed 1, flow depth is displayed as the primary controlling factor for flood damages. Most areas subject to flooding show flood depth, except for areas of higher flow depth and velocity within Lillooet or Green River in the vicinity of the Hamlet of Mount Currie. Higher flow intensities within the Hamlet of Mount Currie may be associated with modelled flow concentrations between buildings.

Note that on both Drawings 08 and 09, the backwater effect caused by the damming of the rivers extended to the upstream limit of the model. Further flooding is possible beyond the model domain limit. For scenario 1, some flooding in the Village of Pemberton may occur but it is expected to be very minor. For scenario 2b, it is expected that the upstream flooding will be more extensive than for scenario 1 due to the blockage of both the Lillooet and Green Rivers. The I_{DF} in the Village of Pemberton for both scenarios will be very low due to the low velocities and depths.

3.10.4. Uncertainties and Limitations

The of Green and Lillooet rivers flow in the model was assumed to be the median annual flood. The actual extent of the flooding associated with a landslide dam could vary based on the flow in the rivers at the time of the damming event. As no bathymetric information was available for the Green and Lillooet rivers, the back-calculated river depth to accommodate normal daily flow does represent of source of uncertainty.

The modelling of the flooding was limited to the footprint of the LiDAR data available. While the modelled water depth and velocity at these boundaries was low, minor difference in the reported flooding extent is anticipated should a larger area of LiDAR was available. The flood modelling was conducted for the August 2017 bare-earth topography. Future changes in dike dimensions and location could influence the results presented in this report.

3.11. Results of Geohazard Numerical Modelling

This section summarizes the results of the runout and flooding numerical modelling analyses and presents the geohazards scenarios (Figure 3-1) to be considered in the risk assessment (Sections 4.0 and 5.0).

Rock avalanches and flooding associated with the damming of Green and Lillooet River was shown to have the potential to affect areas on the north side of Green River (Sections 3.9 and 3.10). The splash zone of potential rock avalanches initiating from source zones 11 and 4 are modelled to only reach Green River and the edge of the golf course (Drawing 07 and Table 3-11). This contrasts with the modelled extent of potential rock avalanches initiating from zones 1a and 2b which could result in impact and flooding with various infrastructure.

Based on the results of the runout and flood modelling, the risk and vulnerability analysis will focus on the geohazard scenarios associated with the direct impact, splash and flood inundation zones resulting from a potential rock avalanche initiating from Zone 1a or 2b. These are referred to as “Scenario 1a” and Scenario 2b” in the risk analysis.

4.0 ELEMENTS AT RISK ANALYSIS

The risk assessment considers the areas potentially impacted by Scenarios 1a or 2b, including the direct impact, splash and flood inundation zones shown on Drawings 8 and 9. This section describes “elements at risk” within these areas and included the following tasks:

- Identifying elements at risk within the assessed area
- Characterizing these elements to allow estimation of spatial-temporal probability and vulnerability to geohazard impact.

Combined, the results of geohazard analysis (Section 3.0) and geohazard exposure analysis (this section) form the basis to estimate risk (Section 5.0).

4.1. Background

According to 2016 Census data, a population of approximately 6,140 people occupies the Village of Pemberton and the Hamlet of Mount Currie over a land area of 92 km² (Statistics Canada, 2017⁷). These communities are home to a total of 2,351 private dwellings with an average household size of 2.7. Note that that the area subject to risk assessment is smaller and is home to fewer people and dwellings.

An extensive lifeline network provides access to food, water, energy, communication and transportation to the communities.

Table 4-1 summarizes elements at risk within the area assessed. A description of each of these elements is provided below. These elements were defined through discussions with the steering committee. Table 4-1 does not include all elements that could suffer direct or indirect consequences due to a geohazard event. Rather, the elements at risk listed in Table 4-1 are limited to those that could be reasonably assessed, based on the information available.

Quantitative assessment of elements other than residential dwellings was limited to identifying their location on drawings in relation to geohazard areas. For example, indirect economic consequences due to highway interruption are not included. This assessment also focuses on risk associated with direct geohazard impact. Additional risk associated with, for example, loss of access to the elements listed in Table 4-1, is not considered.

Risk mitigation decisions based on the elements assessed will also reduce risk for a broader spectrum of elements in protected areas than those explicitly considered.

⁷ Includes Pemberton (Population Centre), Pemberton Village (Census Subdivision), Mount Currie 1, 2, 8, 10 Indian Reserve (Designated Place). Mount Currie 6 is not affected by the hazards, therefore is not included in the census totals.

Table 4-1. Elements at risk within the assessment area.

| Element at Risk | Scenario 1a | | | Scenario 2b | | |
|-------------------------|-----------------------------------|----------------------------|-----------------|-----------------------------------|----------------------------|-----------------|
| | Rock Avalanche Direct Impact Zone | Rock Avalanche Splash Zone | Inundation Zone | Rock Avalanche Direct Impact Zone | Rock Avalanche Splash Zone | Inundation Zone |
| Persons in Buildings | ✓ | ✓ | ✓ | ✓ | ✓ | ✓ |
| Buildings | ✓ | ✓ | ✓ | ✓ | ✓ | ✓ |
| Critical Infrastructure | | | ✓ | ✓ | ✓ | ✓ |
| Roads | ✓ | ✓ | ✓ | ✓ | ✓ | ✓ |
| Transmission | ✓ | ✓ | ✓ | ✓ | ✓ | ✓ |
| Businesses | ✓ | ✓ | ✓ | ✓ | ✓ | ✓ |

4.2. Buildings

Information on building types within the risk assessment area was obtained from census data. The locations of buildings (building footprints) were digitized by McElhanney from orthophotos acquired during the July 2017 LiDAR survey. These data were used in the risk analysis to identify location(s) of buildings within parcels that could be impacted by geohazard scenarios.

The majority (nearly 50%) of private dwellings in the Village of Pemberton and Hamlet of Mount Currie are single detached houses. Other dwelling types include row houses (34%), apartments (12%), semi-detached houses (5%), and movable dwellings (2%). The average household size is 2.7.

The risk assessment area contains approximately 75 residential, 30 commercial, 20 industrial, 15 agricultural, 2 government and 1 religious parcels containing buildings. These are estimated from BC assessment data and review of imagery in the absence of assessment data.

Each land parcel contains a unique identification number (“PID”) and unique lookup code identifying the primary use and type of building within the parcel. In the case of single buildings (e.g. residential houses), each parcel typically contains only one assessed land and building value. However, some parcels contain more than one occupied building (e.g. IR 1 Mount Currie and IR 2 Mount Currie on Drawing 10). Data on building structure type or contents were not available.

In total, about \$55.9 million⁸ (M) of assessed building infrastructure is located within 139 parcels in the risk assessment area, with assessed land values totaling about \$41.5M⁹. The values listed above do not include building contents or inventory and do not necessarily correspond to replacement cost, which may be higher. As such, they should be regarded as minimum costs. Assessment of proposed future development is outside BGC’s scope of work.

Table 4-2 summarizes the main uncertainties associated with the buildings attributes data provided.

Table 4-2. Building data uncertainties.

| Type | Description |
|--------------------|--|
| Building Value | Building value was assigned as the total improvement value within a given parcel according to BC Assessment (BCA 2017). However, buildings exist within some parcels where BCA lists no improvement value, such as in areas under Federal Jurisdiction (First Nations Reserves) or parcels with unrecorded buildings development. In these cases, BGC assigned an improvement value corresponding to the average assessed value of similarly classed parcels within the study area. |
| Building Structure | No information describing building structure was available, such as construction type, foundation type, number of stories, presence of sub-grade basement, Flood Construction Level (FCL) first-floor elevation, or floor area. These data gaps will decrease confidence in damage and risk estimation. BGC understands these data may be contained within building permits. However, these permits are not managed in digital format and manually extracting individual building characteristics from building permits was not included in the scope of work. |
| Building Type | Information on exact building types within parcels was not directly available. Building types were assigned based on the BCA primary actual use codes grouped into residential, commercial, industrial, agricultural, government and religious categories. In the case of missing primary actual use codes, building types were manually assigned based on review of imagery (i.e. Google Maps). |
| Building Location | Ambiguities exist where multiple buildings exist within parcels and where building footprints overlap parcel boundaries. |

4.3. Critical Facilities

Critical facilities are defined as those that:

- Provide vital services in saving and avoiding loss of human life
- Accommodate and support activities important to rescue and treatment operations
- Are required for the maintenance of public order
- House substantial populations

⁸ Improvement values were not available for 35 of the 139 parcels assessed. BGC estimated the improvement values for these buildings based on average values from similar parcels. The sum of the improvement value from BC assessment data is \$34.1 M and the sum of the estimated improvement values is \$21.8 M.

⁹ Note that impacts on land values were not considered in this assessment.

- Confine activities that, if disturbed or damaged, could be hazardous to the region
- Contain hazardous products or irreplaceable artifacts and historical documents.

Critical facilities within the study were identified by SLRD and include: the airport/fire base, RCMP detachment, Ambulance Station, Pemberton Medical clinic, schools, city halls, SLRD and VoP/Lil'wat Band Office, Fire Station (co-located in the SLRD building), Pemberton Community Centre (designated Reception Centre location and alternate Emergency Operations Centre location), hydro substation, water and waste water treatment systems and transfer station. The location of the critical facilities within the risk assessment area is shown on Drawings 08 to 11. Note that the majority of the critical facilities are located within the Village of Pemberton boundaries, outside of the risk assessment area, and are not labelled on the drawing.

4.4. Persons

Population estimates used in this assessment are based on 2016 Census data (Statistics Canada, 2017), dwelling counts from tax roll classification data (BC Assessment 2017), and business data (Hoovers 2017).

Assessment of risk at a parcel level of detail requires estimation of the number of persons in each parcel on the fan. However, Census data does not provide estimates at this resolution. As such, individual parcel populations were estimated based on the number of building units of a given type, in each parcel, and the estimated number of persons in a given unit type. Steps to complete this estimate for residential parcels are described below.

First, BGC estimated the number of building units based on a combination of parcel land usage and tax roll codes. Second, BGC estimated the number of occupants per building unit. Permanent residential occupancy rates were based on 2016 Census data and corresponded to 2.7 persons per dwelling unit. For most residential parcels, it was assumed that there is only one occupied dwelling per parcel. For residential parcels IR 1 Mount Currie and IR 2 Mount Currie, there are multiple residential buildings on a single parcel, therefore occupancy rates were multiplied by the number of buildings impacted by the flow.

Population estimates for non-residential parcels are based on the number of employees listed in business data obtained from Dun & Bradstreet (Hoovers 2017). For parcels where these data are not available, averages from similar parcel types were applied. Populations estimates for the airport and the firebase were provided by SLRD. Attendance estimates for the Mount Currie church were obtained by phoning the church directly.

Table 4-3 summarizes calculated populations used in the risk analysis. The population estimate is approximately 13% of the Census population estimate, which includes a greater geographic extent than the risk assessment area. Implications of the uncertainties listed in Table 4-4 include possible over- or underestimation of group safety risk for particular parcels depending on whether the number of persons was over- or underestimated, respectively. BGC believes that the accuracy of population estimates is sufficient to allow risk management decisions. However, the estimates

should not be used for detailed assessment of individual parcels (e.g. for building permit applications) without being manually checked.

Table 4-3. Summary of calculated population estimates used in risk analysis.

| Population Type | Population Total |
|-----------------|------------------|
| Residential | 289 |
| Commercial | 190 |
| Industrial | 123 |
| Agricultural | 120 |
| Religious | 15 |
| Total | 780 |

Table 4-4. Uncertainties associated with estimating the number of occupants of a building.

| Uncertainty | Implication |
|--|--|
| Average occupancy rates may not correspond to actual occupancy rates for a given dwelling unit. | Over- or underestimation of occupant numbers |
| Seasonal population fluctuations (including tourists) exist that were not accounted for. | |
| Multiple residential dwellings on a single parcel may exist that were not accounted for (these were only accounted for on Mount Currie Indian Reserve 1 and 2). | |
| No employee data available (either not listed in Dun and Bradstreet (D&B) (Hoovers 2017) or could not be assigned to specific parcels. | |
| Errors in employee data sourced from Dun and Bradstreet (D&B) (Hoovers 2017) may exist. These data were not verified by BGC. | |
| Errors in assignment of D&B employee data to specific parcels may exist, due to inconsistencies in building address data. | |
| Overlap between some population types (e.g. employees might also live in the risk assessment area) | Uncertainty in estimation of human vulnerability to geohazard impact |
| Distribution of persons within a building are unknown. As such, the number of persons most vulnerable to geohazard impact on the first floor or basement is unknown. | |
| Seasonal visitors may occupy private residences, and additional temporary visitors occupy restaurants, shops, golf courses, and professional services. | Underestimation of occupant numbers |

4.5. Business Activity

Business activity considered in this assessment includes public and private employers with their primary address located in the risk assessment area. Employer data are based on information compiled by the commercial information provider Dun and Bradstreet (D&B) (Hoovers 2017).

In summary, 46 employers are located in the Mount Currie risk assessment area representing a wide range of economic sectors generating about \$34 CAD¹⁰ M/year and employing approximately 203 people.

The business data used in the assessment are subject to uncertainties associated with both the data itself and how it is assigned to particular parcels. Table 4-5 summarizes uncertainties associated with the data. Business activity impacts listed in this report are likely underestimated due to the uncertainties in the business data.

In addition to the uncertainties listed in Table 4-5, business activity estimates do not include individuals working at home for businesses located elsewhere or businesses that are located elsewhere but that depend on transportation corridors. Inclusion of these figures would substantially increase the level of business activity that could be affected by a geohazard event. Such estimates are outside the scope of this assessment.

Table 4-5. Business data uncertainties.

| Type | Description |
|-------------------|---|
| Revenue data | Missing for 4 workplaces (not available from D&B). |
| D&B data quality | BGC has not reviewed the accuracy of business data obtained for this assessment. |
| Worker location | Whether the employee primarily works at the office or some other location is not known. The estimates also do not include individuals working at home for businesses located elsewhere. |
| Source of revenue | Whether a business' source of revenue is geographically tied to its physical location (e.g. a retail store with inventory, versus an office space with revenue generated elsewhere) is not known and is outside the scope of this assessment. |

4.6. Lifelines

Lifelines considered in this assessment include transportation networks (roads and bridges) and utility systems (power, water, communication lines).

Roads considered in the assessment include the Sea to Sky Highway, Highway 99, municipal roads in the Mount Currie study area and forest service roads (Drawing 10). Hiking/biking trails were not directly considered in the risk assessment.

Utility systems considered in the risk assessment area are shown on Drawings 08 and 09 include the following:

- BC Hydro Transmission Line
- BC Hydro Transmission Line (Local)
- Shaw and Telus local lines

¹⁰ D&B revenue data provided in USD and was converted at 1 USD = 1.28 CAD.

5.0 VULNERABILITY AND RISK ESTIMATION

5.1. Introduction

Quantitative Risk Analysis (QRA) involves estimating the likelihood that a hazard occurs, impacts elements at risk, and causes particular types and severities of consequences. Vulnerability estimation involves estimating the likelihood of consequences, given that a hazard occurs and impacts elements at risk. The key difference between vulnerability and risk estimation is that vulnerability estimates assume impact, whereas risk additionally provides estimates of the likelihood of impact.

This section presents the results of vulnerability and risk estimation for the geohazard scenarios described in Section 3.11 and shown on Drawings 08 and 09. These scenarios are considered separately (e.g. the combined risk from both scenarios is not estimated). Elements at risk considered in the analysis are described in Section 4.0 and shown on Drawing 10. The probability of scenario occurrence is based on the rock avalanche frequency estimates described in Section 3.5.6.

The analysis methods are described in detail in Appendix H, and consider the elements at risk described in Section 4.0. In summary, BGC used QRA methodology to estimate risk to life (safety risk) and probability of building destruction within the direct landslide impact and splash zones. In these areas, impact is assumed to occur suddenly with no opportunity for evacuation, and with high vulnerability to loss of life.

Within the flood inundation zones, many additional variables affect risk that are poorly known, such as levels of warning; flood duration, emergency planning and evacuation; human behavior during an emergency; and differences in human vulnerability due to age and health. BGC did not complete QRA within these areas, but did identify areas with relatively higher vulnerability to loss of life.

This assessment focuses on direct structural building damage, risk to life, and identification of lifelines, critical infrastructure and business activity within impacted areas. It excludes estimation of emergency response and reconstruction costs, or the consequences of severed road access. These consequences would have to be added to assess the total potential costs of landslide and flood scenarios considered in this assessment.

5.2. Safety Risk Tolerance Criteria

Safety risk was estimated from two perspectives: risk to individuals and groups.

Individual safety risk considers the risk to a particular individual exposed to hazard, and is independent of the number of persons exposed to risk.

BGC compared the individual risk estimate results to geohazard tolerance criteria adopted by the District of North Vancouver (DNV), BC and Canmore, AB which are the two jurisdictions in Canada that have formally adopted risk tolerance standards for residential development. Their criteria for individual geohazard risk tolerance are as follows (Figure 5-1):

- Maximum 1:10,000 (1×10^{-4}) risk of fatality per year for existing developments
- Maximum 1:100,000 (1×10^{-5}) risk of fatality per year for new developments.

For context, the DNV risk tolerance threshold of 10^{-4} (1/10,000) for existing development is comparable to the lowest background risk of death that Canadians face, on average, throughout their lives. This tolerance threshold is also similar to the average Canadian’s annual risk of death due to motor vehicle accidents, 1/12,500, for the year 2008 (Statistics Canada 2009).

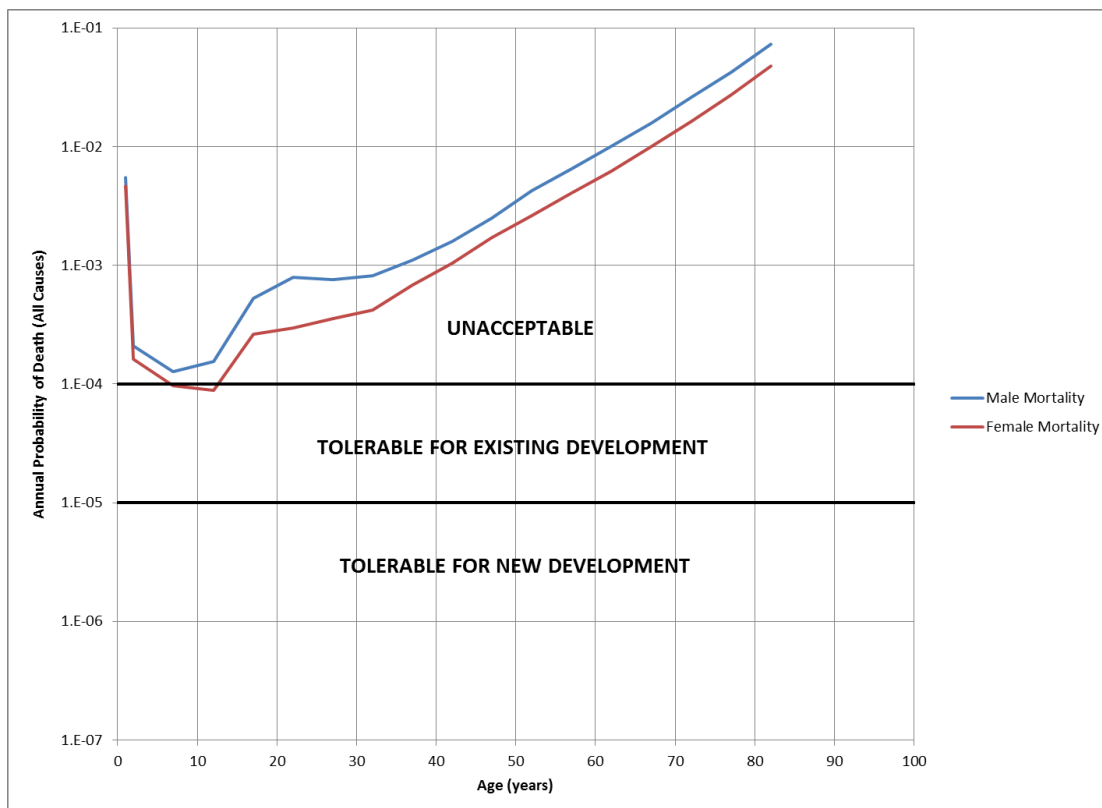


Figure 5-1. DNV individual risk tolerance criteria for landslides compared with Canadian mortality rates (all causes) in 2008.

Group safety considers the collective risk to all individuals exposed to hazard, and is proportional to the number of persons exposed to risk. For risk to groups, estimated risks were compared to group risk tolerance criteria formally adopted in Hong Kong (GEO 1998) and informally applied in Australia (AGS 2007), DNV and Canmore. Group risk tolerance criteria reflect society’s general intolerance of incidents that cause higher numbers of fatalities. Group risk tolerance thresholds based on criteria adopted in Hong Kong (GEO 1998) are shown on an F-N Curve in Figure 5-2. Three zones can be defined as follows:

- Unacceptable – where risks are generally considered unacceptable by society and require mitigation
- As Low as Reasonably Practicable (ALARP) – where risks are generally considered tolerable by society only if risk reduction is not feasible or if costs are grossly disproportionate to the improvement gained (this is referred to as the ALARP principle).

- Acceptable – where risks are broadly considered acceptable by society and do not require mitigation.

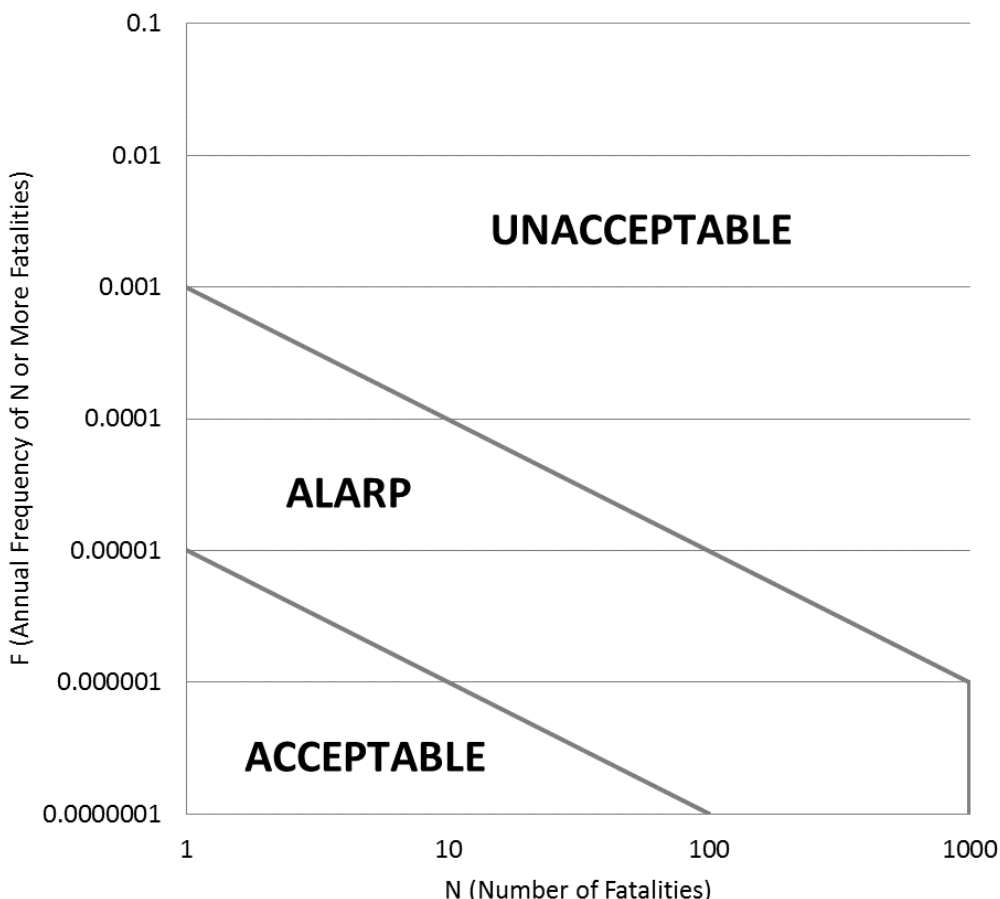


Figure 5-2. Group risk tolerance criteria as defined by GEO (1998).

5.3. Results

This section summarizes results of the risk analysis based on the methods described in Appendix H.

5.4. Individual Safety Risk

Table 5-1 lists the number of parcels exceeding the individual risk tolerance thresholds of 1:10,000 (1×10^{-4}) for existing developments and 1:100,000 (1×10^{-5}) for new developments. Two hazard probability scenarios are listed based on the frequency estimates and the climate factor adjustments listed in Section 3.5.6. This emphasizes that the climate change assumptions have substantial bearing on the risk results. This implies the need for further study of the rock mass thermal characteristics, ice content and its strength with and without ice cohesion to test the climate change hypothesis and provide improved adjustment factors.

Table 5-1. Number of parcels exceeding individual risk tolerance thresholds for current conditions and with consideration of climate change.

| Hazard Probability | PDI > 1:10,000 (1×10^{-4}) | | PDI > 1:100,000 (1×10^{-5}) | |
|--------------------|---------------------------------------|-------------|--|-------------|
| | Scenario 1a | Scenario 2b | Scenario 1a | Scenario 2b |
| Current Climate | 0 | 0 | 2 | 13 |
| Future Climate | 2 | 7 | 2 | 15 |

5.5. Group Safety Risk

Figure 5-3 presents the results of group risk analysis on an F-N curve. Note that the risk results pertain only to the direct impact and splash zones and do not include loss of life risk within flood inundation areas, which was not quantified.

When compared to the international risk tolerance standards described in Section 5.2, estimated overall group risk for Scenario 1a plots within the ALARP range for current climate conditions and the Unacceptable range for potential future climate conditions. Estimated overall group risk for Scenario 2b plots within the Unacceptable range for current and potential future climate conditions considered.

Figure 5-4 compares the results of the group risk analysis from this study to group risk results from a risk analysis of debris flows originating from Mount Meager (Friele et al., 2008). The results indicate that group risk from Mount Currie rock avalanches plot in a similar range as the estimated group risk for Mount Meager debris flows. Friele et al. (2008) estimate a higher number of fatalities (N) for the upper bounds of the largest debris flows. This is attributed to the fact that the largest debris flows reach densely developed areas in the Village of Pemberton.

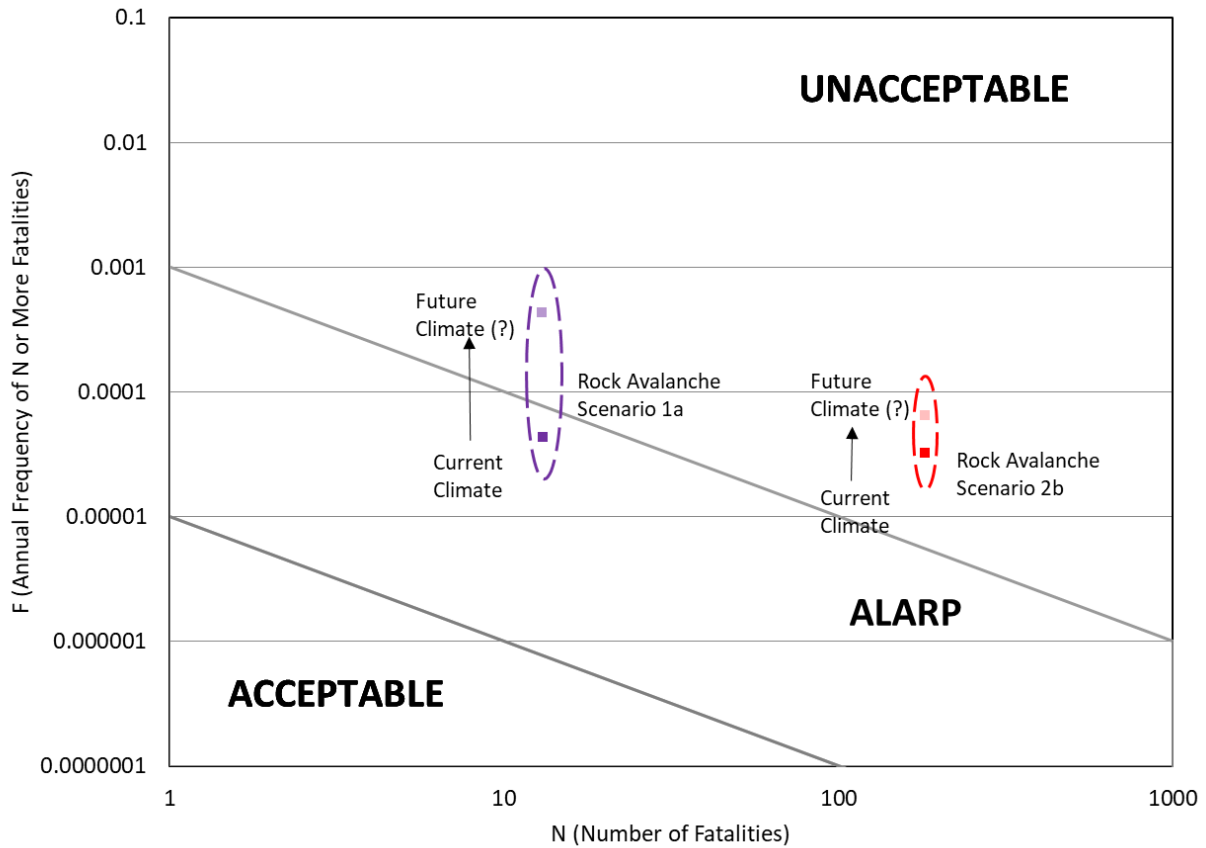


Figure 5-3. F-N curve showing the range of group risk analysis results for Scenarios 1a (purple dots) and 2b (red dots) in the current climate and projected future climate conditions. Note that the latter are associated with substantial uncertainty and are based entirely on judgement. The frequency ranges represented by the ellipses are not based on quantitative analysis, but illustrate subjective ranges in uncertainty in the rock avalanche probability estimates.

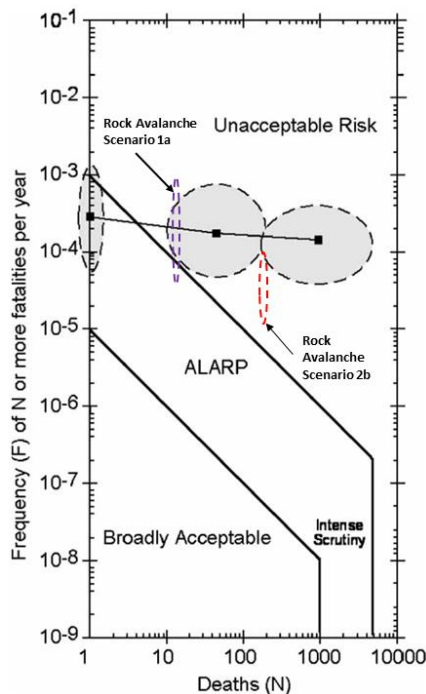


Figure 5-4. F-N plot for group risk for debris flows from Mount Meager (gray shaded ovals represent different debris flow volumes considered in Friele et. al. 2008) with Rock Avalanche Scenario 1a and 2b group risk results from the current study shown for comparison (purple and red ovals). The results of both studies are shown as shaded ovals to indicate uncertainty.

5.6. Human Vulnerability

Drawing 11 shows the spatial distribution of relative human vulnerability for people inside buildings, for Scenario 2b, based on the criteria described in Appendix H. In total, about 160 buildings are subject to maximum flood depths > 1 m above the estimated first floor elevation¹¹. No buildings with maximum flood depths >1 m above the estimated first floor elevation were identified for Scenario 1a.

Human vulnerability to flooding depends on numerous factors. Most of these factors are not considered by the simple criteria described in Appendix H, such as the effects of warning systems, other emergency planning measures, water temperature, ability to swim, health of the individual, and presence of debris. Consequently, the results presented herein should be used with caution and considered only as relative values for the purpose of emergency planning.

5.7. Building Damage

Table 5-2 summarizes total building damage costs for buildings located within the direct landslide impact or splash zone and the flood inundation zone. Building damage costs are estimated based

¹¹ Since most buildings in Pemberton are single story, “top floor” is the same as first floor in most cases.

on the criteria presented in Appendix H. In summary, buildings were assumed as certain to suffer destruction within the direct impact zone, and thus the estimated damage cost corresponds to the total assessed value of improvements within this area. For buildings within the flood inundation zone with higher intensity ($I_{DF} > 1$), the same vulnerability criteria as the splash zone was applied. For areas flooded at lower intensity ($I_{DF} < 1$), BGC estimated direct damages to building structures using flood stage-damage functions.

The estimated direct building damage costs range from \$1.7 million (M) for Scenario 1 to \$12 M for Scenario 2. For comparison, estimated total building value in the risk assessment zone is \$56 M.

It should be emphasized that the estimated building damage costs are based only on a portion of assessed building values and do not include damage to contents or inventory. In addition, costs of cleanup and recovery, are not included. If these were considered, actual damage costs would be much higher. For reference, the Pemberton Valley Dyking District (2016) recently estimated the value of assets potentially at risk of flooding as \$700 M (excluding provincial assets such as highways and power).

Table 5-2. Summary of building consequence estimates.

| Scenario | Zone | Number of Parcels Affected | Building Damage Cost (\$M) |
|----------|-------------------------------|----------------------------|----------------------------|
| 1a | Direct Impact and Splash Zone | 2 | \$1.0 |
| | Inundation | 25 | \$0.7 |
| | Total | 25 | \$1.6 |
| 2b | Direct Impact and Splash Zone | 16 | \$8.2 |
| | Inundation | 139 | \$8.5 |
| | Total | 139 | \$16.0 |

5.8. Business Activity

Table 5-3 summarizes business activity impacts for business located within the risk assessment zone. BGC mapped the distribution of business activity in the risk assessment zone by estimating the total annual revenue for each parcel identified as containing businesses.

Based on the data available, it is not possible to determine the vulnerability of businesses to complete loss of function, and associated economic cost, due to rock avalanche and flooding impacts. For example, a retail store could suffer loss of inventory and business function, whereas a business generating revenue elsewhere could suffer office-related damages without necessarily losing their source of revenue.

As a proxy for level of business impact, BGC summed the annual revenue estimated for parcels impacted by a debris-flood scenario. Additional factors such as indirect losses, damages to business equipment or inventory, interruption of transportation corridors, or effects of prolonged outage, were not estimated.

Table 5-3. Summary of business consequence estimates.

| Debris-flood Scenario | Zone | Number of Businesses Affected | Number of Employees | Annual Revenue (\$M) |
|-----------------------|-------------------------------|-------------------------------|---------------------|----------------------|
| 1a | Direct Impact and Splash Zone | 1 | 6 | \$0.4 |
| | Inundation | 8 | 25 | \$2.0 |
| | Total | 8 | 25 | \$2.0 |
| 2b | Direct Impact and Splash Zone | 7 | 28 | \$3.4 |
| | Inundation | 39 | 175 | \$31.5 |
| | Total | 39 | 175 | \$31.5 |

5.9. Loss of Function

This section summarizes lifelines (roads) and critical facilities located within the direct impact and splash zones that would likely suffer loss of function following impact.

Table 5-4 lists critical facilities listed in Section 4.3 impacted by Scenario 1a and 2b rock avalanche and flooding. The level of damage and functionality of these facilities once impacted is beyond the scope of this assessment. The critical facilities listed include water and sewer infrastructure and facilities near the Pemberton airport. The majority of the other critical facilities listed in Section 4.3 are located within the Village of Pemberton, outside the LiDAR survey and inundation model extents. Flooding to these areas may still occur at relatively shallow depths.

Table 5-4. Summary of critical facilities impacted by Scenario 1 and 2 rock avalanche and flooding.

| Scenario | Hazard | Critical Facilities Impacted |
|----------|----------------|---|
| 1 | Rock Avalanche | Private Sanitary Lift Station (at Big Sky Golf Course) |
| | Flooding | Water Main Sewer Force Main Sanitary Lift Stations (3 private, 1 public) Waste Water Treatment Plant Pemberton Search & Rescue Ministry of Forests Fire Base |
| 2 | Rock Avalanche | Water Main Sewer Force Main Sanitary Lift Station (1 public) Waste Water Treatment Plant (WWTP) WWTP Treated Water Outfall Water Main River Crossing ² Sanitary Forcemain River Crossing ² Water Main from Lil'Wat Nation Pemberton Search & Rescue |

| Scenario | Hazard | Critical Facilities Impacted |
|----------|----------|--|
| | | Ministry of Forests Fire Base |
| | Flooding | Transfer Station Water Main Sewer Force Mains Sanitary Lift Station (3 private, 3 public, 1 strata) Water Booster Station (1 public, 1 strata) Strata Water None identified ¹ |

Note:

1. Potential flooding to critical facilities located in the Village of Pemberton is possible but was beyond inundation model extents and was not assessed as part of the scope of work.
2. Facility is buried 10 m under river bed and may not be impacted. Assessment of the vulnerability of these facilities is beyond the scope of this assessment.

Table 5-5 lists roads impacted by Scenario 1 and 2 rock avalanche and flooding. The sea to sky highway is impacted in Scenario 1 flooding and by Scenario 2 direct landslide impact and flooding. Scenario 1 impacts the highway, Green River forest service road and two other local roads. Scenario 2 impacts the highway and numerous other local roads.

The level of damage and functionality of these roads once impacted is beyond the scope of this assessment. In the emergency response period, evacuation and road closures may also extend beyond the areas directly impacted.

Drawings 8 and 9 indicate that transmission lines and utility lines will also be impacted for Scenarios 1 and 2 (both direct impact and flooding).

Table 5-5. Summary of roads impacted by Scenario 1 and 2 rock avalanche and flooding.

| Scenario | Hazard | Road Impacted |
|----------|----------------|--|
| 1 | Rock Avalanche | Green River Forest Service Road |
| | Flooding | Sea to Sky Highway Green River Forest Service Road Clover Road Airport Road Unnamed dirt roads |
| 2 | Rock Avalanche | Green River Forest Service Road Airport Road Kwesta Road Mount Currie IR 1 Road Sea to Sky Highway Unnamed dirt roads |
| | Flooding | A Avenue Airport Road Artisan Road Carpenter Road Clover Road |


| Scenario | Hazard | Road Impacted |
|----------|--------|---|
| | | Green River Forest Service Road Industrial Way IR 10 Road Kwesta Road Lillooet Lake Road Main Street McKenzie Basin Forest Service Road Mount Currie IR 1 Road Old Mill Road Pemberton Farm Road East Pemberton Way Pinewood Drive Pinewood Place Rancheree Road Rancherie Street Sea to Sky Highway Stone Cutter Place Timberland Road Venture Place Water Street Unnamed dirt roads |

6.0 CONCEPTUAL MITIGATION STRATEGIES

Potential rock avalanches from Mount Currie likely cannot be mitigated at any reasonable cost for two reasons. First, the north face of Mount Currie is too vast and unstable to isolate areas that could be mitigated, for example, by drilling drainage tunnels towards the south. Secondly, unlike for debris flows, where deflection berms or catchment basins can be successful measures for risk reduction, rock avalanches cannot be stopped or slowed without very large-scale earthworks. Those are not feasible in this case as their cost would exceed the values of the elements at risk and would have a lasting effect on the aesthetics and ecosystems in the Green River and Lillooet River valleys.

As engineered mitigation is not practical to reduce risk of rock avalanches at Mount Currie, a monitoring system may be a feasible strategy to manage risk to loss of life. Loss of property, with the potential exception of home contents should evacuations be timely, would be unavoidable in case of a rock avalanche. Numerous monitoring systems exist that could be applied to detect displacement and acceleration of movement. Techniques differentiated by monitoring method, frequency, and required access are listed in Table 6-1.

Table 6-1. Hierarchical approach to potential rock slope monitoring techniques applicable to Mount Currie.

| Relative Risk Level | Monitoring Method | Monitoring Frequency | Access Requirements |
|---------------------|---|--|----------------------|
| Low | Tension crack inspections | Increasing monitoring frequency from once a year to continuous | Via helicopter |
| | Manual reading of crack monitors or surface extensometers | | Via helicopter |
| | Remote radar interferometry | | Remote |
| Moderate | Laser scanners |  | Helicopter or remote |
| | Inclinometers | | Helicopter or remote |
| | Time Domain Reflectometry | | Helicopter or remote |
| | Automated surface extensometers | | Helicopter or remote |
| High | Radar | Real time telemetry (Alert, Alarm, Evacuation) | Remote |
| | Automated surface extensometers with local or remote alarms | | Remote |

An automated data acquisition system (ADAS) could be developed for the monitoring instruments. This system could be installed incrementally on Mount Currie and new component added as further knowledge of the site is gained. ADAS systems typically use radio communication to allow remote downloading of the data loggers from each instrument. The data could be collected in a central database to be overseen by a technical specialist. Remote retrieval of data would be particularly useful during winter months when individual instruments may be difficult to visit due to snow cover. Turtle Mountain, in southeastern Alberta, is a Canadian example where a near real-time early warning monitoring was in place and associated with an emergency response plane for a period of 10 year (Froese and Moreno, 2014). An independent panel of international expert reviewed the data acquired over a 10 year period and recommended that the Turtle Mountain Monitoring Program transitioned to a near-real-time remote monitoring system (Wood et al., 2017a and 2017b).

The overarching idea behind a hierarchical approach to rock slope monitoring is to spend the appropriate effort given the perceived hazard level. Once a change in hazard level has been identified the next higher (or lower) monitoring effort could be initiated. At this stage, BGC recommends the measures listed under Low Hazard. In addition, it would be desirable to complete at least one borehole along the Mount Currie ridge in which instrumentation could be lowered such as thermistor strings and inclinometers as well as borehole telemetry to better characterized rock mass structure. The extraction of the borehole core would also allow the determination of ice content which could, in conjunction with the structural measurement form the basis for numerical rock mass modelling.

The costs of a robust monitoring system even for a Low hazard can be substantial, however, still well below the costs of a statistical life in Canada which ranges between \$ 5 and \$ 10 million (Zhang et al. 2005).

7.0 CONCLUSIONS AND RECOMMENDATIONS

This report provided a landslide risk assessment for the north face of Mount Currie. The types of geohazards within the study area that were considered include: rock avalanches, rock falls, debris flows, rock slides / debris slides, landslide damming and associated flooding. The landslide risk assessment was based on:

- Desktop analysis
- Fieldwork including seismic survey
- Geomorphic mapping
- Rock avalanche probability of occurrence estimate and runout modelling.
- Landslide damming and flood modelling
- Debris flow magnitude-frequency estimate
- Identification and characterization of element at risk
- Vulnerability and risk estimation

7.1. Conclusions

The following key conclusions can be drawn from the above analyses:

1. Mount Currie's morphology and geology lends itself to landsliding and is susceptible to rock avalanches that can travel and impact developed areas, even though no direct evidence of previous events was found on the floodplain or through seismic surveys.
2. Rock slope stability is believed to be influenced, in part, by the assumed existence of permafrost. With climate change, BGC believes that permafrost will degrade and the ice presumed to occur in joint sets melt. This would imply a higher frequency and possibly higher magnitude of rock slope failures in the future. Projected increases in rainfall intensity and frequency could further reduce rock mass strength.
3. Geomorphic mapping and engineering geological characterization allowed the delineation of potential rock avalanche sources zones, two of which were selected for numerical modelling.
4. The numerical modelling results suggest the two rock avalanche scenarios could reach the golf course and airport also potentially blocking the Green and Lillooet rivers. A splash zone (liquefied and displaced floodplain material) was also considered in front of the modelled main rock avalanche deposits.
5. The estimated annual probability of the modeled rock avalanche scenario 1 is approximately 1 in 5,000, or a 0.02% chance of occurrence in any given year while the annual probability of the modelled rock avalanche scenario 2 is approximately 1 in 11,000 or 0.009% chance of occurrence in any given year. These annual probability of occurrence estimates are subject to uncertainty and may be higher or lower than reported. The estimated probability of rock avalanche is expected to be higher under climate change scenarios.
6. BGC modeled flooding associated with the damming of Green and Lillooet rivers by potential rock avalanches and their splash zones. The model suggests that part of the industrial park and a section of the hamlet of Mount Currie could be affected.

7. BGC assessed geohazard risk associated with the direct impact of a rock avalanche and estimated vulnerability for the flooding associated with the damming of the Green and Lillooet rivers. The different approaches are associated with the anticipated response time and vulnerability of the elements at risk to these hazards.
 - a. The risk was calculated for an individual person and for groups of people and compared to risk tolerance criteria developed elsewhere. For the rock avalanche scenarios up to 15 buildings were found to be over the given individual risk tolerance criteria.
 - b. For the flooding hazard, the water depth increases over minutes to hours allowing for people to respond to the hazard. The spatial distribution of vulnerability for people inside buildings was based on the maximum flood depths > 1 m above the estimated first floor elevation. Approximately 160 buildings were identified in the flooding scenario associated with one of the rock avalanche scenarios.
 - c. BGC estimated economic loss in association with direct impact and flooding for building damage (between \$1.6 million and \$16 million) and business activity (between \$2 million and \$31.5 million). Critical infrastructure and lifelines potentially affected by rock avalanche direct impact or flooding include waste water treatment plant, Pemberton search & rescue base, and Ministry of Forest fire base.

7.2. Recommendations

Given the uncertainties and potential risks, additional investigation, analysis, and implementation of a monitoring system likely represent the most practical and cost-effective approach to risk management. This would also allow future refinements or revisions of the current hazard and risk estimates. To further characterize the hazard, it is recommended that the rock mass be investigated including a temperature profile in the tension cracks. Displacement monitoring could provide a better understanding of the current activity of the different sections of Mount Currie. These monitoring measures should be carried out over several years. Specifics of monitoring measures are provided in Section 6.0.

To further characterize the risk associated with the hazard it is recommended to assign individual building IDs and characterize lots at building level of detail (e.g. main house, garage, etc.). Switching to digital building permit records and adopting data management standards that extract information that can be used to determine building vulnerability (e.g. FCL, number of stories, interior area, presence of habitable basement) could be helpful for hazard assessment and for other land use decisions and planning.

It is also recommended to integrate the results from this landslide risk assessment in a total risk framework (i.e., integrate with other geohazards such as floods and lahars) and their consequences.

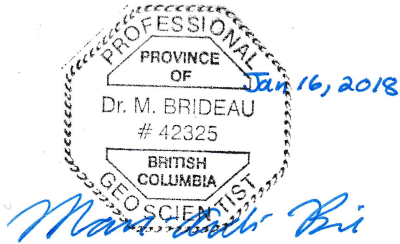
SLRD might consider restricting land use in parts or all of the areas within modeled rock avalanche runout zones as any increase in development density in these areas would further increase the risk estimates.

8.0 CLOSURE

We trust the above satisfies your requirements at this time. Should you have any questions or comments, please do not hesitate to contact us.

Yours sincerely,

BGC ENGINEERING INC.
per:



Marc-André Brideau, Ph.D., P.Geo.
Senior Engineering Geologist

Matthieu Sturzenegger, Ph.D., P.Geo.
Geoscientist

Matthias Jakob, Ph.D., P.Geo.
Principal Geoscientist

Sarah Kimball, M.A.Sc., P.Geo., EIT
Senior Engineering Geologist

Reviewed by:

Kris Holm, M.Sc., P.Geo.
Senior Geoscientist

Derek Kinakin, M.Sc., P.Geo.
Senior Engineering Geologist

MJ/KH/DK/mjp/sjk

REFERENCES

Aaron, J, Hungr, O., 2016. Dynamic simulation of the motion of partially-coherent landslides. *Engineering Geology* 205: 1-11.

Australian Geomechanics Society (AGS), 2007. Guideline for landslide susceptibility, hazard and risk zoning for land use management. *Australian Geomechanics* 42 (1): 13-36.

Bauman, F.W. and Yonin, D., 1994. Terrain stability analysis of the Mount Currie – D’Arcy corridor in southwestern British Columbia. Report completed for the Squamish-Lillooet Regional District

British Columbia Assessment (BCA), 2017. Data provided by BCA via RDCK in Excel Spreadsheet format showing property improvement characteristics and assessed values as of July, 2017, for the Squamish-Lillooet Regional District.

BGC Engineering (BGC), 2017. Quantitative landslide risk assessment, kinematic rock analysis and landslide runout modeling – Mount Currie. Interim Report submitted to the Squamish-Lillooet Regional District, July 2017.

Blais-Stevens, A., 2008. Surficial geology and landslide inventory of the upper Sea to Sky corridor, British Columbia. Geological Survey of Canada, Open File 5324, scale 1:50,000.

Blais-Stevens, A., Hermanns, R. and Jermyn, C., 2011. A 36Cl age determination for Mystery Creek rock avalanche and its implications in the context of hazard assessment, British Columbia, Canada. *Landslides* 8:407–416.

Blais-Stevens, A., Behnia, P., Kremer, M., Page, A., Kung, R. and Bonham-Carter, G., 2012. Landslide susceptibility mapping of the Sea to Sky transportation corridor, British Columbia, Canada: comparison of two methods. *Bulletin of Engineering Geology and the Environment* 71: 447 – 466.

Blikra, L.H., Majala, G., Anda, E., Berg, H., Eikennaes, O., Helgas, G., Oppikofer, T., Hermanns, R., Bohme, M., 2016. Fare- og risikoklassifisering av ustabile fjellparti. Prepared by Norges vassdrags- og energidirektorat, Report Number 77-2016.

Bovis, M.J. and Evans, S.G., 1995. Rock slope movements along the Mount Currie “fault scarp”, southern Coast Mountains, British Columbia. *Canadian Journal of Earth Sciences* 32: 2015 – 2020.

Brideau, M.-A., Shugar, D.H., Wong, C., 2016. Preliminary investigation of the 2014 Vulcan Creek landslide dam, Kluane National Park and Reserve, Yukon. Canadian Geotechnical Conference, Paper

Brückl, E.P., 2001. Cause-effect models of large landslides. *Natural Hazards* 23: 291 – 314.

Bustin, A.M.M., Clowes, R.M., Monger, J.W.H. and Journeay, J.M., 2013. The southern Coast Mountains, British Columbia: New interpretations from geological, seismic reflection, and gravity data. *Canadian Journal of Earth Sciences* 50: 1033-1050.

- Canadian Standard Association (CSA), 1997. Risk management: Guidelines for decision-makers, a national standard of Canada. CAN/CSAQ850-97, 46 pp.
- Clague, J.J. and Souther, J.G., 1982. The Dusty Creek landslide on Mount Cayley, British Columbia. *Canadian Journal of Earth Sciences* **19**: 524 – 539.
- Clague, J.J. and Ward, B., 2011. Pleistocene glaciation of British Columbia. *Developments in Quaternary Science* **15**: 563 – 573.
- Cloutier, C., Locat, J., Geertsema, M., Jakob, M., Schnorbus, M., 2016. Summary of the report Potential Impacts of Climate Change on Landslides Occurrence in Canada. Canadian Geotechnical Conference. Paper.
- Coe, J.A., Bessette-Kirton, E.K., Geertsema, M., 2017. Increasing rock-avalanche size and mobility in Glacier National Park and Preserve, Alaska detected from 1984 to 2016 Landsat imagery. Landslides DOI: 10.1007/s10346-017-0879-7.
- Cruden, D.M., and Hu, X-Q. 1993. Exhaustion and steady state models for predicting landslide hazards in the Canadian Rocky Mountain. *Geomorphology* **8**: 279-285.
- Cruden, D.M. and Hungr, O., 1986. The debris of the Frank Slide and theories of rockslide-avalanche mobility. *Canadian Journal of Earth Sciences* **23**: 425-432.
- Cruden, D.M. and Lu, Z.Y., 1992. The rockslide and debris flow from Mount Cayley, B.C., in June 1984. *Canadian Geotechnical Journal* **29**: 614 – 626.
- Cui, Y., Miller, D., Nixon, G. and Nelson, J. 2015. British Columbia Digital Geology. British Columbia Geological Survey, Open File 2015-2.
- Eisbacher, G.H., 1983. Slope stability and mountain torrents, Fraser Lowlands and Southern Coast Mountains, British Columbia. Field trip guidebook (Trip 15), Geological Association of Canada, Mineralogical Association of Canada, Canada Geophysical Union Joint Annual Meeting, Victoria, May 1983.
- Evans, S.G., 1987. Surface displacement and massive toppling on the northeast ridge of Mount Currie, British Columbia. In: *Current Research, Part A*. Geological Survey of Canada, Paper 87-1A: 181 – 189.
- Evans, S.G. and Brooks, G.R., 1991. Prehistoric debris avalanches from Mount Cayley volcano, British Columbia. *Canadian Journal of Earth Sciences* **28**: 1365 – 1374.
- Evans, S.G. and Brooks, G.R., 1992. Prehistoric debris avalanches from Mount Cayley volcano, British Columbia: Reply. *Canadian Journal of Earth Sciences* **29**: 1343 – 1347.
- Evans, S.G. and Hungr, O., 1993. The assessment of rockfall hazard at the base of talus slopes. *Canadian Geotechnical Journal* **30**: 620 – 636.
- Fournier, G., 2016. 2016 Mount Currie rock fall and local instability. Internal Information Note, File 17275-20, Ministry of Forests, Lands and Natural Resource Operations.

- Friele, P., Jakob, M., Clague, J. 2008. Hazard and risk from large landslides from Mount Meager volcano, British Columbia, Canada. *Georisk*. Vol. 2, No. 1, March 2008, 48-64.
- Froese, C.R., Moreno, F., 2014. Structure and components for the emergency response and warning system on Turtle Mountain, Alberta, Canada. *Natural Hazards* 70: 1689-1712.
- Gischig, V., Preisig, G. and Eberhardt, E., 2016. Numerical investigation of seismically induced rock mass fatigue as a mechanism contributing to the progressive failure of deep-seated landslides. *Rock Mechanics and Rock Engineering* **49** (6): 2457-2478.
- Glastonbury J., and Fell, R. 2010. Geotechnical characteristics of large rapid rock slides. *Canadian Geotechnical Journal* **47**: 116-132.
- Global Greenhouse, 2017. Mountain Permafrost. <http://www.global-greenhouse-warming.com/mountainpermafrost.html>. Access November 26, 2017.
- Gruber, S., 2012. Derivation and analysis of a high-resolution estimate of global permafrost zonation. *The Cryosphere* 6: 221-233.
- Gruber S., Hoelzle, M., Haeberli, W., 2004. Permafrost thaw and destabilization of Alpine rock wall in the hot summer of 2003. *Geophysical Research Letters*, 31: Paper L13504.
- Guthrie, R.H., Evans, S.G., 2007. Work, persistence, and formative events: The geomorphic impact of landslides. *Geomorphology* 88: 266-275.
- Halchuk, S., Allen, T.I., Rogers, G.C., and Adams, J., 2015. Seismic Hazard Earthquake Epicentre File (SHEEF2010) used in the Fifth Generation Seismic Hazard Maps of Canada. Geological Survey of Canada, Open File 7724.1.zip file. doi:10.4095/296908.
- Hensold, G., 2011. An integrated study of deep-seated gravitational slope deformations at Handcar Peak, southwestern British Columbia. Master Thesis, Simon Fraser University, Canada, 145 pp.
- Hermanns, R.L., Oppikofer, T., Anda, E., Blikra, L.H., Bohme, M., Bunkholt, G., Crosta, G.B., Dahle, H., Devoli, G., Fischer, L., Jaboyedoff, M., Loew Simon, Saetre, S., Yugsi Molina, F., 2012. Recommended hazard and risk classification system for large unstable rock slopes in Norway. Prepared by Norges geologiske undersokelse, Report Number 2012.029.
- Hervouet, J.M., Bates, P., 2000. The TELEMAC modelling system, Special Issue. *Hydrological Process*. 14 (13), 2207–2363.
- Hippolyte, J.-C., Bourles, D., Leanni, L., and Braucher, R. 2012. ¹⁰Be ages reveal >12 ka of gravitational movement in a major sackung of the Western Alps (France). *Geomorphology* 171/172: 139-153.
- Holm, K., Bovis, M., Jakob, M., 2004. The landslide response of alpine basins to post-Little Ice Age glacial thinning and retreat in southwestern British Columbia. *Geomorphology* 57: 201-216.

Hong Kong Geotechnical Engineering Office (GEO), 1998. Landslides and Boulder Falls from Natural Terrain: Interim Risk Guidelines. Geo Report 175, Geotechnical Engineering Office, Civil Engineering Department, Hong Kong Special Administrative Region, 184 pp.

Hoovers, 2017. Business Data for Mount Currie and Pemberton purchased from Hoovers Dun & Bradstreet on October 27, 2017.

Huggel, C., Salzmann, N., Allen, S., Caplan-Auerbach, J., Fischer, L., Haeberli, W., Larsen, C., Schneider, D., Wessels, R., 2010. Recent and future warm extreme events and high-mountain slope stability. *Philosophical Transactions of the Royal Society A*, 368: 2435-2459.

Hungr, O., and Evans, S.G. 2004. Entrainment of debris in rock avalanches: An analysis of a long run-out mechanism. *Geological Society of America Bulletin*, 116(9–10): 1240–1252.

Hungr, O., and Evans, S.G. 1996. Rock avalanche runout prediction using a dynamic model. *In Proceedings of the 7th International Symposium on Landslides, Trondheim, Norway. Edited by K. Senneset. A.A. Balkema, Rotterdam, pp. 233–238.*

Hungr, O., Leroueil, S. and Picarelli, L. 2014. Varnes classification of landslide types, an update. *Landslides*, 11: 167-194.

Hungr, O., McDougall, S., Bovis, M., 2005. Entrainment of material by debris flows. In: *Debris-flows Hazards and Related Phenomena*, Jakob, M., Hungr, O. (Eds), pp. 135-155.

Hsu, K.J. 1975. Catastrophic debris streams (sturzstroms) generated by rockfalls. *Geological Society of America Bulletin* 86: 129-140.

International Organization for Standardization (ISO), 2009. Risk management – principles and guidelines, ISO 31000, 24 pp.

IPCC, 2014: Climate Change 2014: Synthesis Report. Fifth Assessment Report of the Intergovernmental Panel on Climate Change. IPCC, Geneva, Switzerland, 151 pp.

ISRM, 1981. Basic geotechnical Description of Rock Masses, *International Journal of Rock Mechanics and Mining Sciences & Geomechanical Abstracts*. 18: 85-110.

ISRM, 1978. Suggested Methods for the Quantitative Description of Discontinuities in Rock Masses. *International Journal of Rock Mechanics and Mining Sciences & Geomechanical Abstracts*, 15: 319-368.

Iverson, R.M., George, D.L., Allstadt, K., Reid, M.E., Collins, B.D., Vallance, J.W., Schilling, S.P., Godt, J.W., Cannon, C.M., Magirl, C.S., Baum, R.L., Coe, J.A., Schulz, W.H., Bower, J.B., 2015. Landslide mobility and hazards: implications of the 2014 Oso disaster. *Earth and Planetary Science Letters* 412: 197-208.

Jaboyedoff, M. and Labiouse, V., 2011. Technical Note: Preliminary estimation of the rockfall runout zones. *Natural Hazards and Earth System Sciences* 11: 819 – 828.

Jackson, L.E. Jr. 2002. Landslides and landscape evolution in the Rocky Mountains and adjacent Foothills area, southwestern Alberta, Canada. *Reviews in Engineering Geology* XV: 325-344.

- Jakob, M., 1996. Morphometric and geotechnical controls of debris flow frequency and magnitude in southwestern British Columbia. Ph. D. Thesis, University of British Columbia, Canada, 232 pp.
- Jakob, M., Stein D., Ulmi, M. 2011. Vulnerability of buildings to debris flow impact. *Natural Hazards*. DOI 10.1007/s11069-011-0007-2.
- Jakob, M., Bale, S., McDougall, S. and Friele, P., 2016. Regional debris-flow and debris-flood frequency-magnitude curves. In *Proceedings of GeoVancouver 2016 Conference*, Vancouver, Canada, October 2016.
- Journey, J.M. and Monger, J.W.H., 1994. Geology and crustal structure of the southern Coast and Intermontane Belts, southern Canadian Cordillera, British Columbia. Geological Survey of Canada, Open File 2490, scale 1:500,000.
- Keefer, D.K., 1984. Landslides caused by earthquakes. *Geological Society of America Bulletin* **95**: 406 – 421.
- Keefer, D.K., 2002. Investigating landslides caused by earthquakes – A historical review. *Survey in Geophysics* **23**: 473 – 510.
- Loye, A., Jaboyedoff, M., Pedrazzini, A., 2009. Identification of potential rockfall source areas at a regional scale using a DEM-based geomorphometric analysis. *Natural Hazards and Earth System Sciences* 9:1643–1653.
- Marinos, P.G., Marinos, V., and Hoek, E. 2007. The Geological Strength Index (GSI): A characterization tool for assessing engineering properties for rock masses. In: *International Workshop on Rock Mass Classification in Underground Mining*, Mark, C., Pakalnis, R., Tuchman, R.J. (Eds), NIOSH Information Circular 9498, pp. 878-94.
- Marinos, V., Marinos, P., and Hoek, E. 2005. The Geological Strength Index; Application and Limitations. *Bulletin of Engineering Geology and the Environment*. **64**: 55-65.
- Mathews, W.H., McTaggart, K.C., 1978. Hope rockslides, British Columbia, Canada. In: Voight, B. (Ed.), *Rockslides and Avalanches*, Elsevier: 259 – 275.
- McDougall, S. 2006. A new continuum dynamic model for the analysis of extremely rapid landslide motion across complex 3D terrain. Ph.D. thesis, The University of British Columbia, Vancouver, B.C.
- McDougall, S., Hungr, O., 2004. A model for the analysis of rapid landslide motion across three-dimensional terrain. *Canadian Geotechnical Journal* 41: 1084-1097.
- McDougall, S., Boulton, N., Hungr, O., Stead, D., Schwab, J.W., 2006. The Zymoetz River landslide, British Columbia, Canada: description and dynamic analysis of a rock slide-debris flow. *Landslides* 3: 195-204.
- McDougall, S., 2017. Landslide runout analysis – current practice and challenges. *Canadian Geotechnical Journal* 54: 605-620.

Ministry of Environment (British Columbia), accessed on June 1, 2017. BC water resource atlas and the WELLS database. <http://maps.gov.bc.ca/ess/sv/wrbc/>.

MFLNRO, 2013. Permafrost distribution model from the BC Ministry of Forests, Lands, and Natural Resource Operations. Unpublished.

Ministry of Forests, Lands and Natural Resource Operations (MFLNRO), 2016. Biogeoclimatic ecosystem classification subzone/variant map for the Sea to Sky Resource District, South Coast Region. Government of British Columbia.

National Earthquake Database (NEDB), accessed on May 16, 2017. <http://www.earthquakescanada.nrcan.gc.ca/stdon/NEDB-BNDS/bull-en.php>.

Noetzli, J., Gruber, S., 2009. Transient thermal effects in Alpine permafrost. *Cryosphere* 3: 85-99.

Noetzli, J., Luethi, R., and Staub, B. (eds.), 2016. Permafrost in Switzerland 2010/2011 to 2013/2014. Glaciological Report (Permafrost) No. 12-15 of the Cryospheric Commission of the Swiss Academy of Sciences, 85 pp.

Pacific Climate Impacts Consortium (PCIC), 2017, accessed on May 19, 2017. <https://pacificclimate.org/data/bc-station-data>.

Pedrazzini, A., Jaboyedoff, M., Loye, A., and Derron, M.-H. 2013. From deep seated slope deformation to rock avalanche: destabilization and transportation models of the Sierre landslide (Switzerland). *Tectonophysics* 605: 149-198.

Pemberton Valley Dyking District (PVDD), 2016. National Disaster Mitigation Program Project Proposal Form dated October 7, 2016.

Prein, A., Rasmussen, R.M., Ikeda, K., Changhi L., Clark, M.P., Holland, G.J., 2016. The future intensification of hourly precipitation extremes. *Nature Climate Change*. DOI 10.1038.

Reed, D.W., 2002. Reinforcing flood-risk estimation. *Philosophical transactions-Royal Society. Mathematical, physical and engineering sciences*, 360(1796), pp.1373-1387.

Riahi, K., Rao, S., Krey, V., Cho, C., Chirkov, V., Fisher, G., Kindermann, G., 2011. RCP 8.5 – A scenario of comparatively high greenhouse gas emissions. *Climate change* 109: 33-57.

Roddick, J.A. and Hutchison, W.W., 1973. Pemberton (east half) map-area, British Columbia. Geological Survey of Canada, Map 13-1973 and Paper 73-17.

Savigny, K.W. and Clague, J.J., 1992. Technical tour no. 2; Fraser Valley and Fraser Canyon areas. Technical Tour Guidebook, Geohazard '92. BiTech Publishers: 47 – 99.

SLRD 201

Statistics Canada, 2009. Mortality, Summary List of Causes. Catalogue no. 84F0209X.

Statistics Canada, 2017. Pemberton [Population centre], British Columbia and British Columbia [Province] (table). Census Profile. 2016 Census. Statistics Canada Catalogue no. 98-316-

X2016001. Ottawa. Released May 3, 2017.
<http://www12.statcan.gc.ca/census-recensement/2016/dp-pd/prof/index.cfm?Lang=E> (accessed June 29, 2017).

Sturzenegger, M., Stead, D., Gosse, J., Ward, B. and Froese, C., 2015. Reconstruction of the history of the Palliser Rockslide based on ³⁶Cl terrestrial cosmogenic nuclide dating and debris volume estimations. *Landslides*, **12** (6): 1097-1106.

Thompson, S.C., Clague, J.J., Evans, S.G., 1997. Holocene activity of the Mount Currie scarp, Coast Mountains, British Columbia, and implications for its origin. *Environmental & Engineering Geoscience*, **3** (3): 329 – 348.

VanDine, D., 2012. Risk management - Canadian technical guidelines and best practices related to landslides: a national initiative for loss reduction. Geological Survey of Canada, Open File 6996.

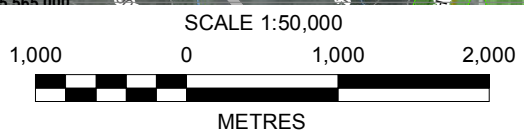
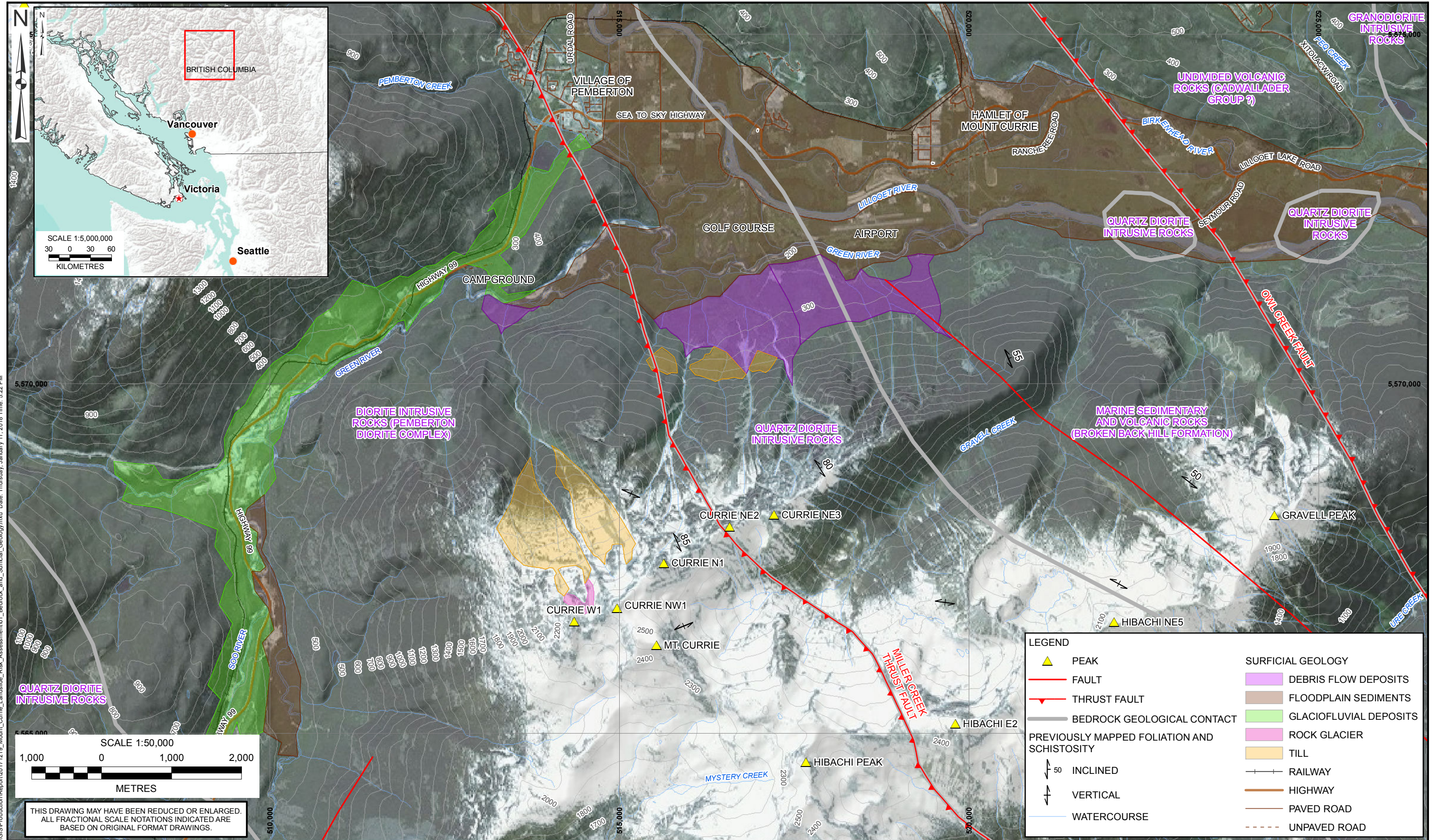
Wood, D.E., Chao, D.K., Guo, J.F., and Shipman, T.C. 2017. AER/AGS Roles and Responsibilities Manual for the Turtle Mountain Monitoring Program, Alberta; Alberta Energy Regulator, AER/AGS Open File Report 2017-04, 38 p.

Wood, D.E., Chao, D.K., and Shipman, T.C. 2017b, Turtle Mountain Field Laboratory, Alberta (NTS 82G): 2015 data and activity summary; Alberta Energy Regulator, AER/AGS Open File Report 2017-03, 21 p.

Woodsworth, G.J., 1977. Geology – Pemberton (92J) map-area. Geological Survey of Canada, Open File 482, scale 1:250,000.

Zhang, A., Boardman, A.E., Gillen, D., Waters, W.G., 2005. Towards estimating the social and environmental costs of transportation in Canada. Revised report issued to Transport Canada September 2005.

DRAWINGS



THIS DRAWING MAY HAVE BEEN REDUCED OR ENLARGED.
ALL FRACTIONAL SCALE NOTATIONS INDICATED ARE
BASED ON ORIGINAL FORMAT DRAWINGS.

X:\Projects\1358\004_Mt_Currie\GIS\Production\Report\20171219_Mount_Currie_Landslide_Risk_Assessment01_Bedrock_and_Surficial_Geology.mxd Date: Thursday, January 11, 2018 Time: 5:22 PM

- NOTES:
1. ALL DIMENSIONS ARE IN METRES UNLESS OTHERWISE NOTED.
 2. THIS DRAWING MUST BE READ IN CONJUNCTION WITH BGC'S REPORT TITLED "MOUNT CURRIE LANDSLIDE RISK ASSESSMENT", AND DATED JANUARY 2018.
 3. SURFICIAL GEOLOGY FROM BLAIS-STEVENS (2008) AND COMPLETED BY BGC ON THE NORTH FACE OF MT. CURRIE.
 4. GEOLOGY FROM JOURNEAY AND MONGER (1994); FOLIATION AND SCHISTOSITY INDICATORS FROM WOODSWORTH (1977).
 5. IMAGERY FROM ESRI WORLD IMAGERY BASEMAP SERVICE.
 6. BASE TOPOGRAPHIC DATA BASED ON CANADIAN DIGITAL ELEVATION DATA (CDED) 25 m. CONTOUR INTERVAL IS 100 m.
 7. PROJECTION IS NAD 1983 UTM ZONE 10N.
 8. UNLESS BGC AGREES OTHERWISE IN WRITING, THIS DRAWING SHALL NOT BE MODIFIED OR USED FOR ANY PURPOSE OTHER THAN THE PURPOSE FOR WHICH BGC GENERATED IT. BGC SHALL HAVE NO LIABILITY FOR ANY DAMAGES OR LOSS ARISING IN ANY WAY FROM ANY USE OR MODIFICATION OF THIS DOCUMENT NOT AUTHORIZED BY BGC. ANY USE OF OR RELIANCE UPON THIS DOCUMENT OR ITS CONTENT BY THIRD PARTIES SHALL BE AT SUCH THIRD PARTIES' SOLE RISK.

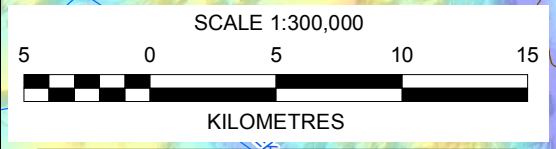
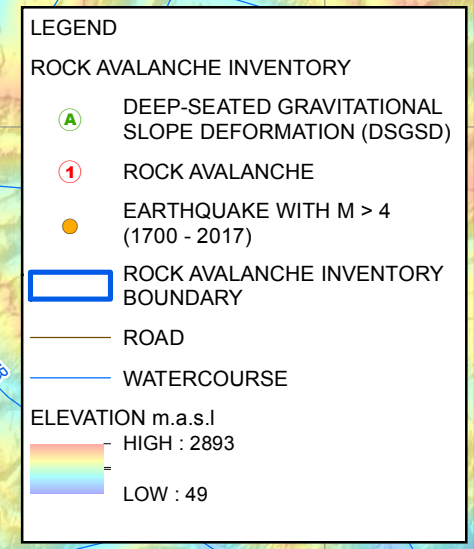
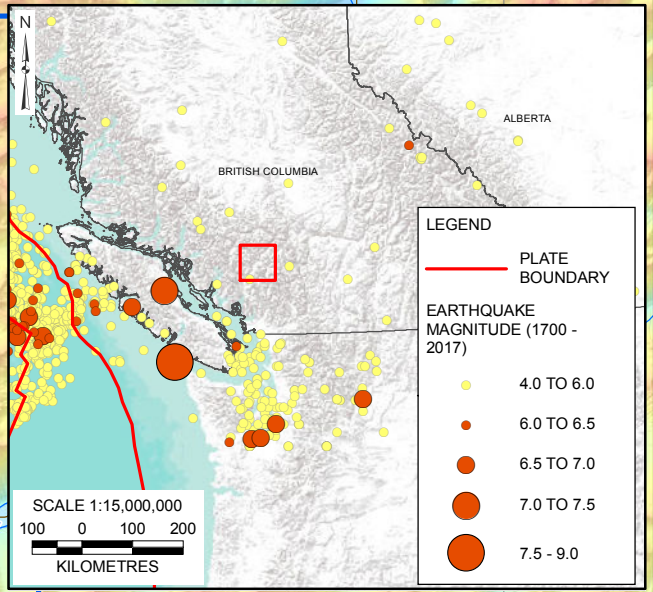
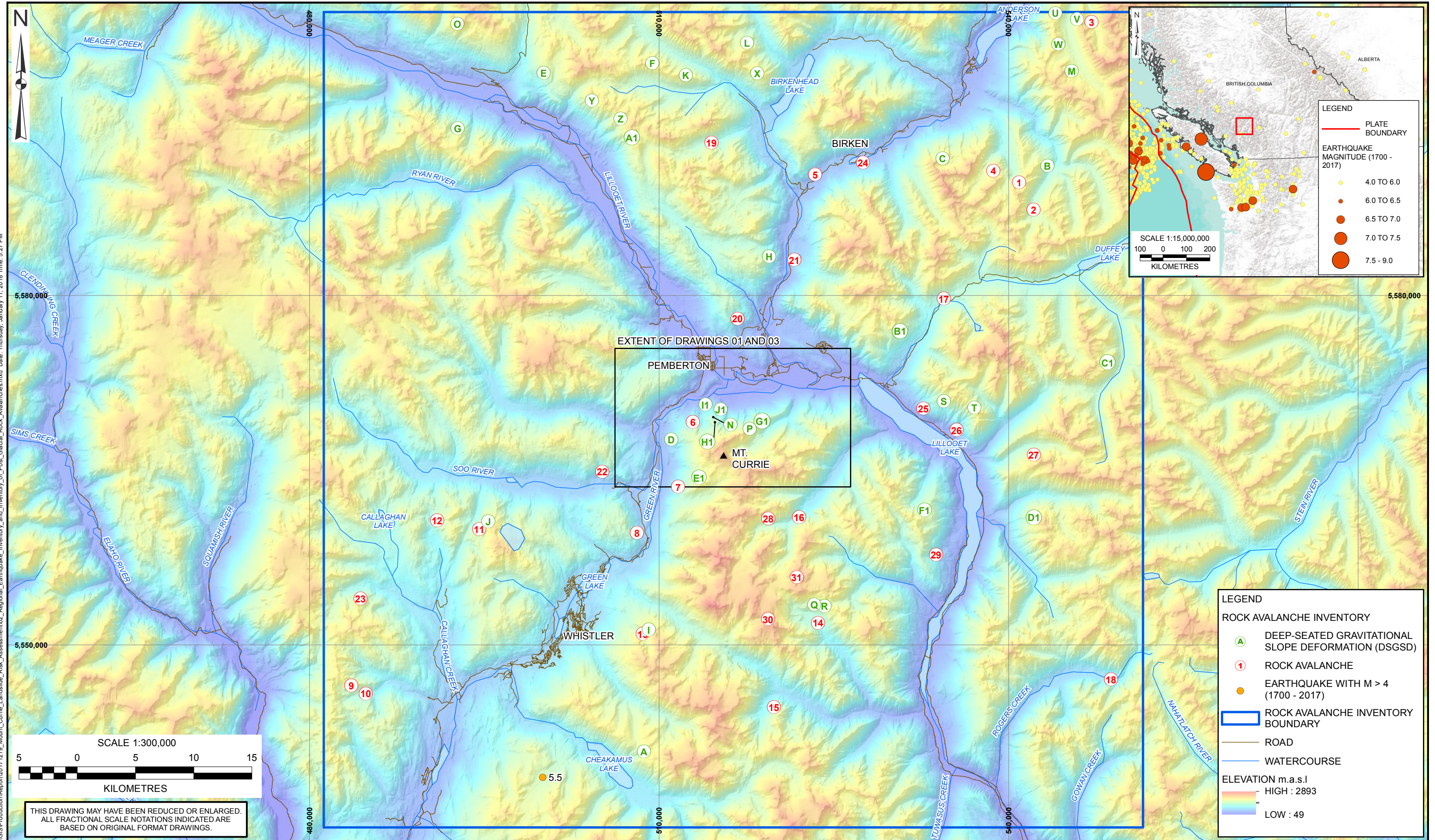
| | |
|-----------|--------------|
| SCALE: | 1:50,000 |
| DATE: | JAN 2018 |
| DRAWN: | LL, MIB, JDC |
| CHECKED: | MS |
| APPROVED: | MAB |

BIGC BGC ENGINEERING INC.
AN APPLIED EARTH SCIENCES COMPANY

CLIENT:
SQUAMISH-LILLOOET REGIONAL DISTRICT (SLRD)

| | | |
|--------------|---|----------|
| PROJECT: | MOUNT CURRIE LANDSLIDE RISK ASSESSMENT | |
| TITLE: | BEDROCK AND SURFICIAL GEOLOGY | |
| PROJECT No.: | 1358004 | DWG No.: |
| | | 01 |

X:\Projects\1368\004_Mt_Currie\GIS\Production\Report\20171219_Mount_Currie_Landslide_Risk_Assessment02_Regional_Earthquake_Inventory_and_Inventory_of_Post-Glacial_Rock_Avalanches.mxd Date: Thursday, January 11, 2018 Time: 5:27 PM



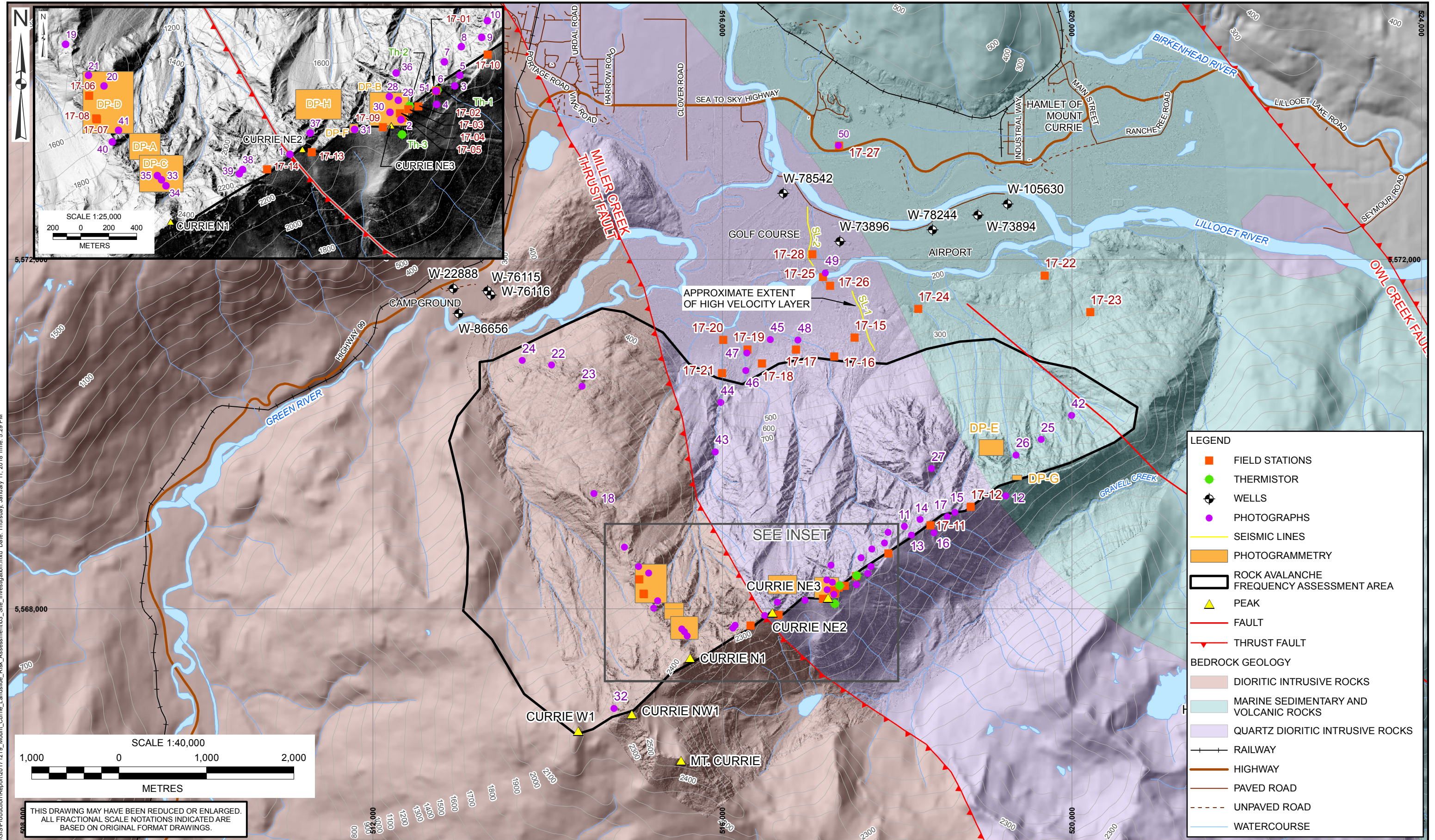
THIS DRAWING MAY HAVE BEEN REDUCED OR ENLARGED.
 ALL FRACTIONAL SCALE NOTATIONS INDICATED ARE
 BASED ON ORIGINAL FORMAT DRAWINGS.

NOTES:
 1. ALL DIMENSIONS ARE IN METRES UNLESS OTHERWISE NOTED.
 2. THIS DRAWING MUST BE READ IN CONJUNCTION WITH BGC'S REPORT TITLED "MOUNT CURRIE LANDSLIDE RISK ASSESSMENT", AND DATED JANUARY 2018.
 3. EARTHQUAKE DATA FROM HALCHUK ET AL., 2015 AND NECB, 2017.
 4. BASE TOPOGRAPHIC DATA BASED ON CANADIAN DIGITAL ELEVATION DATA (CDED) 25m DEM.
 5. ROCK AVALANCHE AND DEEP-SEATED GRAVITATIONAL SLOPE DEFORMATION DETAILS IN APPENDIX A.
 6. PROJECTION IS NAD 1983 UTM ZONE 10N.
 7. UNLESS BGC AGREES OTHERWISE IN WRITING, THIS DRAWING SHALL NOT BE MODIFIED OR USED FOR ANY PURPOSE OTHER THAN THE PURPOSE FOR WHICH BGC GENERATED IT. BGC SHALL HAVE NO LIABILITY FOR ANY DAMAGES OR LOSS ARISING IN ANY WAY FROM ANY USE OR MODIFICATION OF THIS DOCUMENT NOT AUTHORIZED BY BGC. ANY USE OF OR RELIANCE UPON THIS DOCUMENT OR ITS CONTENT BY THIRD PARTIES SHALL BE AT SUCH THIRD PARTIES' SOLE RISK.

SCALE: 1:300,000
 DATE: JAN 2018
 DRAWN: LL, MIB, JDC
 CHECKED: MS
 APPROVED: MAB

BIGC BGC ENGINEERING INC.
 AN APPLIED EARTH SCIENCES COMPANY
 CLIENT:
 SQUAMISH-LILLOOET REGIONAL DISTRICT (SLRD)

PROJECT: MOUNT CURRIE LANDSLIDE RISK ASSESSMENT
 TITLE: REGIONAL EARTHQUAKE INVENTORY AND INVENTORY OF POST-GLACIAL ROCK AVALANCHES
 PROJECT No.: 1358004
 DWG No.: 02



X:\Projects\1358\004_Mt_Currie\GIS\Production\Report\20171219_Mount_Currie_Landslide_Risk_Assessment\03_Site_Investigation.mxd Date: Thursday, January 11, 2018 Time: 5:29 PM

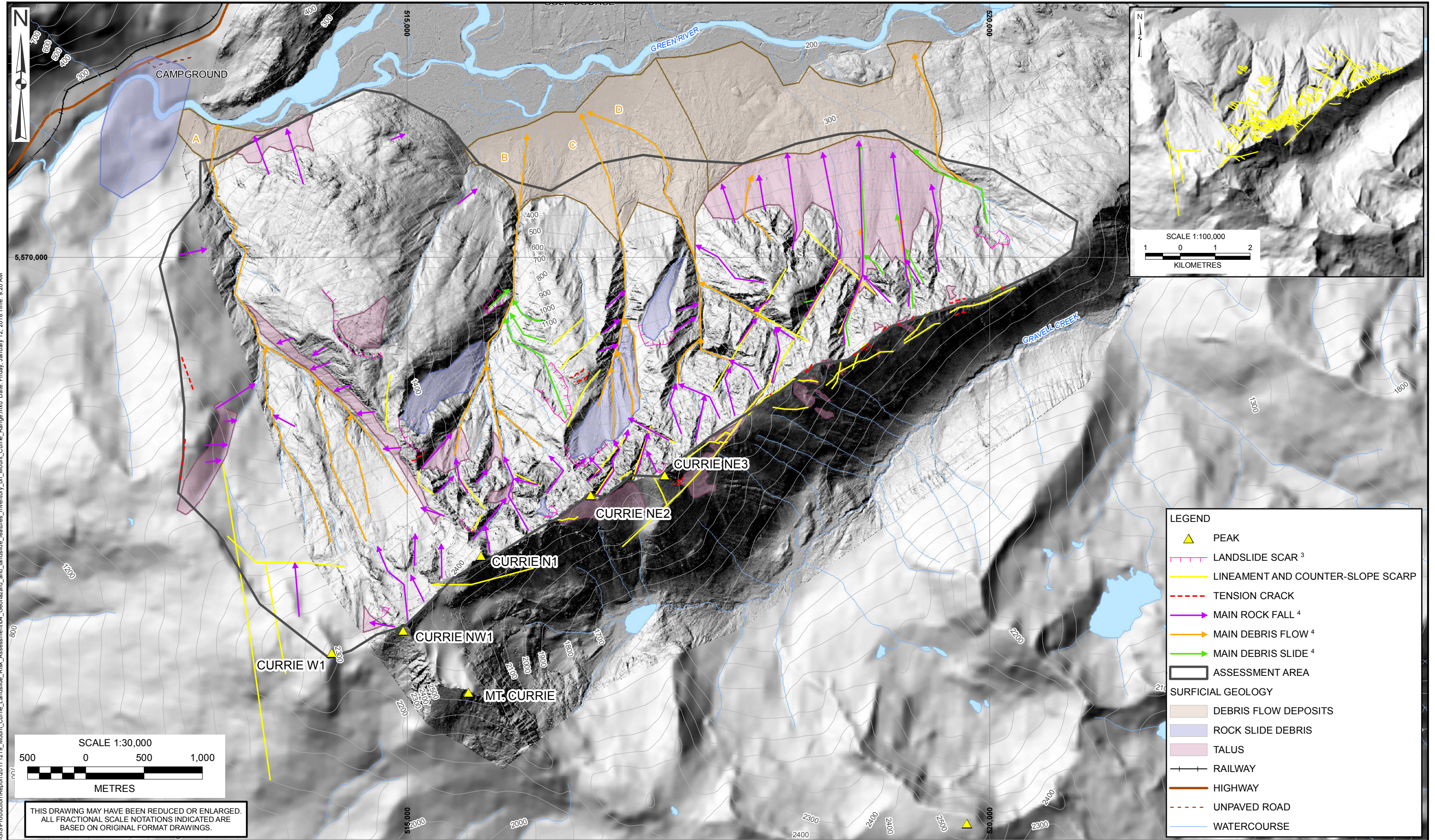
- NOTES:
1. ALL DIMENSIONS ARE IN METRES UNLESS OTHERWISE NOTED.
 2. THIS DRAWING MUST BE READ IN CONJUNCTION WITH BGC'S REPORT TITLED "MOUNT CURRIE LANDSLIDE RISK ASSESSMENT", AND DATED JANUARY 2018.
 3. SURFICIAL GEOLOGY FROM BLAIS-STEVENS (2008) AND COMPLETED BY BGC ON THE NORTH FACE OF MT CURRIE.
 4. GEOLOGY FROM JOURNEY AND MONGER (1994); FOLIATION AND SCHISTOSITY INDICATORS FROM WOODSWORTH (1977).
 5. WELLS ARE FROM BC MINISTRY OF ENVIRONMENT WELL DATABASE.
 6. BASE TOPOGRAPHIC DATA BASED ON LIDAR PROVIDED BY MCELHANNEY DATED AUGUST 26, 2017, AND CANADIAN DIGITAL ELEVATION DATA (CDED) 25 m. CONTOUR INTERVAL IS 100 m.
 7. PROJECTION IS NAD 1983 UTM ZONE 10N.
 8. UNLESS BGC AGREES OTHERWISE IN WRITING, THIS DRAWING SHALL NOT BE MODIFIED OR USED FOR ANY PURPOSE OTHER THAN THE PURPOSE FOR WHICH BGC GENERATED IT. BGC SHALL HAVE NO LIABILITY FOR ANY DAMAGES OR LOSS ARISING IN ANY WAY FROM ANY USE OR MODIFICATION OF THIS DOCUMENT NOT AUTHORIZED BY BGC. ANY USE OF OR RELIANCE UPON THIS DOCUMENT OR ITS CONTENT BY THIRD PARTIES SHALL BE AT SUCH THIRD PARTIES' SOLE RISK.

| | |
|-----------|----------|
| SCALE: | 1:40,000 |
| DATE: | JAN 2018 |
| DRAWN: | JDC |
| CHECKED: | MAB |
| APPROVED: | MAB |

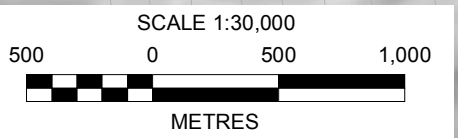
BIGC BGC ENGINEERING INC.
 AN APPLIED EARTH SCIENCES COMPANY

CLIENT:
 SQUAMISH-LILLOOET REGIONAL DISTRICT (SLRD)

| | | |
|--------------|--|----------|
| PROJECT: | MOUNT CURRIE LANDSLIDE RISK ASSESSMENT | |
| TITLE: | SITE INVESTIGATION | |
| PROJECT No.: | 1358004 | DWG No.: |
| | | 03 |



X:\Projects\1358\004_Mt_Currie\GIS\Production\Report\20171219_Mount_Currie_Landslide_Risk_Assessment\04_Geohazard_and_Landslide_Features_Inventory_on_Mount_Currie_Range.mxd Date: Friday, January 12, 2018 Time: 9:20 AM



THIS DRAWING MAY HAVE BEEN REDUCED OR ENLARGED.
ALL FRACTIONAL SCALE NOTATIONS INDICATED ARE
BASED ON ORIGINAL FORMAT DRAWINGS.

NOTES:

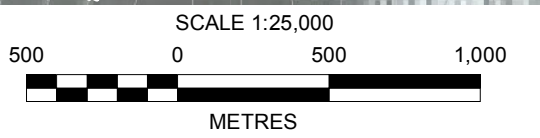
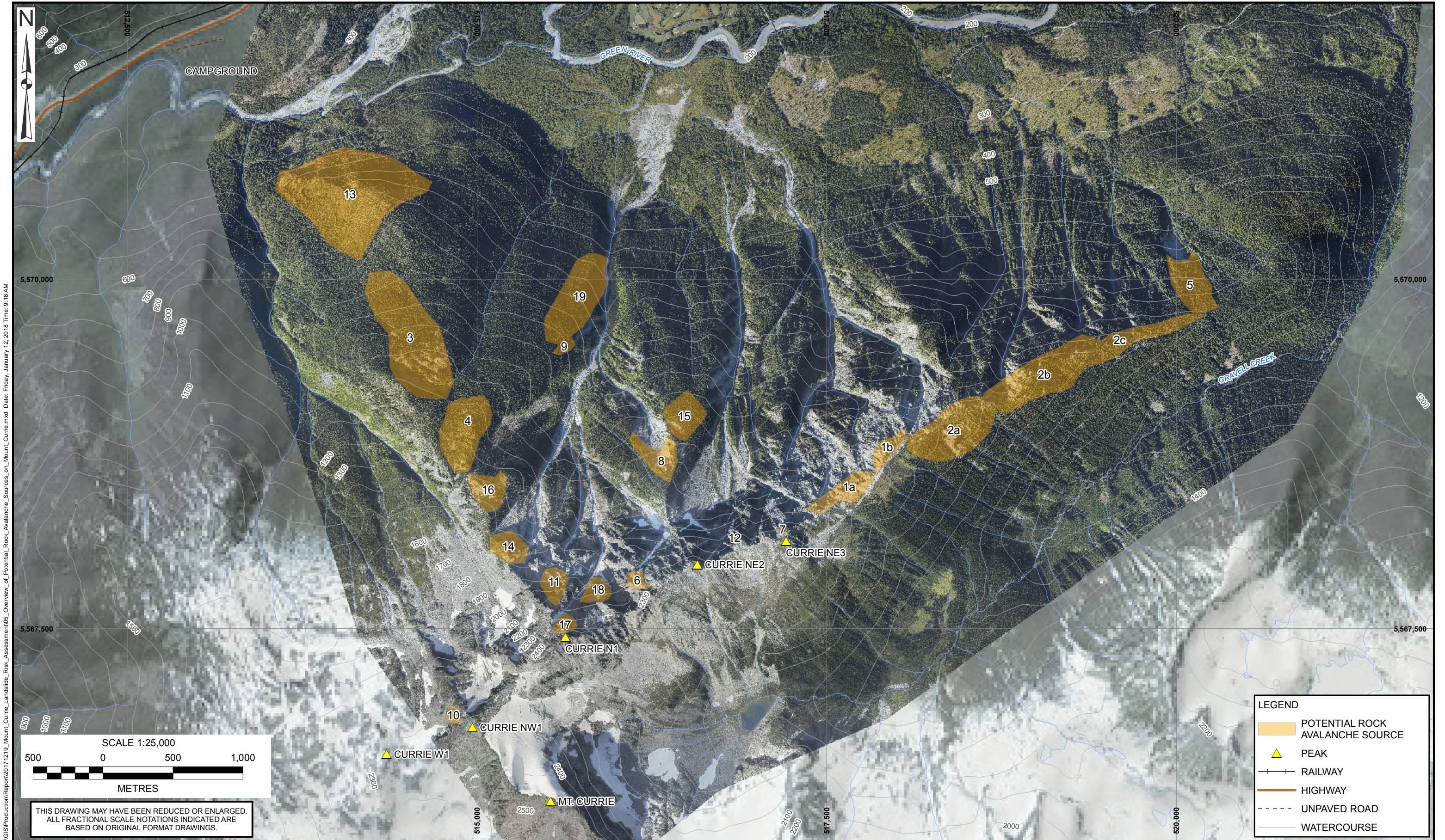
1. ALL DIMENSIONS ARE IN METRES UNLESS OTHERWISE NOTED.
2. THIS DRAWING MUST BE READ IN CONJUNCTION WITH BGC'S REPORT TITLED "MOUNT CURRIE LANDSLIDE RISK ASSESSMENT", AND DATED JANUARY 2018.
3. LANDSLIDE SCARS ARE INTERPRETED AS THE LOCATION OF A SINGLE EVENT.
4. THE ROCK FALL, DEBRIS FLOW AND DEBRIS SLIDE ARROWS INDICATE THE LOCATION AND PATH OF OBSERVED OR INFERRED EVENTS.
5. BASE TOPOGRAPHIC DATA BASED ON LIDAR PROVIDED BY MCELHANNY DATED AUGUST 26, 2017, AND CANADIAN DIGITAL ELEVATION DATA (CDED) 25 m. CONTOUR INTERVAL IS 100 m.
6. PROJECTION IS NAD 1983 UTM ZONE 10N.
7. UNLESS BGC AGREES OTHERWISE IN WRITING, THIS DRAWING SHALL NOT BE MODIFIED OR USED FOR ANY PURPOSE OTHER THAN THE PURPOSE FOR WHICH BGC GENERATED IT. BGC SHALL HAVE NO LIABILITY FOR ANY DAMAGES OR LOSS ARISING IN ANY WAY FROM ANY USE OR MODIFICATION OF THIS DOCUMENT NOT AUTHORIZED BY BGC. ANY USE OF OR RELIANCE UPON THIS DOCUMENT OR ITS CONTENT BY THIRD PARTIES SHALL BE AT SUCH THIRD PARTIES' SOLE RISK.

| | |
|-----------|----------|
| SCALE: | 1:30,000 |
| DATE: | JAN 2018 |
| DRAWN: | JDC |
| CHECKED: | MAB |
| APPROVED: | MAB |

BGC ENGINEERING INC.
AN APPLIED EARTH SCIENCES COMPANY

CLIENT:
SQUAMISH-LILLOOET REGIONAL DISTRICT (SLRD)

| | |
|---|----------|
| PROJECT: MOUNT CURRIE LANDSLIDE RISK ASSESSMENT | |
| TITLE: GEOHAZARD AND LANDSLIDE FEATURES INVENTORY ON MOUNT CURRIE | |
| PROJECT No.: | DWG No.: |
| 1358004 | 04 |



THIS DRAWING MAY HAVE BEEN REDUCED OR ENLARGED.
ALL FRACTIONAL SCALE NOTATIONS INDICATED ARE
BASED ON ORIGINAL FORMAT DRAWINGS.

| LEGEND | |
|--------|---------------------------------|
| | POTENTIAL ROCK AVALANCHE SOURCE |
| | PEAK |
| | RAILWAY |
| | HIGHWAY |
| | UNPAVED ROAD |
| | WATERCOURSE |

NOTES:
 1. ALL DIMENSIONS ARE IN METRES UNLESS OTHERWISE NOTED.
 2. THIS DRAWING MUST BE READ IN CONJUNCTION WITH BGC'S REPORT TITLED "MOUNT CURRIE LANDSLIDE RISK ASSESSMENT", AND DATED JANUARY 2018.
 3. ORTHOPHOTO PROVIDED BY MCELHANNEY AND DATED AUGUST 26, 2017. BACKGROUND IMAGERY FROM ESRI WORLD_IMAGERY BASEMAP SERVICE.
 4. BASE TOPOGRAPHIC DATA BASED ON CANADIAN DIGITAL ELEVATION DATA (CDED) 25 m. CONTOUR INTERVAL IS 100 m.
 5. PROJECTION IS NAD 1983 UTM ZONE 10N.
 6. UNLESS BGC AGREES OTHERWISE IN WRITING, THIS DRAWING SHALL NOT BE MODIFIED OR USED FOR ANY PURPOSE OTHER THAN THE PURPOSE FOR WHICH BGC GENERATED IT. BGC SHALL HAVE NO LIABILITY FOR ANY DAMAGES OR LOSS ARISING IN ANY WAY FROM ANY USE OR MODIFICATION OF THIS DOCUMENT NOT AUTHORIZED BY BGC. ANY USE OF OR RELIANCE UPON THIS DOCUMENT OR ITS CONTENT BY THIRD PARTIES SHALL BE AT SUCH THIRD PARTIES' SOLE RISK.

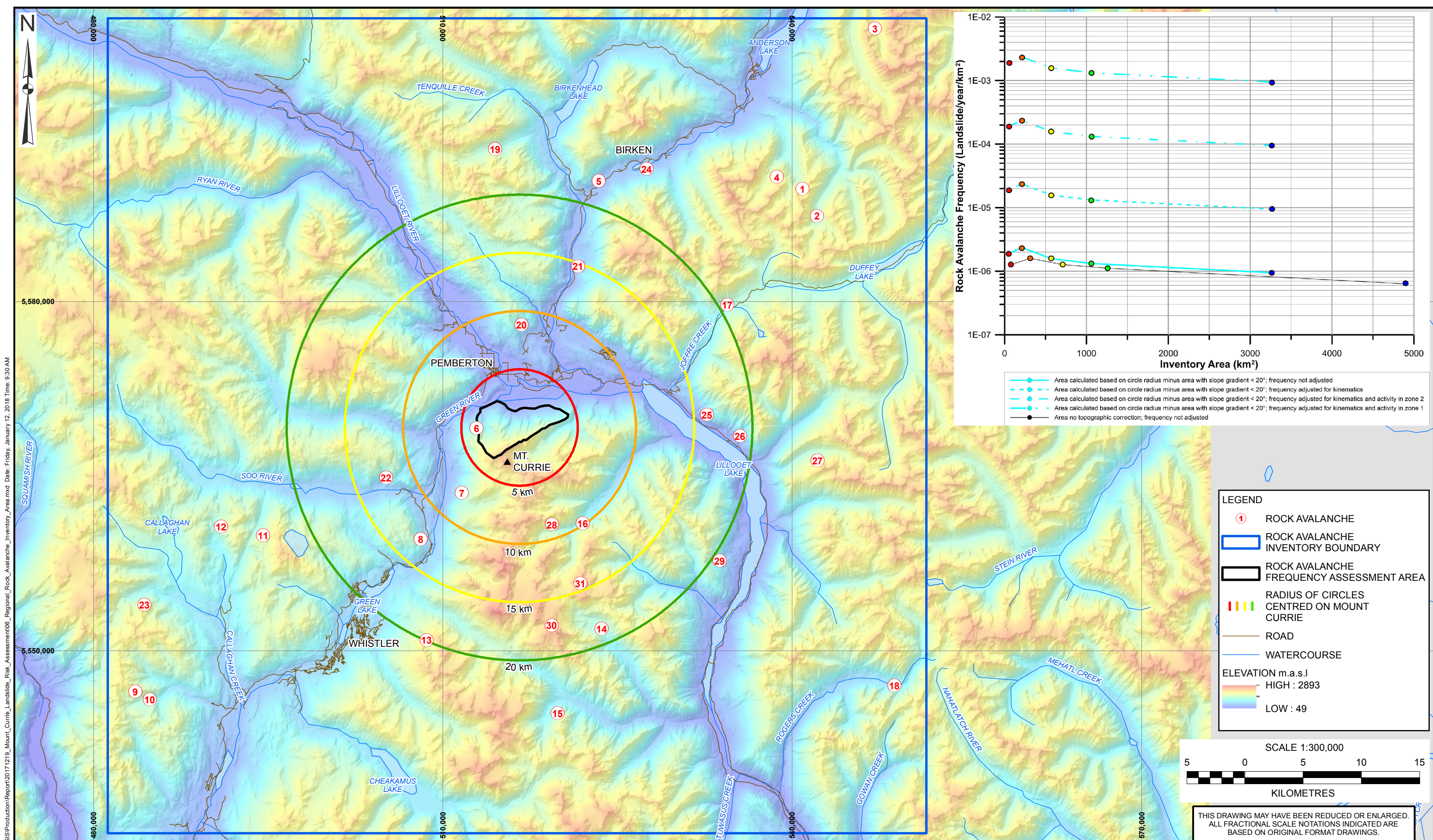
| | |
|-----------|----------|
| SCALE: | 1:25,000 |
| DATE: | JAN 2018 |
| DRAWN: | JDC |
| CHECKED: | MAB |
| APPROVED: | MAB |

BGC ENGINEERING INC.
 AN APPLIED EARTH SCIENCES COMPANY

CLIENT:
 SQUAMISH-LILLOOET REGIONAL DISTRICT (SLRD)

| | |
|---|----------|
| PROJECT: MOUNT CURRIE LANDSLIDE RISK ASSESSMENT | |
| TITLE: OVERVIEW OF POTENTIAL ROCK AVALANCHE SOURCES ON MOUNT CURRIE | |
| PROJECT No.: | DWG No.: |
| 1358004 | 05 |

X:\Projects\1358\004_Mt_Currie\GIS\Production\Report\20171219_Mount_Currie_Landslide_Risk_Assessment05_Overview_of_Potential_Rock_Avalanche_Sources_on_Mount_Currie.mxd Date: Friday, January 12, 2018 Time: 9:18 AM



X:\Projects\1358\004_Mt_Currie\GIS\Production\Report\20171219_Mount_Currie_Landslide_Risk_Assessment\06_Regional_Rock_Avalanche_Inventory_Area.mxd Date: Friday, January 12, 2018 Time: 9:30 AM

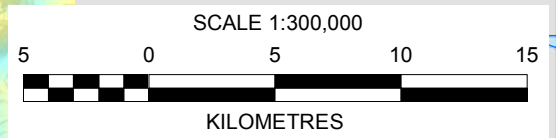
NOTES:
 1. ALL DIMENSIONS ARE IN METRES UNLESS OTHERWISE NOTED.
 2. THIS DRAWING MUST BE READ IN CONJUNCTION WITH BGC'S REPORT TITLED "MOUNT CURRIE LANDSLIDE RISK ASSESSMENT", AND DATED JANUARY 2018.
 3. BASE TOPOGRAPHIC DATA BASED ON CANADIAN DIGITAL ELEVATION DATA (CDED) 25m DEM.
 4. PROJECTION IS NAD 1983 UTM ZONE 10N.
 5. UNLESS BGC AGREES OTHERWISE IN WRITING, THIS DRAWING SHALL NOT BE MODIFIED OR USED FOR ANY PURPOSE OTHER THAN THE PURPOSE FOR WHICH BGC GENERATED IT. BGC SHALL HAVE NO LIABILITY FOR ANY DAMAGES OR LOSS ARISING IN ANY WAY FROM ANY USE OR MODIFICATION OF THIS DOCUMENT NOT AUTHORIZED BY BGC. ANY USE OF OR RELIANCE UPON THIS DOCUMENT OR ITS CONTENT BY THIRD PARTIES SHALL BE AT SUCH THIRD PARTIES' SOLE RISK.

SCALE: 1:300,000
 DATE: JAN 2018
 DRAWN: LL, MIB, JDC
 CHECKED: MAB
 APPROVED: MAB

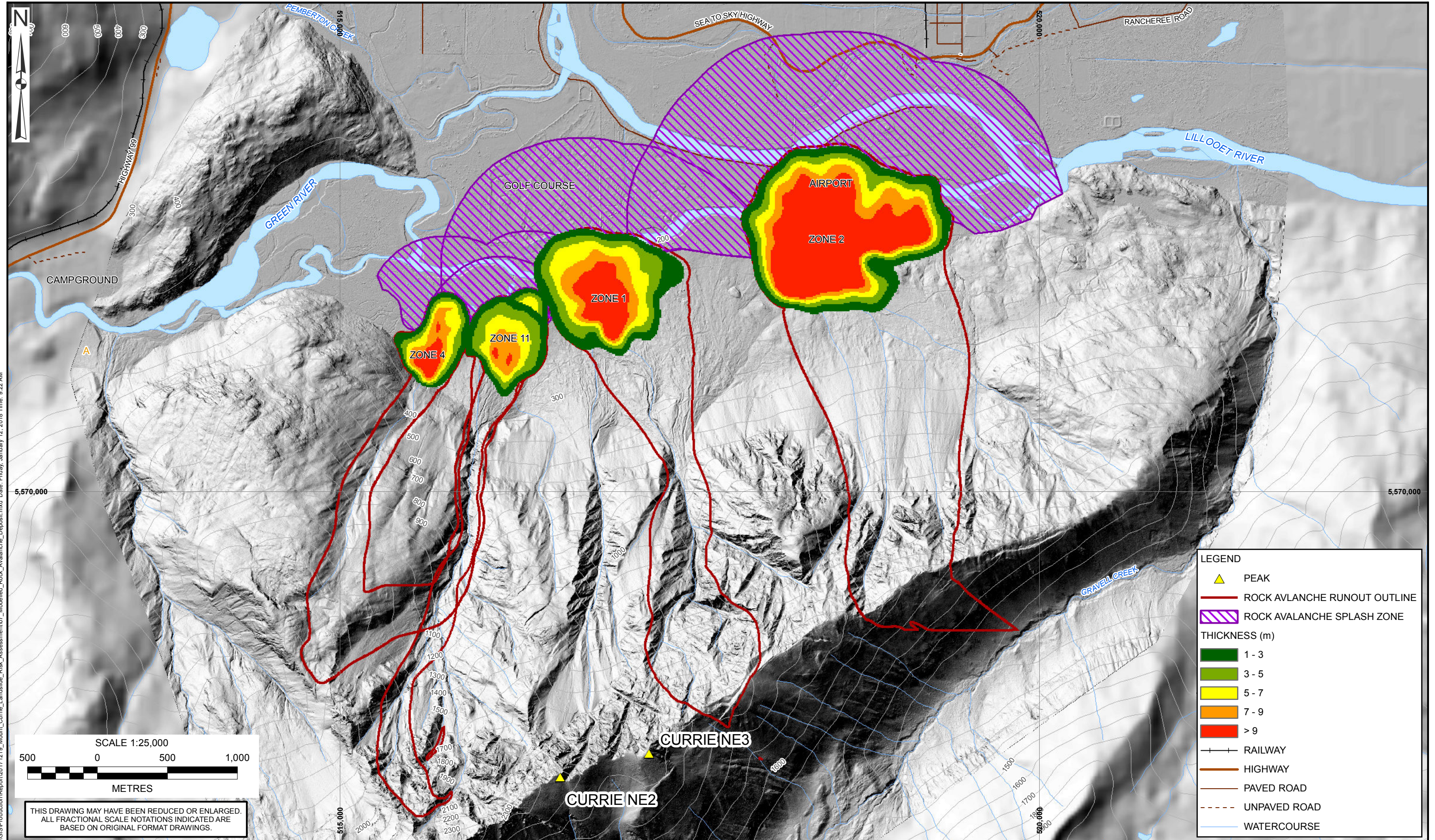
BGC ENGINEERING INC.
 AN APPLIED EARTH SCIENCES COMPANY
 CLIENT:
 SQUAMISH-LILLOOET REGIONAL DISTRICT (SLRD)

PROJECT: MOUNT CURRIE LANDSLIDE RISK ASSESSMENT
 TITLE: REGIONAL ROCK AVALANCHE INVENTORY AREA AND CONCENTRIC AREAS USED IN THE ESTIMATION OF ROCK AVALANCHE FREQUENCY
 PROJECT No.: 1358004
 DWG No.: 06

LEGEND
 ① ROCK AVALANCHE
 [Blue outline] ROCK AVALANCHE INVENTORY BOUNDARY
 [Black outline] ROCK AVALANCHE FREQUENCY ASSESSMENT AREA
 [Colorful lines] RADIUS OF CIRCLES CENTRED ON MOUNT CURRIE
 [Brown line] ROAD
 [Blue line] WATERCOURSE
 ELEVATION m.a.s.l.
 HIGH : 2893
 LOW : 49



THIS DRAWING MAY HAVE BEEN REDUCED OR ENLARGED. ALL FRACTIONAL SCALE NOTATIONS INDICATED ARE BASED ON ORIGINAL FORMAT DRAWINGS.



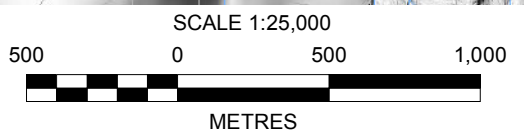
LEGEND

- PEAK
- ROCK AVLANCHE RUNOUT OUTLINE
- ROCK AVALANCHE SPLASH ZONE

THICKNESS (m)

- 1 - 3
- 3 - 5
- 5 - 7
- 7 - 9
- > 9

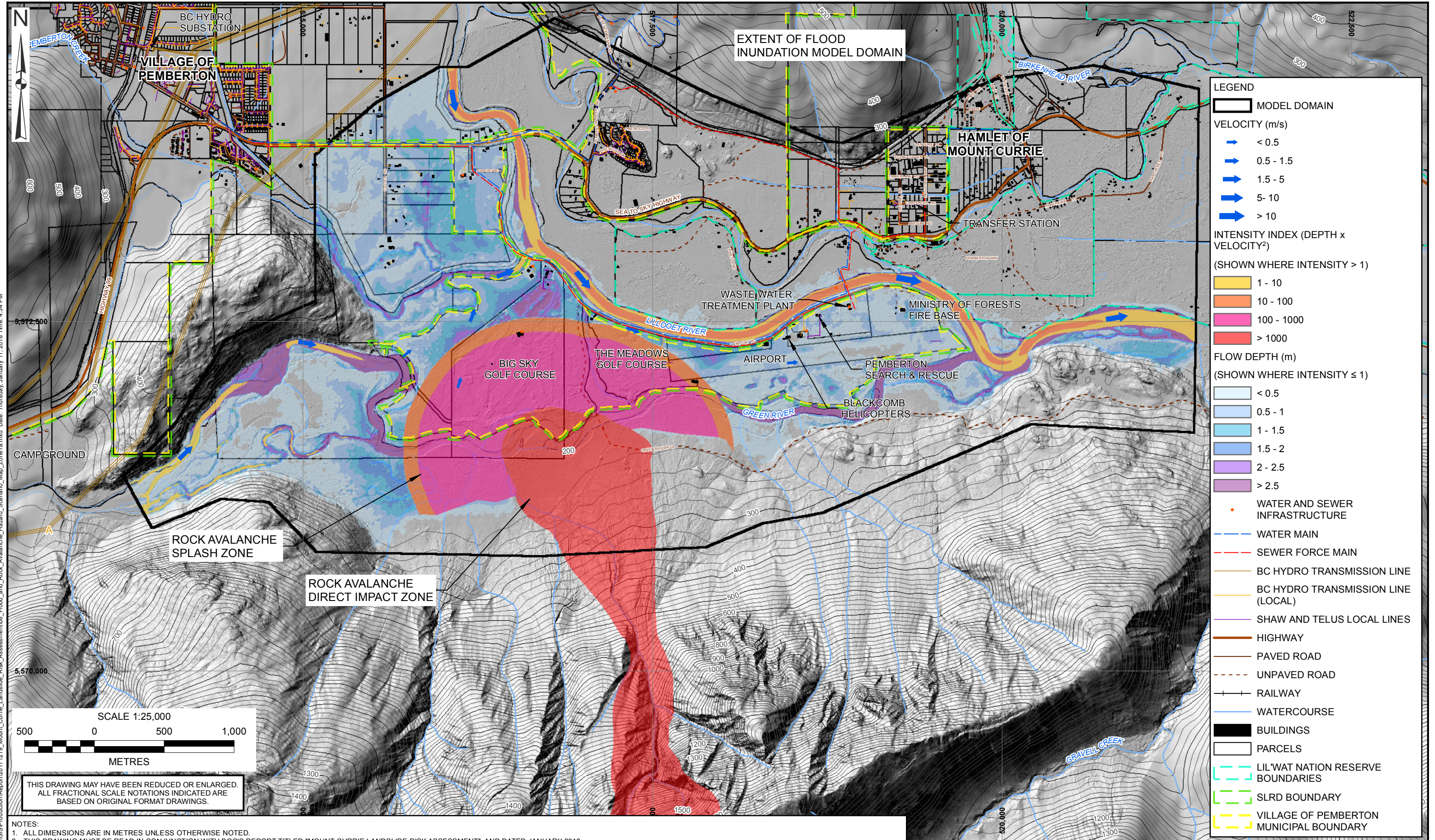
- RAILWAY
- HIGHWAY
- PAVED ROAD
- UNPAVED ROAD
- WATERCOURSE



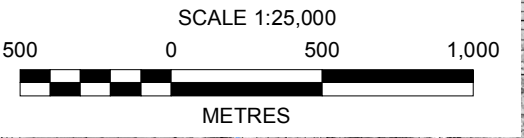
THIS DRAWING MAY HAVE BEEN REDUCED OR ENLARGED.
ALL FRACTIONAL SCALE NOTATIONS INDICATED ARE
BASED ON ORIGINAL FORMAT DRAWINGS.

X:\Projects\1358\004_Mt_Currie\GIS\Production\Report\20171219_Mount_Currie_Landslide_Risk_Assessment07_Modelled_Rock_Avalanche_Deposit.mxd Date: Friday, January 12, 2018 Time: 9:22 AM

| | | | | |
|---|---|--|--|--|
| <p>NOTES:</p> <ol style="list-style-type: none"> ALL DIMENSIONS ARE IN METRES UNLESS OTHERWISE NOTED. THIS DRAWING MUST BE READ IN CONJUNCTION WITH BGC'S REPORT TITLED "MOUNT CURRIE LANDSLIDE RISK ASSESSMENT", AND DATED JANUARY 2018. LANDSLIDE SCARS ARE INTERPRETED AS THE LOCATION OF A SINGLE EVENT. THE ROCK FALL, DEBRIS FLOW AND DEBRIS SLIDE ARROWS INDICATE THE LOCATION AND PATH OF OBSERVED OR INFERRED EVENTS. BASE TOPOGRAPHIC DATA BASED ON LIDAR PROVIDED BY MCELHANNEY DATED AUGUST 26, 2017, AND CANADIAN DIGITAL ELEVATION DATA (CDED) 25 m. CONTOUR INTERVAL IS 100 m. PROJECTION IS NAD 1983 UTM ZONE 10N. UNLESS BGC AGREES OTHERWISE IN WRITING, THIS DRAWING SHALL NOT BE MODIFIED OR USED FOR ANY PURPOSE OTHER THAN THE PURPOSE FOR WHICH BGC GENERATED IT. BGC SHALL HAVE NO LIABILITY FOR ANY DAMAGES OR LOSS ARISING IN ANY WAY FROM ANY USE OR MODIFICATION OF THIS DOCUMENT NOT AUTHORIZED BY BGC. ANY USE OF OR RELIANCE UPON THIS DOCUMENT OR ITS CONTENT BY THIRD PARTIES SHALL BE AT SUCH THIRD PARTIES' SOLE RISK. | <p>SCALE: 1:25,000</p> <p>DATE: JAN 2018</p> <p>DRAWN: JDC</p> <p>CHECKED: MAB</p> <p>APPROVED: MAB</p> | <p>BGC ENGINEERING INC. AN APPLIED EARTH SCIENCES COMPANY</p> <p>CLIENT: SQUAMISH-LILLOOET REGIONAL DISTRICT (SLRD)</p> | <p>PROJECT: MOUNT CURRIE LANDSLIDE RISK ASSESSMENT</p> <p>TITLE: MODELLED ROCK AVALANCHE DEPOSIT</p> | |
| | <p>PROJECT No.: 1358004</p> <p>DWG No.: 07</p> | | | |



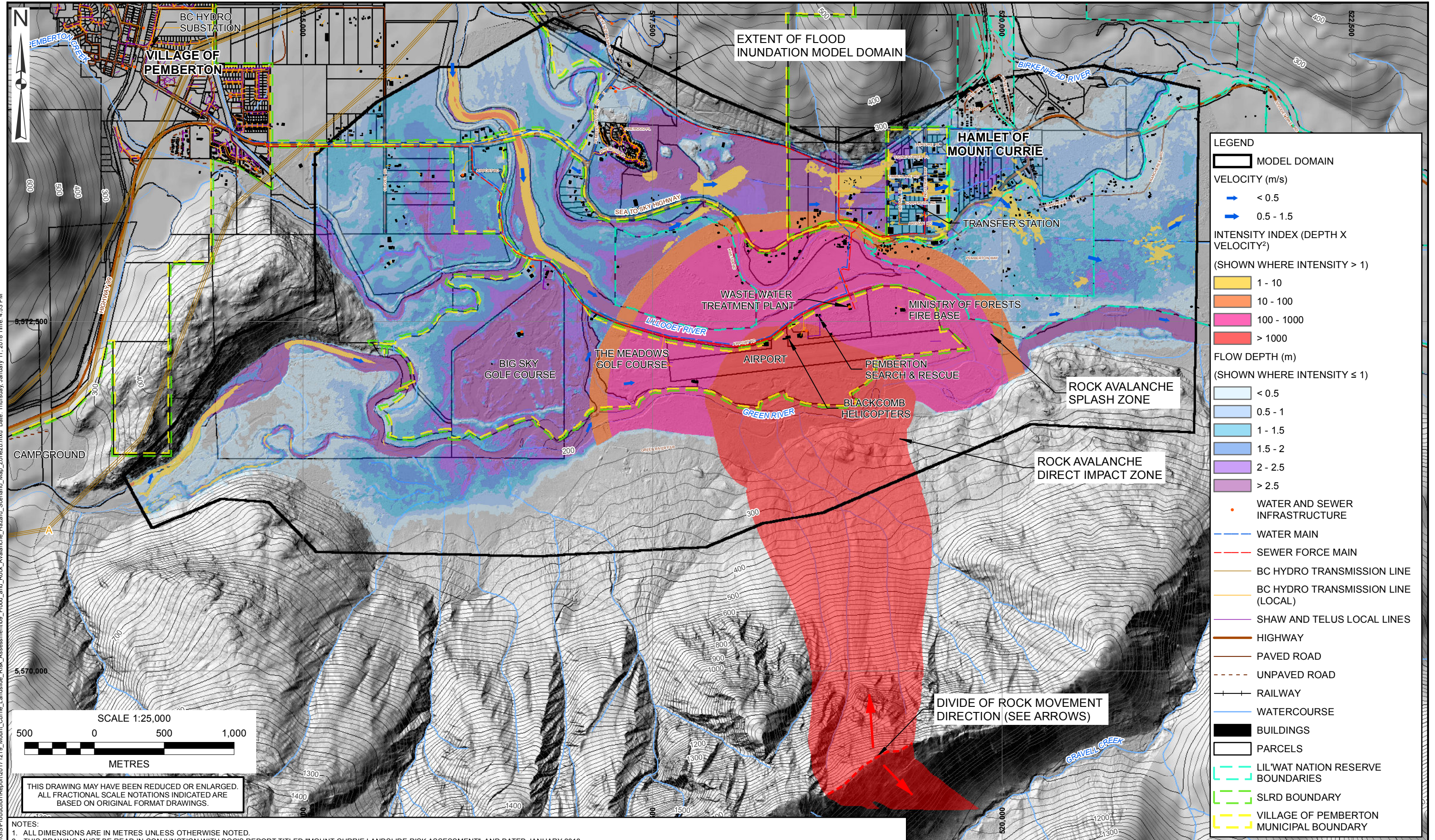
X:\Projects\1358\004_Mt_Currie\GIS\Production\Report\20171219_Mount_Currie_Landslide_Risk_Assessment08_Flood_and_Rock_Avalanche_Hazard_Scenario_Map_Zone1a.mxd Date: Thursday, January 11, 2018 Time: 4:34 PM



THIS DRAWING MAY HAVE BEEN REDUCED OR ENLARGED.
ALL FRACTIONAL SCALE NOTATIONS INDICATED ARE
BASED ON ORIGINAL FORMAT DRAWINGS.

- NOTES:**
1. ALL DIMENSIONS ARE IN METRES UNLESS OTHERWISE NOTED.
 2. THIS DRAWING MUST BE READ IN CONJUNCTION WITH BGC'S REPORT TITLED "MOUNT CURRIE LANDSLIDE RISK ASSESSMENT", AND DATED JANUARY 2018.
 3. BASE TOPOGRAPHIC DATA BASED ON LIDAR PROVIDED BY MCELHANNY DATED AUGUST 26, 2017, AND CANADIAN DIGITAL ELEVATION DATA (CDED) 25 m. CONTOUR INTERVAL IS 20 m.
 4. PARCELS, UTILITIES, AND ROADS WERE OBTAINED FROM SLRD. BUILDINGS WERE PROVIDED BY MCELHANNY DATED OCTOBER 11, 2017.
 5. PROJECTION IS NAD 1983 UTM ZONE 10N.
 6. THIS MAP SHOWS ONLY GEOHAZARD SCENARIOS CONSIDERED IN THE ACCOMPANYING REPORT. OTHER GEOHAZARDS EXIST WITHIN THIS MAP EXTENT THAT ARE NOT SHOWN.
 7. THIS MAP IS A SNAPSHOT IN TIME. FUTURE CHANGES (E.G. CLIMATE CHANGE, RIVER CHANNEL CHANGE, LAND USE, GEOHAZARD EVENTS) MAY WARRANT RE-DRAWING OF CERTAIN AREAS.
 8. THE MODEL DOMAIN BOUNDARY REPRESENTS THE LIMIT OF THE AREA ASSESSED. IT DOES NOT NECESSARILY SHOW THE FULL HAZARD SCENARIO EXTENT.
 9. THE ROCK AVALANCHE DIRECT IMPACT ZONE IS BASED ON THE AREA THAT EXPERIENCED A MODELED FLOW THICKNESS GREATER THAN 1 m.
 10. UNLESS BGC AGREES OTHERWISE IN WRITING, THIS DRAWING SHALL NOT BE MODIFIED OR USED FOR ANY PURPOSE OTHER THAN THE PURPOSE FOR WHICH BGC GENERATED IT. BGC SHALL HAVE NO LIABILITY FOR ANY DAMAGES OR LOSS ARISING IN ANY WAY FROM ANY USE OR MODIFICATION OF THIS DOCUMENT NOT AUTHORIZED BY BGC. ANY USE OF OR RELIANCE UPON THIS DOCUMENT OR ITS CONTENT BY THIRD PARTIES SHALL BE AT SUCH THIRD PARTIES' SOLE RISK.

| | | | | | |
|-----------|----------|--------------|--|---|----|
| SCALE: | 1:25,000 | | PROJECT: | MOUNT CURRIE LANDSLIDE RISK ASSESSMENT | |
| DATE: | JAN 2018 | | TITLE: | FLOOD AND ROCK AVALANCHE HAZARD SCENARIO MAP: ZONE 1a | |
| DRAWN: | JDC | CLIENT: | SQUAMISH-LILLOOET REGIONAL DISTRICT (SLRD) | | |
| CHECKED: | SK, MAB | PROJECT No.: | 1358004 | DWG No.: | 08 |
| APPROVED: | KH, MAB | | | | |



EXTENT OF FLOOD INUNDATION MODEL DOMAIN

HAMLET OF MOUNT CURRIE

WASTE WATER TREATMENT PLANT

MINISTRY OF FORESTS FIRE BASE

AIRPORT

PEMBERTON SEARCH & RESCUE

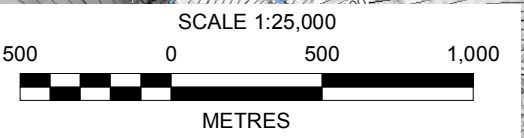
ROCK AVALANCHE SPLASH ZONE

ROCK AVALANCHE DIRECT IMPACT ZONE

DIVIDE OF ROCK MOVEMENT DIRECTION (SEE ARROWS)

LEGEND

- MODEL DOMAIN
- VELOCITY (m/s)**
- < 0.5
- 0.5 - 1.5
- INTENSITY INDEX (DEPTH X VELOCITY²)**
- (SHOWN WHERE INTENSITY > 1)
- 1 - 10
- 10 - 100
- 100 - 1000
- > 1000
- FLOW DEPTH (m)**
- (SHOWN WHERE INTENSITY ≤ 1)
- < 0.5
- 0.5 - 1
- 1 - 1.5
- 1.5 - 2
- 2 - 2.5
- > 2.5
- WATER AND SEWER INFRASTRUCTURE
- WATER MAIN
- SEWER FORCE MAIN
- BC HYDRO TRANSMISSION LINE
- BC HYDRO TRANSMISSION LINE (LOCAL)
- SHAW AND TELUS LOCAL LINES
- HIGHWAY
- PAVED ROAD
- UNPAVED ROAD
- RAILWAY
- WATERCOURSE
- BUILDINGS
- PARCELS
- LIL'WAT NATION RESERVE BOUNDARIES
- SLRD BOUNDARY
- VILLAGE OF PEMBERTON MUNICIPAL BOUNDARY

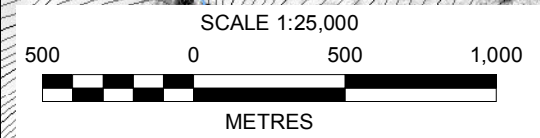
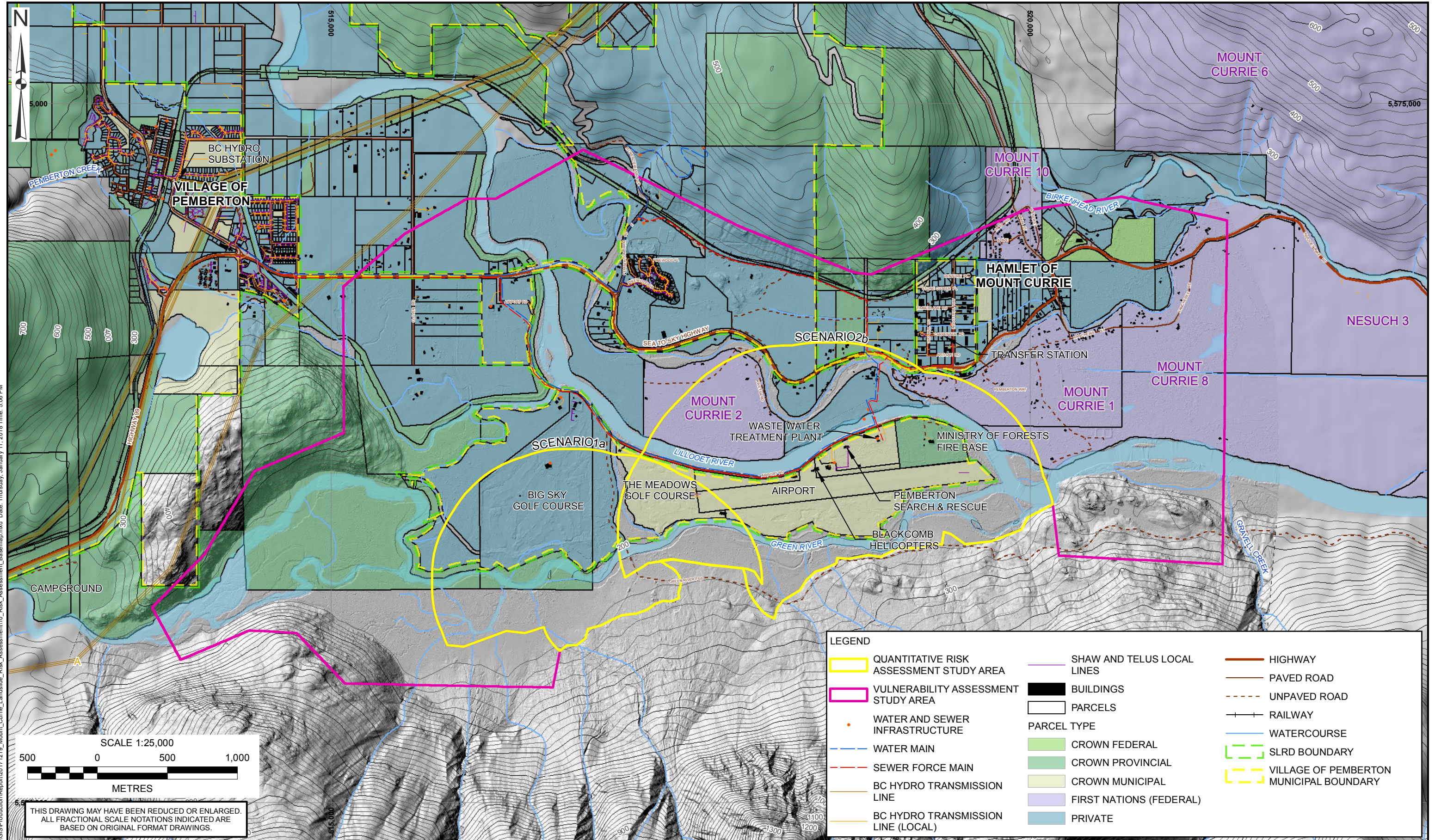


THIS DRAWING MAY HAVE BEEN REDUCED OR ENLARGED. ALL FRACTIONAL SCALE NOTATIONS INDICATED ARE BASED ON ORIGINAL FORMAT DRAWINGS.

- NOTES:**
1. ALL DIMENSIONS ARE IN METRES UNLESS OTHERWISE NOTED.
 2. THIS DRAWING MUST BE READ IN CONJUNCTION WITH BGC'S REPORT TITLED "MOUNT CURRIE LANDSLIDE RISK ASSESSMENT", AND DATED JANUARY 2018.
 3. BASE TOPOGRAPHIC DATA BASED ON LIDAR PROVIDED BY MCELHANNEY DATED AUGUST 26, 2017, AND CANADIAN DIGITAL ELEVATION DATA (CDED) 25 m. CONTOUR INTERVAL IS 20 m.
 4. PARCELS, UTILITIES, AND ROADS WERE OBTAINED FROM SLRD. BUILDINGS WERE PROVIDED BY MCELHANNEY DATED OCTOBER 11, 2017.
 5. PROJECTION IS NAD 1983 UTM ZONE 10N.
 6. THIS MAP SHOWS ONLY GEOHAZARD SCENARIOS CONSIDERED IN THE ACCOMPANYING REPORT. OTHER GEOHAZARDS EXIST WITHIN THIS MAP EXTENT THAT ARE NOT SHOWN.
 7. THIS MAP IS A SNAPSHOT IN TIME. FUTURE CHANGES (E.G. CLIMATE CHANGE, RIVER CHANNEL CHANGE, LAND USE, GEOHAZARD EVENTS) MAY WARRANT RE-DRAWING OF CERTAIN AREAS.
 8. THE MODEL DOMAIN BOUNDARY REPRESENTS THE LIMIT OF THE AREA ASSESSED. IT DOES NOT NECESSARILY SHOW THE FULL HAZARD SCENARIO EXTENT.
 9. THE ROCK AVALANCHE DIRECT IMPACT ZONE IS BASED ON THE AREA THAT EXPERIENCED A MODELED FLOW THICKNESS GREATER THAN 1 m.
 10. UNLESS BGC AGREES OTHERWISE IN WRITING, THIS DRAWING SHALL NOT BE MODIFIED OR USED FOR ANY PURPOSE OTHER THAN THE PURPOSE FOR WHICH BGC GENERATED IT. BGC SHALL HAVE NO LIABILITY FOR ANY DAMAGES OR LOSS ARISING IN ANY WAY FROM ANY USE OR MODIFICATION OF THIS DOCUMENT NOT AUTHORIZED BY BGC. ANY USE OF OR RELIANCE UPON THIS DOCUMENT OR ITS CONTENT BY THIRD PARTIES SHALL BE AT SUCH THIRD PARTIES' SOLE RISK.

| | | | | | |
|-----------|----------|--|--|---|----|
| SCALE: | 1:25,000 | BGC ENGINEERING INC. AN APPLIED EARTH SCIENCES COMPANY | PROJECT: | MOUNT CURRIE LANDSLIDE RISK ASSESSMENT | |
| DATE: | JAN 2018 | | TITLE: | FLOOD AND ROCK AVALANCHE HAZARD SCENARIO MAP: ZONE 2b | |
| DRAWN: | JDC | CLIENT: | SQUAMISH-LILLOOET REGIONAL DISTRICT (SLRD) | | |
| CHECKED: | SK, MAB | PROJECT No.: | 1358004 | DWG No.: | 09 |
| APPROVED: | KH, MAB | | | | |

X:\Projects\1358004_Mt_Currie\GIS\Production\Report\20171219_Mount_Currie_Landslide_Risk_Assessment09_Flood_and_Rock_Avalanche_Hazard_Scenario_Map_Zone2b.mxd Date: Thursday, January 11, 2018 Time: 4:53 PM



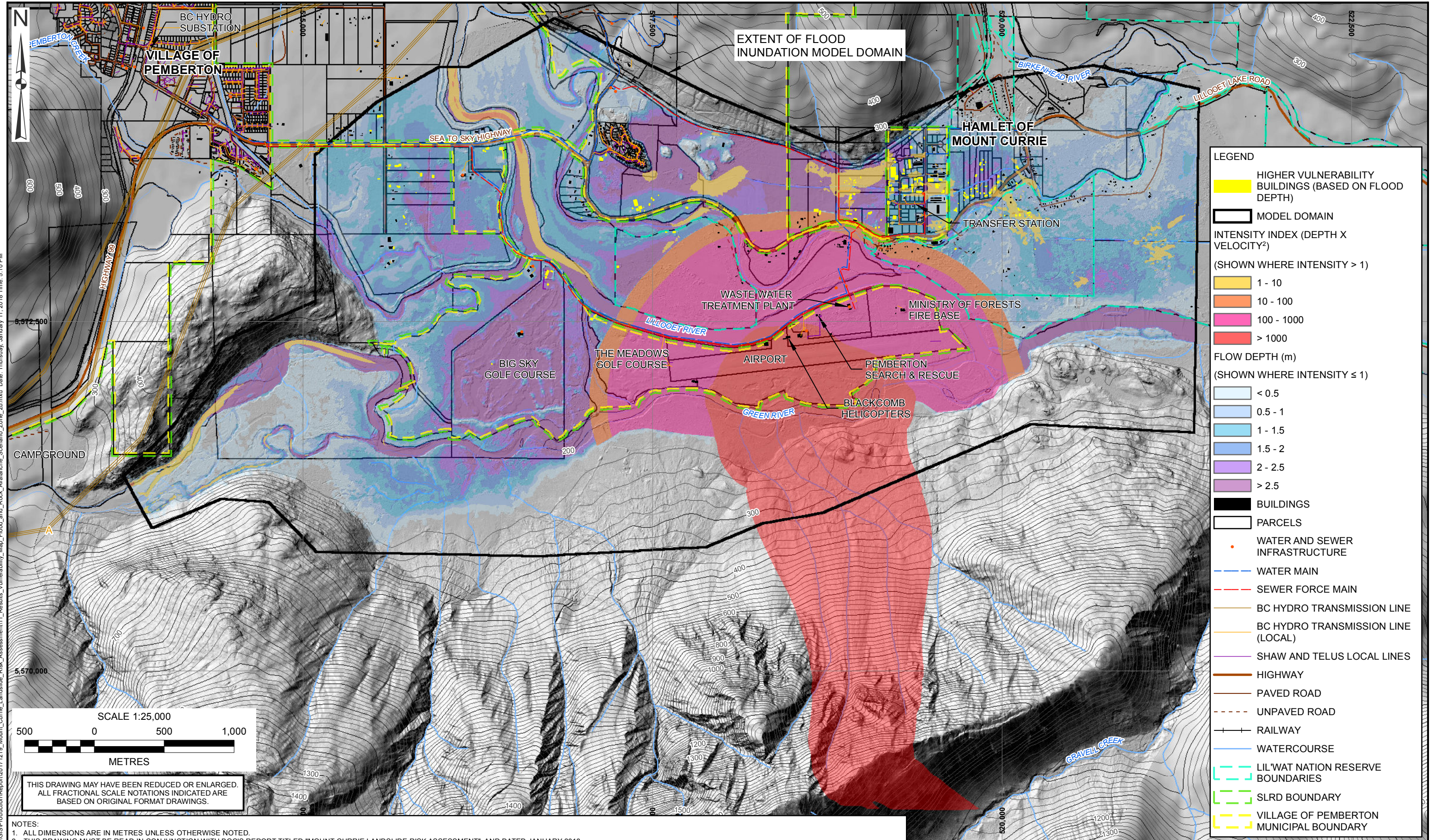
THIS DRAWING MAY HAVE BEEN REDUCED OR ENLARGED. ALL FRACTIONAL SCALE NOTATIONS INDICATED ARE BASED ON ORIGINAL FORMAT DRAWINGS.

| LEGEND | |
|-------------|---|
| | QUANTITATIVE RISK ASSESSMENT STUDY AREA |
| | VULNERABILITY ASSESSMENT STUDY AREA |
| | WATER AND SEWER INFRASTRUCTURE |
| | WATER MAIN |
| | SEWER FORCE MAIN |
| | BC HYDRO TRANSMISSION LINE |
| | BC HYDRO TRANSMISSION LINE (LOCAL) |
| | SHAW AND TELUS LOCAL LINES |
| | BUILDINGS |
| | PARCELS |
| PARCEL TYPE | |
| | CROWN FEDERAL |
| | CROWN PROVINCIAL |
| | CROWN MUNICIPAL |
| | FIRST NATIONS (FEDERAL) |
| | PRIVATE |
| | HIGHWAY |
| | PAVED ROAD |
| | UNPAVED ROAD |
| | RAILWAY |
| | WATERCOURSE |
| | SLRD BOUNDARY |
| | VILLAGE OF PEMBERTON MUNICIPAL BOUNDARY |

NOTES:
 1. ALL DIMENSIONS ARE IN METRES UNLESS OTHERWISE NOTED.
 2. THIS DRAWING MUST BE READ IN CONJUNCTION WITH BGC'S REPORT TITLED "MOUNT CURRIE LANDSLIDE RISK ASSESSMENT", AND DATED JANUARY 2018.
 3. BASE TOPOGRAPHIC DATA BASED ON LIDAR PROVIDED BY MCELHANNEY DATED AUGUST 26, 2017, AND CANADIAN DIGITAL ELEVATION DATA (CDED) 25 m. CONTOUR INTERVAL IS 20 m.
 4. PARCELS, UTILITIES, AND ROADS WERE OBTAINED FROM SLRD. BUILDINGS WERE PROVIDED BY MCELHANNEY DATED OCTOBER 11, 2017.
 5. PROJECTION IS NAD 1983 UTM ZONE 10N.
 6. UNLESS BGC AGREES OTHERWISE IN WRITING, THIS DRAWING SHALL NOT BE MODIFIED OR USED FOR ANY PURPOSE OTHER THAN THE PURPOSE FOR WHICH BGC GENERATED IT. BGC SHALL HAVE NO LIABILITY FOR ANY DAMAGES OR LOSS ARISING IN ANY WAY FROM ANY USE OR MODIFICATION OF THIS DOCUMENT NOT AUTHORIZED BY BGC. ANY USE OF OR RELIANCE UPON THIS DOCUMENT OR ITS CONTENT BY THIRD PARTIES SHALL BE AT SUCH THIRD PARTIES' SOLE RISK.

| | | |
|-------------------|--|--|
| SCALE: 1:25,000 | BGC ENGINEERING INC. AN APPLIED EARTH SCIENCES COMPANY | PROJECT: MOUNT CURRIE LANDSLIDE RISK ASSESSMENT |
| DATE: JAN 2018 | | TITLE: RISK ASSESSMENT BASEMAP |
| DRAWN: JDC | | PROJECT No.: 1358004 |
| CHECKED: SK | | DWG No.: 10 |
| APPROVED: KH, MAB | | CLIENT: SQUAMISH-LILLOOET REGIONAL DISTRICT (SLRD) |

X:\Projects\1358004_Mt_Currie\GIS\Production\Report\20171219_Mt_Currie_Landslide_Risk_Assessment.mxd Date: Thursday, January 11, 2018 Time: 5:06 PM



LEGEND

- HIGHER VULNERABILITY BUILDINGS (BASED ON FLOOD DEPTH)
- MODEL DOMAIN

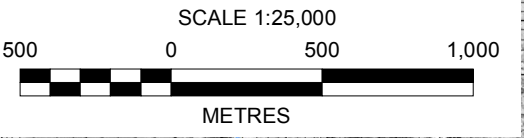
INTENSITY INDEX (DEPTH X VELOCITY²)
(SHOWN WHERE INTENSITY > 1)

- 1 - 10
- 10 - 100
- 100 - 1000
- > 1000

FLOW DEPTH (m)
(SHOWN WHERE INTENSITY ≤ 1)

- < 0.5
- 0.5 - 1
- 1 - 1.5
- 1.5 - 2
- 2 - 2.5
- > 2.5

- BUILDINGS
- PARCELS
- WATER AND SEWER INFRASTRUCTURE
- WATER MAIN
- SEWER FORCE MAIN
- BC HYDRO TRANSMISSION LINE
- BC HYDRO TRANSMISSION LINE (LOCAL)
- SHAW AND TELUS LOCAL LINES
- HIGHWAY
- PAVED ROAD
- UNPAVED ROAD
- RAILWAY
- WATERCOURSE
- LIL'WAT NATION RESERVE BOUNDARIES
- SLRD BOUNDARY
- VILLAGE OF PEMBERTON MUNICIPAL BOUNDARY



THIS DRAWING MAY HAVE BEEN REDUCED OR ENLARGED.
ALL FRACTIONAL SCALE NOTATIONS INDICATED ARE
BASED ON ORIGINAL FORMAT DRAWINGS.

NOTES:

1. ALL DIMENSIONS ARE IN METRES UNLESS OTHERWISE NOTED.
2. THIS DRAWING MUST BE READ IN CONJUNCTION WITH BGC'S REPORT TITLED "MOUNT CURRIE LANDSLIDE RISK ASSESSMENT", AND DATED JANUARY 2018.
3. BASE TOPOGRAPHIC DATA BASED ON LIDAR PROVIDED BY MCELHANNEY DATED AUGUST 26, 2017, AND CANADIAN DIGITAL ELEVATION DATA (CDED) 25 m. CONTOUR INTERVAL IS 20 m.
4. PARCELS, UTILITIES, AND ROADS WERE OBTAINED FROM SLRD. BUILDINGS WERE PROVIDED BY MCELHANNEY DATED OCTOBER 11, 2017.
5. PROJECTION IS NAD 1983 UTM ZONE 10N.
6. THIS MAP SHOWS ONLY GEOHAZARD SCENARIOS CONSIDERED IN THE ACCOMPANYING REPORT. OTHER GEOHAZARDS EXIST WITHIN THIS MAP EXTENT THAT ARE NOT SHOWN.
7. THIS MAP IS A SNAPSHOT IN TIME. FUTURE CHANGES (E.G. CLIMATE CHANGE, RIVER CHANNEL CHANGE, LAND USE, GEOHAZARD EVENTS) MAY WARRANT RE-DRAWING OF CERTAIN AREAS.
8. THE MODEL DOMAIN BOUNDARY REPRESENTS THE LIMIT OF THE AREA ASSESSED. IT DOES NOT NECESSARILY SHOW THE FULL HAZARD SCENARIO EXTENT.
9. THE ROCK AVALANCHE DIRECT IMPACT ZONE IS BASED ON THE AREA THAT EXPERIENCED A MODELED FLOW THICKNESS GREATER THAN 1 m.
10. UNLESS BGC AGREES OTHERWISE IN WRITING, THIS DRAWING SHALL NOT BE MODIFIED OR USED FOR ANY PURPOSE OTHER THAN THE PURPOSE FOR WHICH BGC GENERATED IT. BGC SHALL HAVE NO LIABILITY FOR ANY DAMAGES OR LOSS ARISING IN ANY WAY FROM ANY USE OR MODIFICATION OF THIS DOCUMENT NOT AUTHORIZED BY BGC. ANY USE OF OR RELIANCE UPON THIS DOCUMENT OR ITS CONTENT BY THIRD PARTIES SHALL BE AT SUCH THIRD PARTIES' SOLE RISK.

| | | | | |
|-----------|----------|--|--|--|
| SCALE: | 1:25,000 | <p>BGC ENGINEERING INC. AN APPLIED EARTH SCIENCES COMPANY</p> | PROJECT: MOUNT CURRIE LANDSLIDE RISK ASSESSMENT | |
| DATE: | JAN 2018 | | TITLE: RESULTS, VULNERABILITY MAP: FLOOD AND ROCK AVALANCHE SCENARIO ZONE 2b | |
| DRAWN: | JDC | | PROJECT No.: 1358004 | |
| CHECKED: | SK | | DWG No.: 11 | |
| APPROVED: | KH, MAB | | CLIENT: SQUAMISH-LILLOOET REGIONAL DISTRICT (SLRD) | |

X:\Projects\1358\004_Mt_Currie\GIS\Production\Report\20171219_Mount_Currie_Landslide_Risk_Assessment\11_Results_Vulnerability_Map_Flood_and_Rock_Avalanche_Scenario_Zone_2b.mxd Date: Thursday, January 11, 2018 Time: 5:10 PM

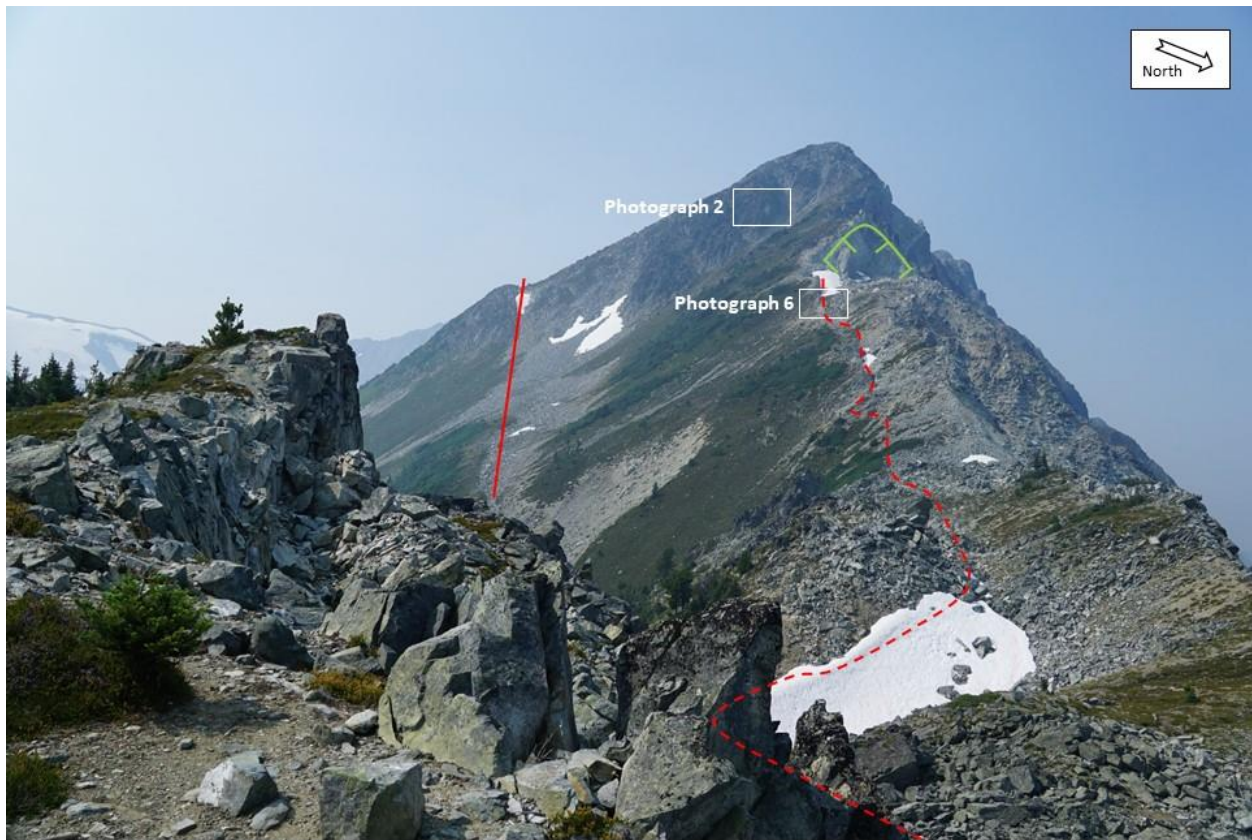
PHOTOGRAPHS



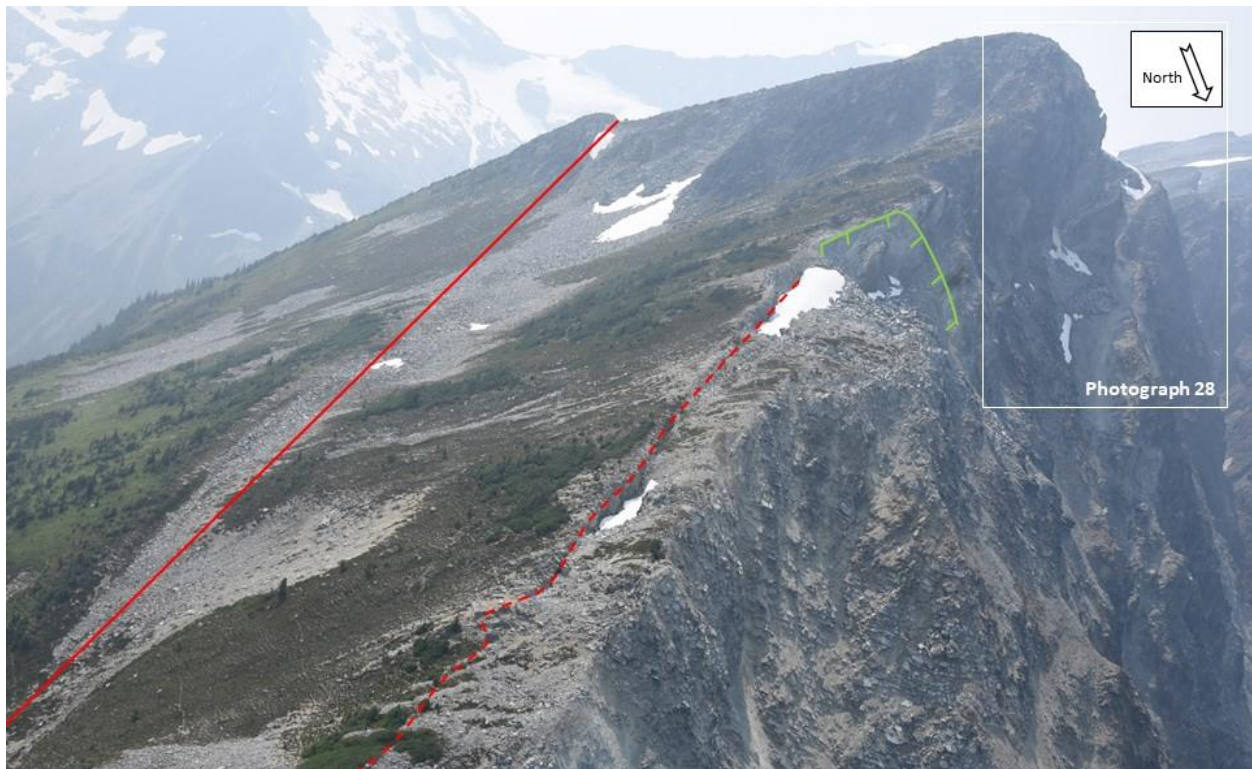
Photograph 1 Diorite intruded by a basaltic dyke.



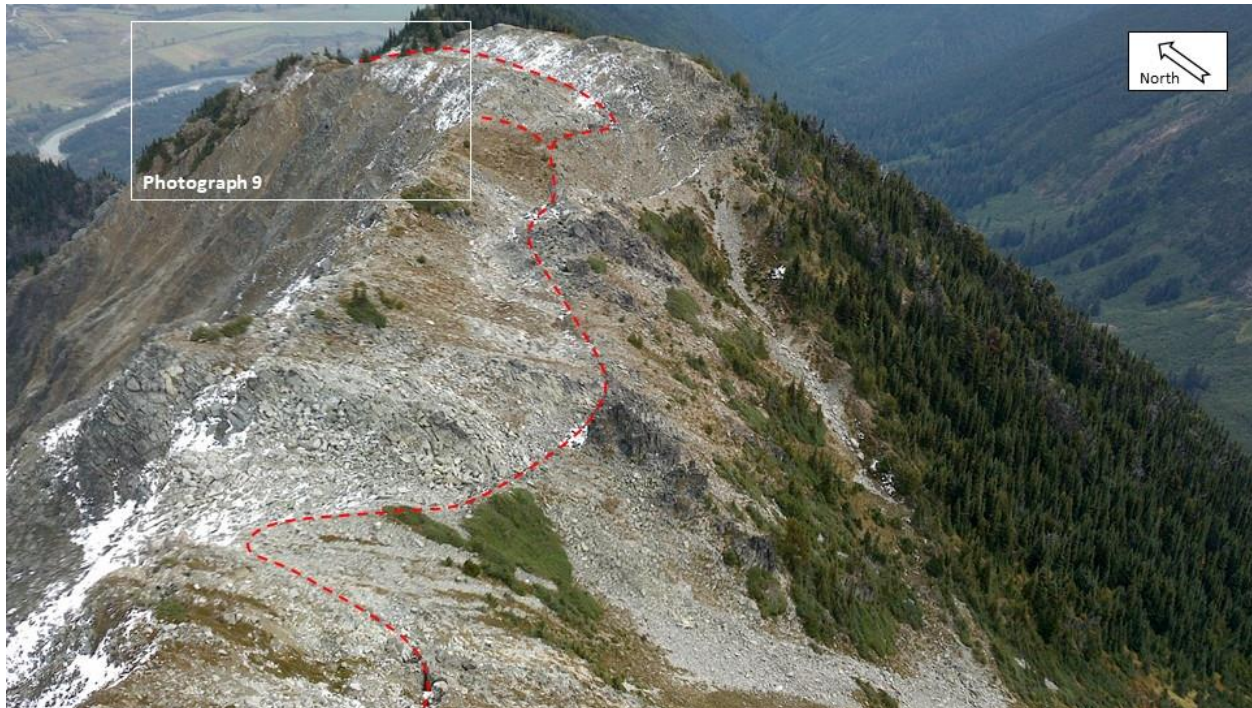
Photograph 2 D5 discontinuities on the southeast slopes, just downslope from the Mt Currie ridgeline.



Photograph 3 Looking west at Mount Currie Ridge and Currie NE2 Summit. The red full line indicates a major lineament. The tension crack or counter-slope scarp (red dashed line) to the right and the scar (green line) appear to mark the upper and lateral extent, respectively, of Source ID 1a.



Photograph 4 Looking southwest at Mount Currie Ridge and Currie NE2 Summit. The red full line indicates a major lineament. The red dashed line to the right and the scar (green line) appear to mark the upper and lateral extent, respectively, of Source ID 1a.



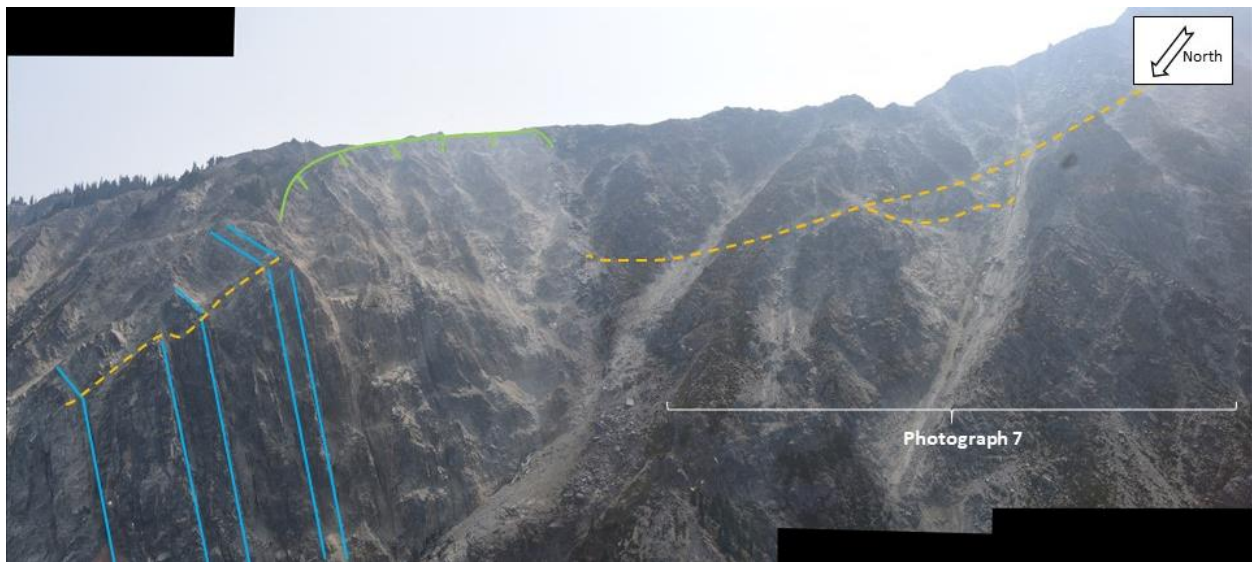
Photograph 5 Looking northeast along Mt Currie ridge. The red dashed line highlights the upper extent of Source ID 1a (at the front) and ID 1b (at the back).



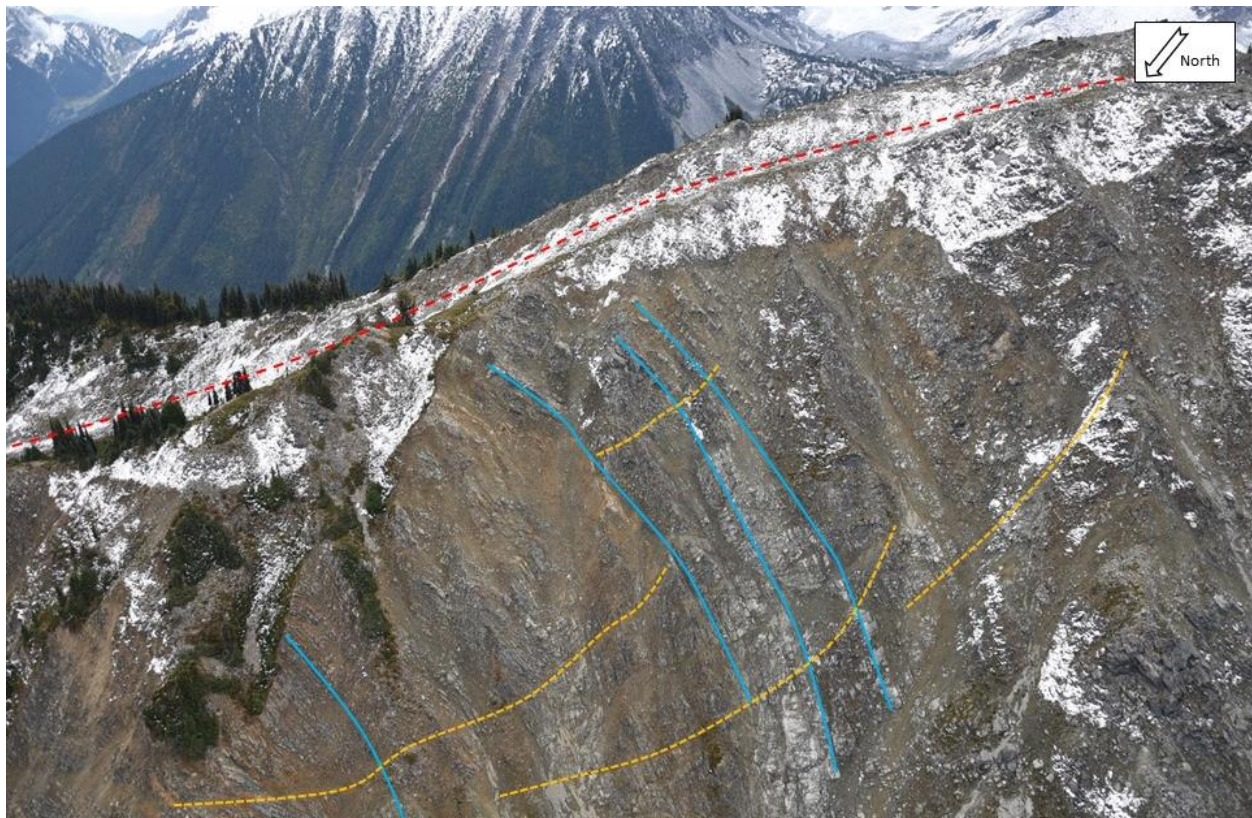
Photograph 6 Disturbed and dilated rock mass (Source ID 1a) with tilted blocks along foliation.



Photograph 7 Scars (green lines) of small landslides initiating on the edge of the disturbed mass (Source ID 1a) and interpreted basal sliding surfaces (orange dashed line) of the disturbed mass.



Photograph 8 Disturbed mass (Source ID 1a) with interpreted basal sliding surfaces (orange dashed line) constrained by the location where undisturbed foliation planes become tilted (blue lines). The green line shows the scar of a small landslide initiating on the edge of the mass.



Photograph 9 Section of Source ID 1b showing the upper extent along a counter-slope scarp (red dashed line), interpreted basal sliding surfaces (orange dashed lines), and inflexed foliation planes (blue lines).



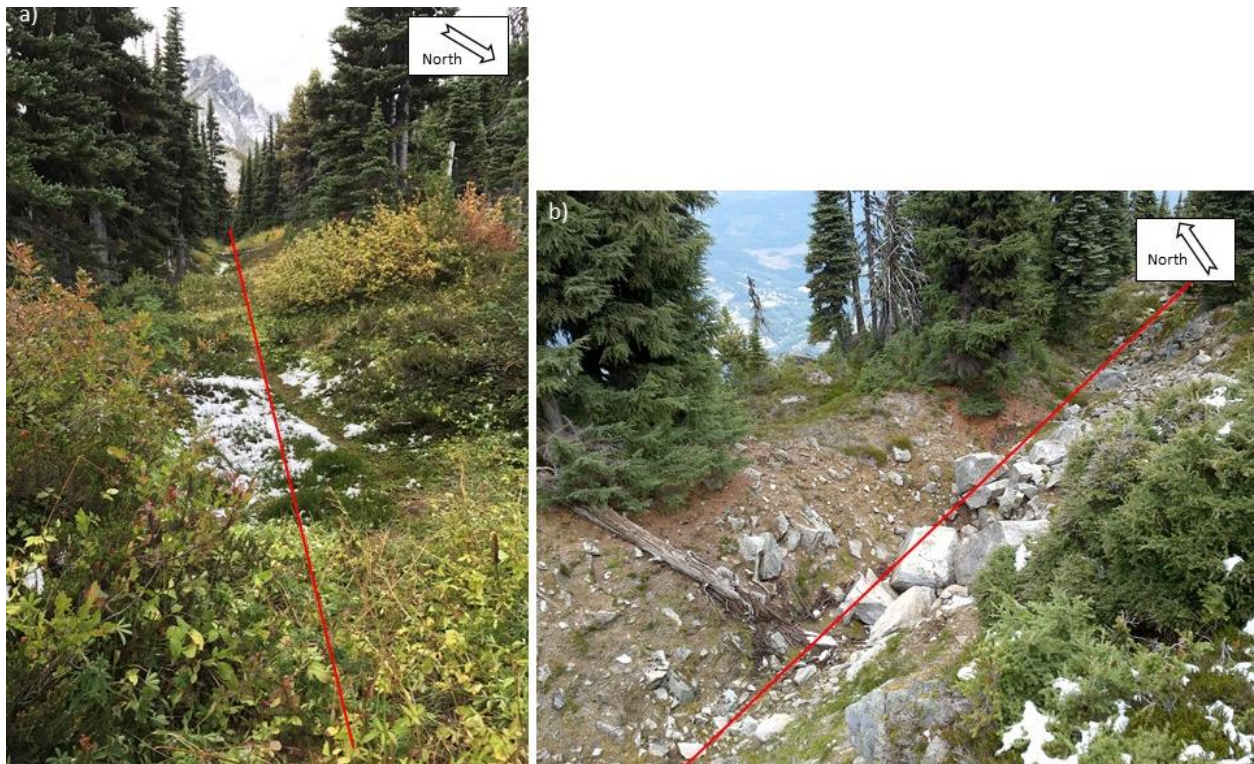
Photograph 10 Disturbed mass (Source ID 1b) with interpreted basal sliding surfaces (orange dashed line) constrained by the location where undisturbed foliation planes become tilted (blue lines). Green lines show scars of small landslides initiating on the edge of the mass.



Photograph 11 Looking southwest at Source ID 1b and the counter-slope scarp marking its upper extent (red dashed line).



Photograph 12 Tension cracks (red dashed lines) subparallel to the ridge at Source ID 2c.



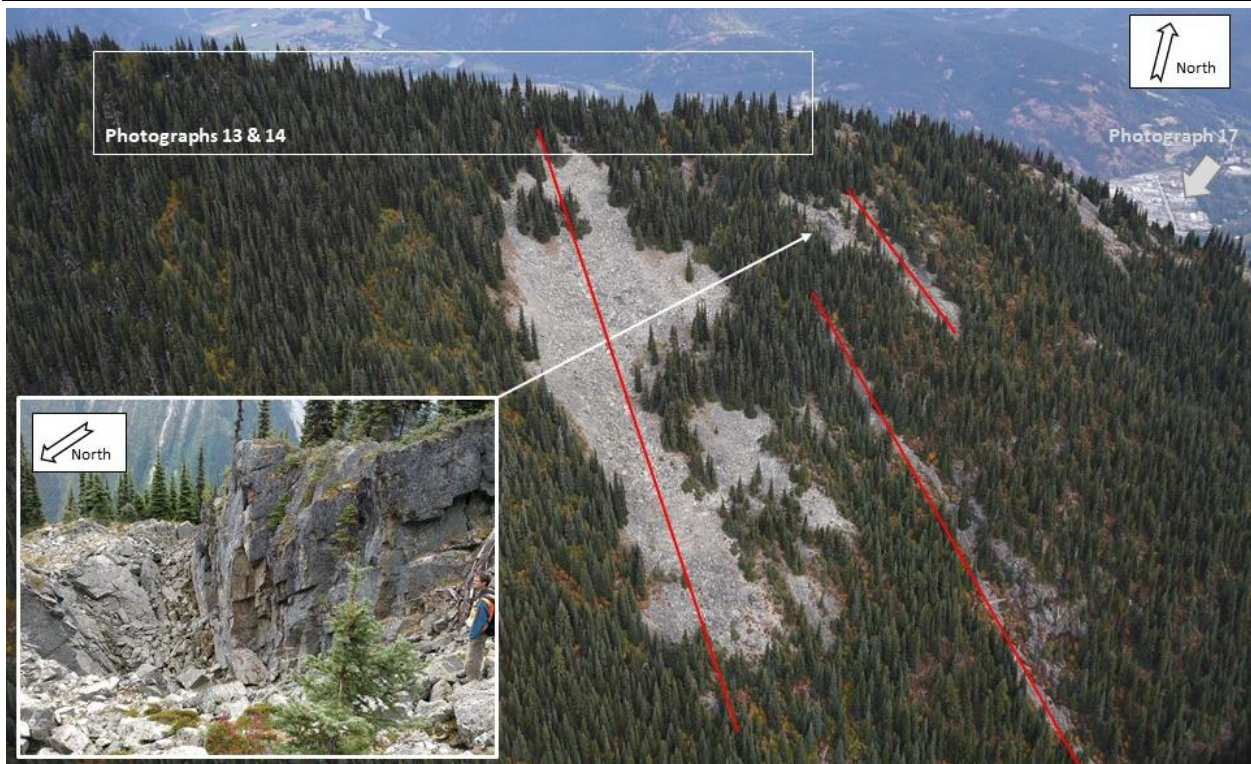
Photograph 13 Lineaments subparallel to the ridge line along Source ID 2a.



Photograph 14 Source ID 2a and the inferred location of its basal sliding surface (orange dashed line).



Photograph 15 Upper part of a section of Source ID 2b showing a disturbed rock mass and moderately dipping discontinuities.



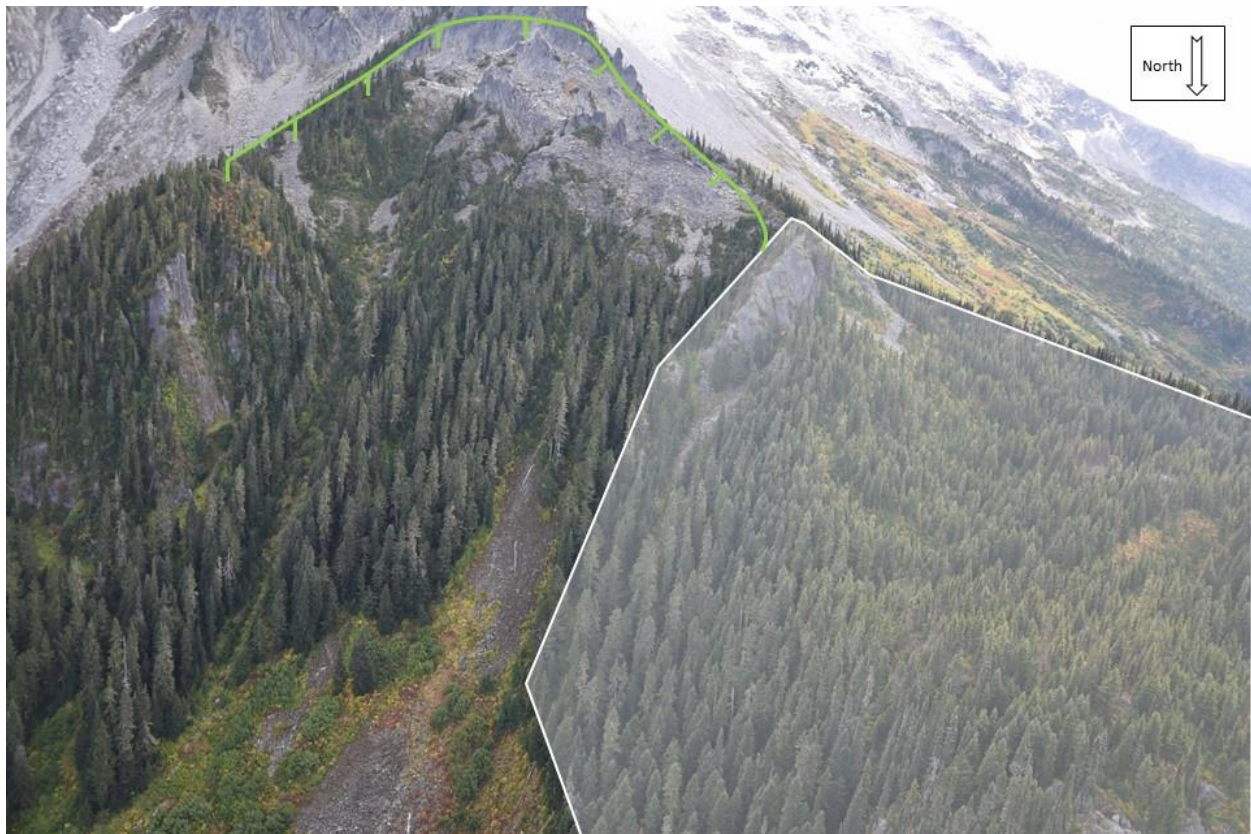
Photograph 16 Lineaments (red lines) and talus slopes subparallel to foliation and oblique to the ridge line along Source ID 2a. Inset picture shows a hole approximately 10 m deep on one of these lineaments.



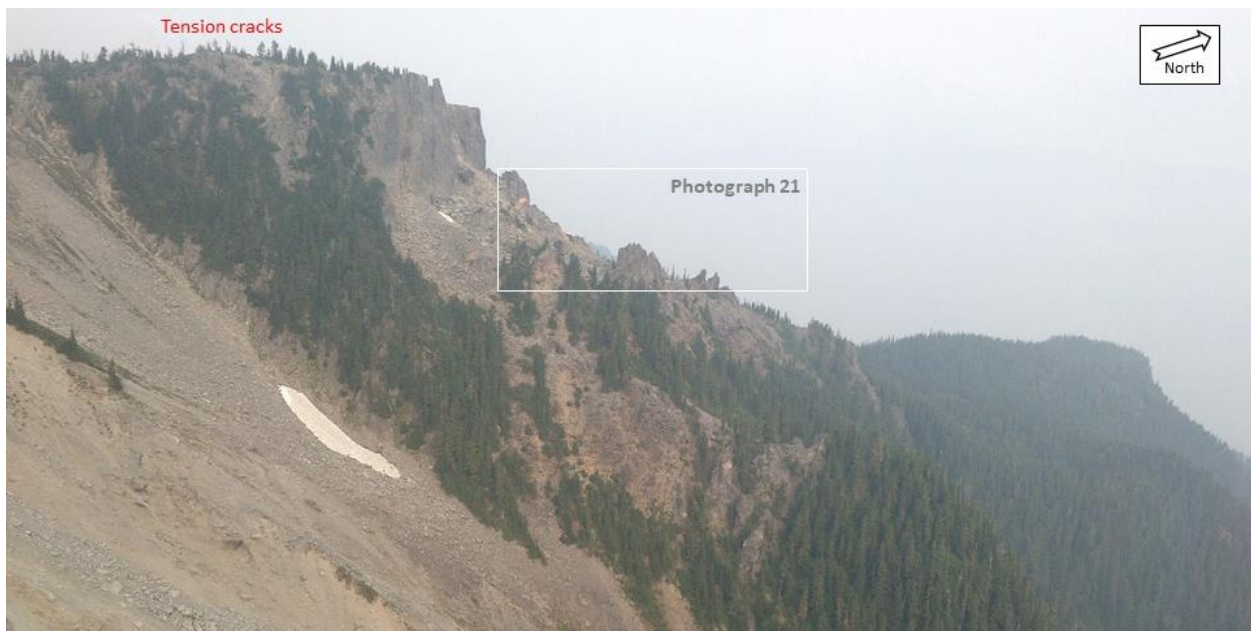
Photograph 17 Right: northeast side of Source ID 2a, showing lineaments (red lines) and associated slope deformation parallel to foliation, and inferred basal sliding surface (orange dashed line). Left: southwest side of Source ID 2b and inferred basal sliding surface (orange dashed line).



Photograph 18 Source ID 3 showing the upper scar (green line) of a DSGSD and talus covered with lichen and some vegetation.



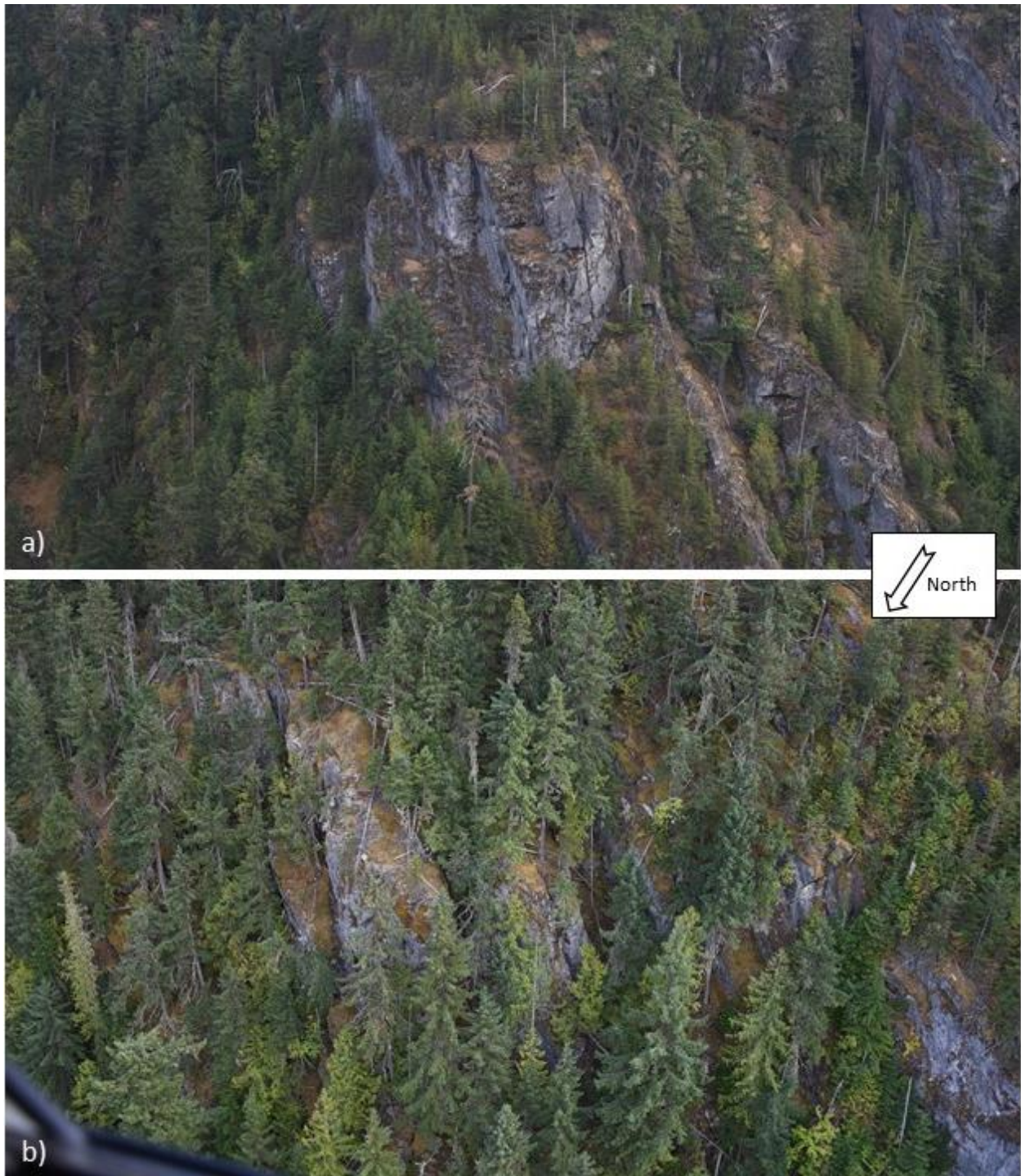
Photograph 19 Upper part of Source ID 4, where tension cracks are developing in the forested area (white transparent polygon) and scar of a past landslide event (green line) where more unstable ground forms Source ID 16 (see Photograph 21).



Photograph 20 Slope deformation and location of the past landslide event described in Photograph 19. Tension cracks were observed behind the upper cliff.



Photograph 21 Bare, unvegetated rock debris at the base of the cliff described in Photograph 19 and Photograph 20. Toppling was identified on the left where undisturbed foliation planes become tilted (blue lines) forming a basal sliding surface (orange dashed line). The red dashed line appears to show a depression within the rock debris, suggesting that further instability (Source ID 16) is possible.



Photograph 22 Dilation along sub-vertical foliation planes within potential Source ID 13.



Photograph 23 Wide northeast trending tension crack filled with rock blocks and vegetation, and marking the upper limit of potential Source ID 13. The surface of the blocks is weathered and appears to be covered with lichen.

Photograph 23



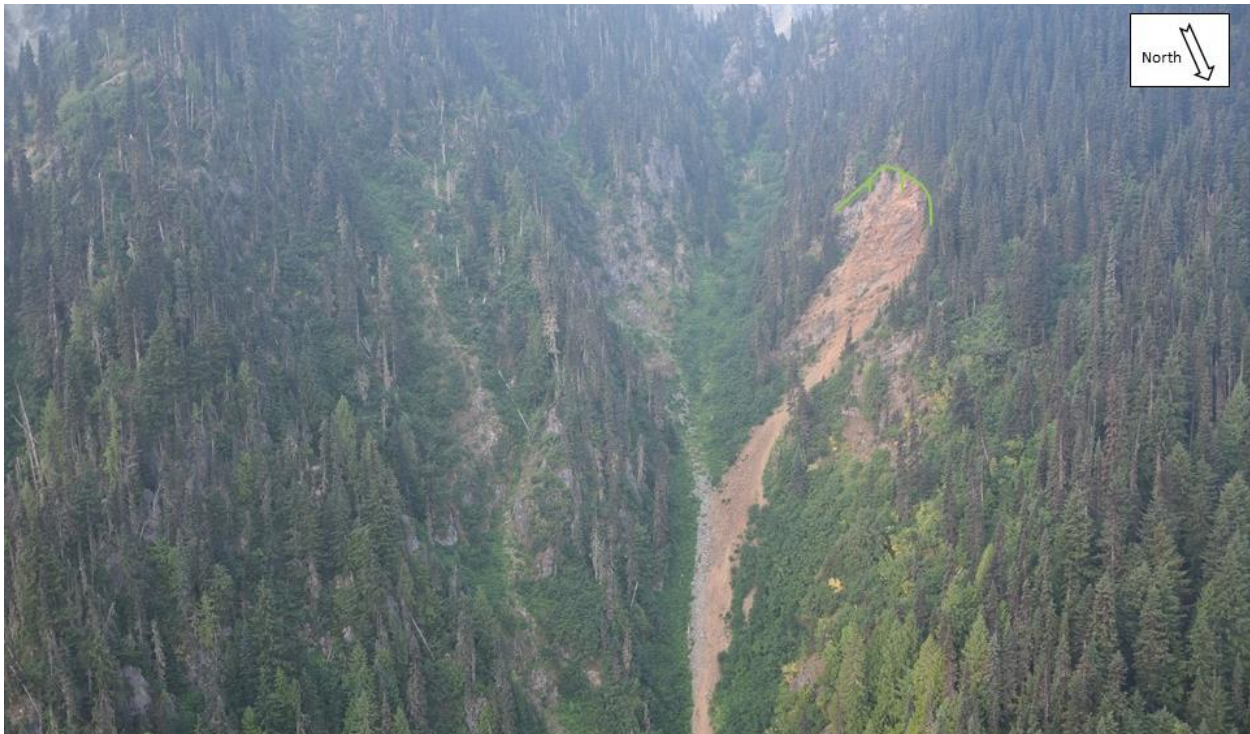
Photograph 24 DSGSD (Source ID 13) showing rock fall debris (weathered and covered with vegetation) at the base of a rock slope. Green River flows at the toe of the debris.



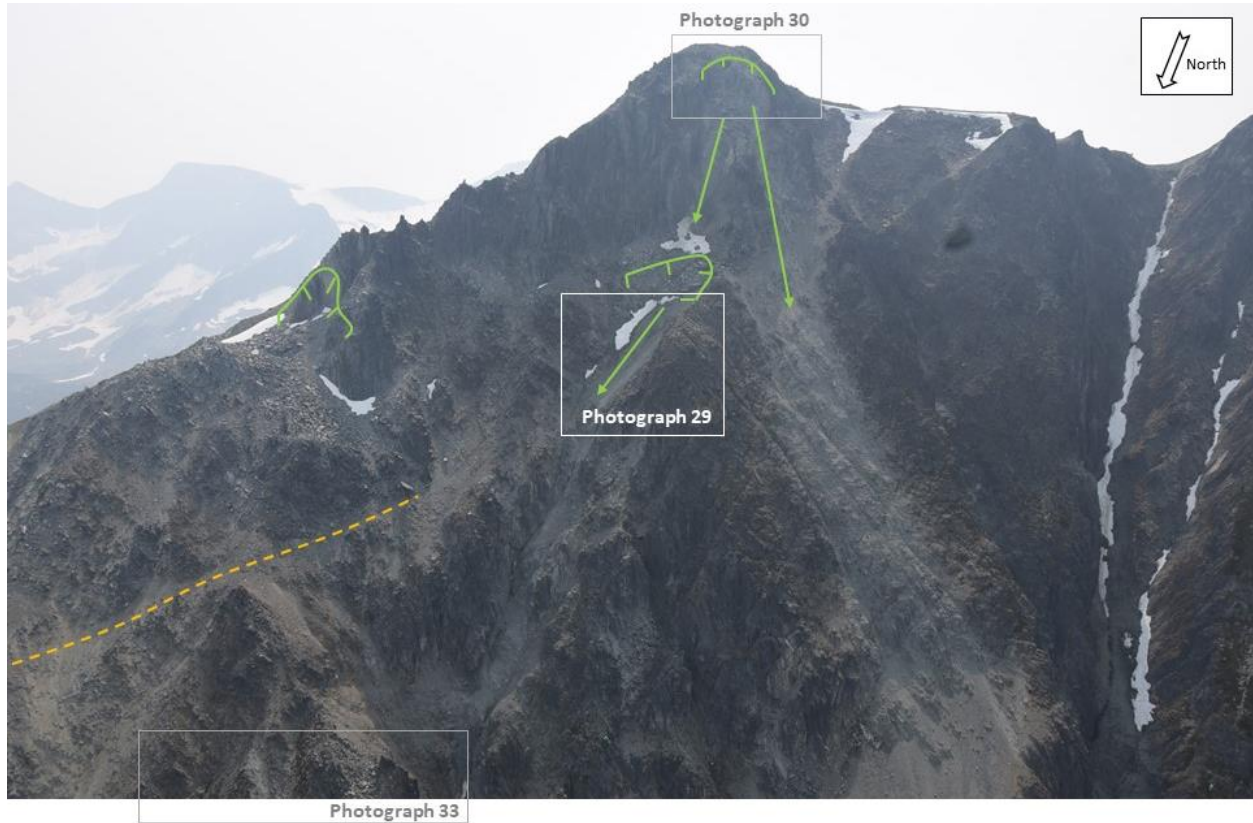
Photograph 25 Rock and debris slides in the easternmost watershed. The green lines highlight the scars.



Photograph 26 Rock and debris slides in the easternmost watershed. The green line highlights the scar.



Photograph 27 Rock and debris slide in the easternmost watershed. The green line shows the scar.



Photograph 28 Currie NE3 summit: on the left, disturbed mass (Source ID 1a) with interpreted basal sliding surface (orange dashed line) and scar (left green line). In the center, upper scar of a rock fall event triggering sliding of small disturbed mass (lower green line).



Photograph 29 Scar of the small disturbed mass, whose failure is assumed to have been triggered by a rock fall event, as explained in Photograph 28.



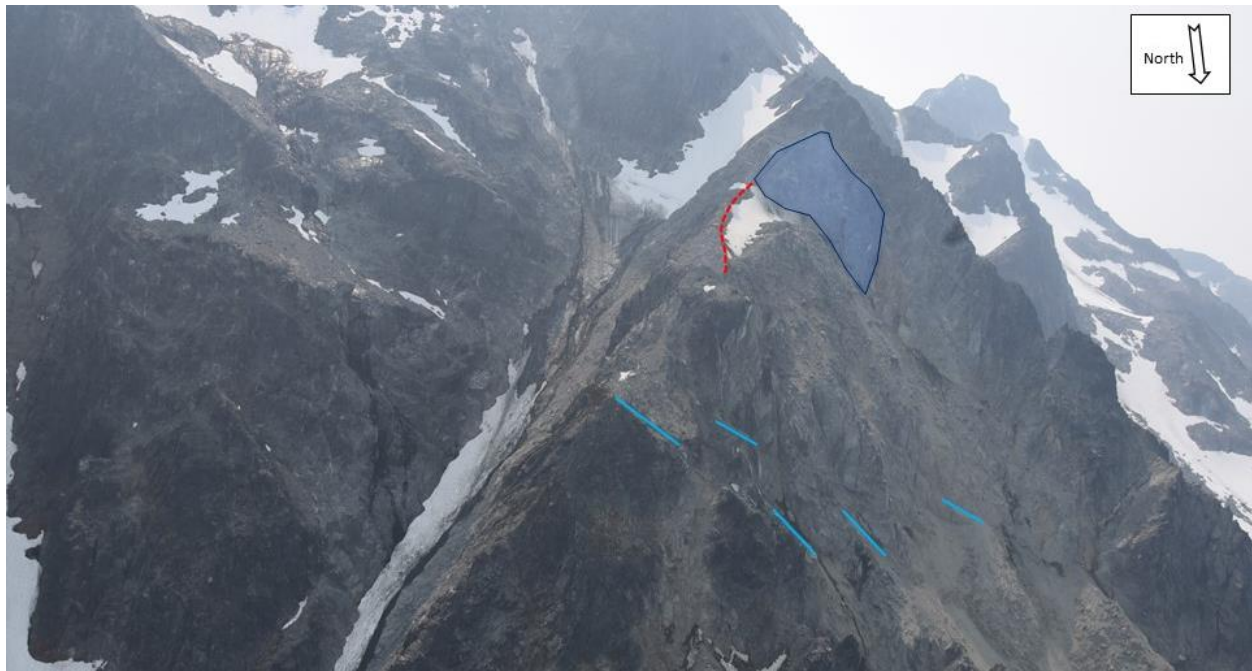
Photograph 30 Upper scar of rock fall event described in Photograph 28 showing dilation and open cracks corresponding to Source ID 7.



Photograph 31 Minor rock fall scars (green lines); and tension crack (red dashed line) defining a potential instability (Source ID 12).



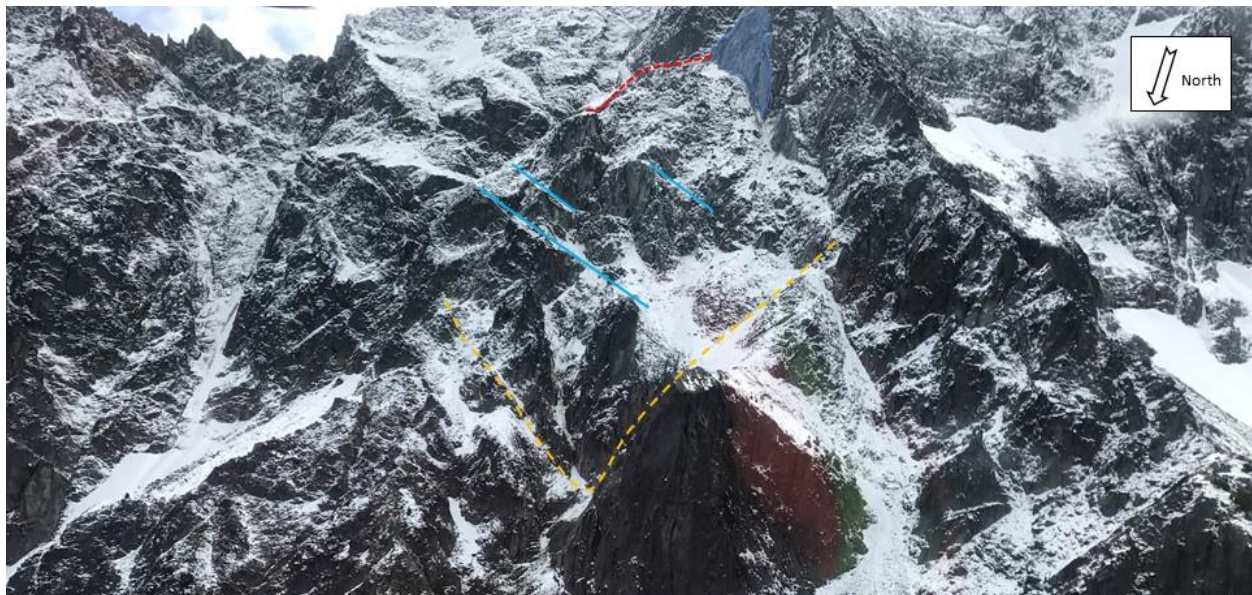
Photograph 32 Inferred location of reported June 29, 2015 rock fall events and location of potential further instability (Source ID 10).



Photograph 33 Location of the July and September 2016 rock slide events with steeply dipping planes (light blue lines), lateral release planes (foliation – dark blue polygon) and upper counter-slope scarp (red dashed line).



Photograph 34 Upper counter-slope scarp (red dashed line) of the July and September 2016 rock slide events.



Photograph 35 Looking up at the location of July and September 2016 rock slide events and its geometry: steeply dipping planes (light blue lines) and lateral release planes (foliation – dark blue polygon) form a wedge whose line of intersection daylight; rear release is provided by the upper counter-slope scarp (red dashed line). The orange dashed line shows the potential location of the lower extent of further instability (Source ID 11).



Photograph 36 Disturbed mass along the crest separating Watershed C and D. The orange dashed line shows interpreted basal sliding surfaces constrained by the location where undisturbed foliation planes are tilted (blue lines).



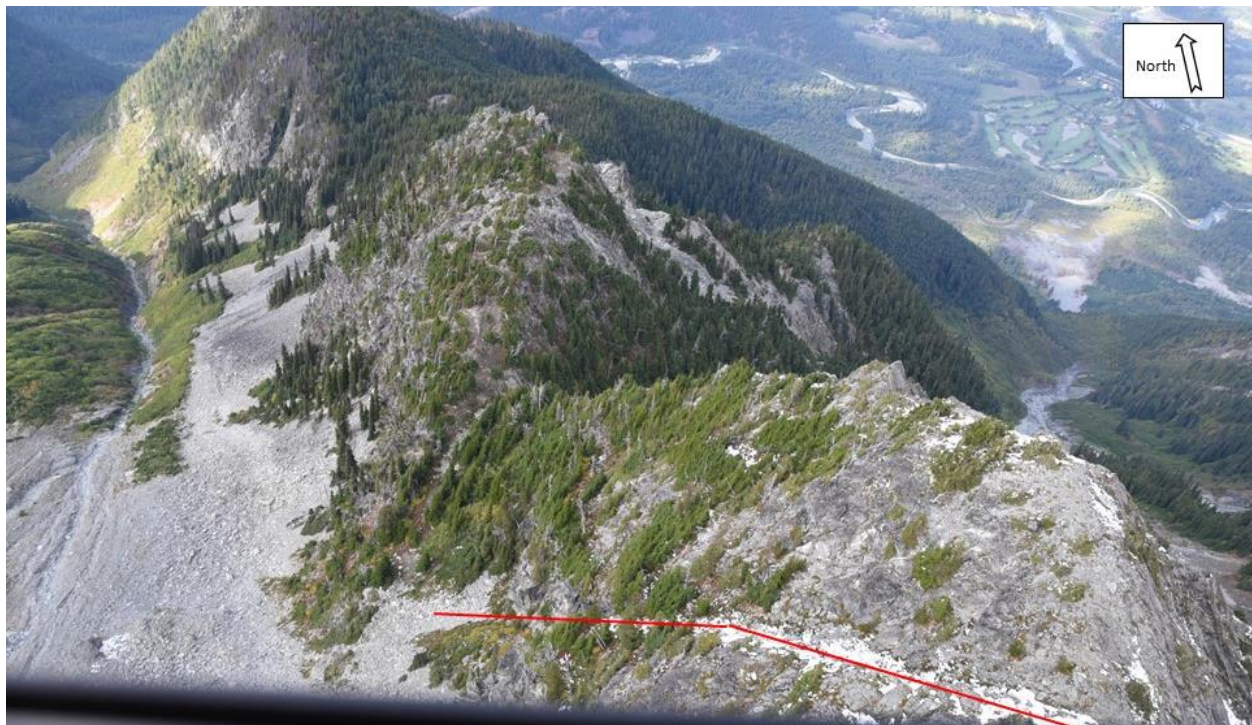
Photograph 37 Toppling mechanism generating a disturbed mass whose interpreted basal sliding surface (orange dashed line) corresponds to the location where undisturbed foliation planes (blue lines) become tilted.



Photograph 38 Debris of a rock slide with its scar (green line) and lower extent (white dashed line). Re-mobilization of the debris corresponds to Source ID 6.



Photograph 39 Debris of a rock slide and its scar (green line). Re-mobilization of the debris corresponds to Source ID 6.



Photograph 40 Lineament (red line) marking the upper extent of potential Source ID 14.



Photograph 41 Lineament (red line) marking the lateral extent of potential Source ID 14.



Photograph 42 Rock and debris slide showing re-vegetation of the scar of the event which occurred between 1948 and 1969. Possible retrogression of this landslide represents Source ID 5.



Photograph 43 Main debris flow path of Watershed B. Some remaining snow patches are visible in picture b.



Photograph 44 Deeply incised gully on the lower part of the debris flow path of Watershed B.



Photograph 45 View of the debris flow fans at the base of Watersheds B and D.



Photograph 46 Debris flow fan at the base of Watershed B.



Photograph 47 Debris flow fan at the base of Watershed B.



Photograph 48 Debris flow fan at the base of Watershed D.



Photograph 49 Green River bank at the base of the north side of Mount Currie showing mostly fine-grained fluvial sediments, and no evidence of past rock avalanche debris.



Photograph 50 Old growth forest on the north side of Highway 99 showing no evidence of past rock avalanche debris.



Photograph 51 Crack at Station 17-01 where the thermistor was used to generate a temperature profile.

APPENDIX A
ROCK AVALANCHE AND DEEP-SEATED GRAVITATIONAL SLOPE
DEFORMATION (DSGSD) REGIONAL INVENTORY

Table A1: Inventory of rock avalanches identified in the study area

| ID | Name | UTM Zone 10 | | Date of slope failure | Volume (m ³) | Area of scar or debris (m ²) | Stratigraphic Unit* |
|----|------------------|-------------|----------|-----------------------|--------------------------|--|---------------------|
| | | Easting | Northing | | | | |
| 1 | Unnamed #1 | 540883 | 5589671 | | | 125,000 (debris) | LKqd |
| 2 | Unnamed #2 | 542134 | 5587338 | | | 150,000 (scar) | LKqd |
| 3 | Unnamed #3 | 547097 | 5603436 | | | 150,000 (debris) | LKTgd |
| 4 | Unnamed #4 | 538664 | 5590680 | | | 130,000 (scar) | LKqd |
| 5 | Unnamed #5 | 523374 | 5590345 | | | 300,000 (debris) | ImJLa |
| 6 | Unnamed #6 | 513123 | 5568986 | | | 700,000 (scar) | LJKP |
| 7 | Mystery Creek | 511613 | 5563543 | 2,200 to 3,600 BP | 40,000,000 | | LJKP |
| 8 | Unnamed #7 | 508080 | 5559573 | | | 600,000 (debris) | LJKqd |
| 9 | Unnamed #8 | 483566 | 5546488 | | | 100,000 (scar) | LJqd |
| 10 | Unnamed #9 | 484815 | 5545798 | | | 250,000 (scar) | LJqd |
| 11 | Unnamed #10 | 494541 | 5559907 | | | 150,000 (scar) | LJKgd |
| 12 | Unnamed #11 | 490936 | 5560643 | | | 100,000 (scar) | LJKgd |
| 13 | Unnamed #12 | 508596 | 5550912 | | | 120,000 (scar) | LJKqd |
| 14 | Unnamed #13 | 523622 | 5551864 | | | 500,000 (scar) | LJKP |
| 15 | Unnamed #14 | 519844 | 5544628 | | | 100,000 (scar) | LJKP |
| 16 | Unnamed #15 | 522001 | 5560935 | | | 150,000 (debris) | Kqd |
| 17 | Unnamed #16 | 534433 | 5579700 | | | 125,000 (debris) | Kgd |
| 18 | Unnamed #17 | 548782 | 5547002 | | | 180,000 (debris) | Migd |
| 19 | Unnamed #18 | 514477 | 5593080 | | | 125,000 (debris) | JKCe |
| 20 | Unnamed #19 | 516735 | 5577983 | | | 1,500,000 (debris) | IKGP |
| 21 | Spetch | 521601 | 5583022 | | | 285,000 (scar) | Kgd |
| 22 | Unnamed #20 | 505111 | 5564844 | | | 450,000 (debris) | LJKqd |
| 23 | Unnamed #21 | 484353 | 5553944 | | | 300,000 (debris) | MKgd |
| 24 | Gates Peak | 527490 | 5591371 | | | 700,000 (debris) | ImJLa |
| 25 | Unnamed #22 | 532669 | 5570269 | | | 300,000 (scar) | LKqd |
| 26 | Unnamed #23 | 535515 | 5568418 | | | 150,000 (debris) | LKqd |
| 27 | Unnamed #24 | 542162 | 5566309 | | | 150,000 (scar) | LKqd |
| 28 | Unnamed #25 | 519360 | 5560827 | | | 120,000 (debris) | LJKP |
| 29 | Unnamed #26 | 533767 | 5557706 | | | 800,000 (debris) | uTrCv |
| 30 | Fingerpost Ridge | 519347 | 5552183 | December 16, 2015 | | Unknown | LJKP |
| 31 | Unnamed #28 | 521803 | 5555769 | 2015? | | Unknown | LJKP |

Note: * based on Cui et al. (2017)

Table A2: Inventory of DSGSDs identified in the study area

| ID | Name | UTM Zone 10 | | Volume (m ³) | scar or debris (m ²) | Reference | Stratigraphic Unit* |
|----|-----------------------|-------------|----------|-----------------------------|-------------------------------------|--|------------------------|
| | | Easting | Northing | | | | |
| A | DSGSD #1 | 508694 | 5540823 | | | | IKGsv |
| B | DSGSD #2 | 543315 | 5591115 | | | | PCh |
| C | DSGSD #3 | 534318 | 5591739 | | | | LKqd |
| D | DSGSD #4 | 511022 | 5567612 | | | | LJKP |
| E | DSGSD #7 | 500091 | 5599088 | | | | uTrCv |
| F | DSGSD #8 | 509402 | 5599910 | | | | ImJLa |
| G | DSGSD #9 | 492697 | 5594322 | | | | LJKqd |
| H | DSGSD #10 | 519454 | 5583311 | | | | Kgd |
| I | DSGSD #11 | 509096 | 5551265 | | | | LJKqd |
| J | DSGSD #12 | 495523 | 5561081 | | | | LJKqd |
| K | DSGSD #13 | 512267 | 5598882 | | | | JKCs |
| L | DSGSD #14 | 517542 | 5601660 | | | | LKqd |
| M | DSGSD #15 | 545406 | 5599245 | | | | JKCs |
| N | DSGSD #16 | 514653 | 5569542 | | | | LJKP |
| O | Handcar Peak | 492674 | 5603295 | | | Hensold (2011) | uTrCsv |
| P | Mount Currie Ridge | 517838 | 5568552 | | | Evans (1987); Bovis and Evans (1995) | Kqd |
| Q | DSGSD #17 | 523296 | 5553435 | | | | LJKP |
| R | DSGSD #18 | 524194 | 5553315 | | | | LJKP |
| S | DSGSD #19 | 534433 | 5570889 | | | | LKqd |
| T | DSGSD #20 | 537042 | 5570343 | | | | LKqd |
| U | DSGSD #21 | 544002 | 5604218 | | | | Evd |
| V | DSGSD #22 | 545870 | 5603705 | | | | LKTgd |
| W | DSGSD #23 | 544259 | 5601555 | | | | JKCs |
| X | DSGSD #24 | 518421 | 5599044 | | | | ImJLa |
| Y | DSGSD #25 | 504230 | 5596706 | | | | uTrCv |
| Z | DSGSD #26 | 506683 | 5595132 | | | | uTrCv |
| A1 | DSGSD #27 | 507659 | 5593515 | | | | uTrCv |
| B1 | DSGSD #28 | 530673 | 5576909 | | | | Kgd |
| C1 | DSGSD #29 | 548465 | 5574201 | | | | PCh |
| D1 | DSGSD #30 | 542156 | 5560907 | | | | LKqd |
| E1 | DSGSD #31 | 513422 | 5564322 | | | | LJKP |
| F1 | DSGSD #32 | 532789 | 5561534 | | | | uTrCv |
| G1 | DSGSD #33 | 518786 | 5569106 | | | | Kqd |
| H1 | DSGSD #34 | 514784 | 5569139 | | | | LJKP |
| I1 | DSGSD #35 | 513990 | 5570627 | | | | LJKP |
| J1 | DSGSD #36 | 515280 | 5570197 | | | | LJKP |

Note: * based on Cui et al. (2015)

APPENDIX B
DETAILS OF PHOTOGRAMMETRY METHODOLOGY TO GENERATE
3D SURFACES AND EXTRACT DISCONTINUITY SURFACE
ORIENTATIONS

APPENDIX B: DETAILS OF PHOTOGRAMMETRY METHODOLOGY TO GENERATE 3D SURFACES AND EXTRACT DISCONTINUITY SURFACE ORIENTATIONS

Characterizing rock mass discontinuity parameters on high mountain rock slopes can be challenging because of limited access and rock fall hazard. Terrestrial digital photogrammetry allows reliable characterization of rock mass discontinuity geometrical parameters, such as orientation, persistence and spacing, based on photographs (Sturzenegger and Stead 2009a, 2009b; Lato et al. 2015). The methodology consists in generating 3D models (point clouds) of rock slopes based on field- or helicopter-based photographs, and then mapping rock mass discontinuities virtually on the 3D models by fitting planes on rock slope surfaces and traces.

B.1 Generating 3D Photogrammetric Models

In this project, 3D models were generated with the software PhotoScan (Agisoft, 2017). PhotoScan uses Structure-from-Motion photogrammetry to build 3D models on a large number of photographs of a scene/object taken from many viewpoints. This technique allows calculation of camera positions and orientations, together with the location of object points in 3D space. Figure B-1 shows an example of dense point cloud generated using helicopter-based photographs on Mount Currie.

In order to make meaningful measurements, the 3D models need to be registered. In this project, registration was achieved using (1) camera location coordinates measured with a GPS unit attached to the camera, or (2) ground control points (GCPs) extracted from the airborne LiDAR data set, where reliable GPS data could not be obtained.



Figure B-1 3D model of a rock slope on the north face of Mount Currie

B.2 Mapping Rock Mass Discontinuities on 3D Models

The generated 3D models were imported into the point cloud processing software CloudCompare (2017). One of CloudCompare tools allows delineating regions of the 3D model corresponding to rock mass discontinuity surfaces or traces. The orientation and size of these regions are then converted into dip and dip direction, and persistence, respectively, for further geotechnical analysis. Figure B-2 shows rock mass discontinuities mapped virtually on the 3D model of Figure B-1.

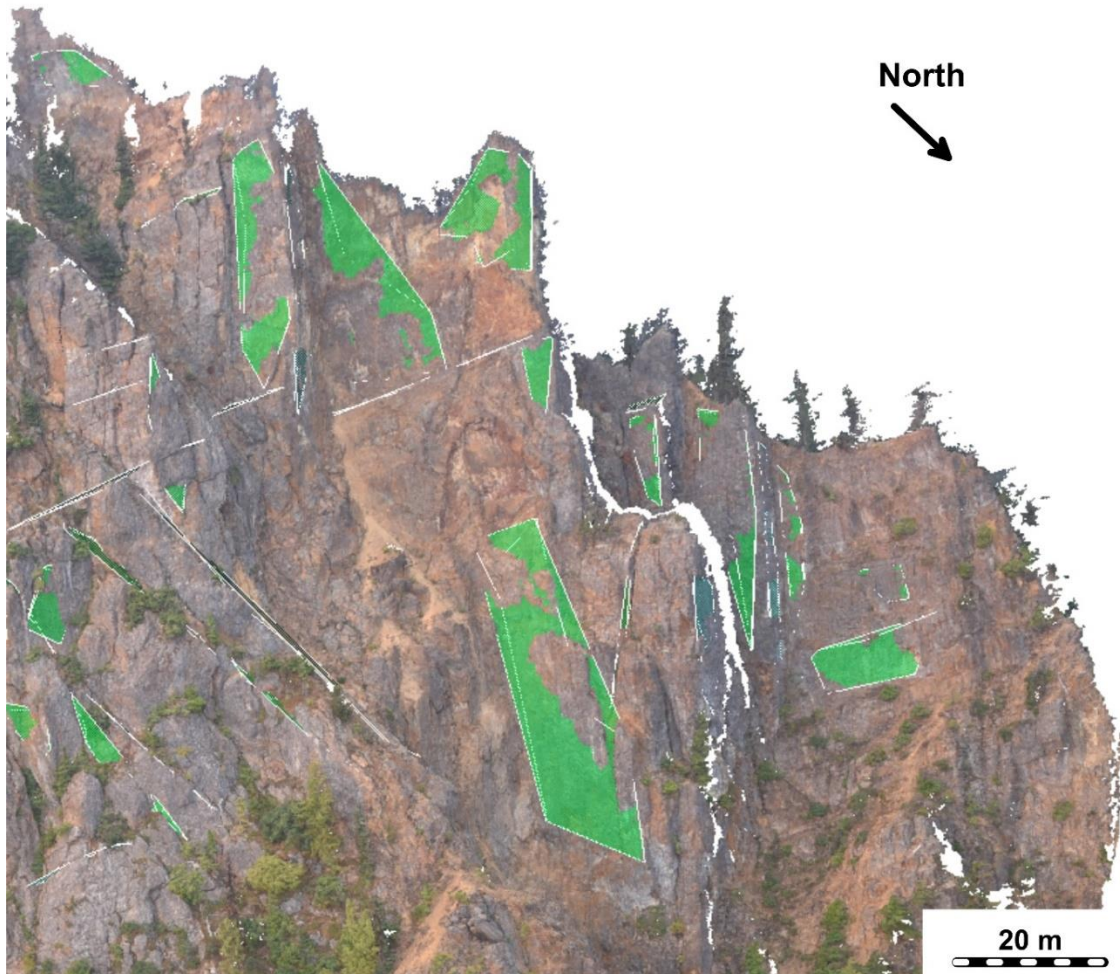


Figure B-2 Rock mass discontinuities (planes) mapped virtually on a section of the 3D model shown on Figure B-1.

References

Agisoft PhotoScan Professional, 2017, version 1.3.2. <http://www.agisoft.com/>

CloudCompare, 2017, version 2.9beta. <http://www.cloudcompare.org/>

Lato, M., Gauthier, D., Hutchinson, D.J., 2015. Selecting the optimal 3D remote sensing technology for the mapping, monitoring and management of steep rock slopes along transportation corridors. Transportation Research Record: Journal of the Transportation Research Board, Nn. 2510: 7 – 14.

Sturzenegger, M., Stead, D., 2009a. Close-range terrestrial digital photogrammetry and terrestrial laser scanning for discontinuity characterization on rock cuts. Engineering Geology 106: 163-182.

Sturzenegger, M., Stead, D., 2009b. Quantifying discontinuity orientation and persistence on high mountain rock slopes and large landslides using terrestrial remote sensing techniques. Natural Hazard and Earth System Sciences 9 (2): 267-287.

APPENDIX C
GEOPHYSICAL SURVEY REPORT FROM FRONTIER GEOSCIENCE
INC.

FRONTIER GEOSCIENCES INC.

SEISMIC REFRACTION AND
SEISMIC REFLECTION SURVEY REPORT
MT. CURRIE LANDSLIDE HAZARD ASSESSMENT
AND RISK ANALYSIS STUDY
PEMBERTON, BC

Submitted to:
BGC Engineering Inc.
September 29, 2017

Authors:
Beth Galambos, P.Geol.
Cliff Candy, P.Geol.

Project: FGI-1507

Table of Contents

| | |
|----------------------------------|---|
| 1. Introduction | 1 |
| 2. The Seismic Refraction Survey | 2 |
| 2.1 Survey Equipment | 2 |
| 2.2 Survey Procedure | 2 |
| 2.3 Interpretive Method | 3 |
| 3. The Seismic Reflection Survey | 4 |
| 3.1 Survey Equipment | 4 |
| 3.2 Survey Procedure | 4 |
| 3.3 Interpretive Method | 5 |
| 4. Geophysical Results | 6 |
| 4.1 General | 6 |
| 4.2 Discussion | 7 |
| 5. Limitations | 9 |

Illustrations

| | Location |
|---|----------|
| Figure 1 Survey Location Plan | Appendix |
| Figure 2 Site Plan | Appendix |
| Figure 3 Interpreted Depth Section SL-1 | Appendix |
| Figure 4 Interpreted Depth Section SL-2 | Appendix |

1. Introduction

During the period of July 27 to July 30, 2017, Frontier Geosciences Inc. carried out a seismic refraction and seismic reflection investigation for BGC Engineering Inc. in support of the Mt. Currie Hazard Assessment and Risk Analysis study in Pemberton, British Columbia. A Survey Location Plan of the area is shown at a scale of 1:50,000 in Figure 1 of the Appendix.

The purpose of the geophysical survey was to determine depth to bedrock and overburden layering information in the southern side of the valley. A Site Plan illustrating the location of the survey lines is presented at a scale of 1:10,000 in Figure 2 in the Appendix.



Seismic Line Location

2. The Seismic Refraction Survey

2.1 Survey Equipment

The seismic refraction investigation was carried out using a Geometrics Geode 24 channel, signal enhancement seismograph and Oyo Geospace 10 Hz geophones. Geophone intervals along the multicored seismic cable were maintained at 10 metres in order to ensure high resolution data on subsurface layering. Seismic energy was provided from small explosive charges buried in hand-excavated shotholes.

2.2 Survey Procedure

For each spread, the seismic cable was stretched out in a straight line and the geophones implanted. Up to seven separate 'shots' were then initiated: one at either end of the geophone array, up to three at intermediate locations along the seismic cable, and one off each end of the line, to ensure adequate coverage of the subsurface. The shots were triggered individually and arrival times for each geophone were recorded digitally in the seismograph. For quality assurance, field inspection of raw data after each shot was carried out, with additional shots recorded if first arrivals were unclear. Data recorded during field surveying operations was generally of good to excellent quality.

Throughout the survey, notes were recorded regarding seismic line positions in relation to topographic and geological features. Relative elevations along the seismic lines were recorded by chain and inclinometer, with absolute elevations referenced to topography from Google Earth.

2.3 Interpretive Method

The final interpretation of the seismic data was arrived at using the method of differences technique. This method utilises the time taken to travel to a geophone from shotpoints located to either side of the geophone. Velocities are calculated as the slope of first break pick times and geophone distances. When there is a significant change in slope a new velocity is calculated and assigned to the new layer. Basal velocities are calculated by the arrivals of off end shots where picked arrivals are refracted from the basal layer. Each geophone is assigned a velocity and time for each layer; in some areas the data provides slope velocities for only two layers, while in other areas four slope velocities are apparent. Using the total time, a small vertical time is computed which represents the time taken to travel from the refractor up to the ground surface. This time is then multiplied by the velocity of each overburden layer to obtain the thickness of each layer at that point. The thicknesses are splined along the seismic line to create a continuous boundary between layers.

3. The Seismic Reflection Survey

3.1 Survey Equipment

The seismic reflection surveying was carried out using four Geometrics Geode 24 channel, signal enhancement seismograph and Oyo Geospace 10 Hz geophones. Seismic energy was provided from small explosive charges buried in hand-excavated shotholes.

3.2 Survey Procedure

In this survey, a 'split spread' configuration was used with the energy source located in the middle of an array of 96 geophone receivers. This receiver array spanned a survey line length of 475 metres, and captured a broad spatial range of energy reflected from the horizons at depth. The survey procedure entailed collection of a 96 geophone record, then advancing the energy source 10 metres down the survey line and repeating the discharge and record process. This method, known as the common mid-point gather (CMP) technique, provides a very high degree of redundancy of sampling of the energy received from a given reflector at depth. The redundancy is used during the data processing procedure to develop an image of the subsurface reflectors of high fidelity. The seismic data acquired in this survey was generally of good to excellent quality.

Throughout the survey, notes were recorded regarding seismic line positions in relation to topographic and geological features. Relative elevations along the seismic lines were recorded by chain and inclinometer, with absolute elevations referenced to topography from Google Earth.

3.3 Interpretive Method

The data were recorded as a set of 2048 millisecond, SEG2 seismograms. The collected data sets were processed using the Seismic Unix software to provide the final stacked seismic profile and filtered shot gathers. The raw data at the first stage of the processing stand as a set of individual seismograms known as 'shot gathers'. The first stage of the processing involves the inspection of each of these records to reject non-relevant seismograms and noisy traces.

The second processing step consists in sorting the seismic traces using the shot and receiver positions to gather together each of the source and receiver pairs that were centred on a common spatial point. This 'common mid-point' or 'CMP gather' brings together each of the reflection ray paths that redundantly sample a given point on a subsurface reflector. First arrival mute was then applied to prevent first break energy from entering the reflection profile. In these CMP gathers, seismic reflections appear as a series of hyperbolic arcs.

Incoherent and coherent noise were then filtered using a frequency domain, band-pass filter with a lower limit of 20 Hz and an upper frequency of 210 Hz. A 100 millisecond automatic gain control was used to balance the trace amplitudes. Finally, the arrival time was adjusted to a reference datum in accordance with the respective relative elevation at each receiver.

The next stage in the processing flow was a determination of the apparent velocities within the CMP gathers from a semblance velocity analysis with a Constant-Velocity-Stack. Based on this velocity analysis, a normal move out correction was applied to derive CMP gathers with the hyperbolas flattened to the equivalent of zero offset records. The stacking process then adds together the energy in each of the traces of the CMP gather, improving the signal-to-noise ratio while reinforcing the reflectors energy. The seismic profile was assembled from all the CMP traces.

4. Geophysical Results

4.1 General

The interpreted results of seismic refraction line SL-1 and seismic reflection line SL-2 are illustrated at a scale of 1:2000 in Figures 3 and 4 in the Appendix. The seismic refraction method was used in the shallower bedrock region of the valley wall for line SL-1. The seismic reflection survey method was employed on SL-2 in the deeper valley sediments, north of the Green River.



Seismograph setup

4.2 Discussion

The interpreted results of the seismic refraction data indicate that line SL-1 is underlain by four seismic velocity layers. The surficial layer is 420 to 480 m/s and consists of loose surface soils. This surficial layer is relatively thin and highly variable, and has a maximum thickness of approximately 4 metres. This is underlain by a layer of 700 to 850 m/s that is likely earth materials of a low degree of compaction. The thickest part of this layer is located towards the uphill end of the coverage, with a thickness of 25 metres noted at station 250N.

The third layer varies between 1700 and 2250 m/s and represents materials with a higher degree of compaction. As well, the higher velocity zones may correspond to more coarse materials, such as cobbles and boulders within the sediments. These higher velocity regions are located in a smaller zone at station 300N and over a larger zone from 550N to 650N. This layer has a maximum interpreted thickness of 116 metres at the north end of the line. The layer three velocities at the north end of the line decrease to 1700 m/s, which may represent the larger influence of finer grained valley filling sediments in the deeper section. The deepest layer is interpreted to represent competent, crystalline bedrock, and exhibits velocities of between 4000 and 5200 m/s.

Line SL-2, surveyed with the seismic reflection method is displayed on Figure 4. The top panel shows the results of tomographic inversion of the compressional wave data to arrive at a velocity profile to a depth of 100 metres. This plot employs the same colour scale as the refraction profile, and as the range of velocity variation is much less, additional contour lines have been included to show the variation. The velocities show a general trend of reducing velocities towards the north, consistent with the presence of finer grained sediments such as clays, sands and gravels seen in nearby boreholes.

The SL-2 reflection data is shown in reflection colour amplitude format in the bottom panel of Figure 4. This shows the presence of a deep reflector, marked as a black line, at approximately sea level, that shows a low at 350N. A very strong, nearly horizontal reflector, indicated with a black dashed line, is seen at an elevation of approximately 75 metres. The southern part of this feature may be a flat lying lacustrine clay which provides a strong acoustic contrast with the overlying sediments. The shallower part of the section

shows a more complex sequence of reflectors. Two events have been identified, marked in green, that show a general dip to the north, ore towards the valley centre. The shallower of these is approximately correlated with the 1800 m/s contour line in the velocity panel.

5. Limitations

The depths to subsurface boundaries derived from seismic refraction and reflection surveys are generally accepted as accurate to within fifteen percent of the true depths to the boundaries. In some cases, unusual geological conditions may produce false or misleading data points with the result that computed depths to subsurface boundaries may be less accurate.

In seismic refraction surveying difficulties with a 'hidden layer' or a velocity inversion may produce erroneous depths. The first condition is caused by the inability to detect the existence of a layer because of insufficient velocity contrasts or layer thicknesses. A velocity inversion exists when an underlying layer has a lower velocity than the layer directly above it. The interpreted depths shown on drawings are to the closest interface location, which may not be vertically below the measurement point if the refractor dip direction departs significantly from the survey line location. Structural discontinuities occurring on a scale less than the geophone spacing or isolated boulders would go undetected in the interpretation of the data.

For seismic reflection, a range of errors from digitising, velocity modelling and data gridding are expected. Reflections can occur from surfaces not in the plane of the seismic reflection profile. As well, some uncertainty is present in correlating reflectors between profiles where there is a lack of cross points.

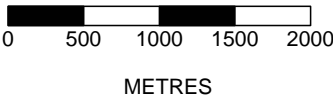
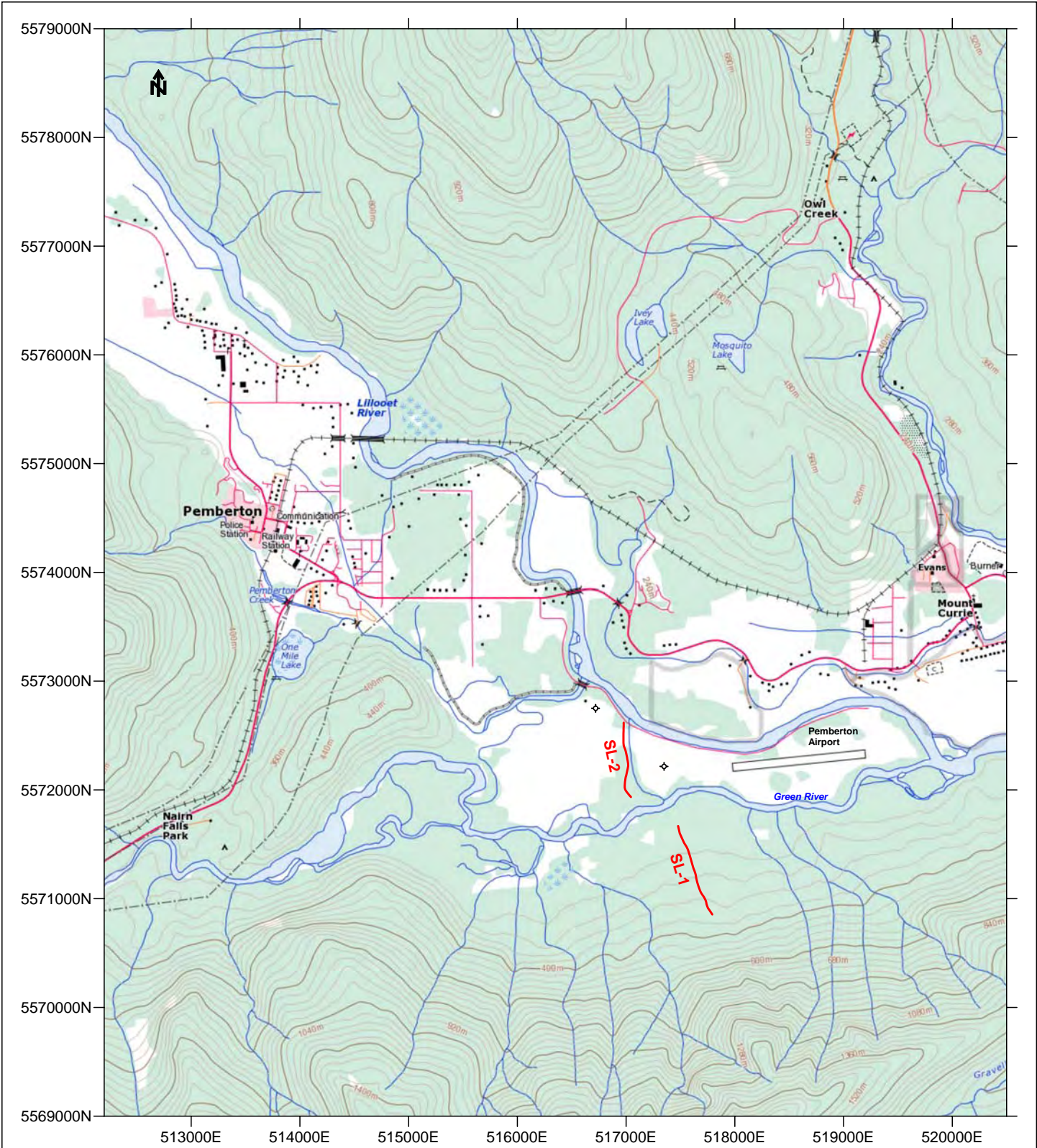
Observed anomalies in seismic data result from integration of perturbation in structure along the ray path. Perturbation is a smoothing operation and long-wavelength components of the structure are much easier to recover than short-wavelength ones.

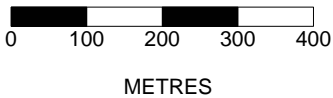
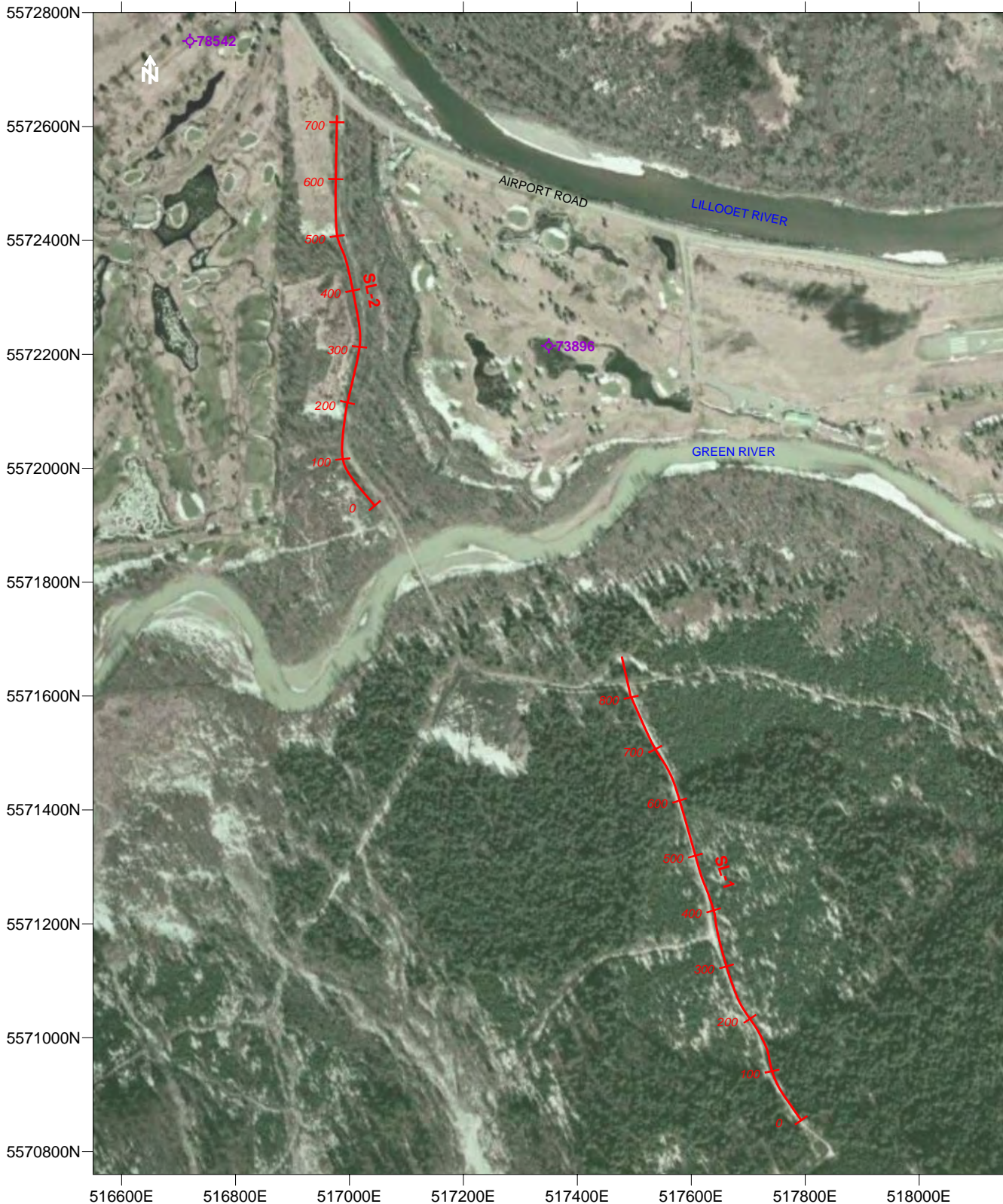
The information in this report is based upon geophysical measurements and field procedures and our interpretation of the data. The results are interpretive in nature and are considered to be a reasonably accurate representation of existing subsurface conditions within the limitations of the seismic refraction method.

For: Frontier Geosciences Inc.

Beth Galambos, P.Geo.

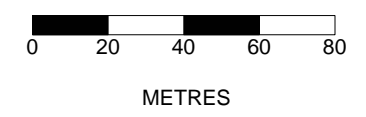
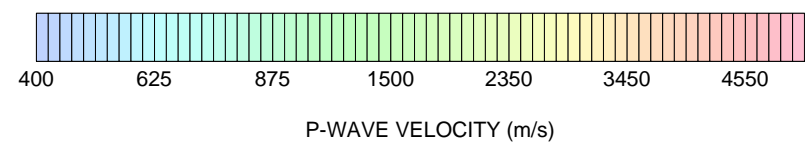
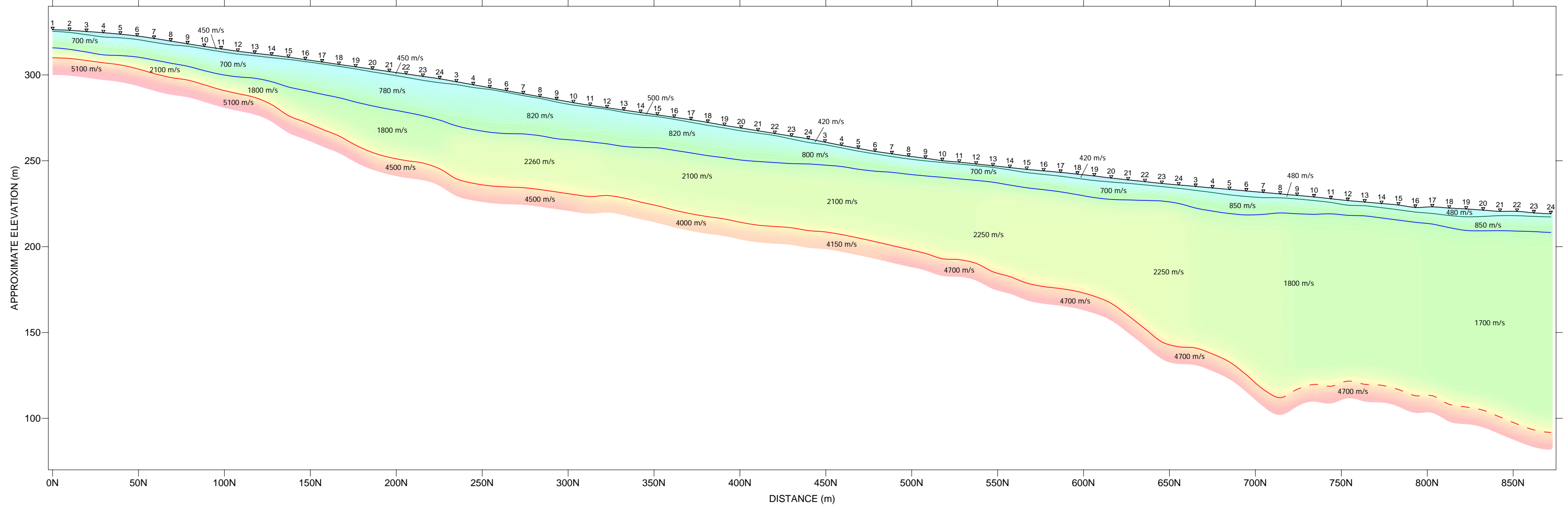
Cliff Candy, P.Geo.





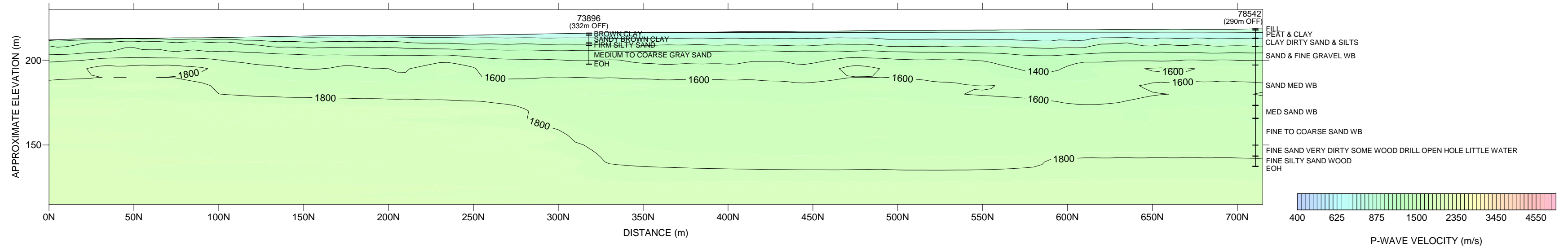
| | | |
|--|----------------|--------|
| BGC ENGINEERING INC. MT CURRIE LANDSLIDE HAZARD ASSESMENT | | |
| SEISMIC SURVEY | | |
| SITE PLAN | | |
| FRONTIER GEOSCIENCES INC. | | |
| DATE: JULY 2017 | SCALE 1:10,000 | FIG. 2 |

SL-1 SEISMIC REFRACTION PROFILE

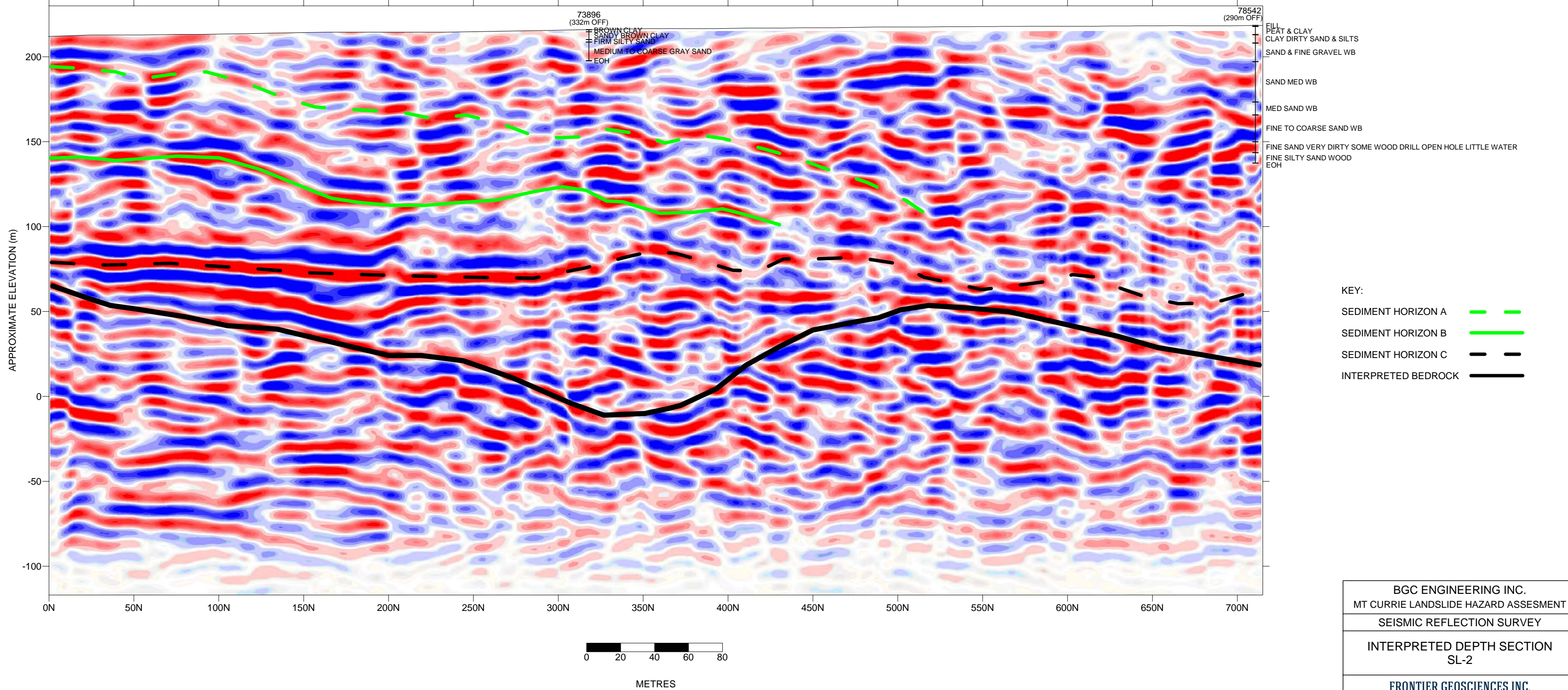


| | | |
|--|---------------|--------|
| BGC ENGINEERING INC. MT CURRIE LANDSLIDE HAZARD ASSESMENT | | |
| SEISMIC REFRACTION SURVEY | | |
| INTERPRETED DEPTH SECTION SL-1 | | |
| FRONTIER GEOSCIENCES INC. | | |
| DATE: JULY 2017 | SCALE 1:2,000 | FIG. 3 |

SL-2 VELOCITY PROFILE



SL-2 SEISMIC REFLECTION PROFILE



| | | |
|--------------------------------------|---------------|--------|
| BGC ENGINEERING INC. | | |
| MT CURRIE LANDSLIDE HAZARD ASSESMENT | | |
| SEISMIC REFLECTION SURVEY | | |
| INTERPRETED DEPTH SECTION SL-2 | | |
| FRONTIER GEOSCIENCES INC. | | |
| DATE: JULY 2017 | SCALE 1:2,000 | FIG. 4 |

APPENDIX D
DETAILS OF KINEMATIC ANALYSES CONDUCTED FOR THE
VARIOUS SECTIONS OF THE NORTH SLOPE OF MOUNT CURRIE

APPENDIX D: DETAILS OF KINEMATIC ANALYSES CONDUCTED FOR THE VARIOUS SECTIONS OF THE NORTH FACE OF MOUNT CURRIE

The upper part of the north face of Mount Currie is composed of a combination of gullies, steep rock slopes, and talus slopes. In order to undertake kinematic analyses in such a complex topography, it is necessary to consider the multiple slope orientations defined by these morphological features.

D.1 Defining Slope Orientation

Geomorphic mapping (Section 3.3) and rock mass characterization (Section 3.4.4) highlighted that the orientation of gullies on the upper part of the north face of Mount Currie is strongly controlled by discontinuity sets S1 (foliation) and D2. As a result, rock face orientations tend to correspond to the orientation of pre-existing discontinuity sets S1 and D2. Discontinuity set D5 was also observed to have a significant influence on the morphology of the mountain.

To confirm the above observations, and to define representative rock face orientations to be used in the kinematic analysis, the airborne LiDAR data was analyzed with the program Coltop3D (Jaboyedoff et al. 2007). Coltop3D uses a Hue-Saturation-Intensity (HSI) wheel system to color-code a point cloud or digital elevation model (DEM) according to ground surface dip and dip direction. Using this software, Figure D-1 shows the distribution of slope angles on the upper part of the north face of Mount Currie.

Figure D-1, Table D-1 and Table D-2 confirms that slope orientations are closely related to the main discontinuity sets characterized in the field and using photogrammetry. The small differences are likely related to a combination of DEM smoothing of the topography (Brideau et al. 2012), and the tendency of large natural slope to form composite surfaces formed by combinations of discontinuity sets (Sturzenegger and Stead 2009).

Table D-1 Slope orientations of the SW Domain on the north face of Mount Currie and corresponding discontinuity sets.

| Slope Orientation | | Controlling Discontinuity Set | | |
|-------------------|-------------------|-------------------------------|---------|-------------------|
| Dip (°) | Dip Direction (°) | Set | Dip (°) | Dip Direction (°) |
| 57 | 015 | S1 | 71 | 031 |
| 68 | 309 | D2 | 78 | 331 |
| 40 | 80 | D5 | 45 | 100 |

Table D-2 Slope orientations of the NE Domain on the north face of Mount Currie and corresponding discontinuity sets.

| Slope Orientation | | Controlling Discontinuity Set | | |
|-------------------|-------------------|-------------------------------|---------|-------------------|
| Dip (°) | Dip Direction (°) | Set | Dip (°) | Dip Direction (°) |
| 47 | 001 | S1 | 85 | 032 |
| 61 | 239 | S1 (opposite quadrant) | 87 | 212 |
| 64 | 304 | D2 | 87 | 312 |
| 46 | 076 | D5 | 30 | 101 |

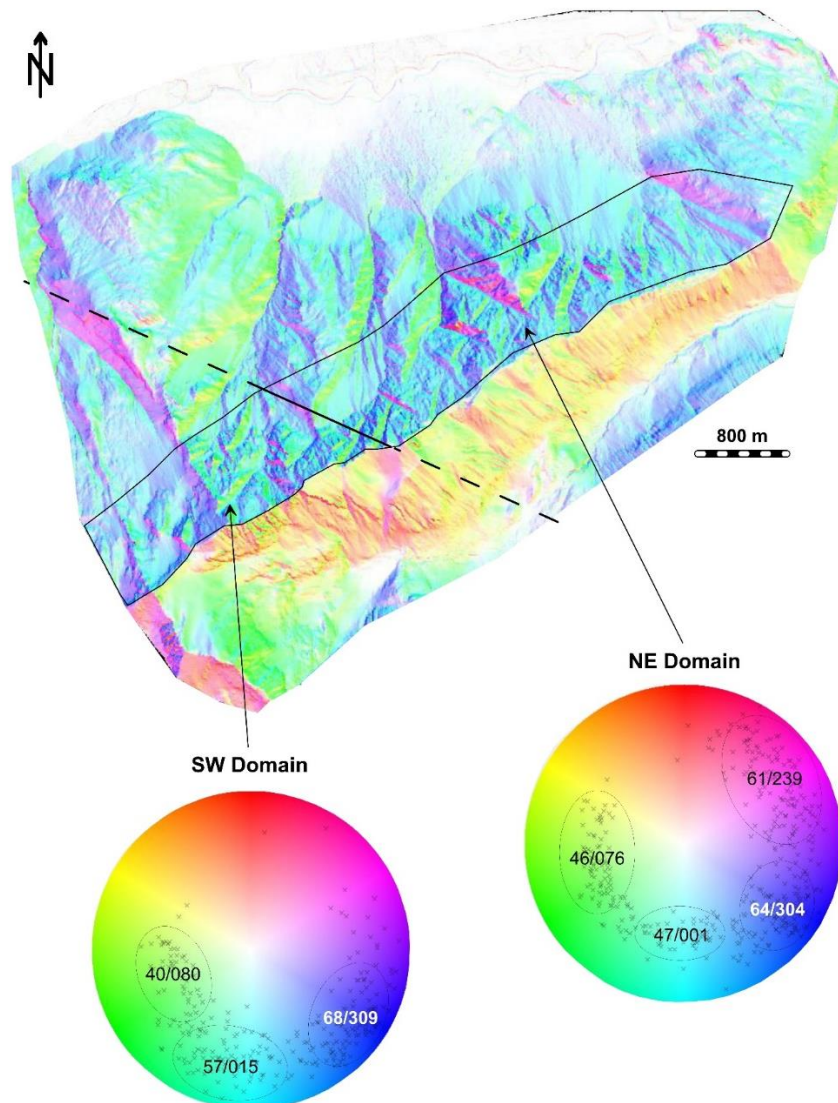


Figure D-1 Airborne LiDAR data of Mount Currie color-coded and processed with the software Coltop3D. The stereonets for each structural domain show slope orientation measurements from the upper part of the north face of the mountain and three or four main slope orientations.

D.2 Kinematic Analysis

The purpose of a kinematic analysis is to identify feasible structurally-controlled failure mechanisms, such as planar sliding, wedge failure and flexural toppling. It considers discontinuity orientation, slope orientation and the friction angle along the discontinuity surfaces. A kinematic analysis asks the questions: (a) Is a slope failure kinematically possible along observed geological structures?; and (b) if so, what mechanisms of slope failure are possible? A kinematic analysis does not calculate a factor of safety and, as such, does not constitute a slope stability assessment which was also outside of BGC's scope. A kinematic analysis also does not provide information regarding the volume of rock mass that could be unstable.

The stereographic techniques for the kinematic analysis of these simple slope failure mechanisms are described in Richards et al. (1978). For a wedge or planar type failure mechanism to be kinematically feasible, a discontinuity set or the line of intersection of discontinuities must have a dip greater than the friction angle along the discontinuity surface. Flexural toppling is possible along discontinuities dipping into the slope at an angle steep enough for interlayer slip to occur. However, flexural toppling generally occurs when the rock mass forms thin and elongated rock blocks.

The software Dips (Rocscience 2017) was used to perform the kinematic analysis. The zone of instability is represented by red zones on the stereonets shown in Figure D-2. The friction angle along all discontinuities was assumed to be 25° based on the planar/undulating and rough discontinuity surface conditions observed in the field. As no site-specific laboratory test results are available to constrain the friction angle used, Barton (1976) and Kulhawy (1975) were consulted for representative values.

The results of the analysis are summarized in Table D-3. Although the results show that one or several failure mechanisms are possible along most slope orientations of the upper part of the north face of Mount Currie, it does not necessarily mean that failure will happen everywhere. Failure likelihood depends on a number of additional parameters, including the actual physical presence of an adversely oriented discontinuity (or combination of discontinuities), discontinuity persistence, and groundwater conditions.

Nevertheless, Figure D-1 illustrates examples of failure mechanism observed or inferred on the north face of Mount Currie:

- Planar sliding along D4 is the assumed potential failure mechanism of Sources ID 1 and 2 (Section 3.3) where the slopes are dipping to the north – northeast (Figure D-2a);
- Wedge sliding along the line of intersection formed by S1 and D4 is the inferred mechanism controlling the August and September 2016 failures north of Currie N1 (SW Domain) where the slope is dipping to the northwest (Figure D-2b).
- Flexural toppling along S1 is a widespread failure mechanism along the NE ridge of Mount Currie (NE Domain), where slopes are dipping to the north – northeast (Figure D-2c).

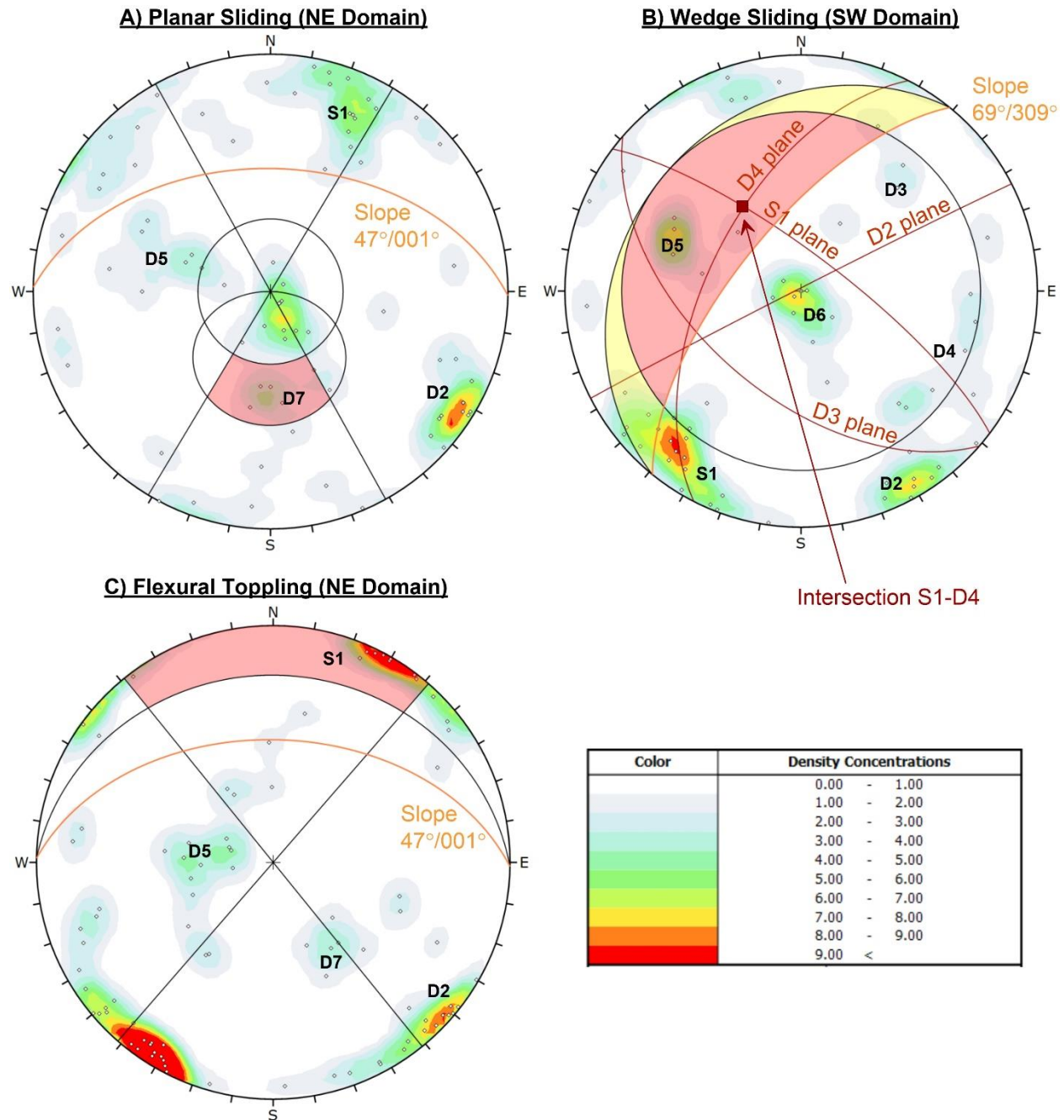


Figure D-2 Example of kinematic analysis for (a) planar sliding, (b) wedge sliding, and (c) flexural toppling. The stereonet shows lower hemisphere equal area projections, and the contours are percentage of total pole measurements per 1% area.

Table D-3 Kinematic analysis results for the Southwest and Northwest Domains. The significance of potential mechanisms is rated as high (red), moderate (yellow) or low (green) based on a relative significance (RS) factor.

| Structural Domain | Slope Orientation (dip/dip direction) (°) | Discontinuity Characterization Method | Failure Mechanism | | |
|-------------------|---|---------------------------------------|-------------------|----------------------------|-------------------|
| | | | Planar Sliding | Wedge Sliding | Flexural Toppling |
| SW Domain | 57/015 | Compass Data | S1*; D6* | D2-D5 | D2; D3* |
| | | Photogrammetry Data | S1*; D2* | D2-D5; S1-D4* | S1*; D2 |
| | 68/309 | Compass Data | D4; D6* | S1-D4; D2-D4; D3-D4; | D2; D5 |
| | | Photogrammetry Data | D2; D4 | S1-D4; D2-D3; D2-D4; D3-D4 | D2; D5 |
| | 40/080 | Compass Data | D5* | D2-D5 | - |
| | | Photogrammetry Data | D5 | D2-D5 | - |
| NE Domain | 47/001 | Compass Data | D7 | S1-D7*; D2-D7; D7-D5* | S1; D2* |
| | | Photogrammetry Data | D7 | S1-D7 | S1; D2* |
| | 61/239 | Compass Data | S1* | S1-D7* | S1* |
| | | Photogrammetry Data | - | S1-D7* | S1 |
| | 64/304 | Compass Data | D7* | - | D2; D5* |
| | | Photogrammetry Data | D7 | S1-D7 | D2 |
| | 46/076 | Compass Data | D5 | S1-D5*; D2-D7; D7-D5* | S1*; D2 |
| | | Photogrammetry Data | D5 | S1-D5* | S1 |

Note:

* Failure mechanism marginally feasible, i.e., poles or lines of intersection plot near the edge of the failure envelope; or only a small number of poles plot within the failure envelope.

To better assess the likelihood of failure mechanisms, BGC developed an approach to estimate the “relative significance” (RS) of discontinuity sets. This method assumes that certain discontinuity sets are more likely to generate failures than others, based on three criteria:

- The RA factor ranks discontinuity based on their geological significance, higher ranking being assigned to regional-scale geology fabrics, such as lineaments (Figure D-3), faults, bedding and/or foliation.
- The SS factor ranks discontinuity sets based on their relative concentration (i.e., frequency of occurrence).

- The IA factor provides more weight to discontinuity sets known to be involved in previous failure events.

The RS score is calculated by multiplying the three factors and the results are shown in Table D-4 and Table D-5 for the Southwest and Northeast Domains, respectively. The failure mechanisms listed in Table D-3 are colored in red (high), yellow (moderate) and green (low) according to the RS score.

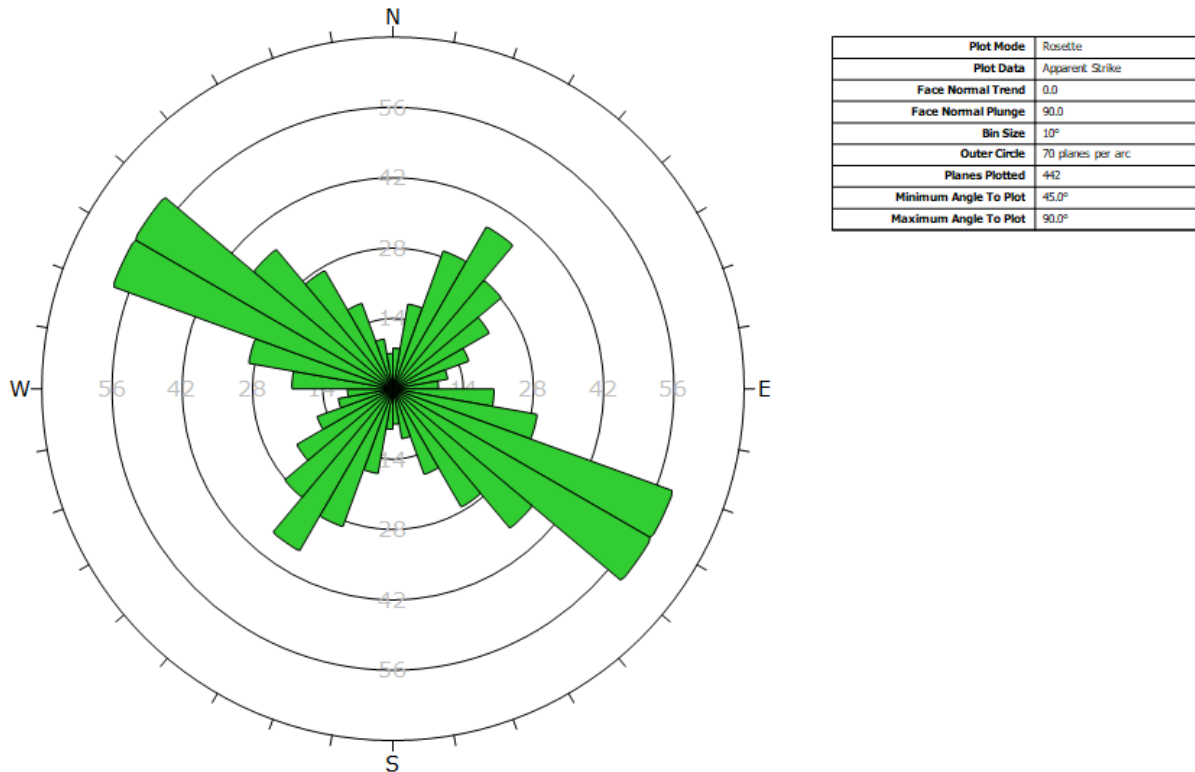


Figure D-3 Rosette diagram of lineaments mapped at Mount Currie (Drawing 04 of main report). The trend of the lineaments corresponds to the orientation of S1 and D2 discontinuity sets.

Table D-4 Relative significance factors for the discontinuity sets of the Southwest Domain

| Discontinuity Set | RA | SS | IA | RS |
|-------------------|------|-----|-----|-------|
| S1 | 1 | 1 | 1 | 1 |
| D2 | 0.75 | 0.8 | 0.5 | 0.3 |
| D3 | 0.5 | 0.1 | 0.5 | 0.025 |
| D4 | 0.5 | 0.3 | 1 | 0.15 |
| D5 | 0.5 | 0.5 | 0.5 | 0.125 |
| D6 | 0.5 | 0.6 | 0.5 | 0.15 |

Table D-5 Relative significance factors for the discontinuity sets of the Northeast Domain

| Discontinuity Set | RA | SS | IA | RS |
|--------------------------|-----------|-----------|-----------|-----------|
| S1 | 1 | 1 | 1 | 1 |
| D2 | 0.75 | 0.8 | 1 | 0.6 |
| D7 | 0.5 | 0.1 | 1 | 0.05 |
| D5 | 0.5 | 0.3 | 0.5 | 0.075 |
| D6 | 0.5 | 0.5 | 0.5 | 0.125 |

References

Barton, N., 1976. The shear strength of rock and rock joints. *International Journal of Rock Mechanics, Mining Sciences and Geomechanics Abstracts* 13: 255-279.

Brideau, M.-A., Sturzenegger, M., Stead, D., Jaboyedoff, M., Lawrence, M., Roberts, N., Ward, B., Millard, T. and Clague, J., 2012. Stability analysis of the 2007 Chehalis Lake landslide based on long-range terrestrial photogrammetry and airborne LiDAR data. *Landslides* 9: 75-91.

Jaboyedoff, M., Metzger, R., Oppikofer, T., Couture, R., Derron, M.-H., Locat, J. and Turmel, D., 2007. New insight techniques to analyze rock-slope relief using DEM and 3D-imaging cloud points: Coltop-3D software. In *Proceedings of the 1st Canada – US Rock Mechanics Symposium*, Vancouver, Canada, May 2007.

Kulhawy F.H., 1975. Stress deformation properties of rock and rock discontinuities. *Engineering Geology* 9: 327-350.

Richards, L.R., Leg, G.M.M. and Whittle, R.A. 1978. Appraisal of stability conditions in rock slopes. In: Bell F.G. (Ed.) *Foundation Engineering in Difficult Ground*, pp. 449-512.

Rocscience Inc. 2017. Dips software, version 7, <https://www.rocscience.com/>

Sturzenegger, M., Stead, D., 2009. Quantifying discontinuity orientation and persistence on high mountain rock slopes and large landslides using terrestrial remote sensing techniques. *Natural Hazard and Earth System Sciences* 9 (2): 267-287.

APPENDIX E
ROCK AVALANCHE PROBABILITY OF OCCURRENCE ESTIMATE
USING THE NORWEGIAN ROCK SLOPE ASSESSMENT APPROACH

APPENDIX E: ROCK AVALANCHE PROBABILITY OF OCCURRENCE ESTIMATE USING NORWEGIAN ROCK SLOPE ASSESSMENT APPROACH

The rock avalanche probability of occurrence estimates outlined in this report used a regional rock avalanche frequency derived from an inventory of large rapid rock slope failures identified in the study area. This method had previously been developed by BGC for other potential rock slope failures in BC. The regional rock avalanche frequency estimates were adjusted to reflect the kinematics and activity conditions (measured movement or signs of movement) specific to the different potential rock avalanche sources identified on Mount Currie based on desktop and field observations. The correction factors applied to the regional rock avalanche frequency are significant sources of uncertainty. While kinematic feasibility and level of activity (displacement rate and rock fall) are generally accepted as factors indicative of a greater susceptibility to rock avalanches, the correction factor is founded on BGC's judgement that was achieved by specialist group consensus.

To compare and validate BGC's probability of occurrence, the hazard and risk assessment methodology by Hermanns et al. (2012) was applied to the potential rock avalanche zones 1 and 2 on Mount Currie. This methodology is a hazard scenario-based system derived from Norwegian experience in assessing large unstable slopes that can cause loss of life. The system focuses on structural criteria (existence of a back-scarp, sliding surface, lateral failure boundaries, as well as kinematics) and the analysis of the slope activity (landslide velocity, change in deformation rate, rock fall activity, and the presence of nearby historic or prehistoric events). The methodology allows the users to assign relative probabilities to account for the uncertainty in their characterization of the site. Based on the site-specific relative probability of each parameter, a relative score and associated hazard class can be calculated. The assumed input for Mount Currie's potential rock avalanche source zones 1 and 2 are shown in Figure E-1 and Figure E-2. The resulting hazard and consequence (based on analyses in Section 5.0) values are presented in the risk matrix (Figure E-3) that is part of the Hermanns et al. (2012) methodology.

Blikra et al. (2016) added a secondary axis to the risk matrix (Figure E-3) which provides an estimate of the probability of rock avalanche occurrence. Table E-1 summarizes the estimates using the Norwegian methodology (Hermanns et al. 2012 and Blikra et al. 2016) and compares it values obtained Section 3.5.6. The rock avalanche probability of occurrence estimate values in are assuming current climate conditions. See Section 3.5.7 of the main report for a discussion on the potential influence of climate change on the rock avalanche probability of occurrence.

Table E-1. Summary of the rock avalanche probability of occurrence estimates based on the Norwegian methodology (Figure E-3) and the BGC methodology discussed in Section 3.5.6 of the main report. The 5th and 95th percentile correspond to 2 standard deviations on either side of the normal distribution.

| Methodology | Rock Avalanche Scenario | Probability of Occurrence Estimate | | |
|--|-------------------------|------------------------------------|----------|-----------------------------|
| | | 5 th Percentile | Mean | 95 th Percentile |
| Hermanns et al., 2012 | Zone 1 | 1/20,000 | 1/5,000 | 1/1,000 |
| | Zone 2 | 1/100,000 | 1/15,000 | 1/4,000 |
| BGC's adjusted regional frequency (from Section 3.5.6) | Zone 1 | - | 1/5,000 | - |
| | Zone 2 | - | 1/11,00 | - |

| | | | | | | | |
|-------------------|--------------|------------------|--------|-----------------|--------------------|--------------|------------|
| Site name: | Mount Currie | Scenario: | Zone 1 | Made by: | Marc-Andre Brideau | Date: | 12/20/2017 |
|-------------------|--------------|------------------|--------|-----------------|--------------------|--------------|------------|

| Hazard classes | Class upper limit | Probability | Cumulative probability | Hazard scores | Fitted normal distribution |
|----------------|-------------------|-------------|------------------------|---------------------------------|-----------------------------|
| Very low | 2.4 | 0.0 % | 0.0 % | Minimum 3.3 | Mean μ 5.2 |
| Low | 4.8 | 32.4 % | 32.4 % | Maximum 9.3 | St. dev. σ 1.1 |
| Medium | 7.2 | 59.7 % | 92.2 % | Mode 5.0 | Mean - 2σ 3.0 |
| High | 9.6 | 7.8 % | 100.0 % | Mean 5.4 | Mean + 2σ 7.5 |
| Very high | 12.0 | 0.0 % | 100.0 % | 5 th percentile 3.7 | Corr. coeff. 0.9997 |
| | | | | 95 th percentile 7.3 | K-S-test (max. diff.) 2.9 % |

| | Score | Rel. prob. | Norm. prob. |
|--|-------|------------|-------------|
| 1. Back-scarp | | | |
| Not developed | 0 | 0 | 0.0 % |
| Partly open over width of slide body (few cm to m) | 0.5 | 0 | 0.0 % |
| Fully open over width of slide body (few cm to m) | 1 | 1 | 100.0 % |
| 2. Potential sliding structures | | | |
| No penetrative structures dip out of the slope | 0 | 2 | 66.7 % |
| Penetrative structures dip on average < 20 degree or steeper than the slope | 0.5 | 1 | 33.3 % |
| Penetrative structures dip on average > 20 degree and daylight with the slope | 1 | 0 | 0.0 % |
| 3. Lateral release surfaces | | | |
| Not developed | 0 | 1 | 25.0 % |
| Partly developed on 1 side | 0.25 | 2 | 50.0 % |
| Fully developed or free slope on 1 side or partly developed on 2 sides | 0.5 | 1 | 25.0 % |
| Fully developed or free slope on 1 side and partly developed on 1 side | 0.75 | 0 | 0.0 % |
| Fully developed or free slope on 2 sides | 1 | 0 | 0.0 % |
| 4. Kinematic feasibility test | | | |
| Kinematic feasibility test does not allow for planar sliding, wedge sliding or toppling | 0 | 0 | 0.0 % |
| Failure is partly kinematically possible (movement direction is more than $\pm 30^\circ$ to slope orientation) | 0.5 | 0 | 0.0 % |
| Failure is kinematically possible (movement direction is less than $\pm 30^\circ$ to slope orientation) | 0.75 | 2 | 40.0 % |
| Failure is partly kinematically possible on persistent discontinuities (movement direction is more than $\pm 30^\circ$ to slope orientation) | 0.75 | 2 | 40.0 % |
| Failure is kinematically possible on persistent discontinuities (movement direction is less than $\pm 30^\circ$ to slope orientation) | 1 | 1 | 20.0 % |
| 5. Morphologic expression of the rupture surface | | | |
| No indication on slope morphology | 0 | 2 | 66.7 % |
| Slope morphology suggests formation of a rupture surface (bulging, concavity-convexity, springs) | 0.5 | 1 | 33.3 % |
| Continuous rupture surface is suggested by slope morphology and can be mapped out | 1 | 0 | 0.0 % |
| 6. Displacement rates | | | |
| No significant movement | 0 | 0 | 0.0 % |
| 0.2 - 0.5 cm/year | 1 | 4 | 80.0 % |
| 0.5 - 1 cm/year | 2 | 1 | 20.0 % |
| 1 - 4 cm/year | 3 | 0 | 0.0 % |
| 4 - 10 cm/year | 4 | 0 | 0.0 % |
| > 10 cm/year | 5 | 0 | 0.0 % |
| 7. Acceleration (if velocity is >0.5 cm/yr and <10 cm/yr) | | | |
| No acceleration or change in displacement rates | 0 | 1 | 50.0 % |
| Increase in displacement rates | 1 | 1 | 50.0 % |
| 8. Increase of rock fall activity | | | |
| No increase of rock fall activity | 0 | 1 | 50.0 % |
| Increase of rock fall activity | 1 | 1 | 50.0 % |
| 9. Past events | | | |
| No post-glacial events of similar size | 0 | 0 | 0.0 % |
| One or several events older than 5000 years of similar size | 0.5 | 1 | 50.0 % |
| One or several events younger than 5000 years of similar size | 1 | 1 | 50.0 % |

Figure E-1. Rock slope hazard assessment score for potential rock avalanche source Zone 1 based on the methodology proposed by Hermanns et al. (2012).

| | | | | | | | |
|-------------------|--------------|------------------|--------|-----------------|--------------------|--------------|------------|
| Site name: | Mount Currie | Scenario: | Zone 2 | Made by: | Marc-Andre Brideau | Date: | 12/20/2017 |
|-------------------|--------------|------------------|--------|-----------------|--------------------|--------------|------------|

| Hazard classes | Class upper limit | Probability | Cumulative probability | Hazard scores | Fitted normal distribution |
|----------------|-------------------|-------------|------------------------|---------------------------------|-----------------------------|
| Very low | 2.4 | 4.6 % | 4.6 % | Minimum 1.8 | Mean μ 3.9 |
| Low | 4.8 | 72.7 % | 77.3 % | Maximum 7.8 | St. dev. σ 1.1 |
| Medium | 7.2 | 22.1 % | 99.4 % | Mode 3.8 | Mean - 2 σ 1.7 |
| High | 9.6 | 0.6 % | 100.0 % | Mean 4.1 | Mean + 2 σ 6.2 |
| Very high | 12.0 | 0.0 % | 100.0 % | 5 th percentile 2.3 | Corr. coeff. 0.9994 |
| | | | | 95 th percentile 6.1 | K-S-test (max. diff.) 4.3 % |

| | Score | Rel. prob. | Norm. prob. |
|--|-------|------------|-------------|
| 1. Back-scarp | | | |
| Not developed | 0 | 0 | 0.0 % |
| Partly open over width of slide body (few cm to m) | 0.5 | 1 | 25.0 % |
| Fully open over width of slide body (few cm to m) | 1 | 3 | 75.0 % |
| 2. Potential sliding structures | | | |
| No penetrative structures dip out of the slope | 0 | 2 | 66.7 % |
| Penetrative structures dip on average < 20 degree or steeper than the slope | 0.5 | 1 | 33.3 % |
| Penetrative structures dip on average > 20 degree and daylight with the slope | 1 | 0 | 0.0 % |
| 3. Lateral release surfaces | | | |
| Not developed | 0 | 2 | 50.0 % |
| Partly developed on 1 side | 0.25 | 1 | 25.0 % |
| Fully developed or free slope on 1 side or partly developed on 2 sides | 0.5 | 1 | 25.0 % |
| Fully developed or free slope on 1 side and partly developed on 1 side | 0.75 | 0 | 0.0 % |
| Fully developed or free slope on 2 sides | 1 | 0 | 0.0 % |
| 4. Kinematic feasibility test | | | |
| Kinematic feasibility test does not allow for planar sliding, wedge sliding or toppling | 0 | 0 | 0.0 % |
| Failure is partly kinematically possible (movement direction is more than $\pm 30^\circ$ to slope orientation) | 0.5 | 0 | 0.0 % |
| Failure is kinematically possible (movement direction is less than $\pm 30^\circ$ to slope orientation) | 0.75 | 3 | 75.0 % |
| Failure is partly kinematically possible on persistent discontinuities (movement direction is more than $\pm 30^\circ$ to slope orientation) | 0.75 | 1 | 25.0 % |
| Failure is kinematically possible on persistent discontinuities (movement direction is less than $\pm 30^\circ$ to slope orientation) | 1 | 0 | 0.0 % |
| 5. Morphologic expression of the rupture surface | | | |
| No indication on slope morphology | 0 | 3 | 75.0 % |
| Slope morphology suggests formation of a rupture surface (bulging, concavity-convexity, springs) | 0.5 | 1 | 25.0 % |
| Continuous rupture surface is suggested by slope morphology and can be mapped out | 1 | 0 | 0.0 % |
| 6. Displacement rates | | | |
| No significant movement | 0 | 2 | 40.0 % |
| 0.2 - 0.5 cm/year | 1 | 2 | 40.0 % |
| 0.5 - 1 cm/year | 2 | 1 | 20.0 % |
| 1 - 4 cm/year | 3 | 0 | 0.0 % |
| 4 - 10 cm/year | 4 | 0 | 0.0 % |
| > 10 cm/year | 5 | 0 | 0.0 % |
| 7. Acceleration (if velocity is >0.5 cm/yr and <10 cm/yr) | | | |
| No acceleration or change in displacement rates | 0 | 1 | 50.0 % |
| Increase in displacement rates | 1 | 1 | 50.0 % |
| 8. Increase of rock fall activity | | | |
| No increase of rock fall activity | 0 | 1 | 50.0 % |
| Increase of rock fall activity | 1 | 1 | 50.0 % |
| 9. Past events | | | |
| No post-glacial events of similar size | 0 | 0 | 0.0 % |
| One or several events older than 5000 years of similar size | 0.5 | 1 | 50.0 % |
| One or several events younger than 5000 years of similar size | 1 | 1 | 50.0 % |

Figure E-2. Rock slope hazard assessment score for potential rock avalanche source Zone 1 based on the methodology proposed by Hermanns et al. (2012).

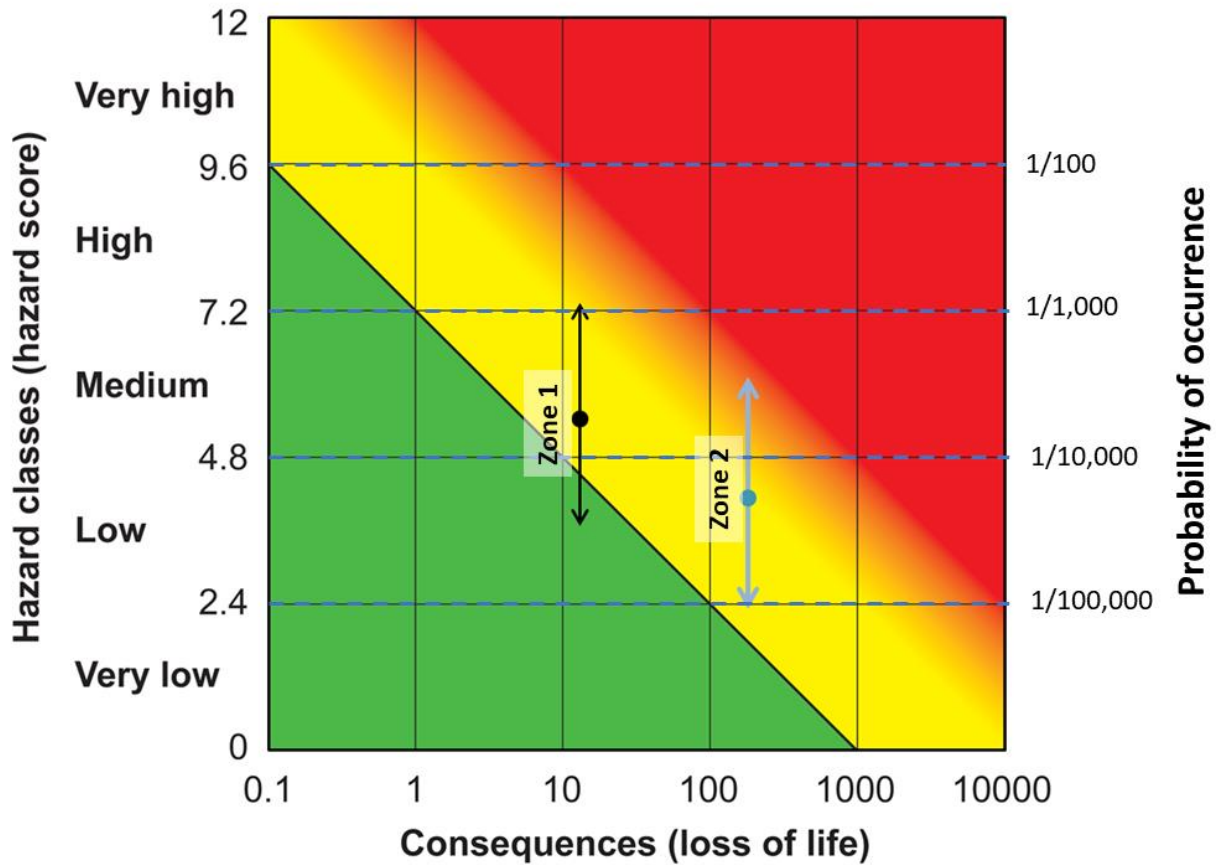


Figure E-3. Risk assessment matrix based on the methodology proposed by Hermanns et al. (2012) and the probability of occurrence presented in (Blikra et al. 2016). The range of hazard score represent the spread between the 5th and 95th percentile based on the relative probability assigned to each parameter in Figure E-1 and Figure E-2.

References

Blikra, L.H., Majala, G., Anda, E., Berg, H., Eikennaes, O., Helgas, G., Oppikofer, T., Hermanns, R., Bohme, M., 2016. Fare- og risikoklassifisering av ustabile fjellparti. Prepared by Norges vassdrags- og energidirektorat, Report Number 77-2016.

Hermanns, R.L., Oppikofer, T., Anda, E., Blikra, L.H., Bohme, M., Bunkholt, G., Crosta, G.B., Dahle, H., Devoli, G., Fischer, L., Jaboyedoff, M., Loew Simon, Saetre, S., Yugsi Molina, F., 2012. Recommended hazard and risk classification system for large unstable rock slopes in Norway. Prepared by Norges geologiske undersokelse, Report Number 2012.029.

APPENDIX F
JAKOB ET AL., 2016. REGIONAL DEBRIS-FLOW AND DEBRIS-FLOOD
FREQUENCY-MAGNITUDE CURVES. PROCEEDINGS OF
GEOVANCOUVER 2016

Regional Debris-flow and Debris-Flood Frequency-Magnitude Curves

Jakob, M., Bale, S., and McDougall, S.
BGC Engineering Inc., Vancouver, BC, Canada
Friele, P.
Cordilleran Geoscience, Squamish, BC, Canada



ABSTRACT

Frequency-magnitude (F-M) relationships of debris flows and debris floods are notoriously difficult to compile because of the paucity of direct observations, the discontinuous nature of the event occurrence, the obfuscation of field evidence due to progressive erosion or debris inundation and, finally, the inherent challenge of finding suitable statistical methods to analyse the dataset. Detailed F-M analyses are also rather costly and invasive given the plethora of field and analytical techniques involved in their generation. Some reprieve can be granted once a number of reliable F-M curves have been assembled in a specific region. These curves can be applied to watersheds for which detailed studies are unavailable, unaffordable or impractical due to lack of datable field evidence. Individual F-M curves require normalization by fan area or fan volume to account for the different geomorphic activity and processes inherent in watersheds with variable sizes, debris production and sediment output. We showcase regional F-M curves for debris flows in southwestern British Columbia and debris floods in the Bow River valley near Canmore. These curves are statistically analysed to estimate error around the logarithmic best-fit estimate. Strong negative deviations of watersheds for which detailed F-M relationships have been established from the fitted curve could herald inherent watershed stability, while strong positive deviations could signal extraordinary watershed mass movement processes or suggest that the fan may be largely of paraglacial origin. We caution against the indiscriminate use of regionally based F-M curves, especially in watersheds where multiple geomorphic upland processes are suspected that result in bi-model data population distributions, thus violating underlying statistical assumptions.

RÉSUMÉ

Les relations entre la fréquence et la magnitude (FM) des coulées de débris et les inondations de débris sont reconnues pour être difficiles à compiler en raison de la rareté des observations directes, la nature épisodique des événements, des évidences de terrain qui s'effritent en raison de l'érosion progressive ou des inondations de débris et, aussi, du défi inhérent à identifier des méthodes statistiques appropriées pour analyser l'ensemble des données. Les analyses détaillées F-M sont également coûteuses et invasives étant donné le nombre de techniques de terrain et d'analyses de laboratoire requis pour leurs créations. Un sursis peut être accordé une fois qu'un certain nombre de courbes F-M fiables ont été assemblés dans une région spécifique et celles-ci peuvent être appliqués aux bassins versants pour lesquels des études détaillées ne sont pas disponibles, inabordable ou impossible en raison du nombre insuffisant d'échantillons de terrain disponible pour la datation. Chaque courbe F-M nécessite une normalisation en utilisant la superficie ou le volume du cône de déjection pour tenir compte de la différence d'activité géomorphologique et des processus inhérents dans les bassins versants de tailles variables, ainsi que de la production de débris et sédiments. Nous présentons des courbes régionales F-M pour les coulées de débris du sud-ouest de la Colombie Britannique et d'inondations de débris dans la vallée de la rivière Bow, près de Canmore. Ces courbes sont analysées statistiquement pour estimer l'erreur autour de l'équation logarithmique ayant la meilleure concordance. Des écarts négatifs prononcés pour des bassins versants pour lesquels des F-M relations détaillées ont été établies à partir de la courbe ajustée pourraient annoncer une stabilité inhérente du bassin versant tandis que de fortes déviations positives pourraient signaler des processus extraordinaires de mouvement de terrain dans ces bassins versants ou suggérer que le cône de déjection est en grande partie d'origine paraglaciale. Nous mettons en garde contre l'utilisation sans fondement des courbes F-M construite à base de données régionale, en particulier dans les bassins versants où on soupçonne la présence de plusieurs processus géomorphologiques de montagne ce qui résulte en des répartitions bimodales de la population de données, ce qui va à l'encontre des hypothèses du model statistiques.

1 INTRODUCTION

Debris flows and debris floods occur almost daily somewhere on Earth. This is unsurprising given the millions of steep mountain creeks globally and the notion that debris flows are often the dominant process in delivering upland sediments to the receiving valley floodplains via their fans or direct confluence. 'Debris flow', as defined by Hung et al. (2014), is a very rapid, channelized flow of saturated

debris containing fines (i.e. sand and finer fractions) with a plasticity index of less than 5%.

Debris flows originate from single or distributed source areas in regolith mobilized by the influx of ground- or surface water. Liquefaction occurs shortly after the onset of landsliding due to turbulent mixing of water and sediment, and the slurry begins to flow downstream, entraining additional water and channel debris. Typical debris flows require a channel gradient of at least 27% (15°) for

transport over significant distances (Takahashi, 1991) and have volumetric sediment concentrations in excess of 50%.

Debris flows are difficult and costly to forecast temporally and are often lethal because they travel long distances at extremely rapid velocities (e.g. Allstadt 2013). Debris flows are characterized by extreme impact forces.

A 'debris flood' is "a very rapid surging flow of water heavily charged with debris in a steep channel" (Hungar et al., 2001). Transitions from water flows to debris floods occur at minimum volumetric sediment concentrations of 3 to 10%, the exact value depending on the particle size distribution of the entrained sediment and the ability to acquire yield strength. Since debris floods are characterized by heavy bedload transport, rather than by a more homogenous mixture of suspended sediments typical of hyperconcentrated flows (Pierson, 2005), the exact definition of sediment concentration depends on how sediment is transported in the water column. Debris floods occur on creeks that are not steep enough to convey debris flows. Unlike the latter, they transport only a portion of the available sediment load in the alluvial beds to the fan. In that they act as a conveyor belt of debris transport with the severity and duration of the storm being the on-off switch for the conveyor. Debris floods are somewhat slower than debris flows and lack the highly destructive frontal surge, but are characterized by the potential for severe bank erosion which can undermine structures even at considerable setback distance to the stream channel.

Fans have long been viewed as the comparatively safer place to live in flood-prone mountain valleys. In more recently developed areas, no records of damaging debris flows or debris floods may exist, instilling the illusion of a lack of hazard. Moreover, hydrogeomorphic hazards are still poorly understood or appreciated by various levels of government and the public alike (Church 2013, Jakob et al. 2015).

Most debris-flow hazard assessments require that the magnitude of events be established for a range of return periods. This is the basis for risk assessments in which life loss and/or economic consequences are systematically included. Magnitude may be expressed as the total volume of debris mobilized, its peak flow rate, or both. Frequency is the annual probability of events, or its inverse, the return period. Debris-flow intensity is estimated by combining velocities and flow depth as a surrogate for impact force, which is a proxy of its destructiveness (Jakob et al. 2012).

Since runoff modelling and risk analysis follow the establishment of the frequency-magnitude (F-M) relationship, any error introduced in its estimate will propagate through the hazard and risk analyses and potentially over- or under-estimate risk. By extension this may lead to over- or under-design of risk reduction measures.

To establish reliable F-M curves, especially for longer return periods (sometimes up to a 10,000-year return period), requires a combination of several absolute dating methods, test trenching, hydrology, sedimentology and geomatics applications to interpolate results across a fan's surface. It also relies on empirical relationships between debris-flow volumes and peak flows as well as areas inundated by debris and their associated volumes. Such

studies can take several months and their costs may range, depending on the size of the fan and assets at risk, from tens of thousands of dollars to \$1,000,000. While such capital expenditures are often justifiable for large urban developments, they are more difficult to justify, or are affordable, for single land owners who wish to subdivide their property. In areas where comprehensive studies on debris-flow or debris-flood frequencies and magnitude have been conducted, a simple normalization procedure based on fan area or fan volume can be applied to approximate F-M relationships and potentially reduce the need for invasive and costly field investigation.

In this paper, we show how regional frequency-magnitude relationships were used to establish a fan-area or fan-volume normalized F-M relationship for two study areas: one focuses on debris flows in southwestern British Columbia and the other relates to debris floods in the Canadian Rocky Mountains. The respective regional F-M curves may be transferred to other locations as a screening tool with caution. Over time, as more detailed debris-flow and debris-flood studies are being conducted and feeding into a common dataset, more regional F-M curves can be developed and refined.

2 STUDY AREA

Two study areas are considered in this paper, as shown in Figure 1. One area is located in southwestern B.C.'s Coast Mountains, and the other is located in the eastern Rocky Mountains of Alberta, centred around the Town of Canmore and the Hamlet of Exshaw.



Figure 1. The left-hand circle pertains to the debris-flow study areas in southwestern British Columbia, and the right hand circle pertains to the debris-flood study area in southwestern Alberta.

2.1 Southwestern British Columbia

The main geological structures in the study area are mid-Cretaceous to early Tertiary in age and include systems of west and east-vergent contractional faults, right-lateral strike-slip faults and extensional faults. The majority of sites included in this study are located in the Coast Plutonic Complex (Wheeler and Gabrielse 1971). One major volcanic centre is included (Mount Garibaldi, drained by Cheekye River) with Quaternary volcanic activity.

Quaternary glaciation has strongly influenced geomorphic processes in the southwestern Coast Mountains. Extensive blankets of basal and ablation till mantle slopes at most sites included in this paper. Mesozoic and late Cenozoic tectonics determined the major alignment of valleys within the study area, which developed from prolonged Cenozoic fluvial erosion. Multiple glaciations during the Pleistocene occurred in which valleys were deepened and widened. At higher elevations, glacial landforms developed, including cirques, horns, arêtes, and overdeepened valley heads. Below approximately 2200 m, glacial erosion developed rounded ridges and roche moutonnée features. The erosional legacy of glaciation was an extensive system of steep,

undercut slopes, many of which are criss-crossed by discontinuities created by earlier tectonic events. Many of these joints, foliations and faults are favorably oriented for slope movement and thus exert an important control on modern-day mass movements (Holm et al. 2004).

2.2 Southwestern Alberta

The Canadian Rocky Mountains are a fold and thrust belt, where thick units of more erosion-resistant Paleozoic carbonates were folded and thrust progressively in a north-westerly direction over more friable Mesozoic sandstones and shales. Four main rock sequences can be characterized in the Canmore region.

The oldest unit at the base is part of the North American cratonic plate. The next unit is the Pre-Cambrian to Lower-Cambrian carbonate rock unit composed of weathered rock. The ~ 6.5 km thick middle carbonate unit consists of marine carbonates (limestone and dolostone) and shale. The upper unit (~ 5 km thick) is a young Jurassic to Tertiary unit of sandstone, shale, conglomerate and coal.

Osborn *et al.* (2006) describe the final stages of mountain building as being associated with differential erosion of various units. The softer Mesozoic rocks led to rounded mountain tops exposing the underlying rocks that can support steeper and higher slopes. Most geologic units flanking Bow River valley are primarily composed of thick Carboniferous and Devonian successions.

The majority of the rock formations are sedimentary with minor metamorphic components. Geologic formations that are more resistant to erosion are more conducive to the formation of cliffs, while more recessive units tend to form sloping ledges.

Thrust faults and folds in the region strike in a northwest to southeast direction. Two common joint sets can be differentiated: strike joints parallel to the orientation of bedding planes and dip joints that are perpendicular to bedding. The main channel of Cougar Creek and adjacent tributaries is oriented approximately at a right angle to the main thrust fault belt. The deep incision through the regional structural grain favours large scale instability in the watershed, primarily rockslides and rock avalanches. Large-scale failures of this type can and have travelled into the valley bottom where they can dam creeks, creating a sizable impoundment given the low overall creek channel gradient (5%). BGC (2014b) has documented at least twelve relic landslide dams along the mainstem channel of Cougar Creek.

3 METHODS

The hypothesis that guided this study is that the fan area or fan volume (where reasonably well preserved) is a proxy for a watershed's geomorphic activity. Larger or more voluminous fans should indicate a higher frequency and/or higher magnitude hydrogeomorphic events compared to smaller or less voluminous fans. According to this hypothesis, it should be possible to normalize detailed site-specific F-M curves by either fan area or fan volume. Combining several detailed F-M curves and plotting a best-fit line with reasonable statistical fit then provides a

regionally-averaged F-M estimate, which can be used to estimate F-M curves for creeks where detailed F-M data are not available. The statistical analysis allows plotting of confidence or prediction intervals that exemplify expected error bounds.

BGC completed quantitative debris-flow and debris-flood hazard assessments for 15 steep creek fans in the Town of Canmore and Municipal District of Bighorn, located about 100 km west of Calgary. Detailed hazard and risk assessments were completed for 10 of those fans (BGC, 2014a,b,c,d,e,f; BGC 2015a,b,c,d,e,f,g), seven of which were prone to debris floods. These fans form the basis for the regional debris-flood F-M curves for southwestern Alberta, as presented in this paper.

Several detailed debris-flow hazard and risk assessments have been completed in southwestern B.C. for different clients over a period of approximately 10 years. The studies were carried out over the past 10 years by BGC Engineering and Cordilleran Geoscience.

The hazard assessments entailed the reconstruction of detailed F-M relationships for debris floods and debris flows. The methods to decipher magnitudes and frequencies of past events included dendrochronology to date events and delineate previous deposits from impact scars and reaction wood, and stratigraphic analysis of natural exposures and backhoe excavated test pits. In stratigraphic analysis, radiocarbon dating and tephrochronology was employed to provide chronological control for frequency analysis. Empirical formulae relating debris-flow or debris-flood area to debris volume allowed back-calculation of debris volumes where only areas had been measured. In two cases, bimodality was identified in the population of hydrogeomorphic events and they were analysed separately. In the case of Cougar Creek (Bow River Valley), rock slide deposits along the creek channel provided evidence of episodic landslide damming. Landslide dams were reconstructed and their respective breaches were modelled numerically to arrive at peak discharge and sediment volume estimates. Frequency of such events were estimated by dividing the number of likely landslide dams by 10,000 years, which encompasses the approximate time of deglaciation in the watershed.

In the case of Cheekye River (southwestern B.C.), three very large events were deciphered. One debris flow, the so-called Garbage Dump event, was reconstructed through excavator-assisted trenching on the fan and radiocarbon dating of organic materials found in the deposit. This allowed extrapolation of the measured thickness in various trenches. In addition, high resolution LiDAR allowed the spatial delineation of the Garbage Dump debris-flow deposit. The other two volumes from Cheekye River debris flows were estimated indirectly: Evidence of two debris flows were found in the lake bottom sediments of Stump Lake (Clague et al. 2003). For debris flows to discharge into this lake, they would have to overflow a bedrock sill separating Cheekye River channel from the lake. The cross-section was measured and the flow velocity estimated to arrive at a peak discharge estimate. Finally, an empirical relationship developed by Mizuyama (1992) between peak discharge and total volume for volcanic debris flows was employed to arrive at a debris-flow volume estimate (Clague et al. 2003). Consequently, those two

event volumes are associated with significant error compared to the Garbage Dump debris flow. The very large debris flows from the Mount Garibaldi volcanic complex are thought to originate from rock avalanches evolving into debris flows and were thus analysed separately from the events thought to be triggered by heavy rain or rain-on-snow events (Jakob and Friele 2010).

For each project, a frequency-magnitude curve was established using a combination of techniques but relying on the Gutenberg-Richter cumulative frequency method (Gutenberg and Richter, 1954) as well as the Pareto distribution (summarized in Jakob, 2012).

The regional relations shown in Figures 2, 3 and 4 predict the sediment volume (V_S) in m^3 generated for various return period (T) events and normalized by fan area (A_f) and fan volume (V_f) in km^2 or km^3 . Log fits were added as they most closely represent the data distributions.

4 RESULTS

F-M curves from southwestern Alberta and southwestern B.C. for debris floods and debris flows were combined to produce regional curves normalized by fan area and fan volume (Figures 2 to 4).

The regional debris-flow relation (Equation 1, Figure 2) was developed by BGC from the detailed study of nine creeks in southwestern BC and has a coefficient of determination (R^2) of 0.65.

$$V_S = A_f[54,230 \ln(T) - 161,714] \quad [\text{Eq. 1}]$$

The regional debris-flood relation (Equation 2, Figure 3) normalized by fan area was developed by BGC from the detailed study of seven creeks in the Bow Valley, near Canmore, Alberta (BGC, 2014d, 2015a, b, c, f) with an R^2 of 0.51.

$$V_S = A_f[4116 \ln(T) + 1786] \quad [\text{Eq. 2}]$$

In the detailed hazard assessment of debris floods and debris flows in the Bow Valley, BGC also estimated the volume of fans by comparing the fan surface topography to the inferred valley bottom surface. These data were used to create a second regional debris-flood relation normalized by fan volume (Equation 3, Figure 4). This relation is based on the detailed study of five creeks and has an R^2 of 0.54.

$$V_S = V_f[353 \ln(T) + 224] \quad [\text{Eq. 3}]$$

In the case of Cougar Creek (Figure 2 and 3), there is a strong deviation from the regional best fit. Not shown on Figures 2 to 4 are confidence bands and prediction limits, though those can be added for the specific creeks as needed. This can be attributed to Cougar Creek also being subject to landslide dam outbreak floods, which implies that a secondary debris-flood generating process is acting in the watershed. The danger of ignoring such process bimodality is further stressed in Section 5. In the case of Mackay Creek (Figure 2), fan erosion has been considered as a process to increase debris flow volumes. This may

explain the strong deviation from the best fit line in this case.

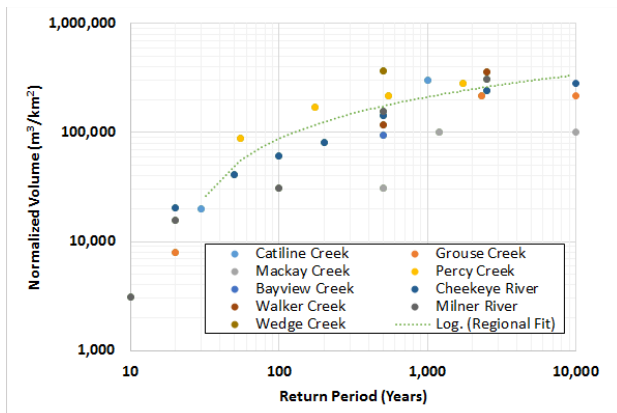


Figure 2. Regional frequency-magnitude curve for southwestern B.C. debris flows normalized by fan area.

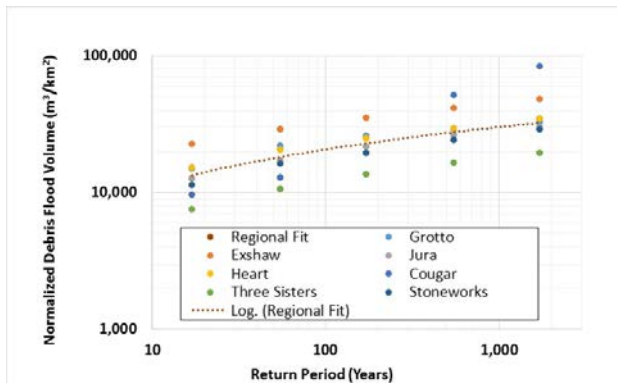


Figure 3. Regional frequency-magnitude curve for Bow Valley debris floods normalized by fan area.

All graphs (Figure 2 to 4) are plotted as log-log graphs, yet show an asymptotic best curve fit. The physical basis for the asymptotic nature of the best fit line lies in the fact that sediment supply (or water) is limited in most instances. Debris flows cannot become indefinitely large due to source material depletion. This is either controlled by the available sediment in a channel system for supply-limited watersheds, or by the volume of landslides that may feed into the debris-flow channel system.

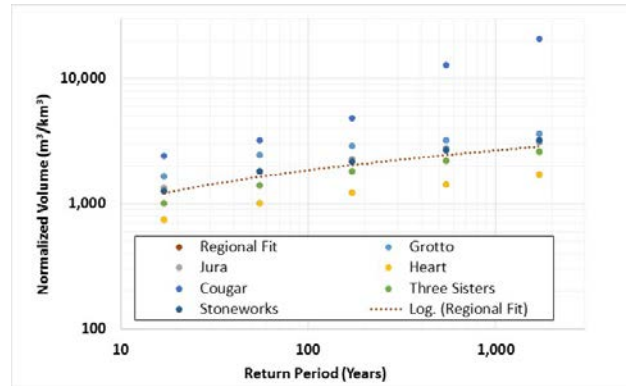


Figure 4. Regional frequency-magnitude curve for Bow Valley debris floods normalized by fan volume.

In the case of debris floods, the amount of debris available to be mobilized is controlled by the duration of a rainstorm with sufficient severity that results in discharge above a critical shear stress threshold for full surface gravel layer mobilization (typically defined as the mobilization threshold for the 95%th percentile grain size). This, in turn, is controlled by the regional meteorology, which again limits the volume and the intensity of rainstorms. In many cases, this implies that, for example, a 10,000-year return period event may not be much larger than a 1,000-year return period event, unless a bi-modal geomorphic process distribution can be identified that acts only at higher return period classes (see the example of Cougar Creek).

5 DISCUSSION

Regionally-based debris-flow and debris-flood frequency-magnitude curves are not to be used indiscriminately or in lieu of detailed hazard assessments, especially where hydrogeomorphic events can result in severe economic losses, environmental degradation or life loss. Regional curves developed in one region are likely not valid in another without some adjustments. Differences in bedrock or surface geology or watershed morphometry as well as the degree of watershed vegetation and regional climate may, to some degree, invalidate the regional curves developed elsewhere. However, they are useful at a screening level in absence of any other method because the general relationship between fan area/volume and geomorphic activity persists irrespective of the above factors.

Another complicating factor is introduced by multiple processes generating debris flood or flows in a watershed. For example, a watershed subject to outburst floods in addition to regular floods may have a deflection point in its F-M curve that would be masked by lumping of data in the regional F-M curves. Cougar Creek serves as an example (Figure 5). Similarly, F-M curves from watersheds with steep fans that are subjected to fan erosion in the proximal portions of a fan and re-deposition in the distal fan segments, may lead to overestimation of debris-flow volumes for respective return periods.

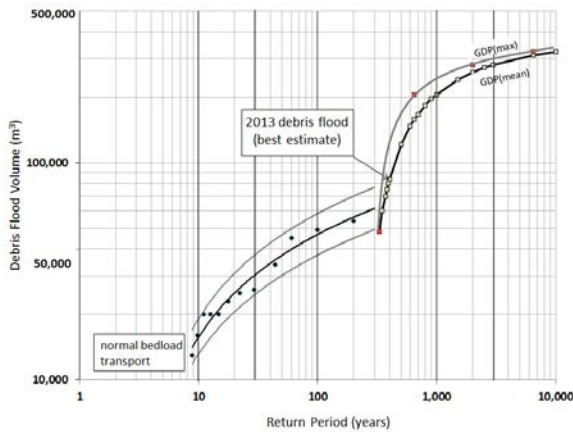


Figure 5. Frequency-magnitude curve for Cougar Creek, Canmore. The change from “normal” debris floods to landslide-generated outbreak floods occurs at approximately the 300 year return period.

The methods introduced in this paper are not suitable for fans that have been truncated by higher-order streams. In those cases, a measurement of fan area or fan volume would underestimate the true values and result in underestimates of debris-flow or debris-flood volumes for the respective return periods. Finally, for those fans bordering lakes or oceans, measuring the fan area or volume could be misleading as parts of the fan are invariably under water and thus not accounted for on topographic maps. Therefore, some bathymetry information is needed, or at least high resolution air photos or satellite images should be used to trace the fringe of the fan visible through shallow water.

6 APPLICATION

BGC applied the regional debris-flow relation developed for southwestern B.C. to Hope Creek as part of a screening-level study. Such studies are frequently being conducted to obtain a preliminary understanding of the nature of the hazard without large capital expenditures necessary for a comprehensive hazard study. They do not, however, replace such studies if the screening-level hazard study indicates a high loss potential.

Hope Creek is located at the fringes of the Town of Hope, B.C and has a history of large debris flows, including an event in 1984, two events in 1995 and an event in 2002. Elements at risk include two highways, a railway, several buildings and an oil pipeline. The fan area is 0.65 km²

The results (Figure 6) suggest that debris-flow sediment volumes range from 23,000 m³ for frequent events (30-year return period) to 210,000 m³ for rare events (1000-year return period).

The 1995 debris flow on Hope Creek had a volume of 50,000 m³ (Jakob et al. 1997) and the 2002 debris flow had a volume of 13,000 m³, as estimated by Linear Consulting and Golder Associates (2002). Based on the F-M relation for Hope Creek, the 2002 event was approximately a 30-year return period event. The volume of sediment mobilized in the 1995 event was equivalent to

approximately a 100-year event. However, Jakob et al. (1997) describe the contribution of sediment in the 1995 event to be largely from the remobilization of fan deposits rather than from sediment recruited in the watershed. The process of debris flows described in the F-M relation above are for the latter (watershed sediment recruitment). Therefore, while peak flows were relatively low for the 1995 event (250 m³/s, Jakob et al. 1997), corresponding to a 30-year return period, the sediment recruitment was atypically high.

The channel upstream of the fan apex has not been surveyed by BGC and the volume of entrainable sediment is unknown. However, between the elevations of 860 m and 1,150 m, an unstable rock mass has been identified on air photographs which frequently supplies debris to the channel.

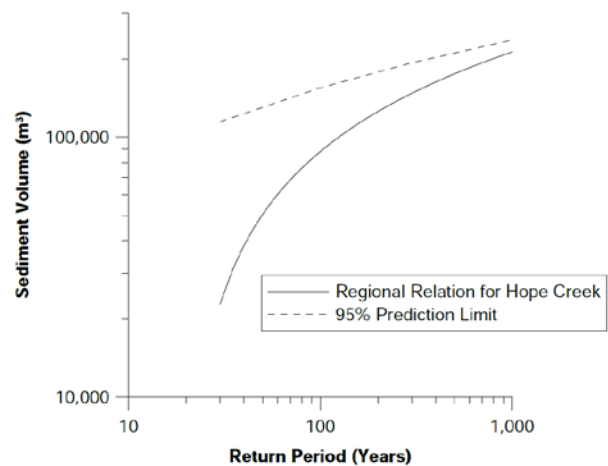


Figure 6. Application of the regional F-M curve for southwestern B.C. for Hope Creek.

It is somewhat contradictory that the 95% prediction limit approaches the best fit line. The prediction intervals define a range of values within which a response is likely to fall given a specified value of a predictor. In hydrology, the confidence and prediction limits result in “trumpet” curves with a widening of the bounds for higher return period. In this case, a narrowing of the 95% prediction limit for higher return periods can be attributed to the supply limitations for all studied fans.

Figure 6 was then used in two ways: First as volume input for a runout model, and second, to solve an empirical relationship between peak discharge and total volume of debris flows to estimate the former. Peak flow rate and volume was then combined to construct a debris flow hydrograph as input to a runout model.

7 CONCLUSION

A reliable debris-flow risk assessment requires an underpinning F-M model (Moon et al. 2005). Those are notoriously difficult and/or costly to develop. Tools to decipher past events in time and magnitude exist. Absolute dating methods such as radiocarbon, dendrochronology and tephrochronology, or varve counting where the

receiving water body is a lake can be combined with empirical formulae, careful mapping and stratigraphic analyses to construct F-M data pairs. Application of extreme value statistics aids to generate F-M curves from the data and allows attribution of error bounds. Consulting practice has demonstrated that combination of such techniques can be very costly and, if not done rigorously, can lead to erroneous results. An incorrect F-M relationship will result in false intensity maps and, in cases of substantial error, fictitious risk estimates. In some cases, budget restrictions simply do not allow application of such rigorous methods and lesser effort is still preferable to poorly supported professional judgment. A regional F-M relationship, as developed in this paper based on fan area or fan volume normalization, provides a tool to constrain debris-flow magnitudes for a variety of return periods with minimal effort and without the necessity of field studies.

It would be naïve to believe that this method can fully replace detailed field studies, especially for high consequence scenarios such as larger urban or industrial developments. For this reason, the technique presented in this contribution is not meant to replace the said F-M estimation methods and rigorous field-based methods. In Canada, the level of effort appropriate for such studies is well described, for example, in the APEGBC Guidelines for Flood Assessments in a Changing Climate (2010) and the Draft Alberta Guidelines for Steep Creek Risk Assessments (2015).

Notwithstanding, the methods discussed herein are beneficial in (a) quickly identifying the scale of a debris-flow- or debris-flood hazard and (b) custom-tailoring efforts suited for a specific debris-flow or debris-flood risk assessment. The practitioner using this technique is cautioned against blind application. An understanding of a watershed's geomorphic processes and hazard chains is still crucial as multiple watershed and fan processes can invalidate the regional approach.

ACKNOWLEDGEMENTS

The authors would like to thank the Town of Canmore, the Municipal District of Bighorn, the Squamish-Lillooet District, David Keir, Mike Milner, Kinder-Morgan Pipelines, Bethel Land Corporation, Lil'wat Construction Enterprises and Emergency BC for their support in conducting the studies that led to this paper.

REFERENCES

- Allstadt, K. 2013. Extracting source characteristics and dynamics of the August 2010 Mount Meager landslide from broadband seismograms, *Journal of Geophysical Research: Earth Surface*, 118(3): 1472-1490.
- AMEC Earth and Environmental. 2006. Geohazards review Highway 40 / Highway 541 corridor, Southwestern Alberta. Report prepared for Alberta Transportation.
- APEGBC. 2010. Guidelines for legislated landslide assessments for proposed residential development in British Columbia. APEGBC, Burnaby, BC.
- APEGBC. 2012. Professional practice Guidelines - Legislated flood assessments in BC. Commissioned by the British Columbia Ministry of Forests, Lands and Natural Resource Operations (MFLNRO). APEGBC, Burnaby, BC.
- BGC Engineering Inc. 2013. Cougar Creek 2013 forensic analysis and short-term debris flood mitigation. Report prepared for the Town of Canmore dated December 11, 2013.
- BGC Engineering Inc. 2014a. Hydroclimatic analysis of the June 2013 storm. Report prepared for the Town of Canmore dated August 1, 2014.
- BGC Engineering Inc. 2014b. Cougar Creek debris flood hazard assessment. Report prepared for the Town of Canmore dated March 7, 2014.
- BGC Engineering Inc. 2014c. Three Sisters Creek debris flood hazard assessment. Report prepared for the Town of Canmore dated October 31, 2014.
- BGC Engineering Inc. 2014d. Jura hazard debris flood hazard assessment. Report prepared for the Municipal District of Bighorn dated March 1, 2015.
- BGC Engineering Inc. 2014e. Cougar Creek debris flood risk assessment. Report prepared for the Town of Canmore dated June 11, 2014.
- BGC Engineering Inc. 2014f. Alberta Ministry of Environment and Sustainable Resource Development provincial guidelines steep creek risk assessments for urban developments – draft. Report prepared for the Alberta Ministry of Environment and Sustainable Resource Development, River Forecasting, Edmonton, Alberta.
- BGC Engineering Inc. 2015a. Harvie Heights Creek debris-flood and debris-flow hazard assessment. Report prepared for the Town of Canmore dated June 5, 2015.
- BGC Engineering Inc. 2015b. Grotto Creek debris-flood hazard assessment. Report prepared for the Municipal District of Bighorn dated May 22, 2015.
- BGC Engineering Inc. 2015c. Heart Creek debris-flood hazard assessment. Report prepared for the Town of Canmore dated April 30, 2015.
- BGC Engineering Inc. 2015d. Stoneworks Creek debris-flow hazard assessment. Report prepared for the Town of Canmore dated April 10, 2015.
- BGC Engineering Inc. 2015e. Exshaw Creek and Jura Creek debris flood risk assessment. Report prepared for the Municipal District of Bighorn dated March 1, 2015.
- BGC Engineering Inc. 2015f. Exshaw Creek debris flood hazard assessment. Report prepared for the Municipal District of Bighorn dated March 1, 2015.
- BGC Engineering Inc. 2015g. Stone Creek debris-flow hazard assessment. Report prepared for the Town of Canmore dated January 16, 2015.
- BGC Engineering Inc. 2015h. Flood mitigation prioritization. Report prepared for Alberta Transportation, January 20, 2016.
- Church M. 2013. Steep headwater channels, *Treatise on Geomorphology*, 9: 528–549.

- Clague, J.J., Friele, P.A. and Hutchinson, I. 2003. Chronology and hazards of large debris flows in the Cheekye River basin, British Columbia, Canada, *Environmental and Engineering Geoscience*, 8(4):75-91.
- Cordilleran Geoscience. 2008. Geologic hazards and risk assessment, Lot 2, DL 1249, Plan 27929, Lillooet land District, Mars Crossing near Birken, BC. Report to Mike Milner, Birken, BC.
- Cordilleran Geoscience. 2015. Geologic hazard assessment for subdivision approval, Keir property on Walker Creek, Gun Lake near Goldbridge, BC. Submitted to David Keir, 100 Mile House, BC.
- Cruden, D.M., and Hu, X-Q. 1999. The shapes of some mountain peaks in the Canadian Rockies, *Earth Surface Processes and Landforms*, 24:1-13.
- Gutenberg, B. and Richter, C.F. 1954. Seismicity of the earth, 2nd ed., Princeton University Press, Princeton, N.J.
- Hungr, O., Leroueil, S., Picarelli, L., 2014. The Varnes classification of landslide types, an update, *Landslides*, 11:167-194.
- Holm, K., Bovis, M. and Jakob, M. 2004. The landslide response of alpine basins to post-Little Ice Age glacial thinning and retreat in southwestern British Columbia, *Geomorphology*, 57 (2004) 201–216.
- Jackson, Jr., L.E. 1987. Debris flow hazard in the Canadian Rocky Mountains, *Geological Survey of Canada Paper*, 86-11.
- Jackson Jr. L.E. Kostaschuk, R.A. and MacDonald, G.M. 1987. Identification of debris flow hazard on alluvial fans in the Canadian Rocky Mountains, *Geological Society of America Reviews in Engineering Geology*, 7: 115-124.
- Jakob, M. 2012. The fallacy of frequency: statistical techniques for debris-flow frequency-magnitude relationships, International Conference on Landslides, Banff, May 2012
- Jakob M. and Jordan J. 2001. Design flood estimates in mountain streams – the need for a geomorphic approach, *Canadian Journal of Civil Engineering*, 28: 425-439.
- Jakob, M., Stein, D. and Ulmi, M. 2012. Vulnerability of buildings to debris-flow impact, *Natural Hazards*, 60(2): 241-261.
- Jakob M. Clague J.J. and Church M. 2015. Rare and dangerous: Recognizing extraordinary events on streams, *Canadian Water Resources Journal*, 41: 161-173.
- Jakob, M. and Friele, P.A. 2010. Landslide hazards and risks from volcanic debris flows at Mount Garibaldi, British Columbia, *Geomorphology*, 114: 382-395.
- Jakob, M., Hungr, O., and Thomson, B. 1997. Two debris flows with anomalously high magnitude, *In Proceedings of the 1st International Conference on Debris-flow hazards mitigation: Mechanics, prediction and assessment. Edited by C.L. Chen, A.S.C.E*, pp. 382-394.
- Linear Consulting and Golder Associates. 2002. Hope Creek Jan. 2002 Debris Flow TMPL Km 1013. Report prepared for Trans Mountain Pipe Line, May, 2002.
- Michael Cullen Geotechnical Ltd & Cordilleran Geoscience 2015. Assessment of debris floods, debris flows and glacial lake outburst floods on the proposed Wedge Creek run of river power project phase 1 Report. Prepared for Lil'wat Construction Enterprises LP, Mount Currie, BC.
- Moon, A.T., Wilson, R.A., and Flentje, P.N., 2005. Developing and using landslide frequency models, *Proceedings of the International Conference on Landslide Risk Management*, Vancouver, BC, 681-690.
- Mizuyama T, Kobashi S and Ou G 1992. Prediction of debris flow peak discharge, *Interpraevent, International Symposium*, Bern, Switzerland, Tagespublikation, 4: 99-108.
- Osborn, G., Stockmal, G., and Haspel, R., 2006. Emergence of the Canadian Rockies and adjacent plains: A comparison of physiography between end-of-laramide time and the present day, *Geomorphology*, 75(3–4): 450-477.
- Pierson, T.C. 2005. Hyperconcentrated flow- transitional process between water flow and debris flow. *In Debris-flow hazards and related phenomena. Edited by M. Jakob and O. Hungr*, Berlin, Springer: 159-202.
- Wheeler, J.O. and Gabrielse, H. 1971. The Cordilleran structural province, *In Variations in tectonic styles in Canada. Edited by R.A. Price and R.J.W. Dougals, Geological Association of Canada Special Paper*, 2: 2-81.

APPENDIX G

DETAILS ON THE DAN3D ROCK AVALANCHE MODELLING

APPENDIX G COMPILATION OF INPUT PARAMETERS USED IN PREVIOUS DAN3D MODELS

G.1 BACK ANALYSES

A database of 16 rock avalanche back-analyses from international case studies (Aaron and Hungr, 2016; Aaron unpublished data) was used to guide selection of the Voellmy parameters used in the runout analysis. The Voellmy model is governed by two parameters:

- a friction coefficient, f . Lower values of friction coefficient correspond to less basal resistance.
- a turbulence parameter, ξ , Higher values of the turbulence parameter correspond to less basal resistance.

The calibrated basal resistance parameters for the 16 international case histories are summarized on Figure G-1. Figure G-1 is divided into four zones corresponding to extremely high mobility, high mobility, intermediate mobility and low mobility. The mobility classes were defined based on clustering of the back-analysed values of basal resistance parameters. Events that experienced low resistance are defined as highly mobile, and those that experienced high resistance are defined as low mobility. In the database, the three case histories that displayed extremely high mobility were channelized rock avalanches that entrained significant quantities of saturated path material. Since a potential rock avalanche originating on the north side of Mount Currie could entrain significant quantities of saturated material, these channelized case histories may provide a good analogue.

Of the 5 case histories that plot in the high mobility zone, 4 were rock avalanches that descended steep slopes and overran flat valley bottoms. Therefore, the cases in this zone are likely good analogues for the behavior of a rock avalanche originating on the north side of Mount Currie. The resistance parameters selected for the high mobility forward analysis are representative of this high mobility zone ($f = 0.1$ and $\xi = 500 \text{ m/s}^2$). To explore the range of potential event mobility, a set of parameters representing the extremely high mobility zone ($f = 0.05$ and $\xi = 500 \text{ m/s}^2$) was also used for the forward analysis. As stated above, these parameters correspond to those analysed by Hungr and Evans (2004) for rock avalanches that entrain significant quantities of saturated path materials.

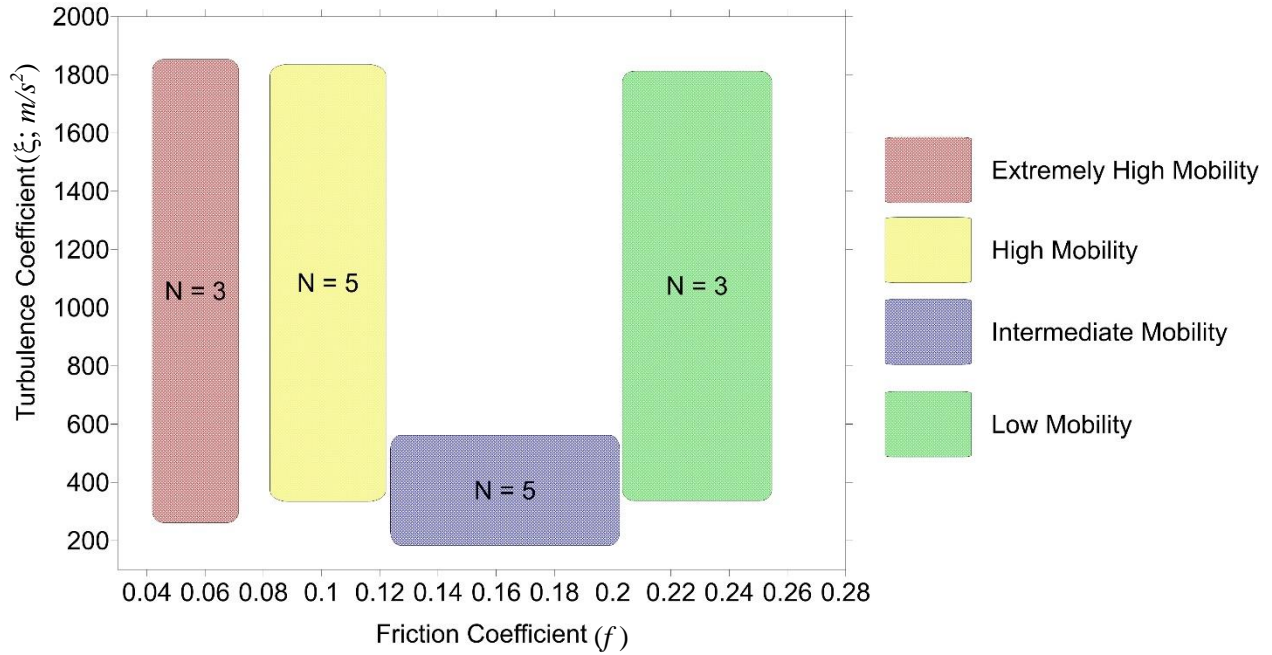


Figure G-1: Summary of calibrated rock avalanche basal resistance parameters. N refers to the number of cases that plot in each mobility zone. The parameters used for the Cheam back analysis are indicated. Units of turbulence are m/s²

References

Aaron, J, Hungr, O., 2016. Dynamic simulation of the motion of partially-coherent landslides. *Engineering Geology* 205: 1-11.

Hungr, O., and Evans, S.G. 2004. Entrainment of debris in rock avalanches: An analysis of a long run-out mechanism. *Geological Society of America Bulletin*, 116(9–10): 1240–1252.

APPENDIX H RISK ASSESSMENT METHODOLOGY

APPENDIX H: RISK ASSESSMENT METHODOLOGY

H.1. INTRODUCTION

Quantitative Risk Analysis (QRA) involves estimating the likelihood that a hazard occurs, impacts elements at risk, and causes certain types and severities of consequences. Vulnerability estimation involves estimating the likelihood of consequences given that a hazard has occurred and impacted elements at risk. The key difference between vulnerability and risk estimation is that vulnerability estimates assume impact, whereas risk additionally provides estimates of the likelihood of impact.

This section describes methods used to estimate vulnerability and risk to buildings and persons within buildings for the geohazard scenarios described in Section H.2 and shown on Drawings 08 and 09¹. As described in the main report, no risk assessment can consider, or quantify, every conceivable risk associated with a geohazard. Therefore, building damage and loss of life were selected as key risks that can serve as proxies informing risk reduction decision making.

Elements at risk considered in the analysis are described in the main report (Section 4.0) and shown on Drawing 10. The probability of scenario occurrence is based on the rock avalanche frequency estimates described in the main report (Section 3.4.5).

Section H.2 describes Scenarios 1a and 2b as an event tree showing key steps leading from landslide occurrence to consequences. Section H.3 describes the risk equation governing QRA methodology.

Different assessment methods were used within areas potentially subject to direct landslide impact compared to flooding from landslide damming of Green or Lillooet Rivers. Section H.4 describes methods used to estimate risk to life (safety risk) and probability of building destruction within the direct landslide impact and splash zones. Section H.5 describes methodology used to estimate the vulnerability of elements at risk to flooding associated with landslide damming of Green River (Scenario 1a) or both Green and Lillooet Rivers (Scenario 2b).

H.2. GEOHAZARD RISK SCENARIOS

Geohazard risk scenarios describe a chain of events where a geohazard occurs and reaches the hazard zone while the element at risk is present in the hazard zone, and causes certain types and severities of damage.

Drawings 08 and 09 show direct impact, splash zone and flooding resulting from a potential rock avalanche initiating from zone 1a (Scenario 1a) or 2b (Scenario 2b). Along with estimates of their likelihood of occurrence, these scenarios are the outcome of the hazard assessment that forms the basis for risk estimation. Figure H-1 visualizes these scenarios as an event tree, which shows

¹ Section 3 of the main report describes methods to develop these scenarios, and describes why these scenarios were chosen to be carried forward to the risk analysis. Other possible geohazard scenarios exist, but either were not considered to have credible potential for consequences or were not considered to be a controlling factor in risk evaluation and risk reduction decision making.

the progression of events leading from hazard occurrence to consequences. Reading the event tree from start (landslide occurrence) to finish (fatality or building damage) shows each step considered in the risk analysis.

The variables cited in Figure H-1 are described in Section H.3, where risk is calculated by multiplying the probabilities along each branch and then summing the results. Vulnerability estimation considers only the end of each branch of the event tree, V_i , given the occurrence of all steps in the event chain leading to impact.

Note that Figure H-1 considers Scenarios 1a and 2b as separate events, which were independently assessed. The combined risk from both scenarios was not estimated, whether occurring separately or simultaneously. This simplification is considered reasonable because the annual probability of both scenarios is very low ($\ll 1:1,000$), which means that the chance of simultaneous occurrence is so low that considering it would not appreciably change the risk estimate.

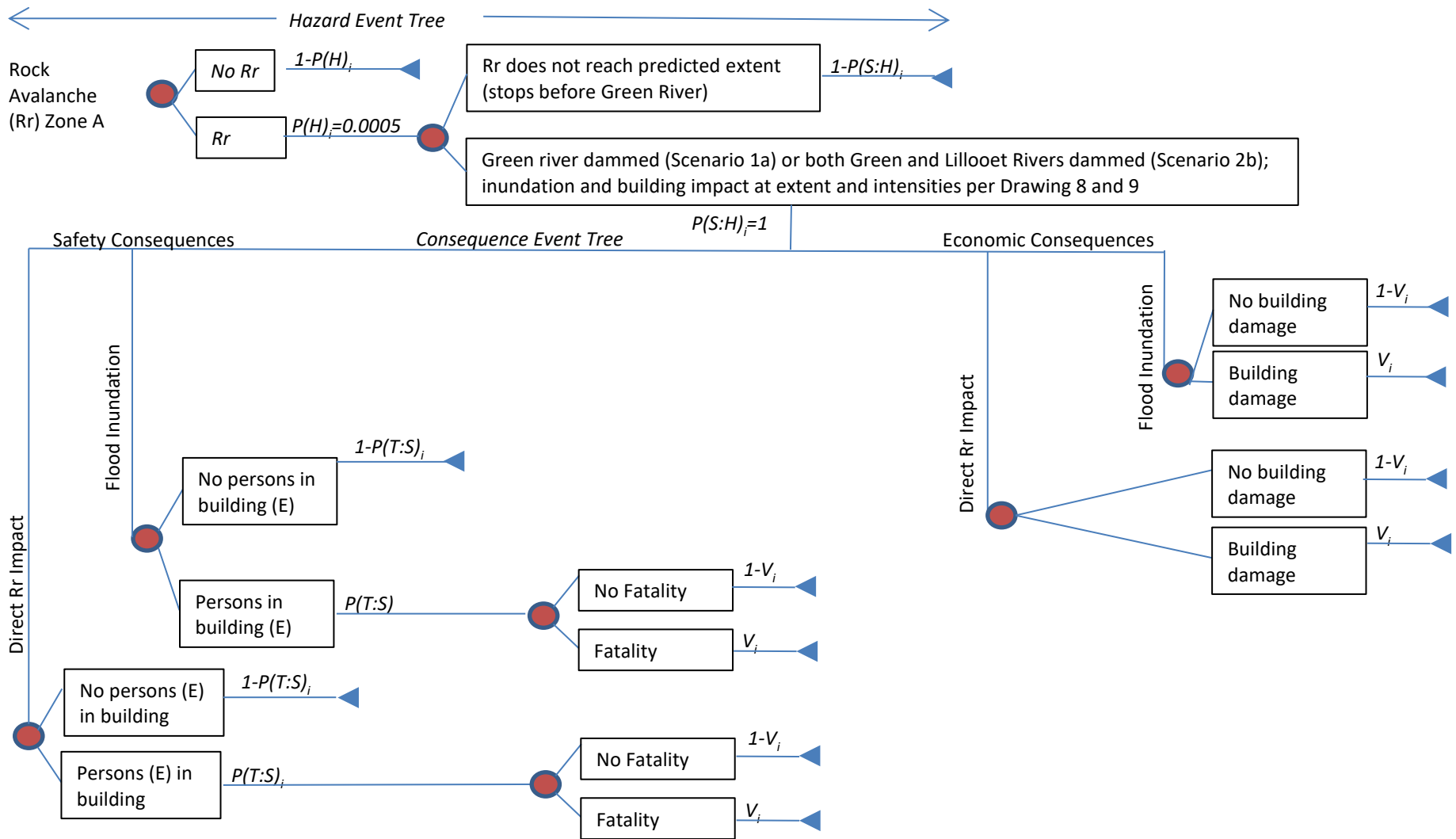


Figure H-1. Geohazard Event Tree, Scenarios 1a and 2b.

H.3. RISK EQUATION

Risk (P_E) was estimated using the following equation:

$$P_E = \sum_{i=1}^n P(H)_i P(S:H)_i P(T:S)_i N \quad [1]$$

where:

$P(H)_i$ Is the annual hazard probability of hazard Scenario 1a or 2b

$P(S:H)_i$ Is the probability that the Scenario 1a or 2b would reach the element at risk, given that it occurs.

$P(T:S)_i$ Is the probability that the element at risk (e.g., persons within buildings) is in the impact zone, given that the Scenario 1a or 2b reaches the location of the element at risk. This parameter is considered certain (equal to 1) for buildings and infrastructure.

$$N = V_i E_i \quad \text{Describes the consequences} \quad [2]$$

where:

V_i Is the vulnerability, which is the probability elements at risk will suffer consequences given hazard impact with a certain severity. For persons, vulnerability is defined as the likelihood of fatality given impact. For buildings, it is defined as the level of damage, measured as a proportion of the building replacement cost or as an absolute cost.

E_i Is a measure of the elements at risk, quantifying the value of the elements that could potentially suffer damage or loss. For persons, it is the number of persons exposed to hazard, equal to 1 in the case of individual risk assessment. For buildings, it is defined as the assessed value of buildings potentially subject to damage.

H.4. DIRECT IMPACT AND SPLASH ZONE

This section describes methods used to estimate risk to life (safety risk) and probability of building destruction within the direct landslide impact and splash zones. In these areas, impact is assumed to occur suddenly with no opportunity for evacuation, and with high vulnerability to loss of life.

H.4.1. Introduction

Building structure and safety risk were estimated according to Equation 1, using risk parameters described in Sections H.4.2 to H.4.6. For simplicity, the analysis considers Scenarios 1a and 2b separately, and does not estimate the combined risk of both scenarios.

Safety risk (risk to life) was estimated separately for individuals and groups (societal) risk. Individual risk considered the probability that a hazard scenario results in loss of life for a particular individual, and was estimated for each occupied parcel as the annual Probability of Death of an Individual (PDI). Unlike group risk, individual risk levels are independent of the number of persons exposed to risk.

Group risk was estimated as the probability of a certain number of fatalities, represented graphically on an F-N curve as shown in Figure H-2. The Y-axis shows the annual cumulative frequency, f_i , of each hazard scenario, and the X-axis shows the estimated number of fatalities, N_i , where:

$$f_i = \sum_{i=1}^n P(H)_i P(S:H)_i P(T:S)_i \quad [\text{Eq. 3}]$$

and N_i is represented by equation [2].

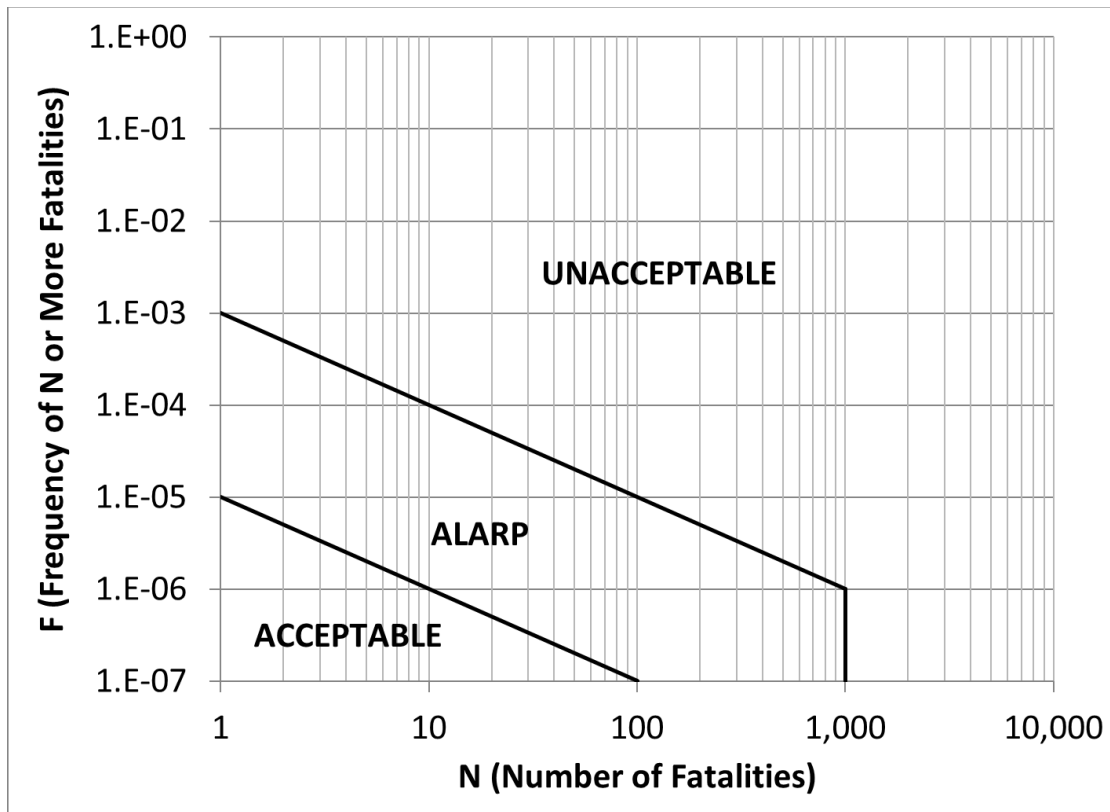


Figure H-2. Group risk tolerance criteria as defined by GEO (1998). ALARP stands for As Low As Reasonably Practical.

H.4.2. Hazard Probability

lists the estimated annual probability of occurrence, $P(H)$, assigned to each scenario. These values correspond to the hazard frequency estimates described in Section 3.4.5 of the main report.

Table H-1. Estimated annual probability of occurrence.

| Scenario | Rock Avalanche Annual Probability of Occurrence |
|----------|---|
| | Existing Conditions |
| 1a | 1.88 * 10 ⁻⁴ |
| 2b | 9.31 * 10 ⁻⁵ |

Table H-2 lists factor adjustments applied as a sensitivity analysis to consider potential changes in hazard probability due to climate change (specifically permafrost degradation and increases in the frequency of extreme precipitation events). As described in Section 3.4.7 of the main report, estimates of $P(H)$ for Scenario 1a are considered sensitive to loss of ice cohesion. Estimates of $P(H)$ for both Scenarios 1a and 2b are considered sensitive to increases in the frequency and magnitude of high intensity rainstorms.

Table H-2. Factor adjustments applied to $P(H)$ to consider climate change.

| Scenario | Likelihood Factor Adjustment | Climate Change Factors |
|----------|------------------------------|---|
| 1a | X 10 | Loss of ice cohesion; increases in the frequency and magnitude of high intensity rainstorms |
| 2b | X 2 | Increases in the frequency and magnitude of high intensity rainstorms |

H.4.3. Spatial Probability

Spatial probability of impact, $P(S:H)$, was assigned as 1 (certain) for all areas shown as impacted on Drawings 08 and 09.

H.4.4. Temporal Probability

For assessment of building damage, temporal probability, $P(T:S)$, was assigned as 1 (certain) based on the assumption that all buildings considered are permanent structures.

For assessment of safety risk, the value of $P(T:S)$ correspond to the estimated proportion of time spent by persons within a building.

For persons in residential buildings, an average value of 0.5 was assigned for analysis of risk to groups, implying that about half of the residents will be in their homes during an event. For businesses, a temporal probability of 0.23 was used, assuming a full-time work schedule of 2000 hours per year. For residential buildings, a more conservative value of 0.9 was used for estimation of individual risk, corresponding to a person spending the greatest proportion of time in the building (e.g. an infant or elderly person).

H.4.5. Building Vulnerability

BGC assigned ratings for building vulnerability, V , using criteria developed from judgement with reference to Jakob et al. (2011). The vulnerability estimates are based on the best information available, but contain uncertainty due to factors that cannot be captured at the scale of assessment, such as variations in the structure and contents of a given building and the location of persons within the building at the time of impact.

Table H-3 shows the building vulnerability ratings used for flows within the direct impact and splash zones. The numerical vulnerability ratings correspond to the estimated proportion of assessed building value based on the hazard intensity index (I_{DF}).

Table H-3. Vulnerability criteria for buildings.

| Hazard Intensity Index, I_{DF} (Range) | Building Damage Description | | Building Vulnerability |
|--|-----------------------------|--|------------------------|
| | Category | Description | Best Estimate |
| 1-10 | Moderate | High likelihood of moderate to major building structure damage due to impact pressure. Certain severe sediment and water damage. Building repairs required, possibly including some structural elements. | 0.5 |
| 10-100 | Major | High likelihood of major to severe building structure damage due to impact pressure. Certain severe sediment and water damage. Major building repairs required including to structural elements. | 0.8 |
| 100-1000 | Complete | Very high likelihood of severe building structure damage or collapse. Complete building replacement required. | 1 |
| >1000 | Complete | Certain building obliteration. Complete building replacement required. | 1 |

¹Numerical ratings are expressed as a proportion of building value for the purpose of damage cost estimation.

H.4.6. Human Vulnerability

Table H-4 shows the criteria used to estimate the vulnerability of persons within buildings to landslide impact, where vulnerability is primarily an indirect outcome of building damage or collapse. The numerical vulnerability ratings indicate estimated probability of loss of life given impact. The values shown are consistent with those used for BGC’s Catiline Creek geohazard risk assessment (BGC 2015).

Table H-4. Human vulnerability criteria, people in buildings ($I_{DF}>1$).

| Hazard Intensity Index, I_{DF} (Range) | Vulnerability Best-Estimate (Individuals) |
|--|---|
| 1-10 | 0.2 |
| 10-100 | 0.6 |
| 100-1000 | 0.9 |
| >1000 | 1.0 |

H.5. FLOOD INUNDATION ZONE

Sections H.5.1 and H.5.2 describes methods to estimate the vulnerability of buildings and persons within buildings to damages due to flooding associated with landslide damming of Green or Lillooet River.

H.5.1. Building Damage

For areas flooded at higher intensity ($I_{DF} > 1$), BGC estimated building damages using the same vulnerability criteria applied to the splash zone (Section H.4.5). For areas flooded at lower intensity ($I_{DF} < 1$), BGC estimated direct damages to building structures using flood stage-damage functions. These functions are widely applied in flood consequence studies and relate flood depth to average damage for certain building types. Damage can be expressed as a percentage of building cost or as an absolute cost per unit building area.

Flood stage-damage functions potentially applicable to this assessment include functions developed following the damaging floods in southwestern Alberta in June 2013 (referred to herein as Alberta depth-damage functions), and those used by the U.S. Federal Emergency Management Agency (FEMA) software program Hazus-MH, which is a multi-hazard loss estimation tool developed by FEMA and adapted for use in Canada by Natural Resources Canada.

The Alberta depth-damage functions are based on an inventory of residential and commercial units in Southern Alberta that were flooded in June 2013, as well as other Alberta flood events dating back to the early 1980s. Damage costs are estimated as a cost per unit floor area, for a given flood depth and building type, and they represent a Canadian source of depth-damage criteria. However, no data was available on building floor area within the study area. While building footprints can be used to approximate floor area, individual building data was also not available to differentiate, for example, a residential home from a large garage. Manually checking all buildings within the study area was not included in the scope of work.

Given the available buildings data, BGC applied Hazus depth-damage functions to estimate direct damages as a proportion of assessed building value (e.g. Figure H-3). Depth-damage functions used as “default” in Hazus-MH are available for 44 average building types. These curves represent the mean of more specific curves (e.g., the default depth-damage curve for retail stores is the average of curves for 144 retail store types).

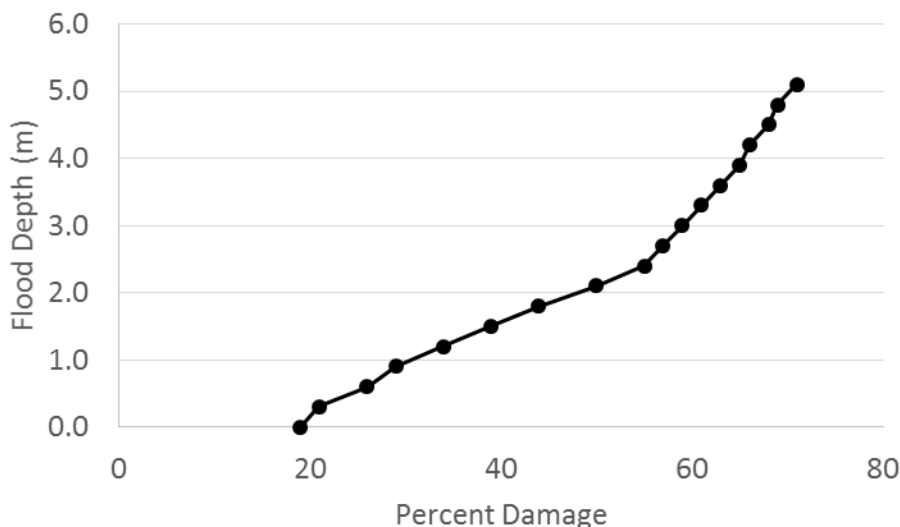


Figure H-3. Example of a flood depth-damage function for a residential home without a sub-grade basement.

On a depth-damage curve, “zero” flood depth corresponds to the first-floor elevation, but no complete dataset exists to determine first floor elevation within the study area. Damage estimates for buildings without basements are particularly sensitive to first floor elevation estimates, because estimated damages increase from zero to at least 20% of the building value once flooding reaches the first floor (FEMA, 2017). Damage cost estimates are also sensitive to whether buildings contain a sub-grade basement. For example, estimated structural damages to residential buildings could exceed 10% of building value even if depths do not reach the first floor, according to Hazus criteria². BGC understands that “many” residential buildings on the floodplain contain a sub-grade basement (pers. comm., SLRD, October 27, 2017). Given these uncertainties, BGC conservatively applied depth-damage curves that assumed the presence of a sub-grade basement for residential buildings, with a first-floor elevation assumed to be 1.2 m above surrounding grade. For non-residential buildings (i.e. industrial, commercial), BGC applied depth-damage curves that assumed a slab elevation of 0.3 m above surrounding grade.

BGC estimated damages to building structure, but not contents or commercial inventory. While Hazus depth-damage curves for contents and inventory are available, there is uncertainty in whether they can be reasonably applied to contents or inventory within the study area. As such, estimated damage costs provide a minimum bound and proxy for risk reduction decision making. Actual flood damage costs could be larger by a factor of two or more.

H.5.2. Human Vulnerability

Numerous workers have developed methods to estimate loss of life due to floods (Jonkman and Vrijling, 2008). These models range from relatively simple relations between inundation depth and

² Hazus “RES1” category, one floor, with basement.

life loss (e.g. Waarts 1992) to attempts to integrate complex human behavior (e.g. Assaf and Hartford 2002).

In general, complex models are sophisticated in theory, but fraught with high uncertainty because they depend on variables that are poorly known and difficult to collect, such as the spatial distribution of people inside buildings, vehicles, or outside; levels of warning; emergency planning and evacuation; human behaviour during an emergency; differences in human vulnerability due to age and health; and whether flood fatality statistics collected elsewhere are appropriate for a particular hazard location.

Given these limitations and uncertainties, risk estimates including probability of death or expected number of deaths for a particular flood scenario were not quantified in this study. Similar reasons have been given by the U.S. Corps of Engineers to explain reluctance to make loss of life estimates for floods (McClelland and Bowles 2002).

Consequently, instead of trying to quantify expected life loss, Table H-5 and Table H-6 lists simple criteria used to estimate relative vulnerability to floods for people in buildings. Table H-4 shows a conceptual sketch of the criteria in Table H-6. These criteria were applied at an individual building level of detail. Because first floor elevations are not known at this level of detail, BGC conservatively assumed a first floor elevation of 0.3 m above surrounding grade to identify higher vulnerability buildings (Drawing 12). No data on number of building stories was available across the study area. As such, BGC also conservatively assumed that the first floor was the highest accessible floor.

Table H-5. Human vulnerability criteria based on IDF, people in buildings.

| IDF | Vulnerability |
|-----|---------------|
| < 1 | Lower |
| > 1 | Higher |

Table H-6. Human vulnerability criteria based on flood depth, people in buildings.

| Estimated max. flood depth above first floor (m) | Vulnerability |
|--|---------------|
| < 1 | Lower |
| > 1 | Higher |

References

Assaf, H, Hartford DND, 2002. A virtual reality approach to public protection and emergency preparedness planning in dam safety analysis. In: Proceedings of the Canadian dam association conference, Victoria.

BGC Engineering Inc. (BGC), 2015. Catiline Creek Debris Flow Hazard and Risk Assessment. Final Report prepared for SLRD dated January 22, 2015.

Jakob, M., Stein D., Ulmi, M. 2011. Vulnerability of buildings to debris flow impact. Natural Hazards. DOI 10.1007/s11069-011-0007-2. Jonkman, S., and Vrijling, 2008. Loss of life due to floods. Journal of Flood Risk Management 1, pp. 43-56

Federal Emergency Management Agency, 2017. Web locations accessed October 30, 2017.

Hazus Program Page: <https://www.fema.gov/hazus>

Hazus Technical Manual Page: <https://www.fema.gov/media-library/assets/documents/24609>

Hong Kong Geotechnical Engineering Office (GEO), 1998. Landslides and Boulder Falls from Natural Terrain: Interim Risk Guidelines. Geo Report 175, Geotechnical Engineering Office, Civil Engineering Department, Hong Kong Special Administrative Region, 184 pp.

McClelland, D.M. and Bowles, D.S. 1999. Life-loss estimation: what can we learn from case histories? Proceedings of the Australian Committee on Large Dams (ANCOLD) Annual Meeting, Jindabyne, New South Wales, Australia, November 1999. 16 p.

Waarts P., 1992. Methode voor de bepaling van het aantal doden als gevolg van inundatie. Report TNO B-91-1099.